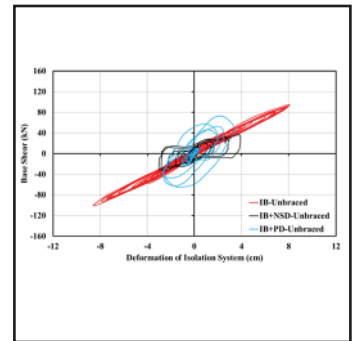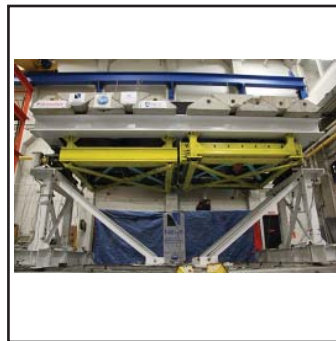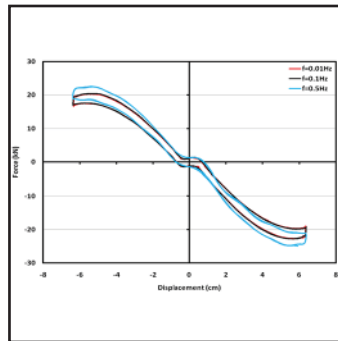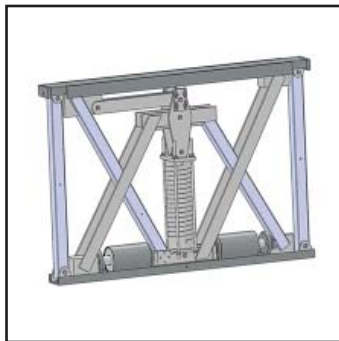# Seismic Protection of Highway Bridges with Negative Stiffness Devices

by

Navid Attary, Michael D. Symans, Satish Nagarajaiah,

Andrei M. Reinhorn, Michael C. Constantinou, Apostolos A. Sarlis,

Dharma T.R. Pasala and Douglas P. Taylor

Technical Report MCEER-13-0013

September 3, 2014

NOTICE

Seismic Protection of Highway Bridges with Negative Stiffness Devices

by

Navid Attary,[1] Michael D. Symans,[2] Satish Nagarajaiah,[3]Andrei M. Reinhorn,[4]
Michael C. Constantinou,[5] Apostolos A. Sarlis,[6] Dharma Theja R. Pasala,[7]
and Douglas P. Taylor[8]

1   Ph.D. Candidate, Department of Civil and Environmental Engineering, Rensselaer Polytechnic Institute
2   Associate Professor, Department of Civil and Environmental Engineering, Rensselaer Polytechnic Institute
3   Professor, Department of Civil and Environmental Engineering & Mechanical Engineering and Material Science, Rice University
4   Clifford C. Furnas Professor, Department of Civil, Structural and Environmental Engineering, University at Buffalo, State University of New York
5   Professor, Department of Civil, Structural and Environmental Engineering, University at Buffalo, State University of New York
6   Ph.D. Candidate, Department of Civil, Structural and Environmental Engineering, University at Buffalo, State University of New York
7   Senior Riser Engineer, Intecsea; Former Graduate Student, Department of Civil and Environmental Engineering, Rice University
8   President, Taylor Devices, Inc.

Project Overview

Development of Next Generation Adaptive Seismic Protection Systems

Design of conventional structures specified by the codes is based on the philosophy that the structure should withstand seismic loads while sustaining an acceptable level of damage. Structures are designed to prevent collapse but their serviceability and functionality in the aftermath of strong earthquake ground motion are not taken into consideration. This is achieved by designing structures to be ductile and letting them yield when subjected to strong earthquake ground motions. Yielding leads to stiffness and strength degradation, increased interstory drifts, and damage with permanent drifts, which render the structure non-functional.

Alternatively, the yielding can be emulated in a structural system by adding an adaptive "negative stiffness device" (NSD) and shifting the yielding away from the main structural system, leading to the new idea of "apparent weakening" that occurs to ensure structural stability at all displacement amplitudes. This is achieved through an adaptive negative stiffness system, a combination of NSD and a fluid damper. By engaging the NSD at an appropriate displacement (apparent yield displacement that is well below the actual yield displacement of the primary structural system), the composite structure-device assembly behaves like a yielding structure (while the primary structure remains mostly elastic). The concept and the NSD have been developed by the project team. The feasiblity of this new concept has been experimetally verified at the University at Buffalo-NEES facility on different structures.

Structural weakening and the addition of damping is an approach previously proposed to reduce seismic forces and drifts in the retrofit of structures. It is also used in the design of new buildings with damping systems. While this approach is efficient, it does not significantly reduce and may even amplify inelastic excursions and permanent deformations of the structural system during a seismic event. A novel negative stiffness device (NSD) is developed in this project that can emulate weakening of the structural system without inelastic excursions and permanent deformations. The NSD produces yielding by engaging at a prescribed displacement and generating negative stiffness, thus reducing the stiffness of the combined primary structure and NSD system, and leading to a bilinear inelastic system.

The new transformative ideas of "Negative Stiffness Device" and "apparent weakening" have been demonstrated in this project by means of experimental and analytical study. The new concept results in significant damage and response reduction. The system can be used in new buildings as well as for retrofit situations. NSD is the first practical negative stiffness device implementable in large structures; such a device did not exist prior to this project. The NSD is adaptive but passive, and exhibits true negative stiffness behavior by possessing predesigned variations of stiffness as a function of structural displacement amplitude. The NSD properties can be easily adapted by changing the lever arm to accommodate any change in the properties of the structure observed over time. It is likely to impact the state of practice of supplemental devices in earthquake protection.

Extensive analytical modeling has also been developed and validated using the shake table test results. The nonlinear analytical models have been incorporated into 3D-BASIS, IDARC and Opensees computer programs, thus enabling technology transfer. The concept of negative stiffness and apparent yielding/weakening has been experimentally verified in a three-story base-isolated structure and base isolated bridge with the NSD at the isolation level and also in a three-story fixed-base steel structure (moment frame) with the NSD in the first story. To accentuate the advantages of incorporating the NSD in structures, the responses of different systems including (1) base structure; (2) base structure with damper; (3) base structure with NSD; and (4) base structure with NSD and damper; are compared for a suite of ground motions. The behavior of all four systems are predicted analytically and the predicted results are in excellent agreement with the experiments. Shake table tests confirmed that by adding the NSD and damper, acceleration, base shear and deformations of the structure can be significantly reduced. In bilinear inelastic structures, the addition of the NSD and damper will prevent collapse as well as reduce its response during severe earthquakes.

The primary focus of this research is to analyze, implement and experimentally test the NSDs in a highway bridge. The bridge was configured with various isolation system components (isolation bearings, negative stiffness devices, and viscous dampers). In addition, the bridge was designed to mimic either a single-span bridge supported on abutments or an interior span of a multi-span bridge. The results of the investigation clearly demonstrate the effectiveness of the negative stiffness devices in limiting the seismic response of the bridge for multiple bridge configurations.

Project Management Committee

Satish Nagarajaiah, Principal Investigator, Rice University, Department of Civil and Environmental Engineering and Mechanical Engineering and Material Science, Houston, TX 77005; *Satish.Nagarajaiah@rice.edu.*

Andrei M. Reinhorn, Co-Principal Investigator, Department of Civil and Environmental Engineering, University at Buffalo, State University of New York, Buffalo, NY 14260; *reinhorn@buffalo.edu.*

Michael C. Constantinou, Co-Principal Investigator, Department of Civil and Environmental Engineering, University at Buffalo, State University of New York, Buffalo, NY 14260; *constan1@buffalo.edu.*

Michael Symans, Co-Principal Investigator, Department of Civil and Environmental Engineering, Rensselaer Polytechnic Institute, Troy, NY 12180; s*ymans@rpi.edu.*

Jian Zhang, Co-Principal Investigator, Department of Civil and Environmental Engineering, University of California, Los Angeles, CA 90095; *zhangj@ucla.edu.*

Douglas P. Taylor, Co-Principal Investigator, Taylor Devices Inc., North Tonawanda, NY 14120; *taylordevi@aol.com.*

ABSTRACT

A new control device has been developed and implemented for seismic response control of highway bridges. The device produces negative stiffness in a completely passive manner via a mechanical mechanism. Numerical simulations and experimental shaking table tests have demonstrated the effectiveness of the device in limiting the seismic demands on bridge structures. The main feature of the negative stiffness device is a pre-compressed spring, which can push the structure away from its center position and thus induce negative stiffness. When implemented in parallel with a structure having positive stiffness, the combined system appears to have substantially reduced stiffness while remaining stable. Thus, there is an "apparent weakening" of the structure that results in an "apparent yield point," reduced forces and increased displacements. The increase in displacement response can be limited by incorporating a damping device in parallel with the negative stiffness device or by adding friction to the device assembly.

In this report, the negative stiffness devices are described along with their hysteretic behavior as obtained from a series of cyclic tests that were utilized to calibrate the parameters of a numerical model. In addition, results from numerical simulations and seismic testing of a quarter-scale bridge model are presented wherein the bridge was configured with various isolation system components (isolation bearings, negative stiffness devices, and viscous dampers). In addition, the bridge was designed to mimic either a single-span bridge supported on abutments or an interior span of a multi-span bridge. The results of the investigation clearly demonstrate the effectiveness of the negative stiffness devices in limiting the seismic response of the bridge for multiple bridge configurations.

"This Page Intentionally Left Blank"

ACKNOWLEDGEMENTS

"This Page Intentionally Left Blank"

TABLE OF CONTENTS

TABLE OF CONTENTS (CONT'D)

LIST OF FIGURES

LIST OF FIGURES

LIST OF FIGURES

LIST OF FIGURES

Figure	Title	Page

LIST OF FIGURES

Figure	Title	Page

LIST OF FIGURES

LIST OF FIGURES

LIST OF FIGURES

LIST OF FIGURES

LIST OF FIGURES

Figure	Title	Page

"This Page Intentionally Left Blank"

LIST OF TABLES

"This Page Intentionally Left Blank"

SECTION 1. INTRODUCTION

A new passive seismic response control device has been developed and implemented in a bridge model and shown to be capable of producing negative stiffness via a purely mechanical mechanism. The main feature of the Negative Stiffness Device (NSD) is a large pre-compressed spring, which can push the structure away from its center position and thus induce negative stiffness behavior. Only a few researchers have investigated the application of the negative stiffness concept to bridge structures. Their work has demonstrated the potential effectiveness of such devices for seismic protection. Although the concept of negative stiffness may appear to be a reversal on the desired relationship between the force and displacement in structures (the desired relationship being that the product of restoring force and displacement is nonnegative), when implemented in parallel with a structure having positive stiffness, the combined system appears to have substantially reduced stiffness while remaining stable. Thus, there is an "apparent weakening and softening" of the structure that results in reduced forces and increased displacements. Any excessive displacement response can then be limited by incorporating a damping device in parallel with the negative stiffness device. The combination of negative stiffness and passive damping provides a large degree of control over the expected performance of the structure.

In the first chapter of this report, initial numerical studies are presented on the performance of a seismically-isolated highway bridge model that is subjected to various strong earthquake ground motions. The Negative Stiffness Devices (NSDs) are described along with their hysteretic behavior as obtained from a series of cyclic tests wherein the tests were conducted using a modified design of the NSDs (modified for testing within the bridge model). Using the results from the cyclic tests, numerical simulations of the seismic response of the isolated bridge model were conducted for various configurations (with/without negative stiffness devices and/or viscous dampers). The results demonstrate that the addition of negative stiffness devices reduces the base shear substantially, while the deck displacement is limited to acceptable values. This assessment was conducted as part of a NEES (Network for Earthquake Engineering Simulation) project which included shaking table tests of a quarter-scale bridge model to validate the results from the numerical simulations presented in this chapter.

In the second chapter, the implementation of the device within a quarter-scale bridge model and its performance under seismic loading conditions is evaluated via shaking table tests. For these tests, the bridge is seismically isolated using elastomeric bearings and includes some tests with NSD's and some with viscous dampers. Four different isolation system configurations are considered: isolated bridge (IB), IB with viscous dampers, IB with NSDs and IB with viscous dampers and NSDs. In addition, two bridge pier configurations were considered, one with flexible piers (mimicking a middle span of a multi-span bridge) and one with braced piers (mimicking a single span bridge supported on abutments). The experimental results clearly demonstrate the effectiveness of the NSDs in limiting the seismic response of the bridge and provide validation of numerical simulation results wherein the numerical models of the bridge model components were calibrated via system identification testing.

In the third chapter, details of the experimental results and their comparison with numerical simulations under a wide range of ground motions are presented. In addition, performance indices were developed to systematically and quantitatively evaluate the relative performance of different isolation system configurations that employ combinations of positive and negative stiffness as well as various levels of positive damping. Further, the influence of

boundary conditions (rigid versus flexible bridge piers) on the effectiveness of employing negative stiffness devices has been evaluated. Finally, concepts for graphical interpretation of the performance indices are presented and used to demonstrate the degree to which employing negative stiffness may be beneficial in improving the seismic response of bridge structures. Finally, results from cyclic testing of the NSDs and shake table testing of the bridge model for the eight configurations described previously, are provided in the appendices along with the details of bridge model instrumentation and fabrication drawings.

SECTION 2. NUMERICAL SIMULATIONS OF A HIGHWAY BRIDGE STRUCTURE EMPLOYING ADAPTIVE PASSIVE NEGATIVE STIFFNESS DEVICE FOR SEISMIC PROTECTION

2.1 Introduction

Bridge structures provide a vital link in many transportation systems and thus their damage during earthquakes can have severe consequences. In an effort to improve the seismic performance of bridges, different types of protection devices (passive, active and semi-active) have been analyzed, tested, and implemented. Common passive seismic protection devices for bridges include elastomeric bearings, sliding bearings, viscous dampers, and viscoelastic dampers. Through numerical simulations and experimental testing, a number of researchers have demonstrated the effectiveness of such devices. However, there have been studies on seismically-isolated bridges that indicate that passive systems may have reduced effectiveness (and sometimes can degrade performance) in cases where the ground motion exhibits strong velocity pulses (e.g., Nagarajaiah et al., 1993). In such near-fault ground motion conditions, the velocity pulse can amplify the dynamic response of the isolated bridge when the pulse period is close to the fundamental period (Shen et al., 2004). Furthermore, it is generally understood that passive seismic protection devices that are effective in reducing the displacement of the bridge deck may not reduce the shear force in the piers and the acceleration of the bridge deck since such force-related response quantities have peak values that are dictated by the yield strength of the structure.

In addition to passive devices, active and semi-active devices have been tested and implemented in bridges. As an example, Sahasrabudhe and Nagarajaiah (2005a and 2005b) conducted experimental and numerical studies on semi-active control of sliding isolated bridges using magneto-rheological (MR) dampers and variable stiffness systems. About a decade ago, Iemura and Pradono (2003) and Iemura et al. (2006) evaluated an application of actively controlled pseudo-negative stiffness via numerical simulations of a benchmark cable-stayed bridge, the intent being to reduce both the base shear of the bridge and the deck displacements. The negative stiffness was provided by a variable hydraulic damping device whose mechanical properties could be controlled in such a way that the device force was in phase with the bridge deck inertia force, thereby producing negative stiffness ("pseudo" in that the device must be externally controlled with feedback to produce the desired behavior). However, the variable damper required external power and a feedback signal to be able to generate negative stiffness, thus reducing its reliability relative to passive devices. Following Iemura's work, Han et al. (2010) performed numerical simulations on a four-span bridge model, using Iemura's actively controlled pseudo-negative stiffness device and compared its performance with other isolation systems. Han et al. (2010) showed that, for various ground motions, the combination of Iemura's pseudo-negative stiffness system with rubber bearings reduced the base shear by more than 40% with respect to the rubber bearings alone and by more than 20% with respect to lead rubber bearings or rubber bearings with viscous dampers. Han et al. (2010) went on to recommend the use of pseudo-negative stiffness systems in bridges, especially in areas prone to high seismic intensity.

With the intent of reducing both acceleration and base shear along with deformations, Reinhorn et al. (2005 and 2009) introduced the concept of weakening of structures (reducing strength) to reduce earthquake forces. Although this can be effective, it is often at the expense of

increased displacements, which, however, can be limited through the use of a damping system. Although weakening of structures with added damping is capable of reducing both the accelerations and deformations, it may lead to early yielding of the structural system resulting in damage to the structure and permanent deformations. In 2009, Iemura and Pradono developed and tested a passive device in a scaled bridge model, capable of producing negative stiffness, using a portion of the weight of the structure in which the bridge deck was placed on top of convex pendulum bearings. Their device was similar to an upside-down friction pendulum bearing in which the negative stiffness is generated due to the weight of the structure applied to the convex surface (such a configuration is inherently unstable at all displacements). Using the device in parallel with elastomeric bearings (which provide positive stiffness), the combined system is a soft system with low horizontal effective stiffness wherein excessive displacement is controlled by friction damping. Although they were able to test the system on a small-scale bridge model, transferring the large gravity loads of real full-scale bridges through an unstable system, which continuously generates negative stiffness between the deck and piers, appears to be impractical.

Since 2008, our research team worked on the development and experimental testing of a new seismic protection device that could change its properties passively and mechanically and, for the first time, could create true negative stiffness behavior (not pseudo-negative stiffness by means of hydraulic devices, as described previously) to substantially reduce earthquake forces in structures through "apparent weakening" or softening behavior, additional damping, and elongation of the fundamental period. The device was a passive device, but it was considered to be adaptive in the sense that it could change its behavior based on the displacement response of the structure. In addition, it could create true negative stiffness behavior by using a pre-compressed spring within an innovative geometrical arrangement of steel braces and levers. Nagarajaiah and Reinhorn (1994), Nagarajaiah (2010) and Nagarajaiah et al. (2010) showed that using the negative stiffness device (NSD) in structures would result in decreased dynamic forces and increased displacements (although the displacements could be limited by including a damping device in parallel with the NSD) (see Fig. 2.1 where the "assembly" represents the combined effect of the components). By engaging the NSD's at certain displacements and using its negative stiffness to create "apparent weakening" or softening behavior, the combined behavior of the primary structure (which has positive stiffness) with NSD's (which have negative stiffness) is one in which there is an apparent or virtual yield point at a small force level, followed by increasing displacement. The response is virtual in that the framing of the primary structural system does not actually yield; rather, the composite system appears to yield (i.e., apparent weakening). Thus, the softening response is of a non-damaging nature in that it occurs in the NSD's rather than within the primary structural framing system. The combination of adaptive negative stiffness and passive damping devices provides a large degree of control over the expected performance of the structure and thus is well suited to performance-based approaches to seismic design.
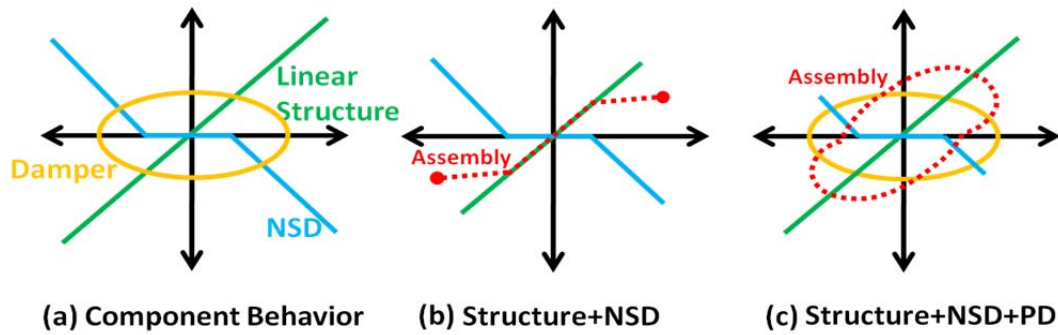
Figure 2.1. Working principle of NSD: (a) Force-displacement relation for each component
(b) Behavior of linear system with NSD (c) Behavior of linear system with NSD and damper
(Green: Base structure, Blue: NSD, Yellow: Passive damper, Red: Assembly)

Two prototypes of the NSD (see Fig. 2.2) were fabricated by a leading manufacturer of seismic protection devices and tested to evaluate their response to cyclic loading. In addition, the effects of the devices on the seismic response of two different three-story scale-model buildings (one, an isolated structure that behaved elastically and, two, a fixed-base structure that behaved inelastically) was evaluated via shaking table tests (Sarlis et al, 2011 & 2012 and Pasala et al, 2011, 2013a and 2013b). In the final stage of the project, the NSD's were implemented in a quarter-scale highway bridge model and tested on a shaking table (Attary et al., 2012a, 2012b & 2013). Unlike the previous two phases of experimental testing of the NSDs within three-story buildings, in this set of experimental tests the NSDs react against flexible bridge piers rather than being directly connected to the foundation of the structure. This chapter focuses on work that was conducted to prepare for the seismic shaking table tests of the bridge model, including results from cyclic testing of the NSD, associated analytical modeling of the device, and numerical simulations of the response of the seismically-isolated bridge model in various configurations including those that employ NSD devices and/or viscous damping devices.
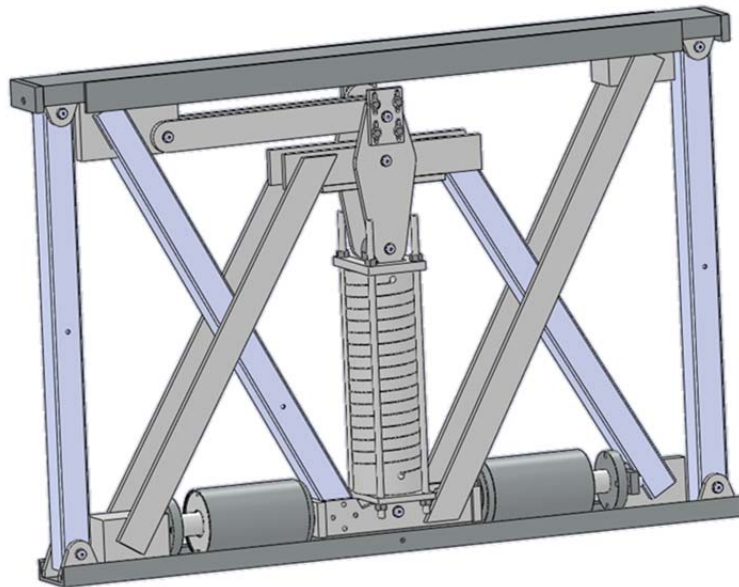
Figure 2.2. Prototype Negative Stiffness Device

2.2 Negative stiffness device: behavior and analytical model

As described previously, the negative stiffness device (NSD) is a completely mechanical device that develops a force that is in-phase with the motion of the device. This force is created using a pre-compressed main spring, which is originally parallel to the sides of the NSD (see Fig. 2.2). When the NSD frame is subject to a shearing deformation, the main spring becomes inclined, creating a force in the same direction as the imposed motion. The deformed shape of the NSD is shown in Figure 2.3 where the top of the NSD is deformed to the right relative to the bottom of the NSD. The gap spring assemblies shown in Figure 2.3 provide an initial phase of response where the NSD provides positive stiffness to ensure stability at small displacements. Beyond some displacement, the gap springs provide negligible positive stiffness, resulting in negative tangent stiffness for the NSD. The use of gap springs results in a so-called adaptive passive device since the gap springs can be designed such that the behavior of the NSD is based on the response (deformation) of the structure to which it is attached. Thus, by using the gap springs, the designer can dictate the level of deformation at which the composite NSD/structure system exhibits a definitive reduction in stiffness. Based on the free body diagram shown in Figure 2.3, the horizontal force developed by the NSD can be obtained from equilibrium of the pivot plate along with the geometry of the deformed shape:

$$F_{NSD} = -F_S \left(\frac{L_1}{L_2} \right) \left(2 + \frac{L_2}{L_1} + \frac{L_p + L_1}{\sqrt{L_2^2 - u^2}} \right) + F_g \tag{2.1}$$

where L_p is the initial length of the main spring, L_1 and L_2 are the lengths of the two sides of the pivot plate, F_g is the force in the gap-spring assembly, u is the shear deformation of the NSD, and F_s is the force in the pre-compressed main spring as given by (assuming linear elastic behavior of the main spring):

$$F_S = \left(\frac{F_{pc} + K_s L_p}{L_s} - K_s \right) u \tag{2.2}$$

where F_{pc} is the initial force in the pre-compressed main spring, K_s is the stiffness of the main spring and L_s is the length of the deformed shape of the main spring. For the case of no gap spring assemblies, imposed motion of the NSD results in immediate development of negative tangent stiffness (see Fig. 2.4). Beyond some displacement, the main spring loses its pre-compression and begins to develop tensile force. At that point, the tangent stiffness becomes positive, ensuring stability of the structure at large displacements (see Fig. 2.4). As the displacement approaches the length L_2, the pivot plate becomes horizontal and the device locks up with high positive stiffness.
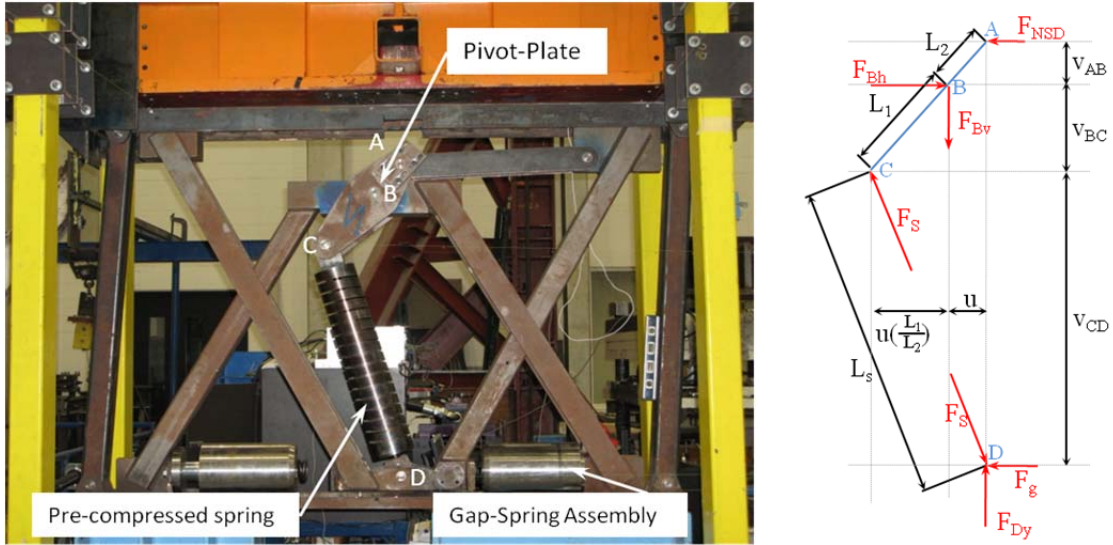
Figure 2.3. Prototype NSD undergoing cyclic testing and free-body diagrams for evaluation of lateral force

The properties and characteristics of the NSD have been presented in details by Sarlis et al. (2011 & 2012), Pasala et al. (2011, 2013a & 2013b) and Attary et al. (2012a). In anticipation of the shaking table tests of the aforementioned bridge model, the properties of the NSDs were modified to optimize their effect on the structure. The key feature of the device is its negative stiffness, which is controlled by the stiffness and pre-compression of the primary spring. The pre-compression force of the primary spring was set equal to 19.57 kN. A summary of the values of the parameters, which were used in experimental testing of the bridge model, is provided in Table 2.1.
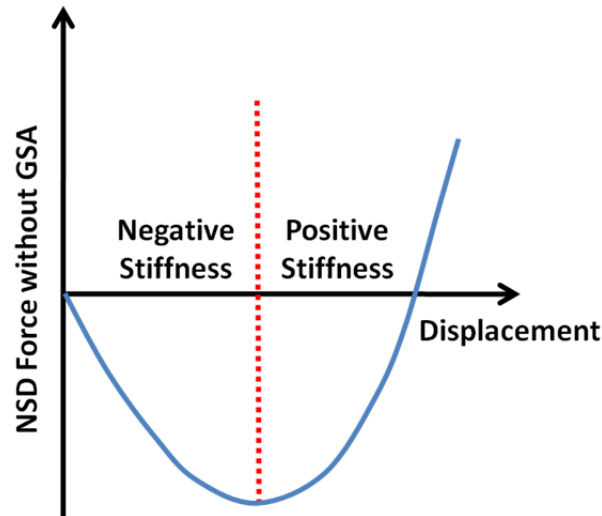
Figure 2.4. Behavior of NSD without gap spring assembly

Table 2.1. Values of parameters used to define NSD behavior for implementation in bridge model

Parameter	Value
Distance from spring pin to fixed pin (l_1)	0.254 m
Distance from lever pin to fixed pin (l_2)	0.127 m
Initial length of main spring (L_p)	0.762 m
Stiffness of main spring (K_s)	140 kN/m
Preload of main spring (F_{pc})	19.57 kN

To optimize the behavior of the NSD for the bridge model testing, the gap-spring assemblies (GSAs) were redesigned such that the negative stiffness is engaged after 0.5 cm of shearing deformation, creating a virtual yield point at 0.5 cm of relative displacement between the bridge deck and the top of the piers. The GSAs consist of a pre-compressed soft spring and a stiff spring in series (see Fig. 2.5) which results in the bilinear behavior shown in Figure 2.6. Also shown in this figure is one of the GSAs at four different stages of operation. At stage S0, the device displacement is negative and the GSA is not in contact with the lower part of the main spring (see GSA on lower left of Fig. 2.6). At stage S1, the lower part of the main spring (point D in Fig. 2.3) just comes into contact with the GSA. Beyond stage S1, the stiff spring is engaged and is compressed until stage S2 is reached (gap spring displacement is equal to d_g). Beyond that displacement, stage S3 occurs wherein the soft spring is also engaged (soft and stiff springs act in series to produce a combined stiffness that is smaller than that of either of the two springs acting alone). The force that develops in the GSAs is defined as follows (elastic nonlinear behavior):

$$
F_g = \begin{cases}
k_{stiff} u & |u| < d_g \\
\left[F_{comp} + \dfrac{k_{stiff} k_{soft}}{k_{stiff} + k_{soft}} \left(|u| - d_g \right) \right] \operatorname{sgn}(u) & |u| > d_g
\end{cases} \tag{2.3}
$$

where k_{stiff} is the stiffness of the outer spring of the GSA (stiffer spring), k_{soft} is the stiffness of the inner spring of the GSA (softer spring), and d_g is the amount of shear deformation of the negative stiffness device prior to initiation of global negative stiffness behavior (i.e., the combined effect of the GSAs and the main spring produces negative stiffness for displacements larger than d_g). The pre-compressed force in the soft spring (which prevents its engagement until the displacement d_g is reached) is given by

$$
F_{comp} = k_{stiff} d_g \tag{2.4}
$$

The values of each parameter that defines the behavior of the GSAs (for application to the bridge model) are given in Table 2.2.
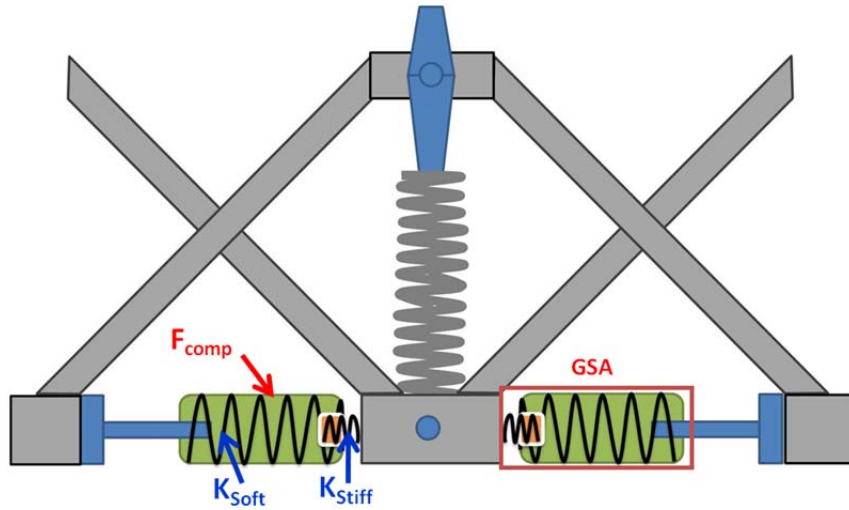
Figure 2.5. Schematic illustrating soft and stiff springs in gap spring assemblies

Table 2.2. Values of parameters used to define gap-spring assembly for application to bridge model

Parameter	Value
NSD engagement displacement (d_g)	0.5 cm
Stiffness of soft spring (K_{soft})	6.59 kN/m
Stiffness of stiff spring (K_{stiff})	491.2 kN/m
Pre-compressed force of soft spring (F_{comp})	2.8 kN
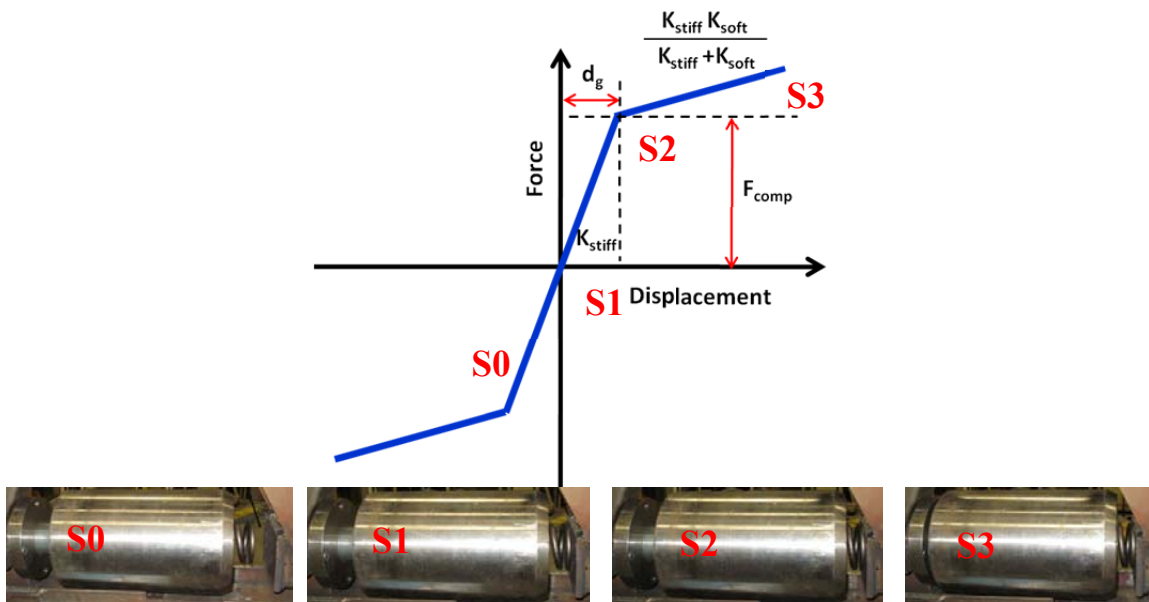
Figure 2.6. Force-displacement behavior of gap-spring assembly

11

2.3 Design of NSDs for application to bridge model

The scale-model structure used in the experimental validation phase of the project was a quarter-scale single-span steel highway bridge (see Fig. 2.7). The numerical simulations presented herein provide predictions of the response of the bridge to seismic loading. The bridge consists of an essentially rigid deck supported on elastomeric bearings which in turn are supported on two piers (the bridge piers are from a bridge model that was previously tested by Tsopelas and Constantinou, 1994). The piers are flexible but can be readily braced to mimic an abutment support condition. The bridge has a clear span of 4.8 m, a height of 2.7 m, and two custom-designed NSD support frames attached below the 5.4 m long bridge deck. The deck of the bridge is supported on a seismic isolation system consisting of four elastomeric bearings and includes NSDs and/or viscous dampers within the isolation system. Note that one of the major differences between testing of the NSDs within the aforementioned building models and the bridge model is that the bridge piers introduce a layer of flexibility between the NSDs and the earthquake ground motion. Such conditions did not exist in the building model wherein the NSD's were located either within an isolation system that was directly attached to the building foundation (shake table) or within the framing of the building.
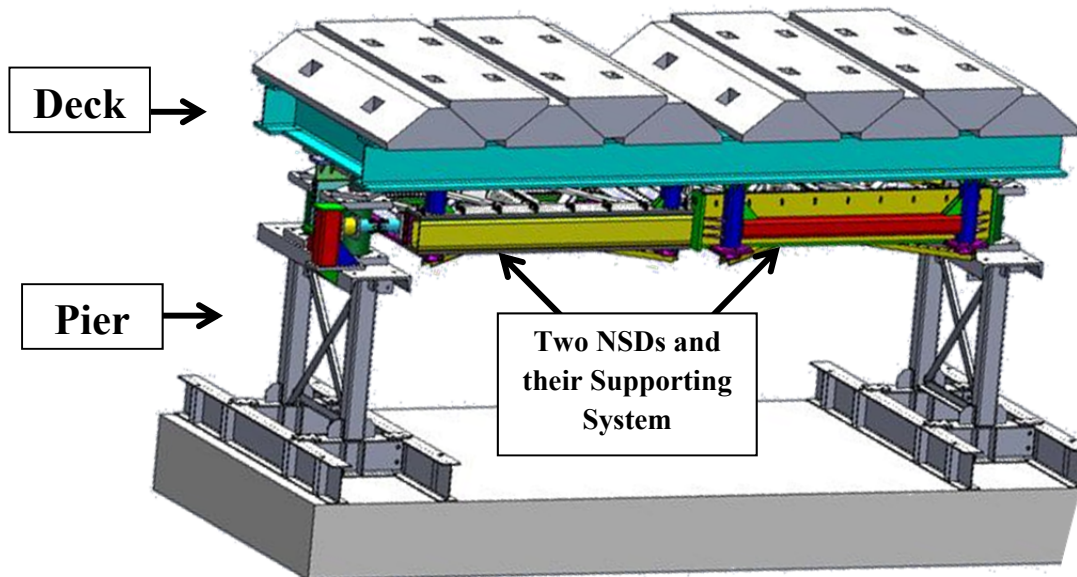
Figure 2.7. Detailed 3D model of quarter-scale bridge test specimen

The bridge deck consists of two W12x96 sections as the main longitudinal beams and two W12x96 sections as transverse beams at the two ends of the deck and four W10x88 transverse beams within the span. Ten concrete blocks are attached to the top of the deck to provide seismic mass. Two support frames are attached to the underside of the deck to carry the NSDs (see Fig. 2.8).
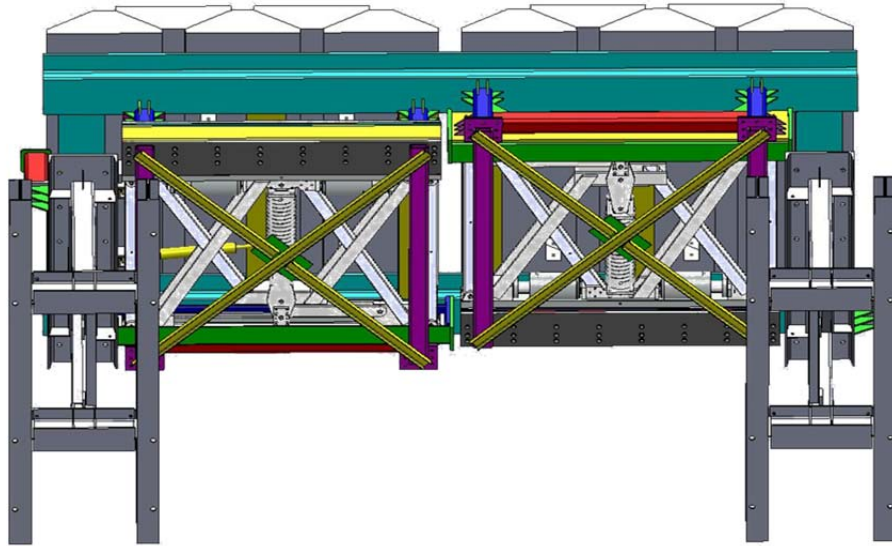
Figure 2.8. View of underside of bridge model (looking up) showing two NSDs installed below the deck

The two NSD support frames were custom-built to support the weight of the NSDs while incorporating a special railing system to allow sliding of the NSDs on the side that was attached to the top of the bridge piers (the other side was rigidly attached to the underside of the bridge deck) (see Fig. 2.9). With this system, the NSDs were subjected to shearing deformation as the bridge deck displaced relative to the bridge piers. Since the shearing deformation results in a reduced width of the NSDs, the NSD support frame was also designed to accommodate lateral motion of the NSD via roller bearings attached to various parts of the frame. The weight of the bridge deck, including the two NSDs with their support frames, is 68.9 kN.
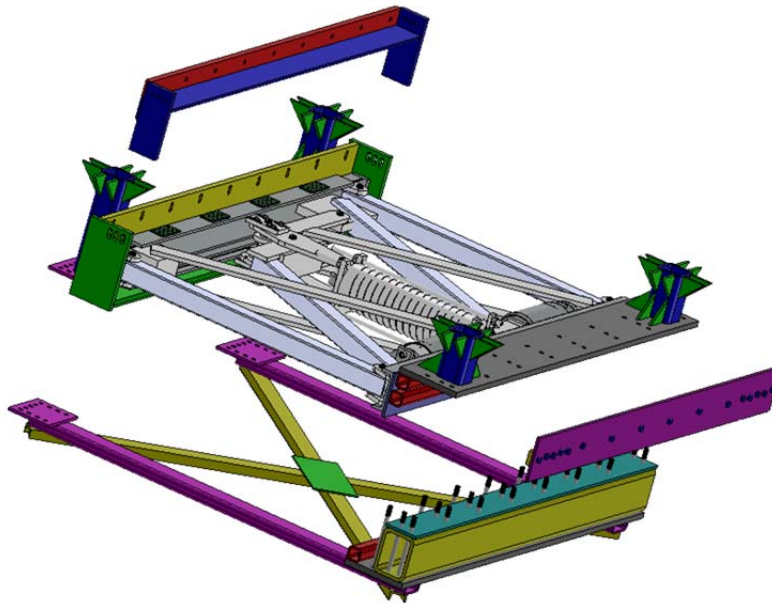
Figure 2.9. Details of the custom-designed NSD support frame with special railing system

The ten concrete blocks attached to the top of the bridge deck each weigh 8.9 kN, resulting in a total bridge deck weight of 157.9 kN. Each bridge pier consists of two columns (tube sections), a pier cap beam (channel section), and lateral bracing (angle sections) between the columns. The elastomeric bearings that are used within the isolation system are low damping bearings that primarily provide a linear restoring force. They are made of natural rubber of grade 5 and Shore durometer Type A hardness of 50. The effective stiffness of each of the bearings can be determined as follows (Naeim and Kelly, 1999):

$$K_{eff} = \frac{GA_r}{T_r}$$ (2.5)

where G is the shear modulus of the rubber, A_r is the bonded rubber area and T_r is the total rubber thickness. Assuming a typical shear modulus of 0.7 MPa for this type of material and using the known total rubber thickness and bonded area (5.7 cm and 243 cm^2, respectively), the effective stiffness of each bearing is calculated as 298 kN/m (total stiffness of four bearings is approximately 1200 kN/m). Using the stiffness of the bearings and the weight of the deck, the fundamental period of the isolated bridge model is estimated to be 0.7 seconds. In some of the tests, two linear viscous dampers, each having a damping coefficient of 66.4 kN-s/m, were installed within the isolation system (in parallel with the elastomeric bearings).

The modified design of the NSDs results in the analytical force-displacement relations shown in Figure 2.10 wherein separate curves are shown for the following cases: 1) NSDs alone, 2) bridge isolation system without NSDs, 3) bridge isolation system with NSDs, and 4) bridge isolation system with NSDs and in series with the bridge piers. Figure 2.7 clearly shows that the NSDs introduce a virtual yield point in the system and continuously changes the secant stiffness of the system (see Fig. 2.11). Further, it can be seen that the effect of the flexible piers (in series with the NSDs) is to reduce the tangent stiffness of the system at any given displacement.
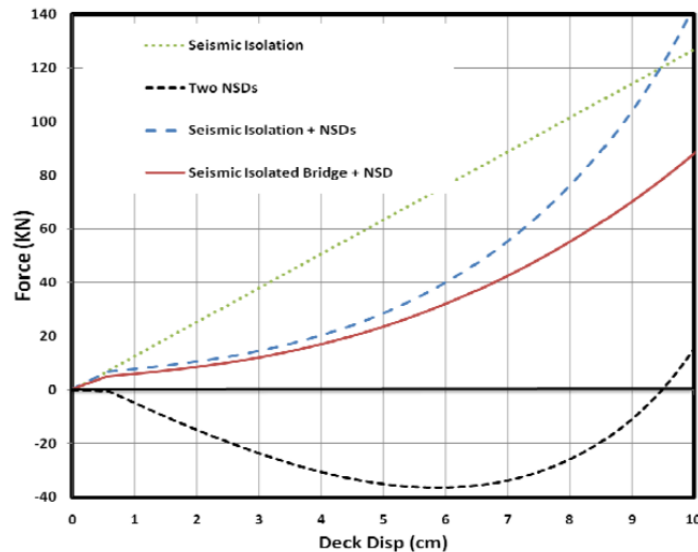
Figure 2.10. Analytical force-displacement relations for NSDs alone, isolation system without NSDs, isolation system with NSDs, and isolation system with NSDs and in series with the bridge piers
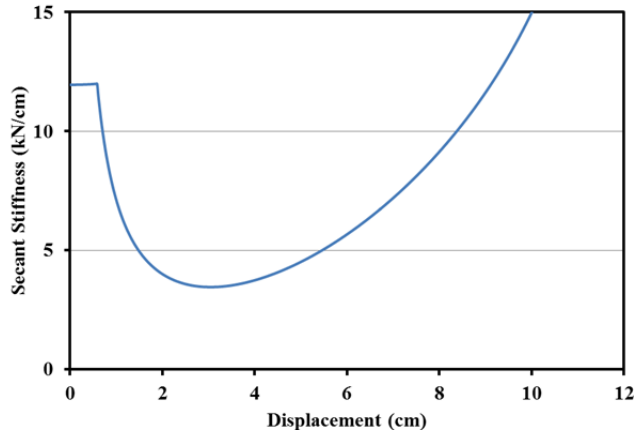
Figure 2.11. Continuous change of secant stiffness of the bridge model combined with NSDs (braced piers)

2.4 Experimental validation of negative stiffness device properties

Having redesigned the NSDs, it was necessary to conduct tests to verify their behavior relative to the analytical model and to calibrate the numerical model to be used within the numerical simulations of the isolated bridge model. The NSDs were installed within a load frame at the UB-SEESL laboratory at the University at Buffalo, wherein they were anchored at the bottom and allowed to displace laterally at the top (see Fig. 2.12). A hydraulic actuator was attached at the top of the NSD and was used to impose harmonic motions.
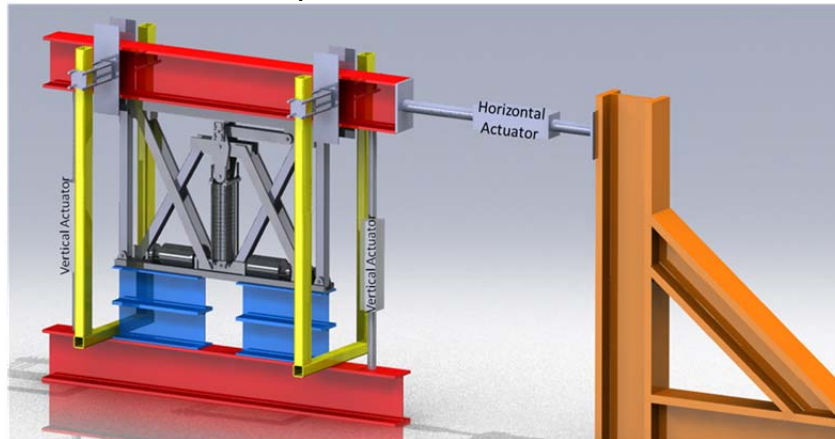
Figure 2.12. Test setup for system identification testing of NSDs

Twenty-five cyclic tests were conducted for each NSD to determine the effect of frequency and amplitude of motion on the behavior of the NSDs. Although the behavior of the two NSDs is nominally the same, to distinguish between the two, they were designated as NSD-South and NSD-North based on their location inside the bridge model. The input motion for the tests was harmonic (four cycles) at three different frequencies (0.01, 0.1 and 0.5 Hz) and amplitudes ranging from 0.38 to 7.62 cm. The undeformed and deformed shape of the NSD during one of the tests is shown in Figure 2.13.
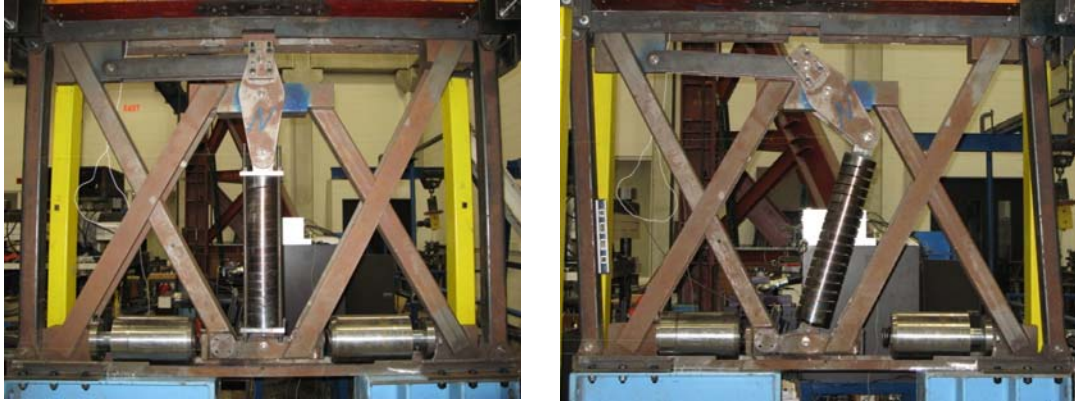
Figure 2.13. Undeformed and deformed shape of the NSD inside load frame at University at Buffalo

The force-displacement relation for three of the experimental tests (NSD-North, ±2.5 in, and 0.01, 0.1 and 0.5 Hz) is shown in Figure 2.14. As can be seen, and as described by Sarlis et al. (2012), due to the masses of different parts of the device, there is some influence of frequency of motion on the device behavior with higher frequencies increasing the negative tangent stiffness. However, as noted by Sarlis et al. (2012), for practical purposes, the frequency-dependencies have a minor effect on the overall seismic response of structures.
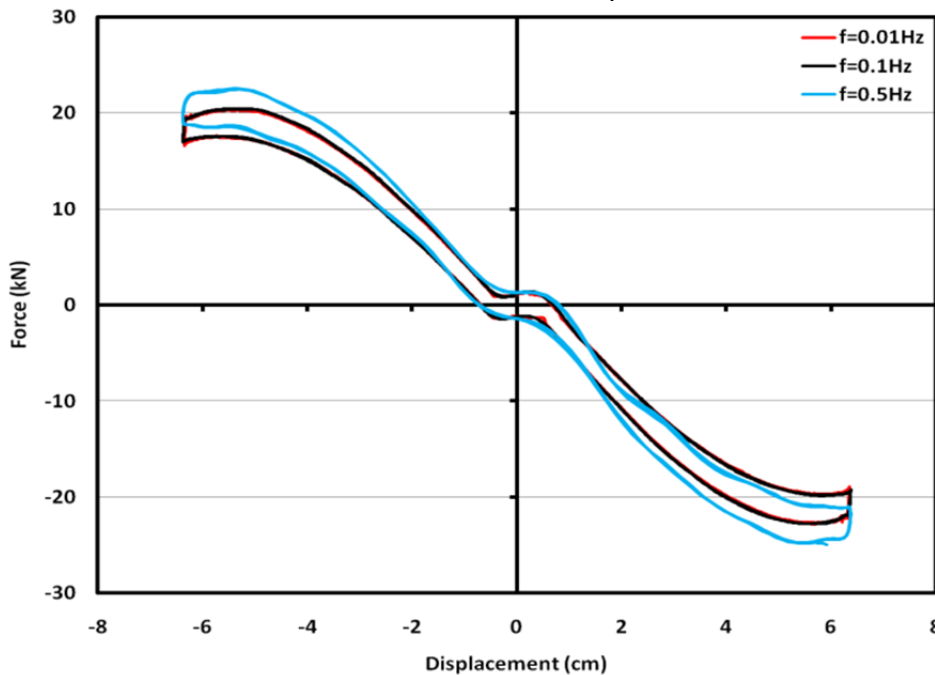
Figure 2.14. Results of experimental tests of the NSD for harmonic tests at different frequencies

A comparison of experimental test data (NSD-South, ±3in, 0.01 Hz) with the analytical model defined by Eqs. 2.1-2.3 is shown in Figure 2.15. The general shape of the analytical curve follows the experimental data with the main discrepancy being the presence of friction in the experimental data. More complex models of the NSDs can be developed to more accurately capture the physical behavior of the device (see Sarlis et al., 2012 for details) but the model defined by Eqs. 2.1-2.3 is deemed sufficient for prediction of the response of the bridge model

employing the NSDs. Furthermore, the two NSDs (North and South) have similar behavior (see Fig. 2.16) and thus the same analytical model is applicable to both devices.
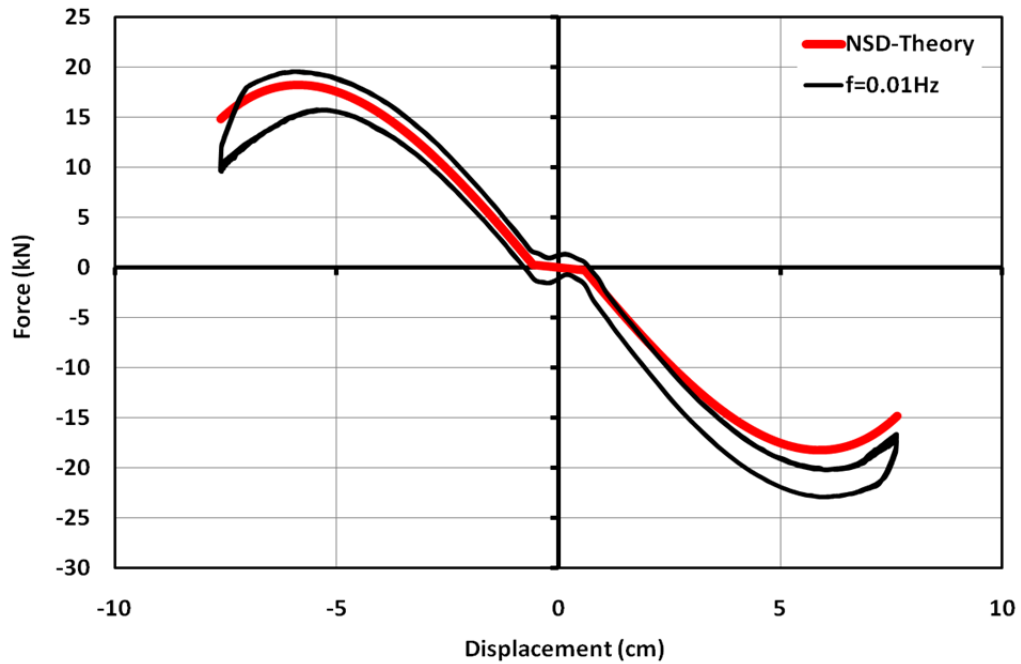
Figure 2.15. Comparison of experimental response and analytical solution (NSD-South, ±7.62 cm (±3 in), 0.01 Hz)
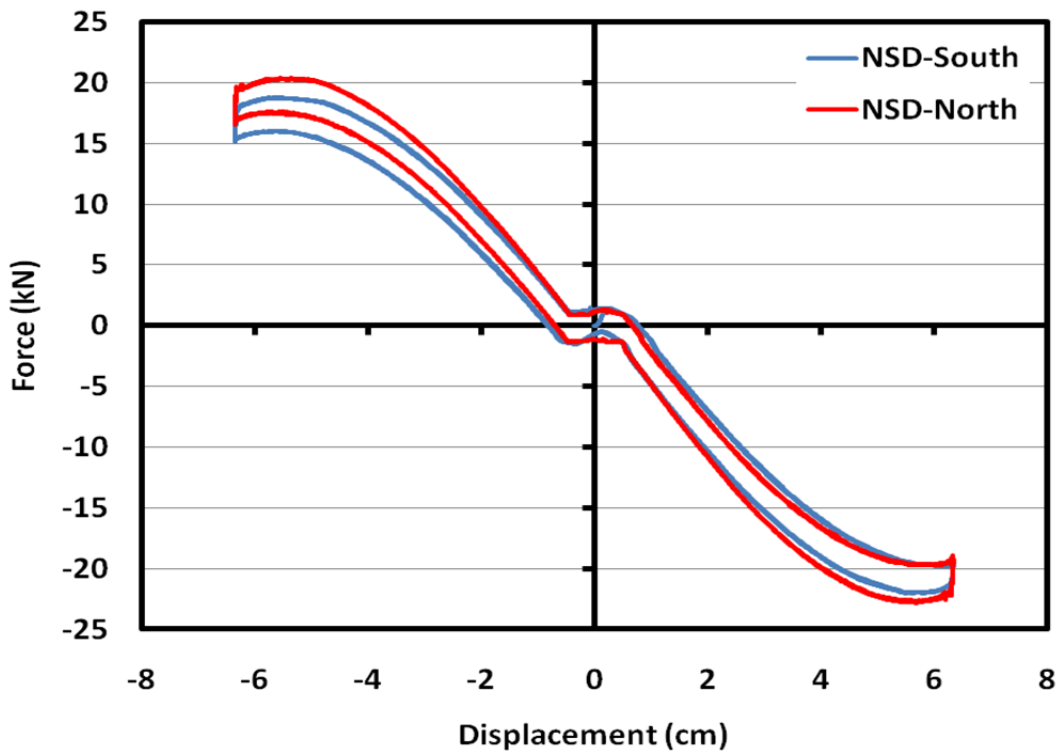
Figure 2.16. Experimental response of NSD-South and NSD-North (±6.35 cm (±2.5 in), 0.01 Hz)

2.5 Numerical modeling of NSDs within bridge model

To develop a numerical model of the NSDs and to aid in understanding their behavior, a 3D finite element model of the device was created in SAP2000 and its behavior assessed using nonlinear analysis, considering P-Delta and large-displacement geometric nonlinearities (see Fig. 2.17). The NSD models were imported into a 3D finite element model of the bridge in SAP2000 (see Fig. 2.18) and placed below the bridge deck. To make the model as realistic as possible, the aforementioned NSD support frames were included in the finite element model.
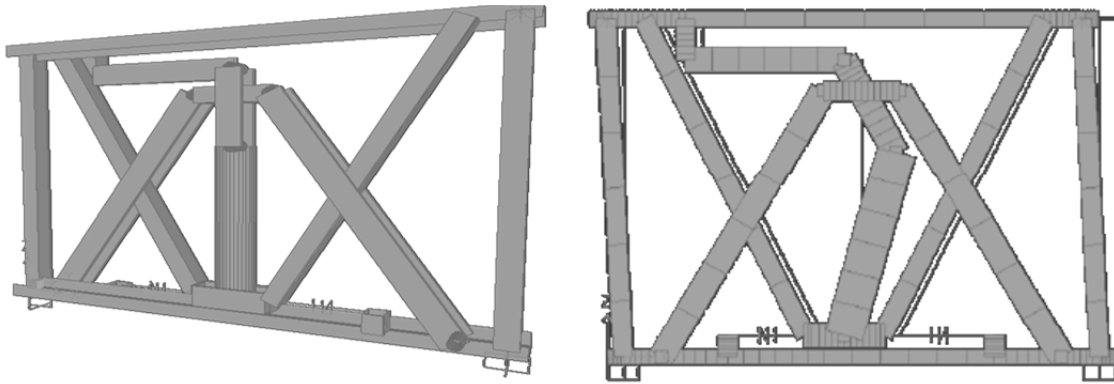
Figure 2.17. Detailed 3D finite element model of NSD and its first mode of vibration
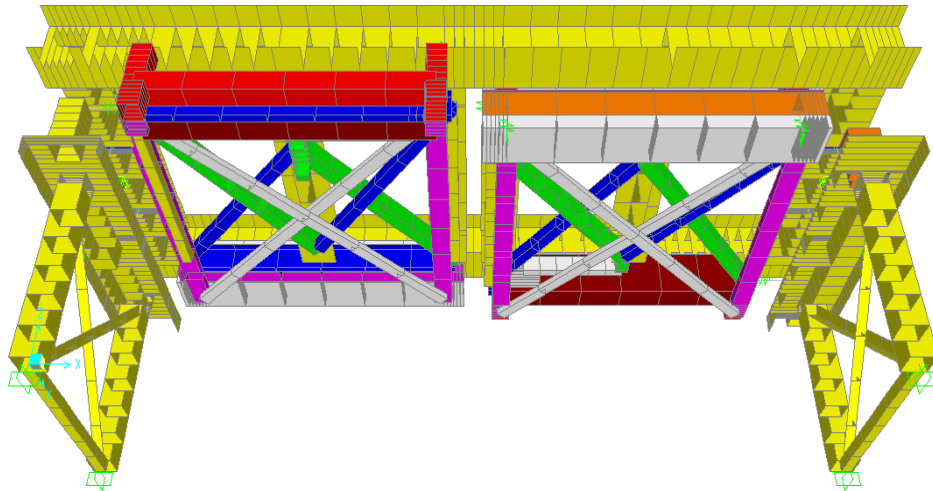
Figure 2.18. Detailed 3D finite element model of bridge structure with two NSDs below bridge deck

Using the detailed finite element models of the NSDs to simulate their behavior in a time history analysis of the bridge is very time consuming since large-displacement geometric nonlinearities need to be considered. To simplify the analysis, the results from the experimental cyclic tests of the NSDs (e.g., see Fig. 2.14) were used to develop an equivalent model consisting of two elements in parallel: a nonlinear elastic element and a friction element. The detailed 3D finite element models of the NSDs were kept in place (without pre-compressed force and with very small stiffness values for the springs) to account for their mass and to monitor their deformations so as to ensure that the NSDs would not collide with each other or the elastomeric bearings during the shake table testing. The behavior of the nonlinear elastic element was

defined by removing the friction from the experimental hysteresis loops from cyclic testing of each of the NSDs. The tests that were utilized corresponded to the maximum displacement amplitude that was used during all tests (±3 in) and a frequency of 0.01 Hz (recognizing that the effects of excitation frequency on the behavior of the device are minor). The friction was removed via a process whereby the average value of the force at each displacement was determined for one cycle of motion. This resulted in a single curve for defining the nonlinear elastic force-displacement relation for each NSD. The removed friction was then accounted for via a friction element where the magnitude of the friction force was taken as constant and equal to the average width of the experimental hysteresis over one cycle of motion. Figure 2.19 depicts this process and provides a comparison of the theoretical curve (defined by Eqs. 2.1-2.3) with the averaged data for NSD-South. The average experimental force-displacement curve for each of the NSDs was then obtained and selected data points (at 0.025 cm displacement increments) were used to model the nonlinear elastic component of behavior. These data points were used to define multi-linear link elements in the finite element model of the bridge.

In order to define the properties of the friction elements, the average width of the hysteresis loops of all of the experimental tests with different amplitudes and frequencies was determined (result was rounded to 4.0 kN) and used to define a plastic Wen link element in SAP2000 for each of the NSDs. The width of the Wen element hysteresis loop is constant but, as can be seen in the NSD experimental hysteresis loops (e.g., see Fig. 2.19), the width of the loop actually changes with displacement. An improved model could be obtained by using a multi-linear plastic element that can account for the displacement-dependency of the width of the hysteresis loop. However, since the displacement-dependency is relatively minor with respect to the overall force-displacement behavior, an average value of the experimental hysteresis loop width was used to define a Wen element and the results were deemed to be accurate enough. For example, a comparison of the hysteresis loops for the combined element (multi-linear link element and Wen element) and the experimental test data for one of the cyclic tests is shown in Figure 2.20. Clearly, there is very good correlation between the predicted hysteresis loop from the nonlinear analytical model of the NSD and that from the experimental testing of the NSD. Similar results are obtained for other frequencies of motion and amplitudes. The Wen element was placed in parallel with the multi-linear link elements. These combined elements were located between the top of the piers and the supporting frame of the NSDs, at the exact location that they would be connected to each other within the bridge model.
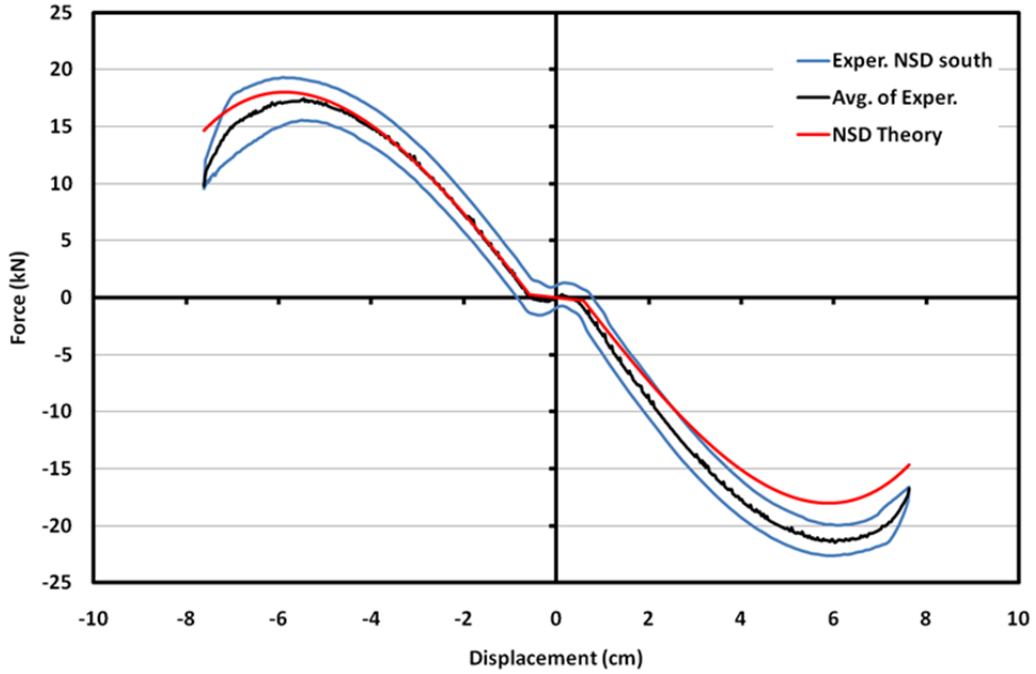
Figure 2.19. Simplification of experimental force-displacement relation by using average force data (NSD-South, ±7.62 cm (±3 in, 0.01Hz)
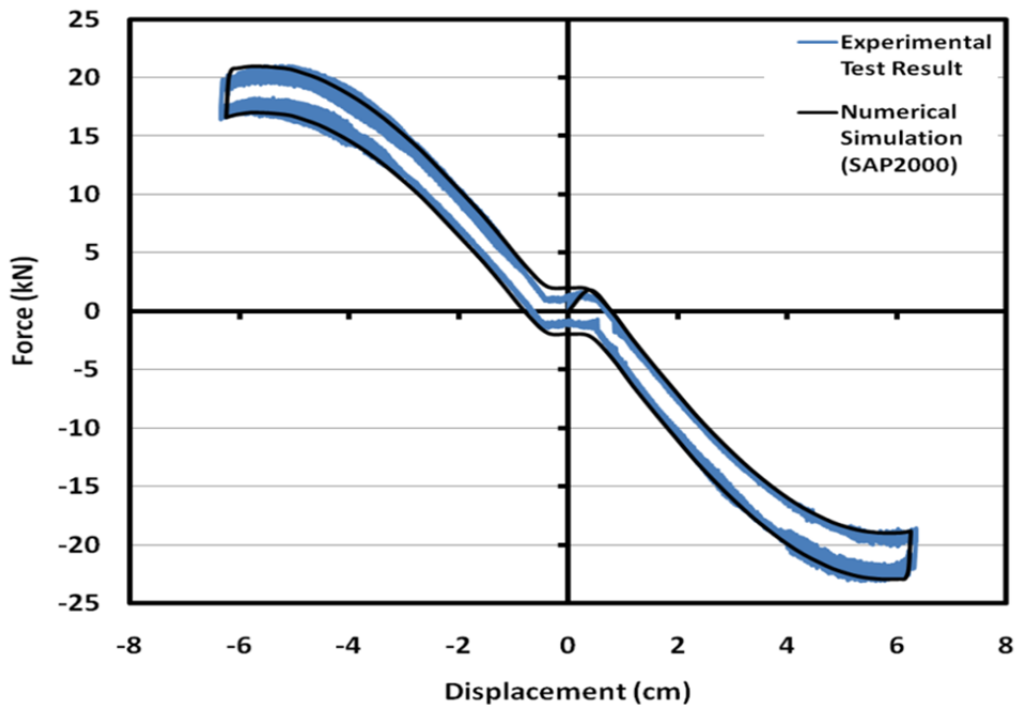
Figure 2.20. Comparison of numerical simulation of NSD hysteretic response and experimental test data (NSD-North, ±6.35 cm (±2.5 in), 0.01 Hz)

Using the average experimental force-displacement curves described above, the properties of the springs (both the main spring and the gap spring assemblies) of the NSDs in the analytical model can be adjusted to improve the ability of the model to predict the NSD behavior. The experimental hysteresis loops are not symmetric with regard to force (e.g., see Fig. 2.19) and thus the two GSAs do not have identical properties. Thus, by modifying the stiffness of the stiff and soft spring within the GSAs, predictions of response from the analytical model can be improved. As an example, Figure 2.21 shows such predicted behavior using a modified version of the analytical model for one of the NSDs (modifications were made via a simple trial-and-error procedure). The nonlinear elastic portion of the response matches very well with the experimental test data.
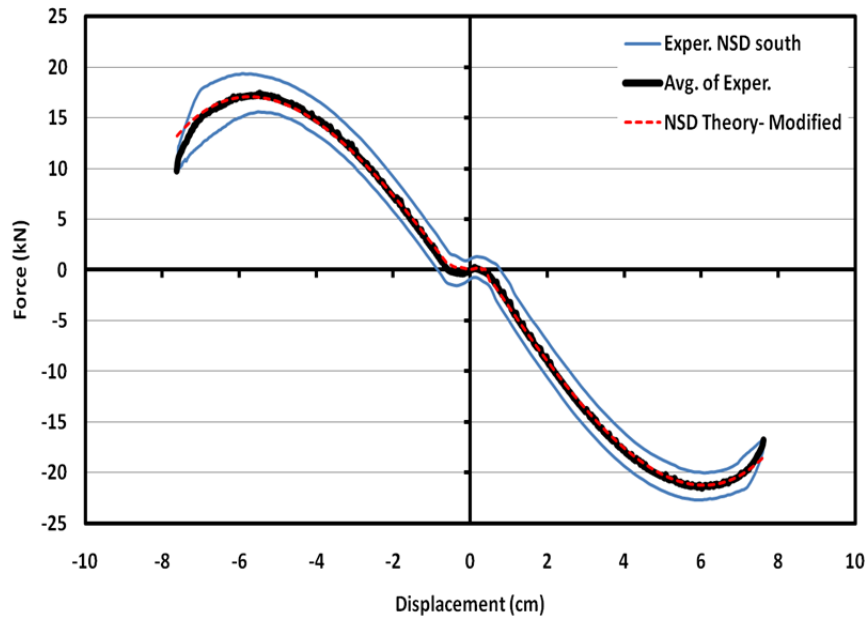
Figure 2.21. Comparison of predicted response (using modified analytical model) and experimental test data (NSD-South, ±7.62 cm (±3 in), 0.01 Hz)

2.6 Numerical predictions of seismic response

Using nonlinear response-history analysis within SAP2000, the detailed 3D finite element model of the bridge test specimen was subjected to seven historical earthquake records (see Table 2.3). These ground motions were selected so as to provide a range of acceleration amplitudes and frequency content (see Fig. 2.22).

Table 2.3. Ground motions used in numerical simulations

No.	Earthquake	Record	Mw
1	Northridge, 1/17/1994	637-270	6.69
2	Loma Prieta, 10/18/1989	CAP-000	6.93
3	Cape Mendocino, 4/25/1992	PET-090	7.01
4	Kobe, 1/16/1995	KJM-000	6.90
5	Northridge, 1/17/1994	Sylmar-000	6.69
6	Landers, 6/28/1992	Yermo-000	7.3
7	Landers, 6/28/1992	Yermo-270	7.3
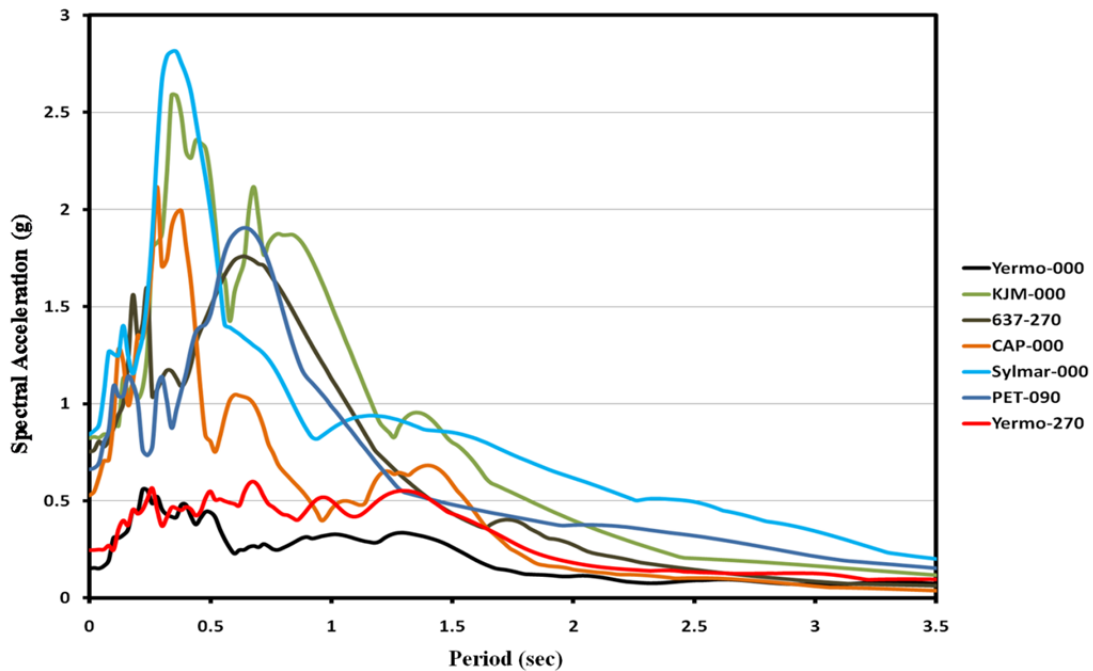
Figure 2.22. Response spectrums for seven ground motions used in numerical simulations (prototype scale)

The simulations were performed for four different bridge configurations: 1) Isolated Bridge (IB), 2) Isolated bridge with NSDs (IB-NSD), 3) Isolated bridge with passive viscous dampers (IB-PD), and 4) Isolated bridge with NSDs and passive viscous dampers (IB-NSD-PD). These simulations were carried out for each of these configurations and for two cases of bridge pier flexibility (one case where the piers are braced at the top and thus are very stiff, mimicking a single-span bridge deck supported on abutments at each end, and the other case where the piers are unbraced and thus are flexible, mimicking an interior span of a multi-span bridge). Using nonlinear response-history analysis, these eight models were subjected to the aforementioned seven ground motions.

Since most damage in bridge superstructures is associated with column failure, shear key failure, or the deck falling off its supports (Chen and Duan, 2003) and the main damage to elastomeric bearings is due to excessive shear strain, the effects of the NSDs on the response of the bridge model are presented in the form of base shear coefficient (peak base shear normalized by weight of bridge model (173 kN)) and peak shear strain of the elastomeric bearings (displacement of bridge deck relative to the top of the piers normalized by total thickness of rubber in each bearing (5.7 cm)).

As shown in Figures 2.23 and 2.25, the NSDs are able to reduce the base shear in the bridge model in comparison with the isolated bridge without the NSDs. Although it is expected that adding NSDs to an isolation system will generally increase the displacements, Figures 2.24 and 2.26 show that in almost all cases the displacements were actually reduced. This was due to the significant damping provided by the devices through friction between its elements. Thus, the NSDs simultaneously provided a reduction in forces and displacements in the system. For the bridge model with flexible piers, in all but one case, adding the passive dampers (PD) in parallel with the NSDs resulted in increased forces and reduced displacements relative to the isolated bridge with NSDs alone. It should be noted that the piers of the bridge model are designed to

22

yield when the bearing shear force exceeds 50% of its axial load (Tsopelas and Constantinou, 1994), which is equivalent to a base shear coefficient of 0.5. As can be seen in Figures 2.23 and 2.25, for some of the cases without NSDs. the base shear coefficient exceeds this value and thus the piers would actually be expected to deform inelastically in these cases (for simplicity, the analysis was conducted under the assumption of elastic behavior of the bridge piers but with the recognition that base shears in excess of about 50% could not actually be achieved due to material inelasticity).
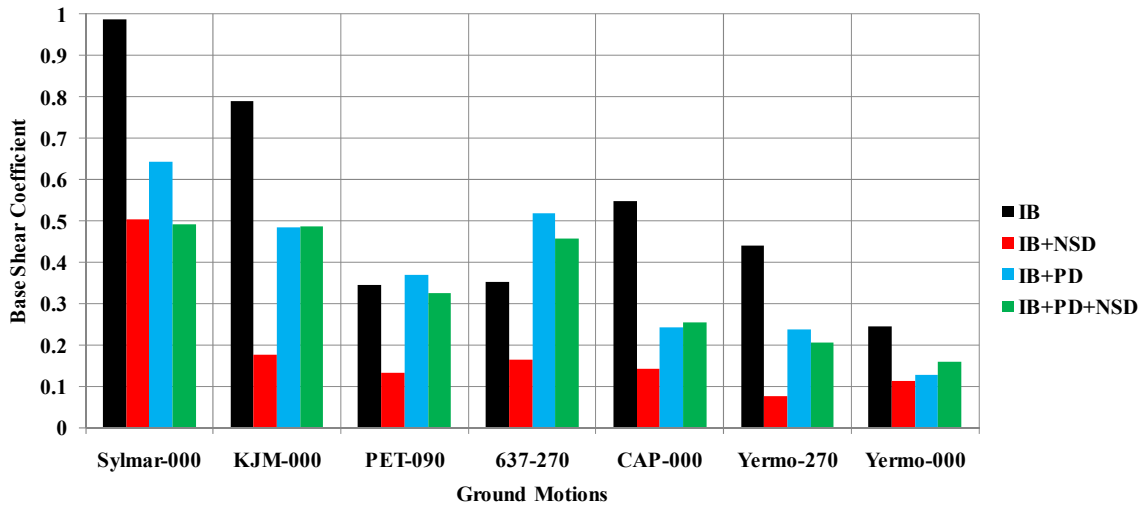
Figure 2.23. Base shear coefficient in bridge model with flexible piers for cases of isolated bridge (IB), isolated bridge with NSDs (IB+NSD), isolated bridge with passive fluid viscous dampers (PD), and isolated bridge with NSDs and PDs (IB+PD+NSD) for different ground motion
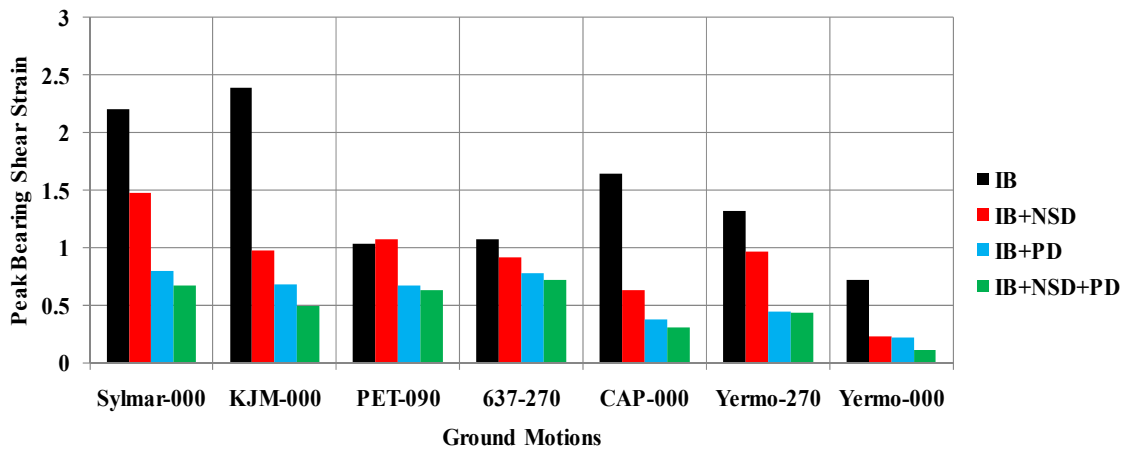
Figure 2.24. Peak bearing shear strain in bridge model with flexible piers for cases of isolated bridge (IB), isolated bridge with NSDs (IB+NSD), isolated bridge with passive fluid viscous dampers (PD), and isolated bridge with NSDs and PDs (IB+PD+NSD) for different ground motion
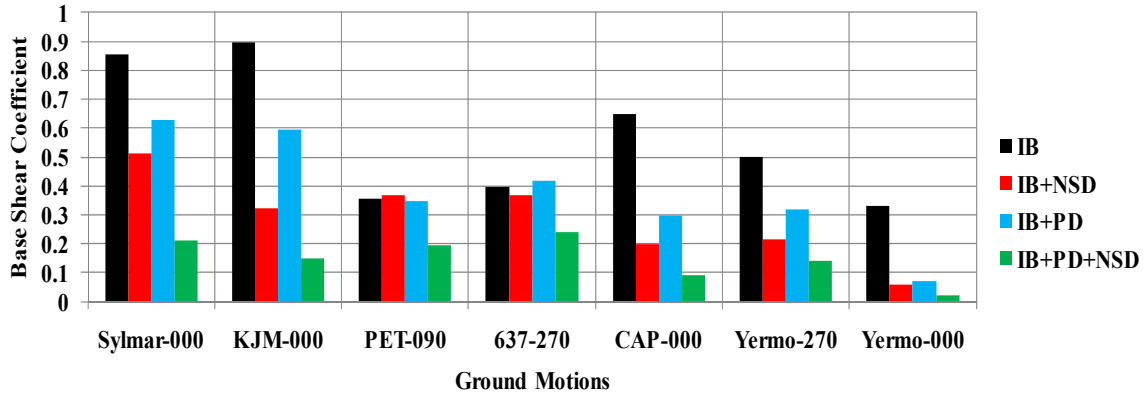
Figure 2.25. Base shear coefficient in bridge model with stiff piers for cases of isolated bridge (IB), isolated bridge with NSDs (IB+NSD), isolated bridge with passive fluid viscous dampers (PD), and isolated bridge with NSDs and PDs (IB+PD+NSD) for different ground motion
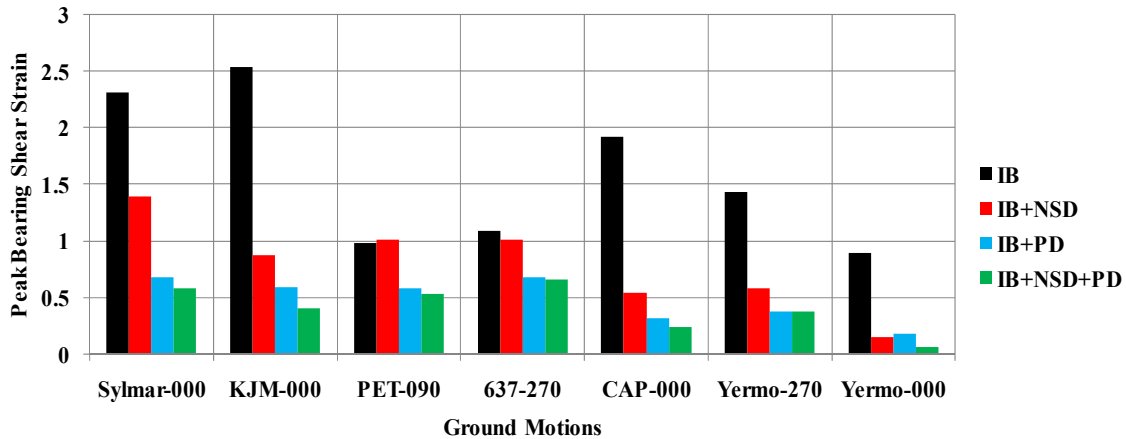
Figure 2.26. Peak bearing shear strain in bridge model with stiff for cases of isolated bridge (IB), isolated bridge with NSDs (IB+NSD), isolated bridge with passive fluid viscous dampers (PD), and isolated bridge with NSDs and PDs (IB+PD+NSD) for different ground motion

To evaluate the performance of the NSDs in the bridge model, the presented results can be compared with other research results and guidelines for seismic performance of isolated bridges. As an example, in the 1990s, researchers from the United States and Japan worked together on a joint project to develop seismic protection systems for bridges for use in areas with strong seismic activity. Their specific goal was to develop a system that could reduce the forces transmitted to the elastic substructure to about one-third of the deck weight, while limiting the bearing deformation to less than 20 cm at prototype scale (Tsopelas et al, 1996). Based on the results presented in Figures 2.23-2.26, this bearing deformation limit (corresponds to a shear strain of 0.88 at model scale) is satisfied for all of the ground motions for the case where NSDs are used in combination with PDs and, furthermore, is satisfied for nearly all the ground motions for the case of NSDs alone.

As shown in Figure 2.27, the NSDs are able to reduce the base shear for both cases of the bridge with braced (stiff) and unbraced (flexible) piers with maximum reductions of about 80% with respect to the case of the isolated bridge without any additional seismic protection device. However, since the effective stiffness of the two cases was different and the properties of the springs of the NSDs were designed to be most effective in the bridge model with flexible piers, it

can be seen in Figure 2.27 that the NSDs were not effective or were minimally effective in reducing the base shear for a few ground motions (PET090 and 637-270) specially for the stiff pier case. As shown in Figure 2.28, similar results are obtained for the bearing shear strain. Figure 2.29 and 2.30 compare the effectiveness of the cases of IB+NSD with IB+PD for the same quantities and, as expected, the NSDs decrease the peak base shear much more than viscous dampers in almost all of the cases. However, they are not as effective as viscous dampers in reducing the deformations of the isolation system.
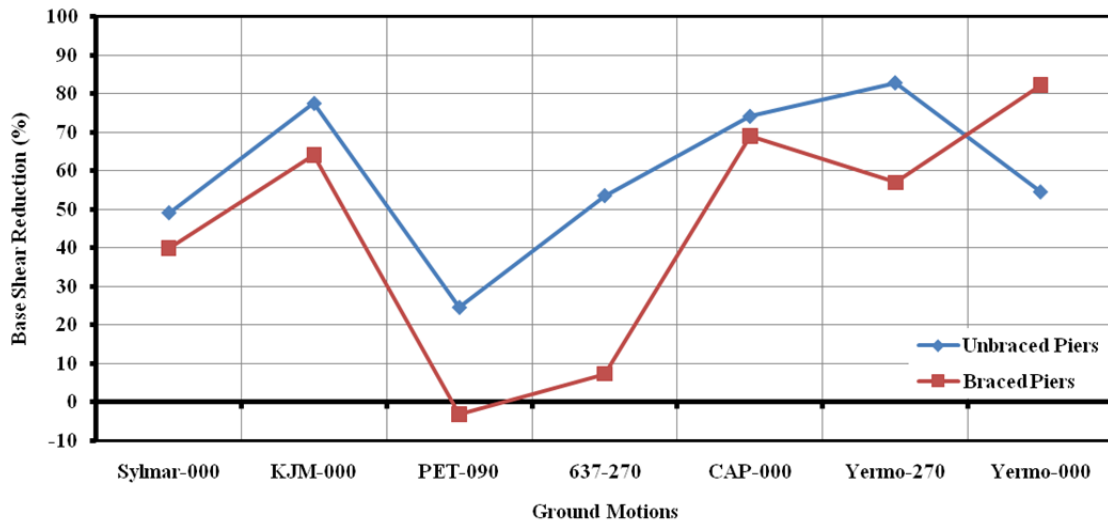
Figure 2.27. Effectiveness of NSDs in reducing base shear (IB+NSD versus IB) for cases of bridge model with braced and unbraced piers
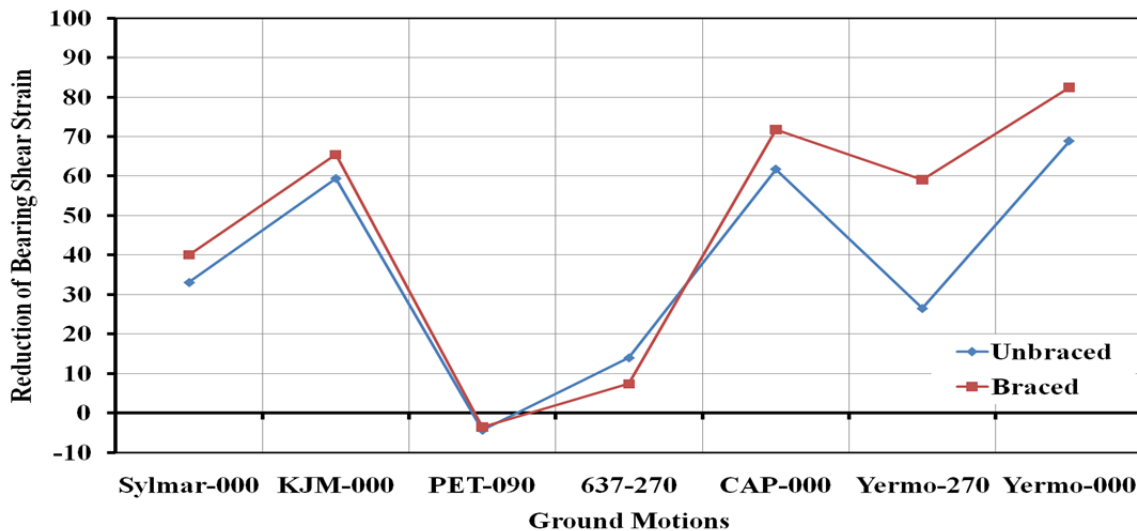
Figure 2.28. Effectiveness of NSDs in reducing bearing shear strain (IB+NSD versus IB) for cases of bridge model with braced and unbraced piers
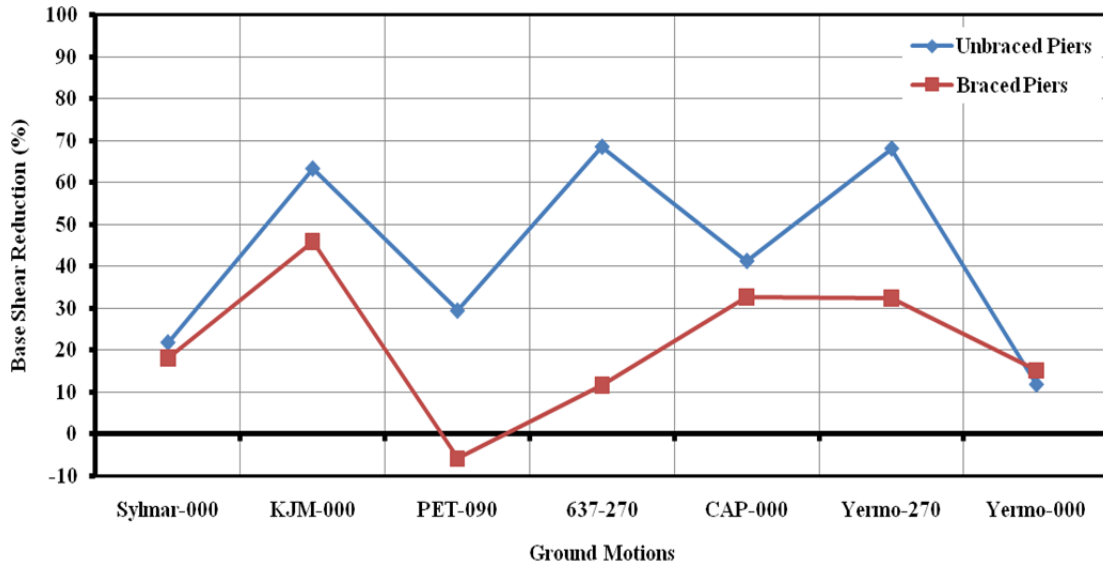
Figure 2.29. Effectiveness of NSDs in reducing base shear (IB+NSD versus IB+PD) for cases of bridge model with braced and unbraced piers
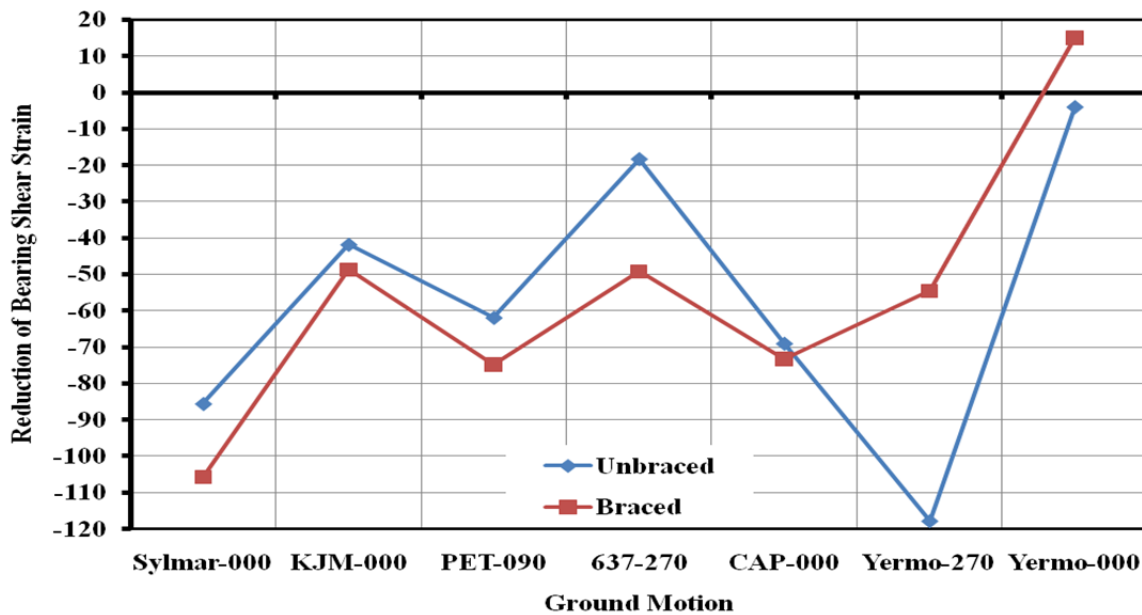
Figure 2.30. Effectiveness of NSDs in reducing bearing shear strain (IB+NSD versus IB+PD) for cases of bridge model with braced and unbraced piers

2.7 Influence of ground motion characteristics on effectiveness of NSDs

The lack of effectiveness of the NSDs in reducing the base shear for two of the ground motions can be explained by examining their acceleration-displacement response spectrums (ADRS). As shown in Figure 2.31, the ADRS curves for the PET-090 and 637-270 ground motions (shown at model scale) are distinctly different from the two other ground motions shown (Sylmar-000 and CAP-000) and thus, depending on which ground motion is considered, the natural period of the

26

structure can have a significant influence on the response. As an example, if we consider a general structure without NSDs and having a natural period of less than 0.25 sec (at model scale) and the effective natural period of the structure with the NSDs is between 0.25 and 0.5 sec. (at model scale), the NSDs would substantially reduce the peak acceleration (and thus base shear) in the case of Sylmar-000 and CAP-000 ground motions but would increase the acceleration for the case of PET-90 and 637-270 ground motions.
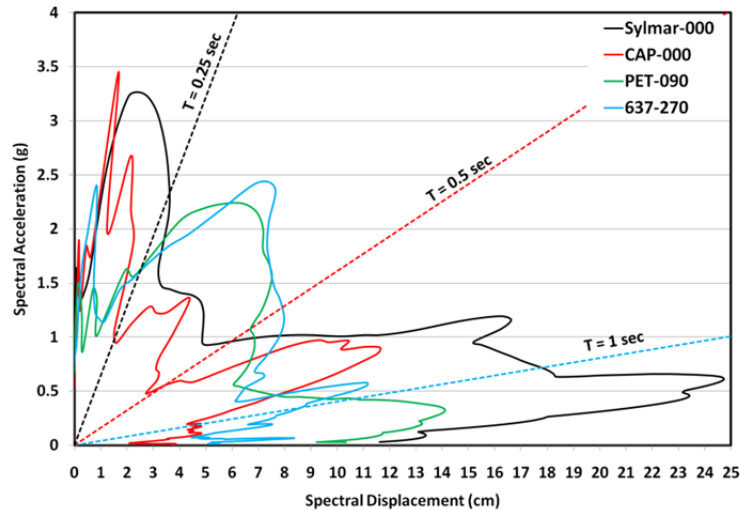
Figure 2.31. Acceleration-displacement response spectrum curves for four ground motions (model scale)

Although a rigorous analysis of the bridge model is complicated due to the presence of both positive and negative stiffness and different types of damping and nonlinearities in the system, a simplified capacity spectrum analysis can be performed to get a general sense for the behavior of the model for different cases. The approach used here is to develop a simplified acceleration-displacement capacity curve for the system (Ray et al., 2013) and use it in conjunction with ADRS curves to predict the bridge response. Using the effective stiffness of the elastomeric bearings, the force-displacement curve for the case of the isolated bridge with braced piers can be obtained. Dividing the force in the force-displacement curve by the mass of the bridge deck results in an approximate acceleration-displacement capacity curve for the bridge model, which can then be overlaid with ADRS curves to estimate the response of the isolated bridge. Using Equations 2.1-2.3, force-displacement curves that define the NSD behavior can be generated and, recognizing that the NSDs act in parallel with the elastomeric bearings, the force-displacement capacity curve for the combined system (i.e., including isolation bearings and NSDs) can be determined. These capacity curves can be overlaid with the ADRS curves to predict the response of the isolated bridge with NSDs.

In Figures 2.32 and 2.33, the process described above is shown for the CAP-000 ground motion and for the PET-090 ground motion, respectively. In these figures, the inherent damping of the bridge model (without NSDs and with braced piers) was taken as 5% based on the properties of the elastomeric bearings (tested by Wolff and Constantinou, 2004). This damping value was used to generate the ADRS curve for predicting the response of the bridge model without the NSDs. For the case of the bridge model with NSDs, since the force-displacement behavior of the NSDs and the combined system is nonlinear, the equivalent viscous damping of the NSDs/bridge system (due to friction) is dependent on the deformation of the isolation system. The damping ratio of the NSDs/bridge system (assuming infinitely rigid piers) at different

deformation levels can be computed using the energy dissipated per cycle by the NSDs (from cyclic tests performed at various displacement amplitudes) and the peak elastic strain energy of the combined NSDs/bridge system (see Fig. 2.34). This process leads to the deformation-dependent damping ratio shown in Figure 2.35. Using the peak deformations of the isolation system for the case of IB + NSD (for PET-090 and with braced piers, the peak deformation is 5.77 cm, and for CAP-000, the corresponding deformation is 3.1 cm; see Figs. 2.24 and 2.26), the damping ratio of the NSDs/bridge system for each of these two cases is estimated as 2% based on Figure 2.35. Thus, an ADRS curve for 7% viscous damping was used for predicting the acceleration response of the bridge model with braced piers.
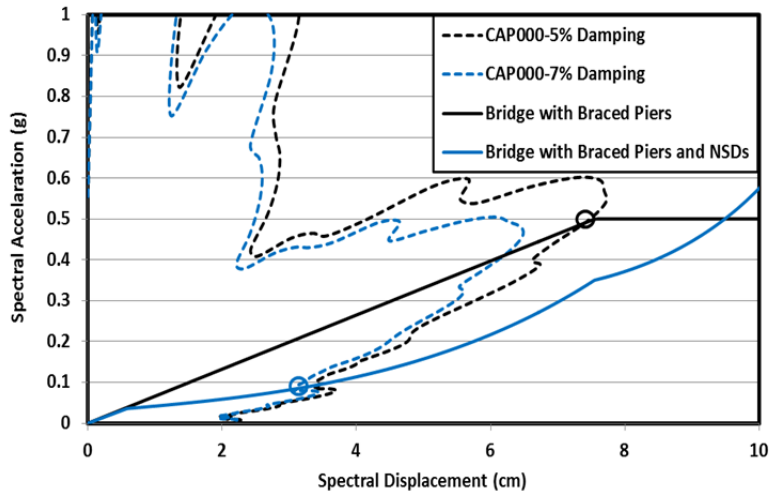
Figure 2.32. Prediction of peak displacement and acceleration demands on bridge subjected to CAP-000 ground motion (model scale); Performance point is shown for two different cases of the bridge model.
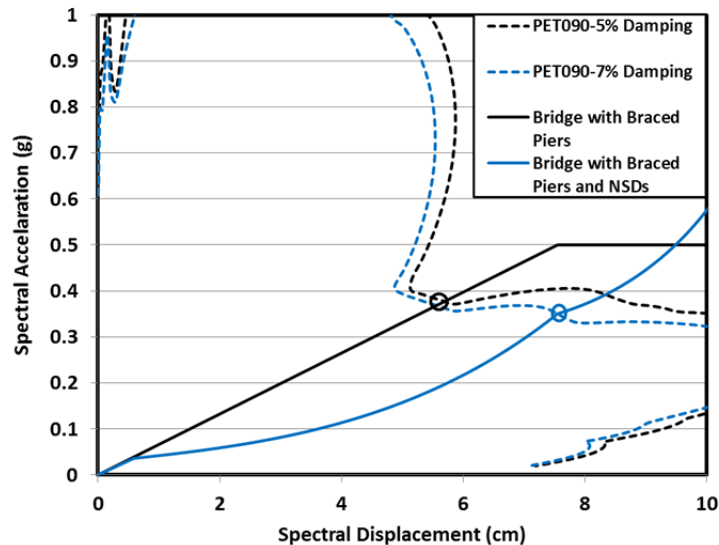
Figure 2.33. Prediction of peak displacement and acceleration demands on bridge subjected to PET-090 ground motion (model scale); Performance point is shown for two different cases of the bridge model.
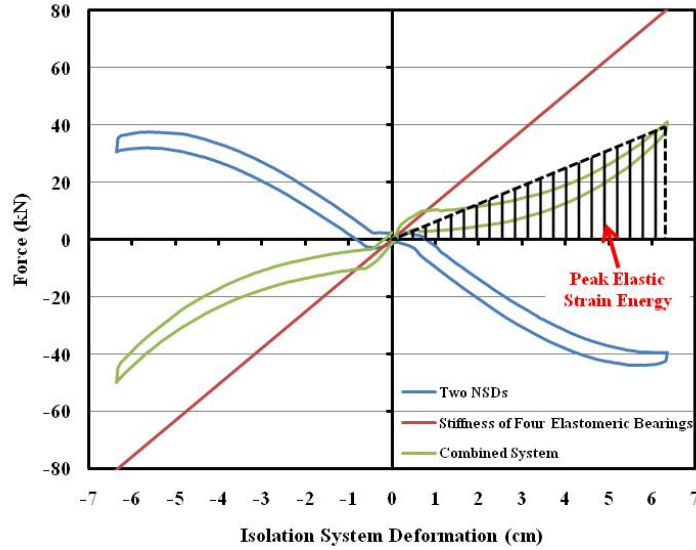
Figure 2.34. Illustration of method for computing peak elastic strain energy for use in obtaining equivalent viscous damping ratio of the NSD/bridge system
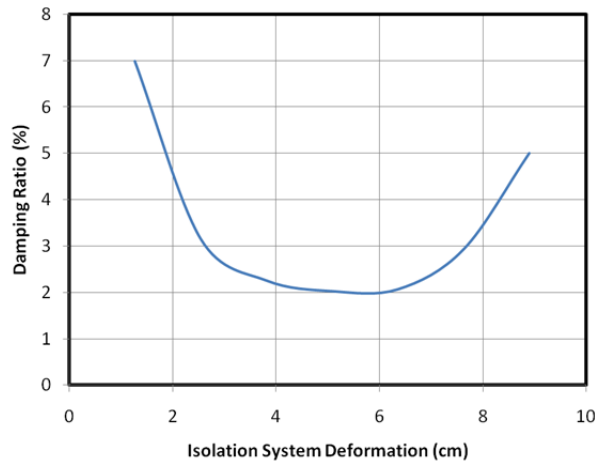
Figure 2.35. Displacement-dependent damping ratio for the IB+NSD case

As shown in Figure 2.32, for the CAP-000 ground motion, adding the NSDs to the bridge model reduces the acceleration and deformation responses of the model for the case of the bridge model with braced piers. In addition, it should be noted that this reduction in force and displacement is mainly caused by the negative stiffness behavior of the device with changes in damping having a minor effect on the response of the system. In contrast, as shown in Figure 2.33, for the PET-090 ground motion, adding the NSDs to the bridge model with braced piers does not result in a significant reduction in acceleration response. The minor effect that the NSDs have on the acceleration (and force) response is due to the shape of the PET-090 ground motion ADRS curve. On the other hand, and for the same reason, from Figure 2.33 it is clear that for this particular ground motion, if a method were used to make the system stiffer, it would have resulted in a large increase of the deck acceleration and base shear of the bridge model. Based on Figure 2.33, to reduce acceleration of the deck, either damping should be added to the system or the NSDs should be redesigned to delay their hardening behavior (i.e., maintain negative stiffness through large deformations).

29

Although a number of approximations are involved in this process of predicting the response of the different configurations of the bridge model, it is useful for explaining why the NSDs are not effective in reducing the base shear in some cases. However, it should be noted that this process is based on a number of assumptions and simplifications (e.g., accounting for friction damping and nonlinear negative stiffness with equivalent viscous damping and assuming that the bridge model with braced piers acts as a single-degree-of-freedom system) and, as a result, the process is not able to properly predict the influence that the ground motion has on the peak displacement response (even though it does predict the influence on the peak acceleration response). Based on what is described here, adding the designed NSDs to the bridge model will not be beneficial for some ground motions based on the shape of the ADRS spectrum (this is also consistent with the results shown in Fig. 2.27 and 2.29 which were obtained from response-history analysis). However, since the behavior of the NSDs is dependent on various parameters which can be readily modified (e.g., by changing the device geometry via alteration of the NSD lever arms and/or by changing the stiffness values for each spring), the device can be designed such that it is most effective for the particular characteristics of the ground motions expected at a site (e.g., based on site-specific ground motion records). In addition, the NSDs can substantially reduce the base shear for most ground motions and thus are generally effective in protecting bridges against earthquakes.

2.8 Summary

In this chapter, the performance of a seismically-isolated bridge structure that incorporates negative stiffness devices was examined via numerical simulations. The numerical simulations demonstrated that the use of NSDs within the isolation system can significantly reduce the peak base shear. In general, it is expected that adding NSDs to a structural system would result in increased peak displacements. However, the friction within the NSDs introduces appreciable damping that results in a reduction of the peak displacements of the system. To decrease the displacements further, passive dampers can be added in parallel with the NSDs. The addition of passive dampers will decrease the displacements further but will generally increase the base shear, although the base shear will still generally be less than the case in which the bridge only employs isolation bearings, thus providing good overall performance with regard to both forces and displacements. Furthermore, this study has demonstrated that NSDs are effective in cases where the isolation system that incorporates the NSDs is reacting against a flexible layer (i.e., the bridge piers) and deforming based on the relative deformation between two degrees of freedom rather than being directly connected to the foundation of the structure (as was the case for the previous two phases of experimental testing by others of the NSDs within three-story buildings). It is also shown that the NSDs are not effective in reducing the force for some ground motions due to the unique characteristics of the ground motions. The performance of all passive seismic protection systems which change the stiffness of a structure during an earthquake depends on the unique characteristics of each ground motion and it is possible that these systems will be ineffective for some particular ground motions due to the shape of their ADRS curves. However, it is known that, in general, the base shear force in soft structures is smaller in comparison with stiff structures. Therefore, in a majority of earthquakes, the NSDs would be effective in reducing base shear and deck acceleration of bridges. In addition, to optimize its effectiveness, the design of the device can be tuned in accordance with the types of ground motions expected at the site.

SECTION 3. EXPERIMENTAL SHAKE TABLE TESTING OF AN ADAPTIVE PASSIVE NEGATIVE STIFFNESS DEVICE WITHIN A HIGHWAY BRIDGE MODEL

3.1 Introduction

Bridge structures are one of the most important structures in the built environment, often serving as critical lifelines and thus requiring protection against natural hazards such as earthquakes. A variety of seismic protection devices, which are either passive, active or semi-active, have been developed by researchers around the world, all seeking to produce the optimal response of bridge structures during strong earthquakes. One commonly used passive device for seismic protection of bridges is viscous dampers. However, it has been shown that in some cases, especially in cases where the ground motion exhibits strong velocity pulses (e.g., Nagarajaiah et al., 1993), these devices may have reduced effectiveness (and sometimes can degrade performance). In general, viscous dampers are effective in reducing the displacement of the bridge deck but may not reduce the shear force in the piers and the acceleration of the bridge deck. In addition to passive devices, many active and semi-active devices have been developed and implemented in bridges to modify the damping and/or stiffness of the structure in real-time based on the response of the structure during an earthquake. As an example, Sahasrabudhe and Nagarajaiah (2005a and 2005b) used magneto-rheological (MR) dampers and variable stiffness systems in semi-active control of sliding isolated bridges. In 2003, Iemura and Pradono proposed application of pseudo-negative stiffness control in seismic protection of bridges to simultaneously reduce base shear and the deck displacements. In his simulations, negative stiffness was produced through a variable hydraulic damping device whose mechanical properties could be controlled externally, creating a force in phase with the bridge deck inertia force and thereby producing negative stiffness behavior. However, since the device required external power and feedback control signals, it generated "pseudo-negative" stiffness rather than true negative stiffness.

Recently, first prototype of a seismic protection device which utilizes the concept of negative stiffness to significantly reduce the response of structures has been developed. The developed Negative Stiffness Device (NSD) is a completely mechanical device that exhibits "true" negative stiffness behavior using a pre-compressed spring (as contrasted with other similar devices that employ pseudo-negative stiffness; e.g., see Iemura and Pradono, 2003 and Iemura et al., 2006). The device is considered to be an "adaptive passive" device since the force produced by the device is displacement-dependent with distinctive behavior at certain displacement levels. By engaging the NSDs at certain displacements and using its negative stiffness to create softening behavior, the combined behavior of the primary structure (having positive stiffness) and the NSDs is one in which there is a virtual yield point. By creating such a virtual yield point at a small force level, the device produces a force reduction in the combined structure-NSD system while potentially allowing for an increase in displacements. The apparent inelastic response may be regarded as "apparent yielding" in that the framing of the primary structural system does not actually yield. Further, any increase in displacements can be controlled by implementing a damper in parallel with the NSD (Nagarajaiah et al., 2010 and Reinhorn et al., 2009). As part of a NEES (Network for Earthquake Engineering Simulation) research project, the effects of such devices on the seismic responses of two different 1/3-scaled three-story building models (one, a base-isolated structure with linear elastic behavior and the other, a fixed-

base structure with inelastic behavior) have been evaluated via shaking table tests (Sarlis et al, 2011 & 2012 and Pasala et al, 2011, 2013a & 2013b). In the final stage of the project, the NSDs were modified and implemented within the isolation system of a quarter-scale bridge model (see Fig. 3.1) and tested on a shake table at the University at Buffalo NEES Laboratory (UB-NEES) (Attary et al., 2012a, 2012b, 2013).
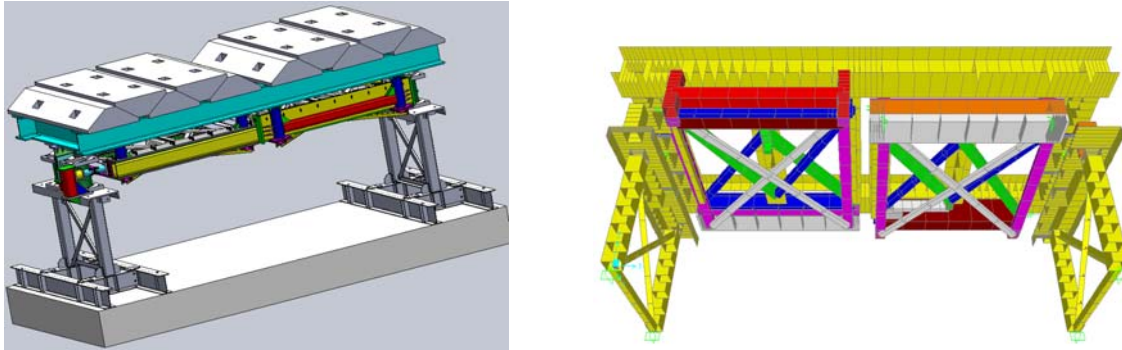
Figure 3.1. (Left) Solid model and (Right) finite element model of bridge structure with NSDs

The bridge model was tested on the shake table for four different bridge configurations: 1) Isolated Bridge (IB), 2) Isolated bridge with NSDs (IB+NSD), 3) Isolated bridge with passive viscous dampers (IB+PD), and 4) Isolated bridge with NSDs and passive viscous dampers (IB+NSD+PD). Each of these configurations was tested for the case of flexible piers (mimicking the middle span of a multi-span bridge) and the case of fixed piers (mimicking a single span bridge supported on abutments) and with ground motions of varying intensity. The results from the shake table tests are presented herein and compared with numerical simulations.

3.2 Description of negative stiffness device

As noted previously, the general behavior of the NSDs has been presented by Sarlis et al. (2012); however, the NSDs were redesigned to optimize their effect on the aforementioned bridge model. The main part of the device is a pre-compressed primary spring, which can rotate and apply a force that is in phase with the motion of the structure, thus creating true negative stiffness (see Fig. 3.2). As described above, in order to exhibit a virtual yield point, the NSDs are designed to have no effect on the structure until a specified displacement is exceeded (the effect of the primary spring is canceled out by so-called gap-spring assemblies (GSAs) up to the specified displacement, beyond which the device produces negative stiffness). In order to optimize the behavior of the device for the bridge model testing, the GSAs were redesigned such that the negative stiffness is engaged after 0.2 in. of displacement.

For the redesigned NSDs, cyclic tests were performed to verify their force-displacement behavior and to calibrate the numerical models to be used within the numerical simulations of the isolated bridge model (as discussed in previous chapter). The NSDs were tested within a load frame at the UB-SEESL laboratory wherein they were anchored at the bottom and allowed to displace laterally at the top. A hydraulic actuator was attached at the top of the NSD and was used to impose harmonic motions. A range of tests with different amplitudes and frequencies were performed (0.01, 0.1 and 0.5Hz; 0.38-7.62 cm amplitude) (see Fig. 3.3).
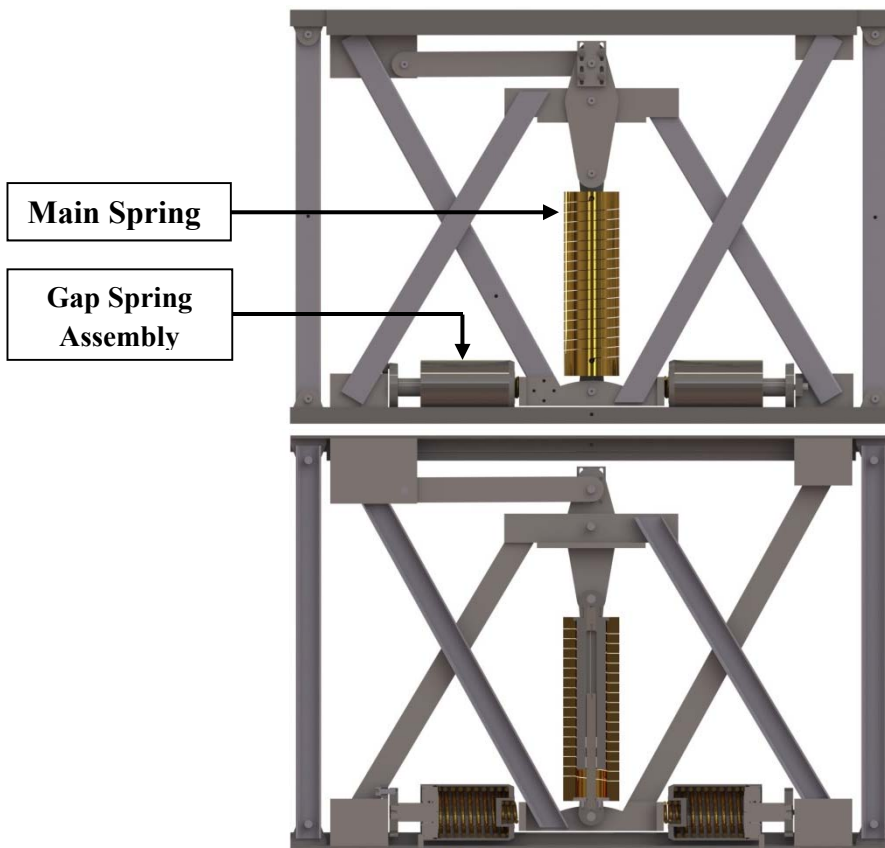
Figure 3.2. Prototype negative stiffness device: Elevation view (top) and cross-section view showing inside of spring assemblies (bottom)
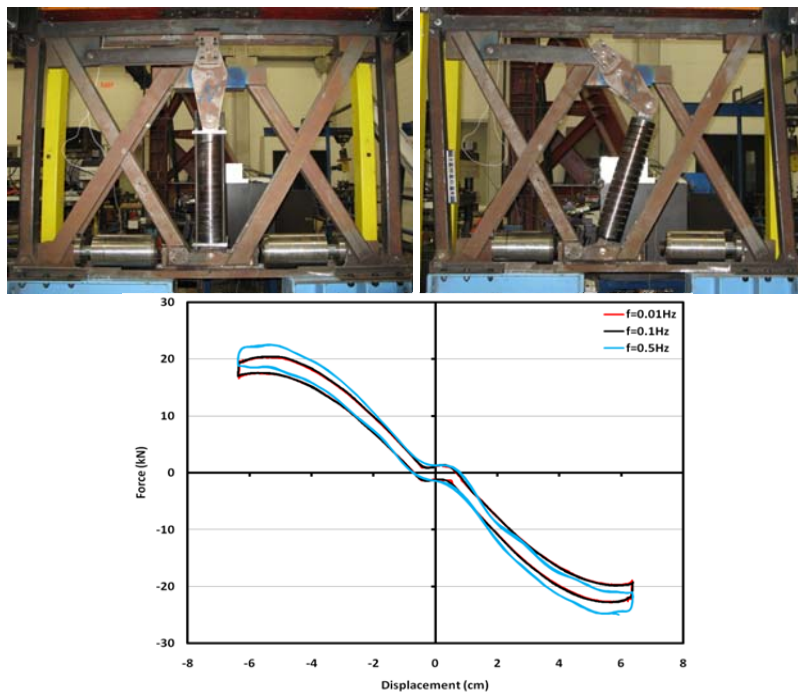
Figure 3.3. Undeformed (Top left) and deformed (Top Right) shape of the NSD inside load frame at University at Buffalo and an example of its hysteresis loops for harmonic tests (Bottom)

3.3 Description of highway bridge model

A quarter-scale highway steel bridge model was tested on the concrete shake table at the University at Buffalo. The single-span bridge model had a rigid deck and two piers, which could be flexible or rigid (using four removable diagonal braces) (see Fig. 3.4). The bridge has a clear span of 4.8 m, a height of 2.7 m, and two custom-designed NSD support frames attached below the 5.4 m long bridge deck. The deck of the bridge is supported on a seismic isolation system consisting of four elastomeric bearings and includes NSDs and/or viscous dampers within the isolation system (see Fig. 3.5).
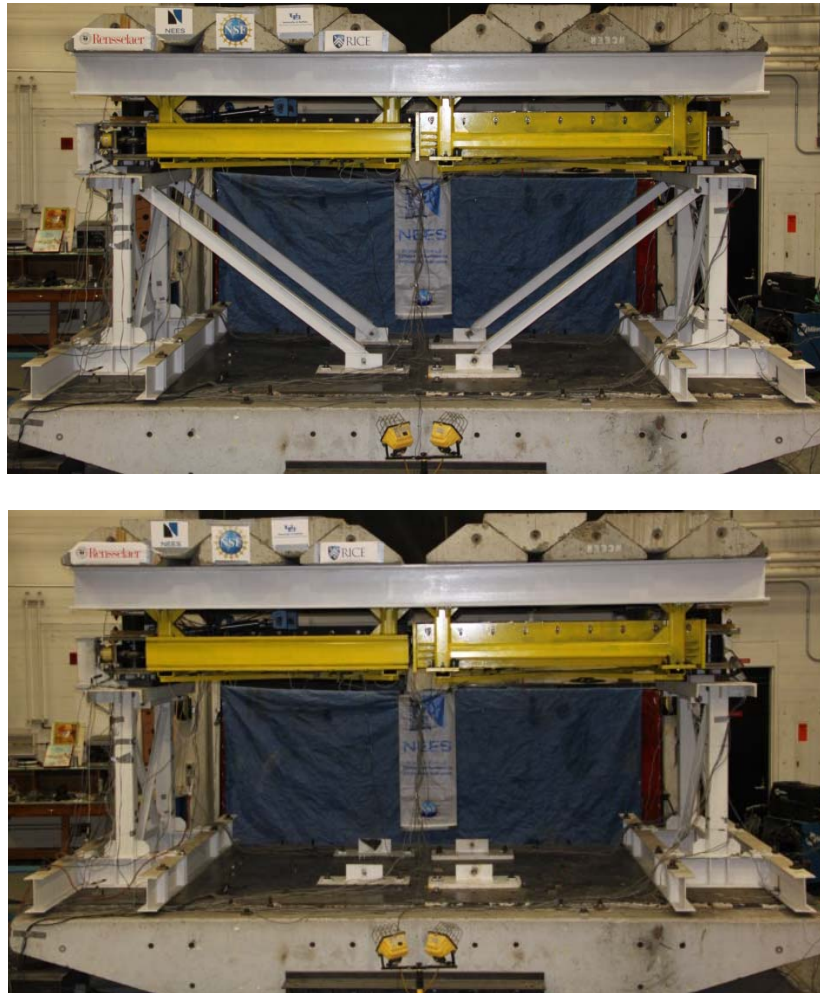
Figure 3.4. Bridge model on the shake table with (top) and without (bottom) diagonal braces
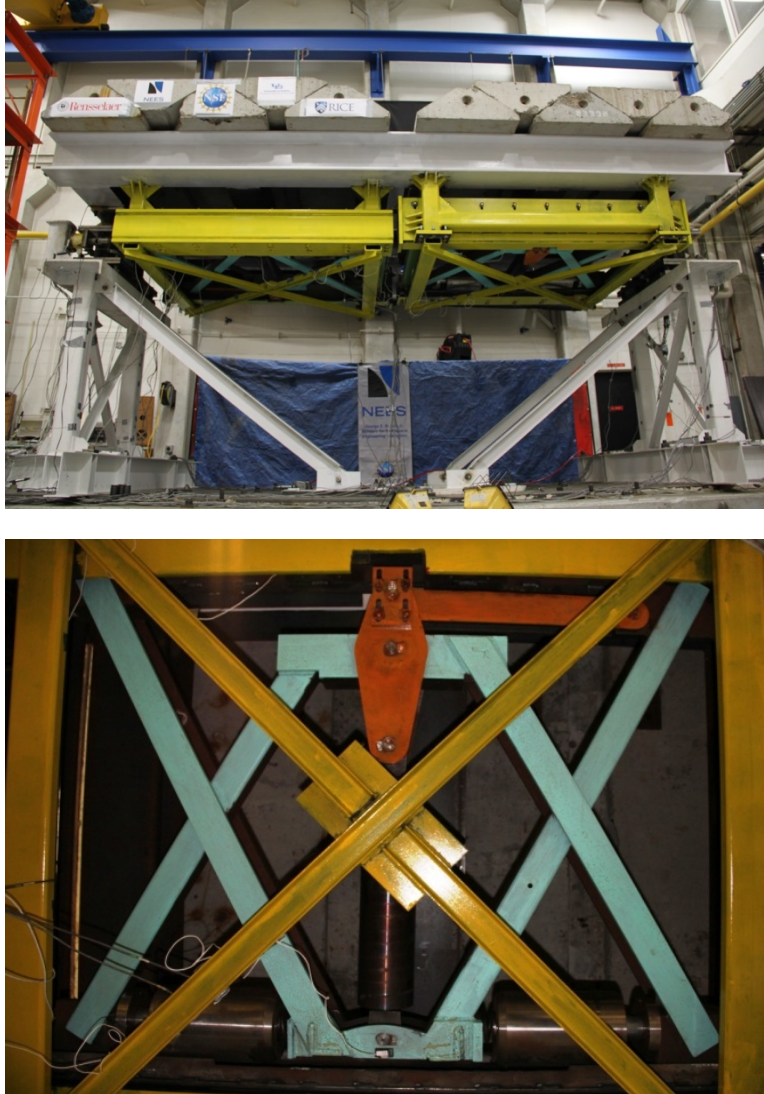
Figure 3.5. Two NSDs within support frames located under bridge deck (top) and close-up view of one of the NSDs as viewed from under the bridge deck (bottom)

Each pier (previously tested by Tsopelas and Constantinou, 1994) consists of two columns (TS6x6x5/16), a pier cap (C18x58), and two lateral braces (L2.5x2.5x1/4). The bottom of the tube columns are connected to beams which are in turn bolted to the shake table. The piers are detailed to yield under the combined effects of a vertical load of 40 kN for each column with 20 kN horizontal loads applied at each bearing location. The stiffness of each pier along the longitudinal direction of the model is increased to a large value by adding two diagonal braces (WT4x5) between the top of the piers and the shake table. The shear force within the piers is measured via 16 strain gauges (4 on each column, 2 at the top and 2 at the bottom, wired together so as to effectively form a load cell). After placing the piers on the shake table and attaching the strain gauges, calibration of the strain gauges was performed by pulling the two piers toward each other using a chain ratchet and a calibrated tension loadcell in the middle of the chain.

The bridge deck consists of two W12x96 sections as the main longitudinal beams and two W12x96 sections as transverse beams at the two ends of the deck and four W10x88 cross

beams within the span. Two supporting systems for carrying the NSDs are connected to the bottom of the deck. These two NSD support assemblies, which are 2.28 m x 2.00 m x 1.25 m, were custom built to support the weight of the NSDs while incorporating a special railing system to allow sliding of the NSDs on the side that was attached to the top of the bridge piers. Since the deformation of the device during motion was based on the shear deformation of its frame, the width of the frame decreases during seismic testing and thus the side of the device which nominally is rigidly attached to the deck, is actually located within a fitted adjustable cap containing roller plates on all contact surfaces, allowing the necessary change in width and transferring the NSD force to the deck. To allow for removal of the NSDs during testing (for possible damage inspection or design modification), special attention was given to making all parts of the assembly removable and adjustable (see Fig. 3.6). The total weight of the deck, including the two NSD support systems and the NSDs themselves, was measured via a load cell attached to the laboratory crane (total weight = 68.9 kN).
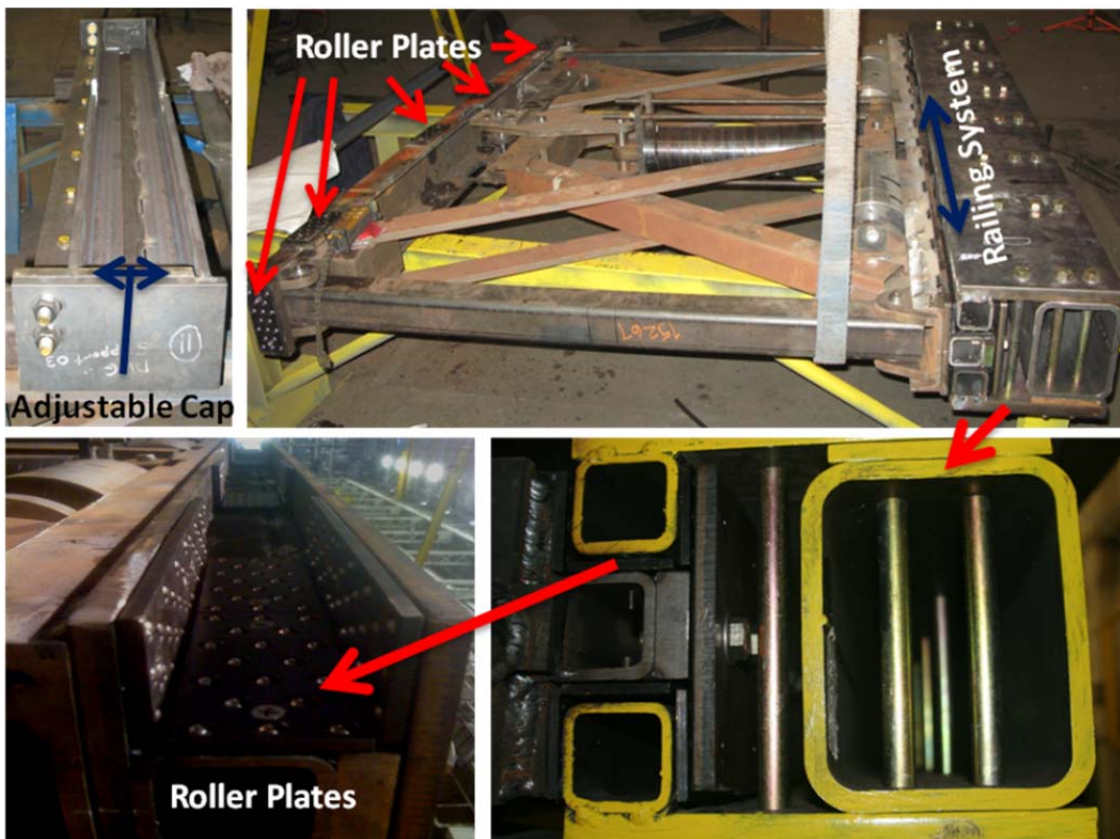
Figure 3.6. Details of the custom-designed NSD support system with special railing system (Top Right: Modified NSD for implementation in bridge model; Railing system installed on one end and multiple roller plates attached to other end. Top Left: Cap that is placed over end of NSD with roller plates; Cap is adjustable to ensure that NSD attachment to deck is as rigid as possible while allowing for shearing deformation. Bottom Right: Close-up view of railing system (yellow painted pieces move with the deck while unpainted pieces move with the piers). Bottom Left: Roller plates inside railing system allow square tubes to freely translate along their length)

To achieve a suitable seismic weight, ten concrete blocks, with an average weight of 8.9 kN each, were placed on the top of the bridge deck and bolted to each other and the cross beams of the deck, resulting in the total weight of the bridge deck being 157.9 kN (see Fig. 3.7).
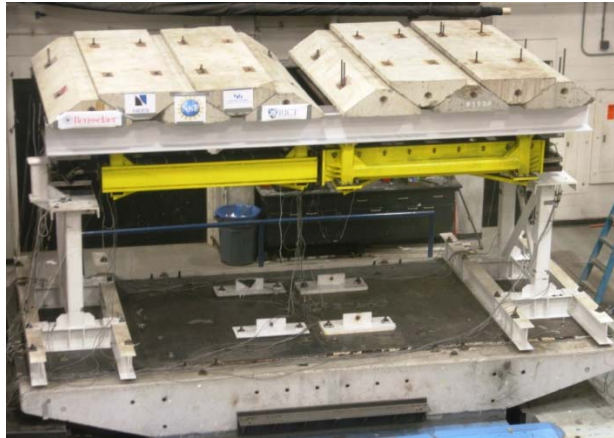
Figure 3.7. Concrete blocks attached to top of bridge deck

The deck of the bridge was seismically-isolated from the bridge piers via four elastomeric bearings. The bearings were supported on four loadcells which provide measurements of shear forces at the isolation level. Each of the loadcells was attached to the top of the piers using a system of threaded rods and leveling nuts (see Fig. 3.8) so that the height of each of the loadcell-elastomeric bearing assemblies is adjustable, resulting in bearings that were level and thus a level bridge deck. The elastomeric bearings, which were used within the isolation system, were low damping bearings that primarily provide a linear restoring force (combined stiffness of four bearings is 12.1 kN/cm).

Figure 3.8. Elastomeric bearings supported on load cells (Left) and close-up view showing bolt/nut leveling system (Right)

The NSDs were not designed specifically for implementation in the bridge model (they were longer and wider than desired) but, due to restrictions on fabricating another set of NSDs and shake table schedule constraints, their length was accommodated by moving the elastomeric bearings (and loadcells located under the bearings) in a transverse direction toward the centerline of the deck, allowing each NSD to react against a reaction block at one end of the bridge pier (see Fig. 3.9a) and to displace into the region between the top of the pier and bottom of the deck at both ends of the pier. The NSDs were attached to the reaction blocks via universal joints, preventing lock-up between the deck and piers in the transverse direction through the NSDs and

their support assemblies. A five degree-of-freedom loadcell was also placed in line with each of the universal joints, to directly measure the force developed by the NSDs (see Fig. 3.9b). Since each NSD was connected to only one side of their respective bridge piers, the forces applied to the bridge deck from the pair of NSDs act on opposite sides of the bridge deck. Thus, the bridge deck is prone to torsion (especially since the elastomeric bearings were moved transversely toward the center of the deck). To minimize any torsional response, two custom-built torsion restraint systems (guide and guide plate) were employed at the middle of each pier cap (see Fig. 3.10). The torsional restraint system included a thick guide plate, with roller bearing sheets on each side of the plate, attached to the underside of the deck. The motion of the guide plate was constrained by a guide consisting of two thick plates attached to the top of the pier cap. To maintain a constant mass for all of the test configurations, the NSDs were disengaged for tests in which NSDs were not utilized. Disengagement was accomplished by removing the loadcells that connected the NSDs to the reaction blocks at the top of the pier caps (see Fig. 3.9c) and holding the main pre-compressed spring in place using threaded restraining rods. The ideal situation for testing the NSDs within the bridge model would have been to fabricate four smaller NSDs (less pre-compression force in each one) and to place them in a manner that essentially eliminates the possibility of torsion (two NSDs attached to each pier, thus applying symmetric forces to the pier caps, with the other end of the two NSDs attached to the middle of the deck, thus applying symmetric forces to the deck).

(a)

(b)

(c)
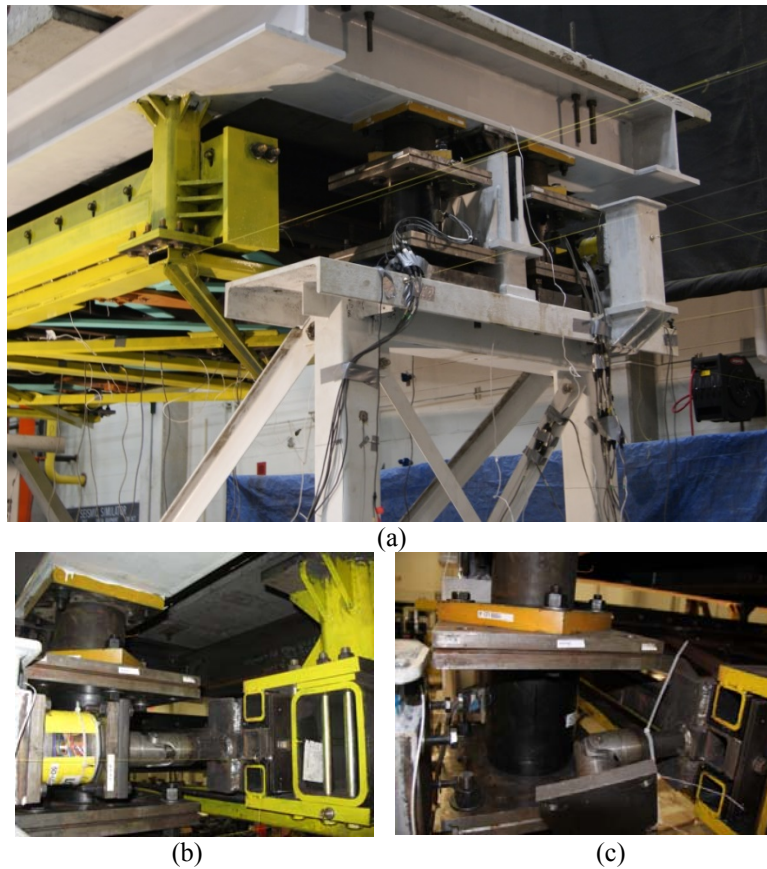
Figure 3.9. Connection of NSDs to top of bridge pier: (a) Reaction block attached to bridge pier cap; (b) universal joint and loadcell attached between reaction block and NSD; and (c) disengagement of NSDs through removal of loadcell and rotation of universal joint
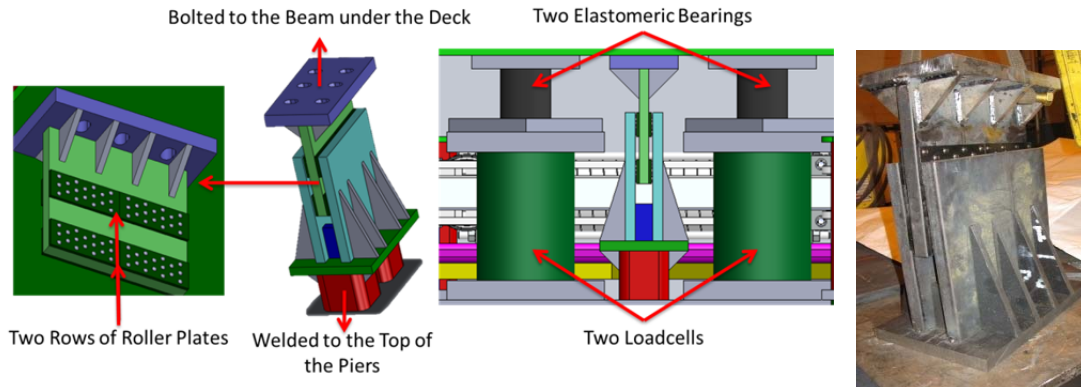
Figure 3.10. Details of torsional restraint system

In some of the tests, two linear viscous fluid dampers (see Fig. 3.11) were installed at the isolation level in parallel with the elastomeric bearings and in line with the longitudinal direction of the bridge deck, and in line with the primary direction of deck motion. The dampers were inclined in elevation by approximately 10 degrees (thus slightly reducing their effectiveness for reducing the deck motion). Each damper had a 1.0-m installed length, a stroke of +/- 6.35 cm, and a damping coefficient of 66.4 kN-s/m.

Figure 3.11. Two viscous dampers installed as part of isolation system

3.4 Measurement sensors

A variety of measurement sensors were attached to the bridge test specimen for monitoring its response during the shaking table tests. Forces were measured using four load cells (five degrees-of-freedom) located directly below the elastomeric bearings (for measuring the forces and moments that develop in the elastomeric bearings), two load cells (five degrees-of-freedom) between the bridge pier cap and the NSDs (for measuring the forces developed by the NSDs), and two load cells (uniaxial) between the bridge pier cap and dampers (for measuring the axial force in the dampers). In addition, the shear force in the columns of the piers was obtained via

eight strain gauges attached to each of the piers. The longitudinal, transverse and vertical acceleration at different locations within the model were obtained from 29 accelerometers. Absolute displacements and relative displacements were measured using 40 string potentiometers (for absolute displacement, a large steel frame attached to the laboratory strong floor was used as an inertial reference frame). The location of most of the measurement sensors is shown in Figure 3.12. All of the sensors were calibrated and tested to ensure proper operation before placing on the specimen.

View from West

View from South
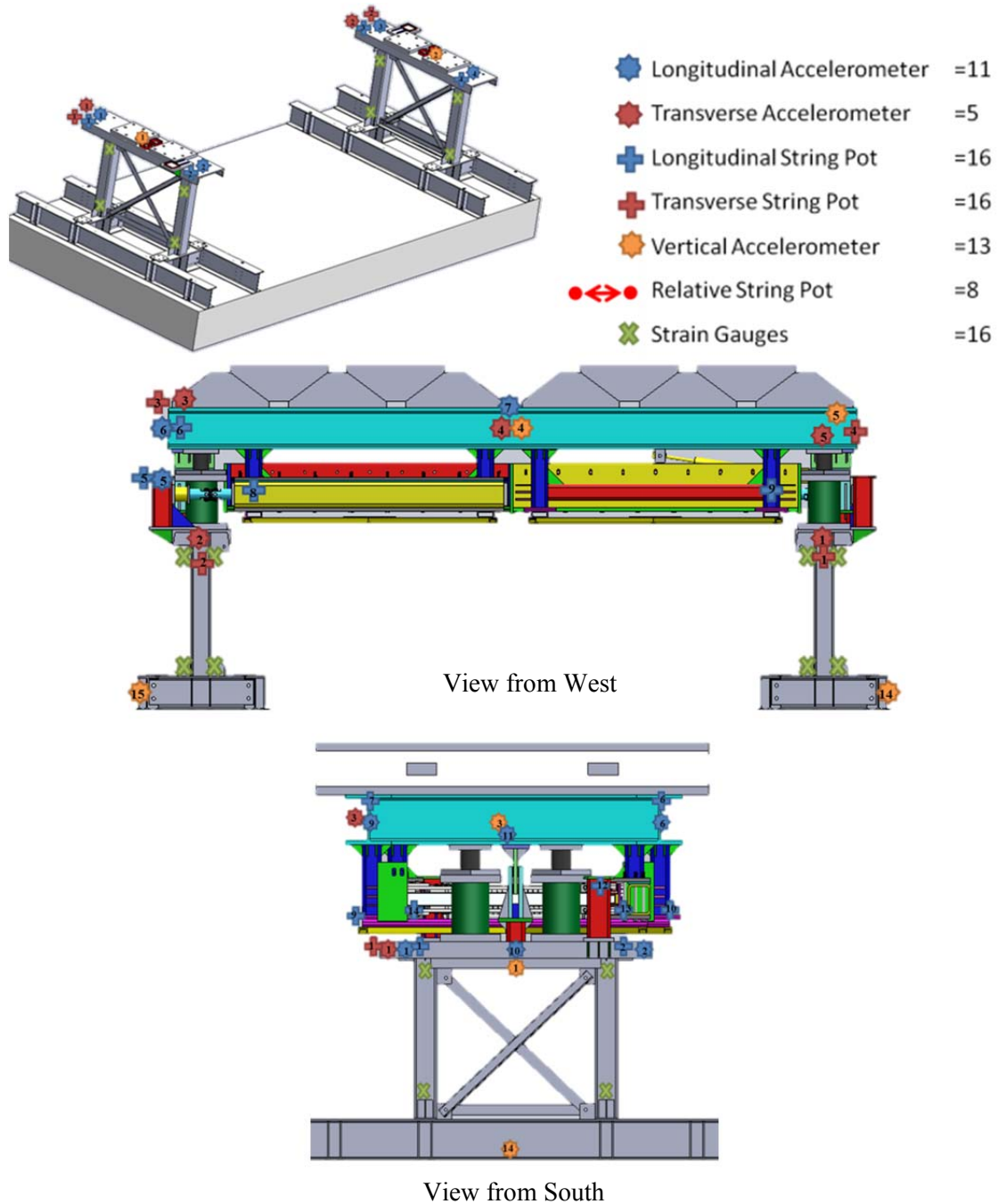
Figure 3.12. Location of measurement sensors on bridge test specimen

40

3.5 System identification of bridge model

As mentioned previously, the experimental tests were performed for the bridge model either with or without pier bracing and for four different configurations: 1) Isolated Bridge (IB), 2) Isolated bridge with NSDs (IB+NSD), 3) Isolated bridge with passive viscous dampers (IB+PD), and 4) Isolated bridge with NSDs and passive viscous dampers (IB+NSD+PD). In order to determine the dynamic properties of the model and verify the properties of its components, system identification tests were performed using white noise, sine-sweep and sinusoidal excitations applied to the base of the model via the shake table.

Elastomeric bearings
The in-situ properties of the elastomeric bearings were determined by performing tests of the bridge with braced piers and only elastomeric bearings engaged (IB). For this configuration, the deformation of the system occurs only at the isolation level and the motion of the top of the piers (bottom of the elastomeric bearings) is nearly identical to that of the shake table. The hysteretic response of the isolation level for sine-sweep excitation over a frequency range of 0.1-2 Hz and with amplitude of 0.51 cm and duration of 20 sec is shown in Figure 3.13. In this figure, the force is directly measured as the shear force in the loadcells located directly below the elastomeric bearings. As shown in Figure 3.13, the hysteresis loop of all four bearings combined has a small amount of damping associated with it (consistent with the elastomeric bearings being made of low damping rubber). In addition, the hysteresis loop shows that the stiffness of the four bearings combined is approximately 1068 kN/m (based on linear regression), which gives an average stiffness of 268 kN/m for each individual bearing.
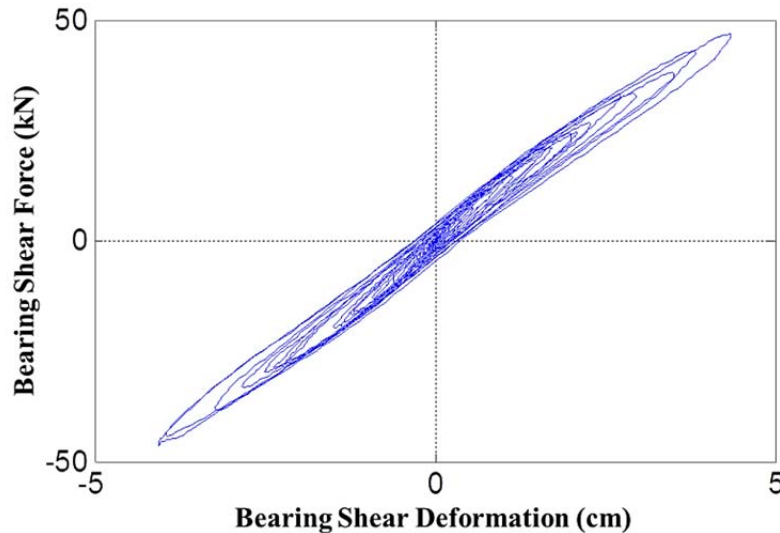
Figure 3.13. Hysteretic response of elastomeric bearings (all four bearings combined) for the case of IB with braced piers for sine-sweep motion having a frequency range of 0.1-2 Hz and with amplitude of 0.51 cm and duration of 20 sec

Using the results of the same test, the acceleration of the deck is plotted in the frequency domain in Figure 3.14. The peak in the Fourier amplitude spectrum occurs at 1.31 Hz, indicating that the system (which is mainly the bridge deck assembly on top of the four bearings) has a

natural period of 0.76 sec. This measured value compares well with a single degree-of-freedom model of the system where the average lateral stiffness of the bearings is utilized (1068 kN/m) along with the weight of the deck (158 kN), resulting in a natural period of 0.77 sec.
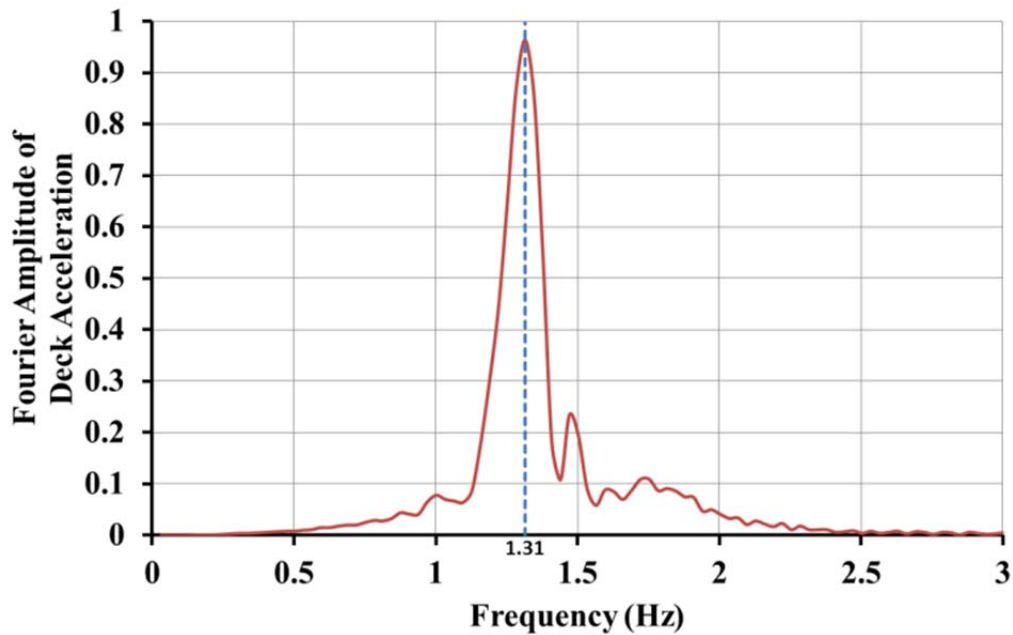
Figure 3.14. Deck Acceleration of model in frequency domain for the case of IB with braced piers for sine-sweep motion having a frequency range of 0.1-2 Hz and with amplitude of 0.51 cm and duration of 20 sec

Viscous Dampers

As discussed previously, in some test configurations, two viscous dampers were installed at the isolation level (connected between underside of bridge deck and to one of the pier caps). The same basic method that was used for identification of the bearing properties was used for identification of the in-situ viscous damper properties. In this case, the bridge model with braced piers and an isolation system consisting of elastomeric bearings and viscous dampers (IB+PD case) was tested. To determine the properties of the dampers, both sine sweep and sinusoidal shake table motions were imposed on the model and the resulting axial force and displacement of the dampers was measured via load cells and string potentiometers attached directly to the dampers. To determine the damping coefficient of each damper, the velocity was computed from the measured displacement via numerical differentiation and linear regression was applied to the force-velocity data. As an example, the force-velocity experimental data for one of the dampers is shown in Figure 3.15 for sinusoidal shake table motion at a frequency of 1.7 Hz. In addition, a "best-fit" curve using linear regression is shown. As can be seen, the experimental data follows a linear trend (consistent with linear viscous damping model), resulting in a damping coefficient of 60 kN-s/m (close to the expected value of 63 kN-s/m based on manufacturer test data). Data from the second damper resulted in a damping coefficient of 58 kN-s/m.
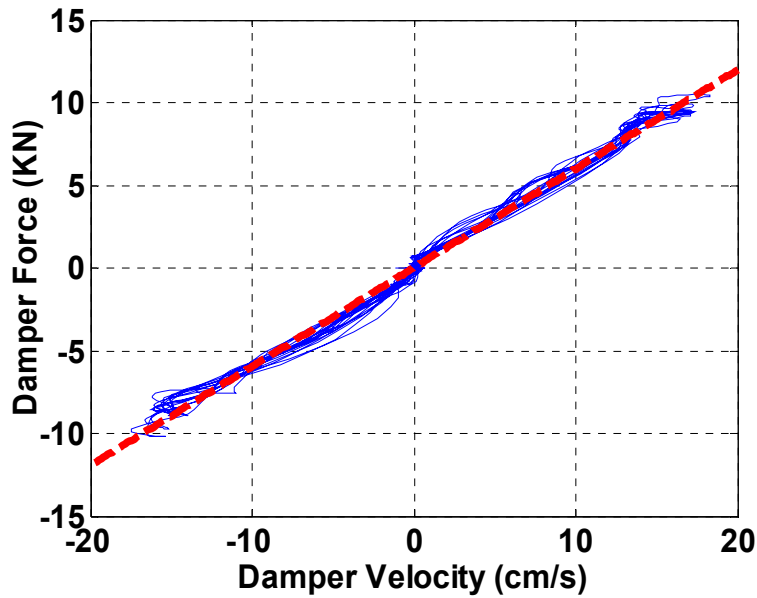
Figure 3.15. Damper force-velocity relation for harmonic shake table motion having a frequency of 1.7 Hz and with amplitude of 1.27 cm

The hysteretic response of the combination of two dampers for the test described above is shown in Figure 3.16. As can be seen, the dampers primarily provide energy dissipation. The small rotation of the hysteresis loop indicates that the dampers also provide some stiffness (slope between peak displacements is 190 kN/m giving an average stiffness for each damper of 95 kN/m). Note that both the force and displacement shown in Figure 3.16 are projections along a horizontal axis (along same axis as isolation system deformation), facilitating their direct use in the dynamic analysis of the bridge deck (the difference in the projected and non-projected displacements/forces is small since the angle of inclination of the dampers is small).
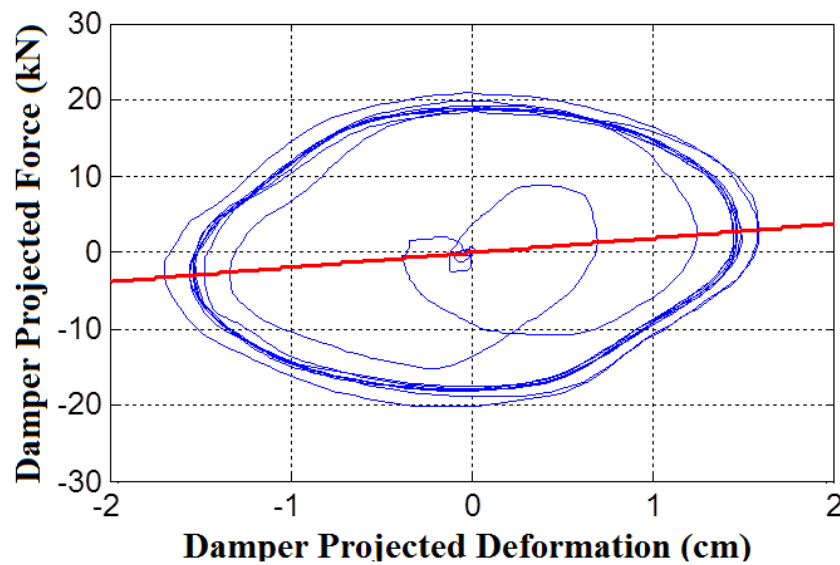
Figure 3.16. Force-displacement relation for both dampers for harmonic motion with frequency of 1.7 Hz with amplitude of 1.27 cm. and duration of 10 sec

43

Negative Stiffness Device
As mentioned previously, the two negative stiffness devices were re-designed for implementation in the bridge model. To experimentally identify the properties of the re-designed devices, they were subjected to cyclic loading within a loadframe at the University at Buffalo (see previous chapter). The cyclic tests were performed using harmonic motions with different amplitudes (ranging from 0.38 to 7.62 cm) and frequencies (0.01, 0.1 and 0.5 Hz). Due to limitations of the test setup, the maximum frequency used in the testing was 0.5 Hz. To determine the in-situ properties of the NSDs and to determine the amount of friction/damping associated with the interaction between the NSDs and their supporting system (i.e., at the sliding interfaces that allow the NSDs to be sheared while simultaneously supporting the weight of the NSDs), the bridge model with braced piers was tested for harmonic shake table motion at a frequency of 0.5 Hz and an amplitude of 10.2 cm. The force developed by the NSDs was measured directly by the load cells that connect the devices to the piers and the shearing deformation of the NSDs was calculated based on measurements from string potentiometers attached to the NSDs. The resulting hysteretic response of the two NSDs combined is shown in Figure 3.17 where the negative stiffness behavior is evident along with the initial small displacement delay in development of negative stiffness due to the gap spring assemblies. The hysteretic response of the four elastomeric bearings during this same test is also shown in Figure 3.17 along with the hysteretic response of the complete isolation system (four elastomeric bearings plus two NSDs) which exhibits the expected softening behavior. The hysteretic response of one of the NSDs (NSD north) for this same test is compared in Figure 3.18 with the hysteretic response of the same device from the cyclic load tests (excitation frequency of both tests is 0.5 Hz). The in-situ NSD exhibits a hysteresis loop that is roughly twice as wide (increased energy dissipation due to friction at the sliding interfaces of the NSD supporting system) and has slightly reduced negative stiffness (due to the flexibility of various components that connect the NSDs to the bridge) relative to the hysteresis loop from cyclic testing of the NSD alone.
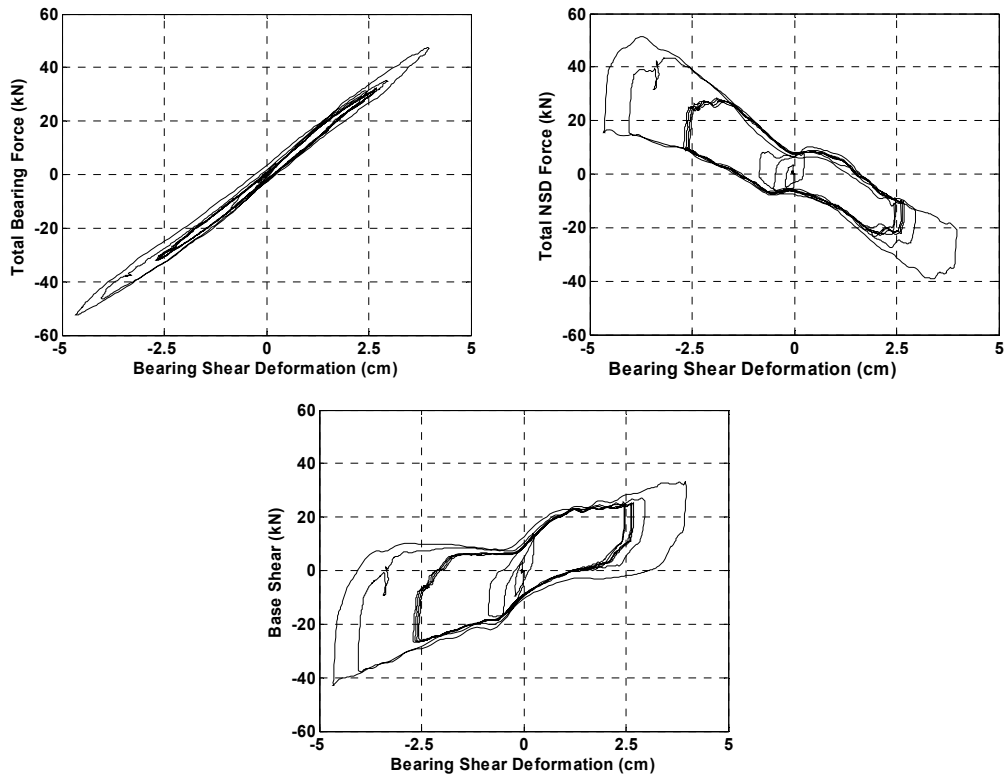
Figure 3.17. Hysteretic response of elastomeric bearings (Top Left), NSDs (Top Right) and the isolation system (Elastomeric bearings + NSDs) (Bottom) for the case of IB+NSD with braced piers and for harmonic shake table excitation at a frequency of 0.5 Hz and amplitude of 10.2 cm.
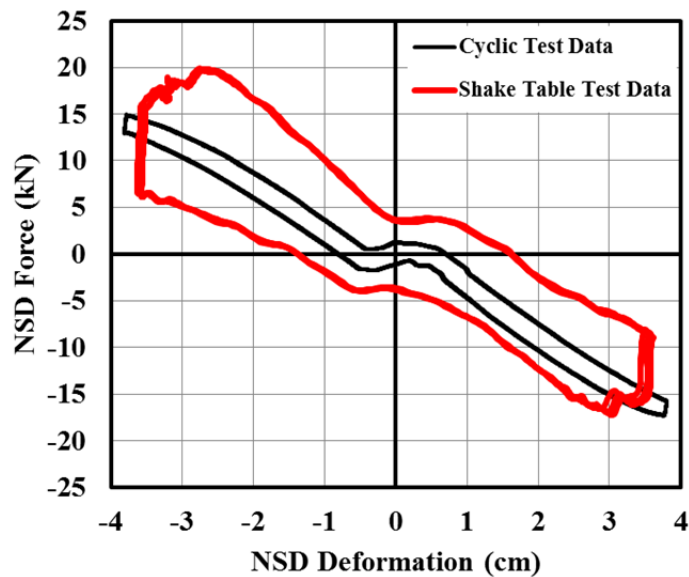
Figure 3.18. Comparison of hysteretic response of in-situ NSD (North) and NSD in load frame for harmonic motion at a frequency of 0.5 Hz

45

Bridge Piers
Many of the shaking table tests were performed for both the cases of braced and unbraced piers. These tests can be used to determine the dynamic properties of the bridge piers. As an example, a sine-sweep motion having a frequency range of 0.1-2 Hz and an amplitude of 0.51 cm was applied to the bridge model for the case of both braced and unbraced piers and only elastomeric bearings engaged (IB). The resulting deck acceleration, for the unbraced case, is shown in the frequency domain in Figure 3.19 where it can be seen that the peak in the spectrum is at 1.14 Hz which is 13% less than the 1.31 Hz for the bridge with braced piers (see Fig. 3.14) (i.e., the bridge model becomes more flexible). Using the weight of the deck (158 kN) and assuming a single degree-of-freedom (SDOF) system (i.e., neglecting the pier mass distribution and considering the pier and bearing stiffnesses to act in series), the effective stiffness of the bridge model with unbraced piers is 823 kN/m. With this model, the lateral stiffness of the piers is determined to be 1794 kN/m. Note that a multi degree-of-freedom (MDOF) version of the bridge model in which the pier mass is considered results in a fundamental natural frequency that matches that of the SDOF model (half of pier mass (full weight of each pier equals 17.8 kN) lumped at top of pier and full mass of deck lumped at deck level). The MDOF also predicts a second mode natural frequency of approximately 8 Hz and thus does not appear in Figure 3.19.
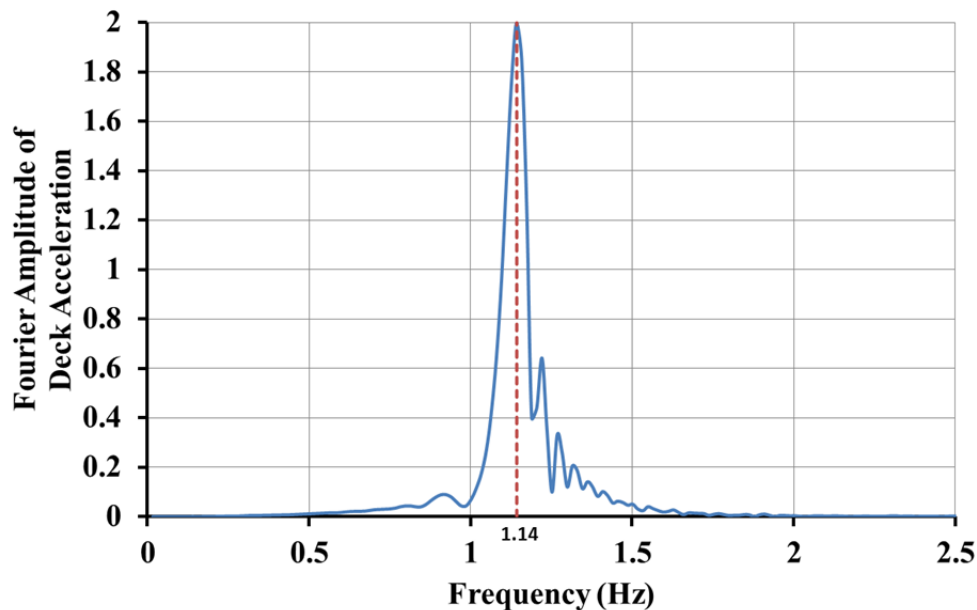
Figure 3.19. Evaluation of fundamental frequency for the case of IB with unbraced piers

3.6 Modification of numerical simulations based on system identification tests

Numerical simulation results from analysis of the bridge structure subjected to seismic loading was presented in a previous chapter. Those simulations were performed prior to the experimental testing. In this chapter, an updated set of simulations is presented wherein the actual properties of the components of the system are used (as obtained from the previously described system identification tests) and the earthquake ground motions that are used for excitation comes directly from sensors (displacement and acceleration sensors) attached to the shaking table near

the base of the model. Note that there were some appreciable differences between the desired shake table motion (historical earthquake record) and the actual motion of the table (recorded from the sensors attached to the table). These differences were caused by interaction of the bridge model with the shaking table. As shown in Figure 3.7, the shaking table includes a concrete cap extension that allows larger models to be tested. However, due to the location of the bridge piers (on the two cantilevered portions of the concrete extension), the concrete extension was prone to a rocking motion.

Nonlinear response-history analysis was performed for the eight bridge model configurations that were experimentally tested using the seven ground motions shown in Table 3.1 (ground motions scaled to meet similitude requirements of the quarter-scale model). Since most damage in bridge superstructures is either caused by excessive shear forces in their supporting members (damages to piers and shear keys) or excessive deck displacements (falling off its supports or damage to isolation system) (Chen and Duan, 2003), the comparison of the numerical predictions for two response parameters that are examined herein are peak base shear force and peak isolation system deformation. It should be noted that the base shear is equal to the shear force transferred to the deck supporting system, which are the piers in the case of the bridge model with unbraced piers and the abutments (piers and braces in the model) for the case of the bridge model with braced piers. A comparison of numerical simulation results for the case of unbraced piers is provided in Figures 3.20 and 3.21. Similar results are shown in Figure 3.22 and 3.23 for the case of braced piers. From the figures, it can be seen that, for almost all of the ground motions, the case of IB+NSD has the smallest base shear and deck accelerations relative to all other cases (and is substantially less than the IB case). In addition, deformations of the isolation system for the case of IB+NSD for all ground motions are smaller than the IB case and similar to the cases with viscous dampers. Further interpretation and discussion of the results are provided after the experimental results are presented.

Table 3.1. Ground motions used in numerical simulations and experimental tests

No.	Earthquake	Record	Mw
1	Northridge, 1/17/1994	637-270	6.7
2	Loma Prieta, 10/18/1989	CAP-000	6.7
3	Cape Mendocino, 4/25/1992	PET-090	7.0
4	Kobe, 1/16/1995	KJM-000	6.9
5	Northridge, 1/17/1994	Sylmar-000	6.7
6	Landers, 6/28/1992	Yermo-000	7.3
7	Landers, 6/28/1992	Yermo-270	7.3
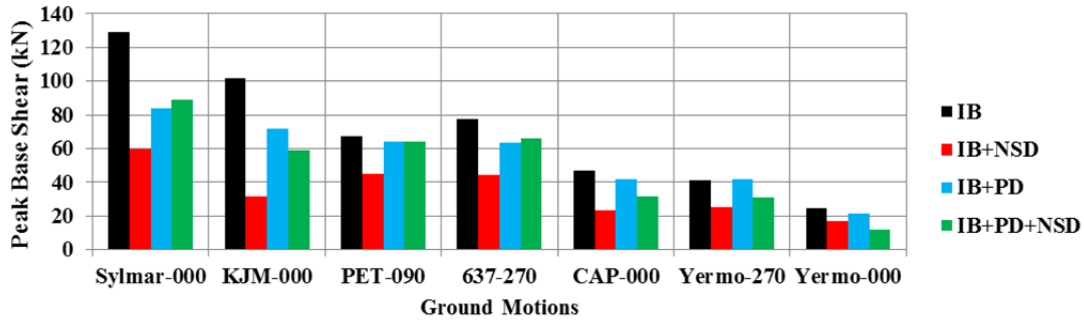
Figure 3.20. Numerical predictions of peak base shear in the bridge model with unbraced piers for the cases of isolated bridge (IB), isolated bridge with NSDs, isolated bridge with passive fluid viscous dampers (PD), and isolated bridge with NSDs and PDs
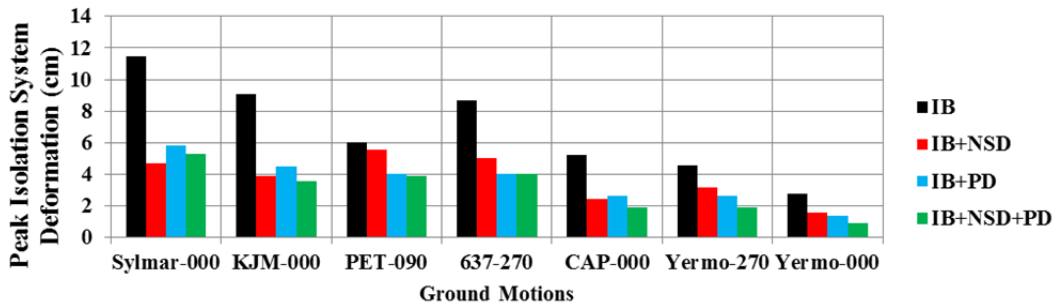
Figure 3.21. Numerical predictions of peak isolation system deformation in the bridge model with unbraced piers for the cases of isolated bridge (IB), isolated bridge with NSDs, isolated bridge with passive fluid viscous dampers (PD), and isolated bridge with NSDs and PDs
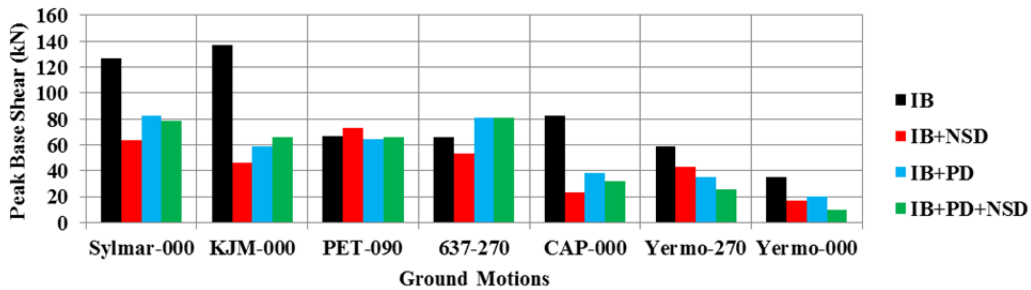
Figure 3.22. Numerical predictions of peak base shear in the bridge model with braced piers for the cases of isolated bridge (IB), isolated bridge with NSDs, and isolated bridge with NSDs isolated bridge with passive fluid viscous dampers (PD), and isolated bridge with NSDs and PDs
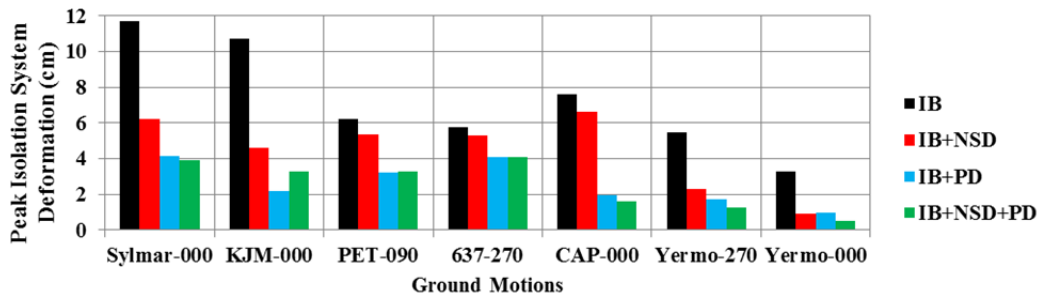
Figure 3.23. Numerical predictions of peak isolation system deformation in the bridge model with braced piers for the cases of isolated bridge (IB), isolated bridge with NSDs, isolated bridge with passive fluid viscous dampers (PD), and isolated bridge with NSDs and PDs

3.7 Shake table test results and discussion

As mentioned previously, the bridge model was tested with four different isolation system configurations (IB, IB+NSD, IB+PD, and IB+NSD+PD) and two different bridge pier bracing conditions (braced or unbraced). Since each of the components of the bridge model has limited capacity, the ground motion intensity was incrementally increased to allow for monitoring of the behavior of these components and to ensure that the experimental results are consistent with the numerical simulations (thus avoiding any possible damage to individual components of the structure). The shake table tests started with the weakest motion and progressed toward the strongest motion, usually with ground motion amplitude scaling of 25%, 50%, 75% and 100% (there were exceptions since, in some cases, the specimen was vulnerable to higher intensity motions while, for other cases, the specimen could readily withstand more than 100% of the ground motion). Since the model is a quarter-scale model (from a length scaling perspective), artificial mass simulation was utilized to meet similitude requirements. This resulted in the ground motion records being compressed in time by a factor of 2.

The measured peak base shear and peak isolation system deformation for all of the ground motions are provided in Figures 3.24 and 3.25 for the case of unbraced piers. Similar results are shown in Figures 3.26 and 3.27 for the case of braced piers. In order to be able to compare different cases with each other, the ground motions associated with the peak responses shown in Figures 3.24-3.27 were all scaled to 100% (however, for the IB cases, scaling of some of the ground motions was limited to ensure that the bearings would not be damaged during the tests and thus the values shown in the figures are calculated via extrapolation of results from lower intensity motions, assuming linear behavior of the bearings; note that the IB case is highly vulnerable due to its low lateral stiffness combined with a small amount of damping). As shown in Figures 3.24-3.27, in nearly all cases, adding the NSDs to the isolation level reduced both the peak base shear and the peak isolation system deformation relative to the IB case. Recall that the NSDs and their support system provide appreciable friction damping and thus the reduction in deformation was not unexpected. Furthermore, in all cases, adding the NSDs to IB results in a larger reduction in peak base shear relative to the addition of dampers (although the dampers produce larger reductions in peak deformation). Although adding the viscous dampers to the NSDs (IB+NSD+PD cases) is beneficial for reducing peak deformation, due to the high friction damping provided by the NSDs and their supporting system, the combined damping (friction plus viscous) resulted in an increase in peak force in most cases relative to the IB+NSD configuration and in some cases it is even larger than that in the IB+PD configuration. Among all of the ground motions, results of the PET090 ground motion are unique in that the NSDs have minimal effect on the base shear and isolation system deformations (this can be explained via examination of the ground motion effects as defined by an ADRS spectrum; for detailed explanation, see previous chapter).
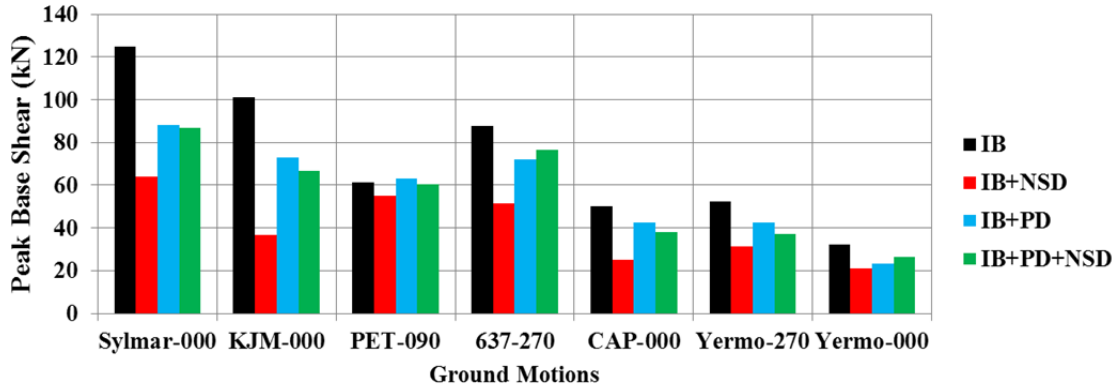
Figure 3.24. Experimental results for peak base shear in the bridge model with unbraced piers for the cases of isolated bridge (IB), isolated bridge with NSDs, and isolated bridge with NSDs isolated bridge with passive fluid viscous dampers (PD), and isolated bridge with NSDs and PDs
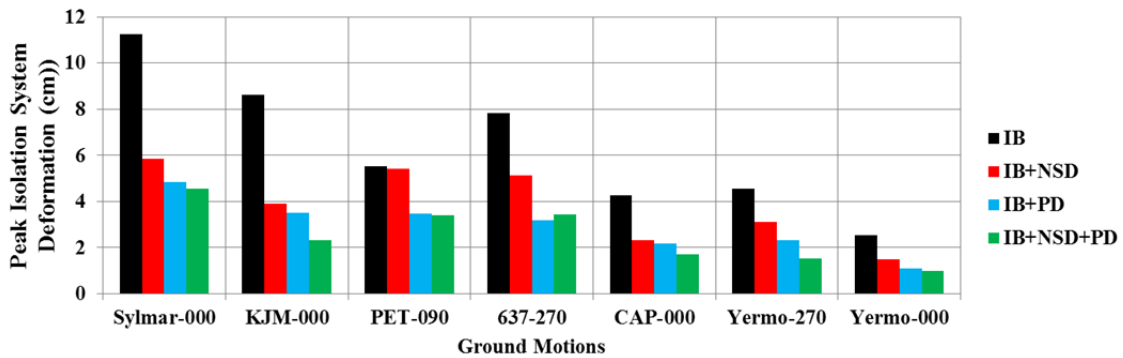
Figure 3.25. Experimental results for peak isolation system deformation in the bridge model with unbraced piers for the cases of isolated bridge (IB), isolated bridge with NSDs, isolated bridge with passive fluid viscous dampers (PD), and isolated bridge with NSDs and PDs
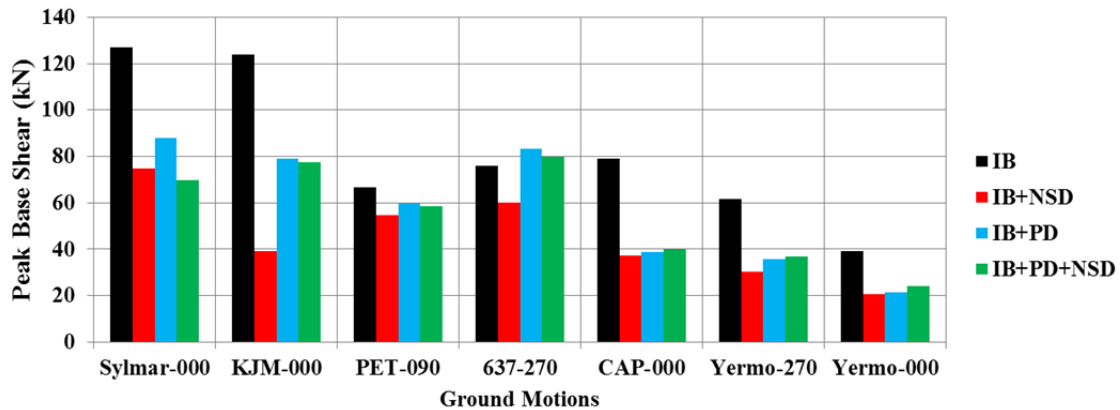
Figure 3.26. Experimental results for peak base shear in the bridge model with braced piers for the cases of isolated bridge (IB), isolated bridge with NSDs, and isolated bridge with NSDs isolated bridge with passive fluid viscous dampers (PD), and isolated bridge with NSDs and PDs

50
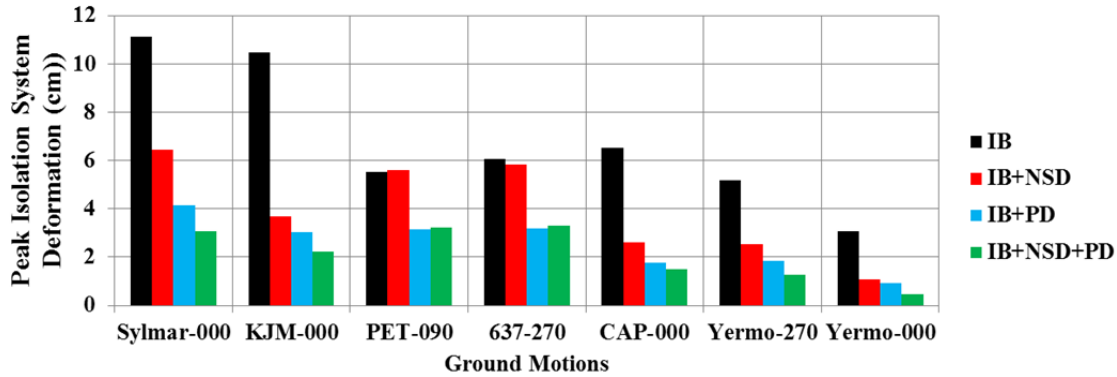
Figure 3.27. Experimental results for peak isolation system deformation in the bridge model with braced piers for the cases of isolated bridge (IB), isolated bridge with NSDs, isolated bridge with passive fluid viscous dampers (PD), and isolated bridge with NSDs and PDs

To further evaluate the performance of the bridge model with NSDs, the case of the Kobe earthquake ground motion is selected for detailed examination. The base shear and isolation system deformation for the cases of IB, IB+NSD and IB+PD and for both braced and unbraced piers are shown as a function of time in Figures 3.28-3.31. As can be seen in these figures, the NSDs (IB+NSD case) reduce the peak base shear and peak isolation system deformation by up to 69% and 65%, respectively, for the case of braced piers, and 64% and 55%, respectively, for the case of unbraced piers, relative to the IB case (note that the dashed lines shown in the plots represent the absolute maximum values for each particular case and are shown on the same side of the plot for comparison purposes). The effect of adding the NSDs to the IB case on the isolation system deformation is similar to that of adding viscous dampers (see Fig. 3.29 and 3.31). However, the force reduction providing by the NSDs is appreciably larger than that provided by the viscous dampers (64% reduction versus 28% for the unbraced case and 69% versus 36% for the braced case; see Fig. 3.28 and 3.29). With regard to pier bracing, as mentioned previously, the NSDs and PDs produce larger response reductions for the bridge model with braced piers as compared to that with unbraced piers, indicating that such devices are more effective when they are installed in a manner that allows them to react against rigid abutments rather than flexible piers.
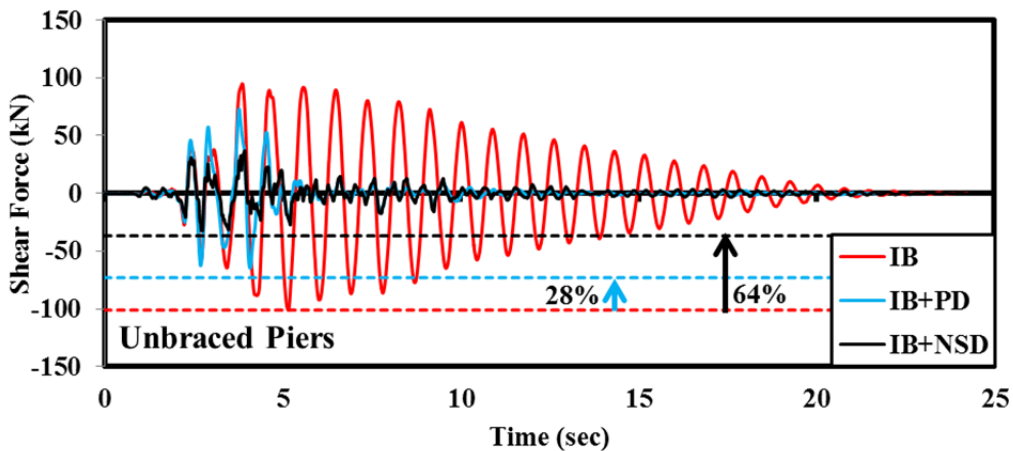
Figure 3.28. Isolation system shear force response for three different isolation system configurations for the bridge with unbraced piers; Excitation is 100% KJM ground motion from 1995 Kobe, Japan Earthquake
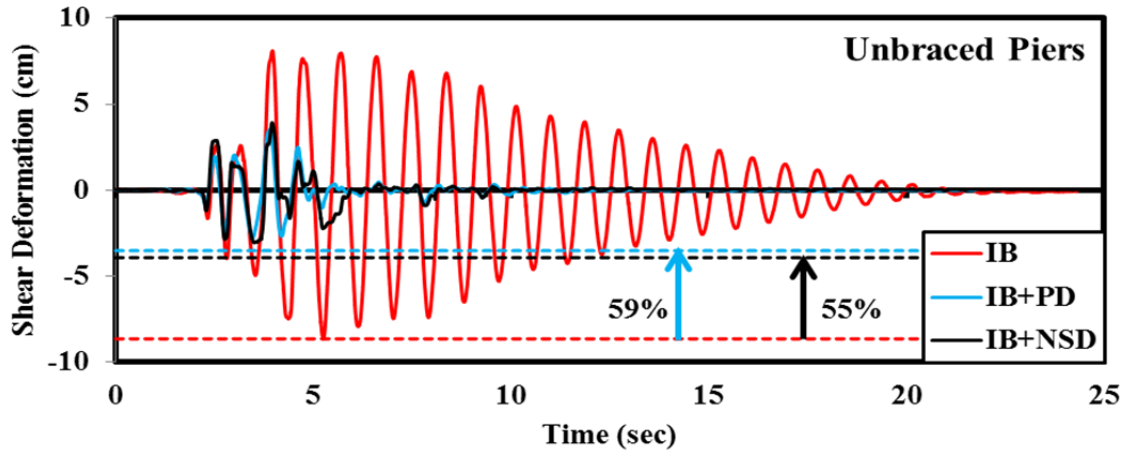
Figure 3.29. Isolation system shear deformation response for three different isolation system configurations for the bridge with unbraced piers; Excitation is 100% KJM ground motion from 1995 Kobe, Japan Earthquake
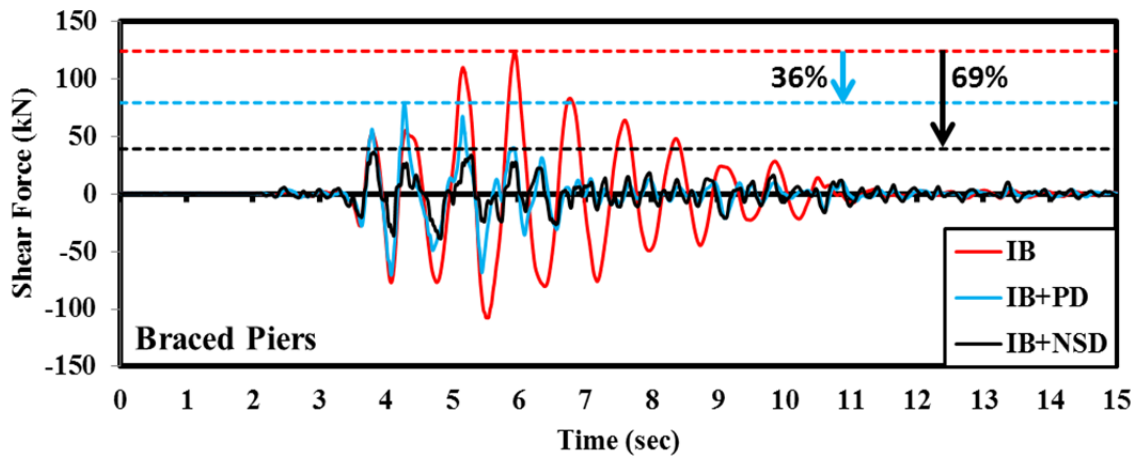
Figure 3.30. Isolation system shear force response for three different isolation system configurations for the bridge with braced piers; Excitation is 100% KJM ground motion from 1995 Kobe, Japan Earthquake
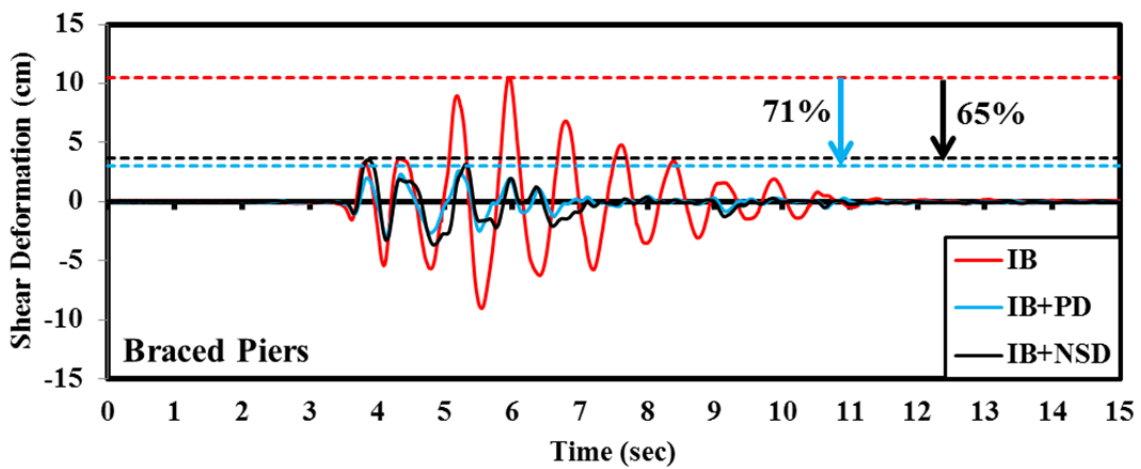
Figure 3.31. Isolation system shear deformation response for three different isolation system configurations for the bridge with braced piers; Excitation is 100% KJM ground motion from 1995 Kobe, Japan Earthquake

The hysteretic response of the bridge model (both the complete bridge structure response and component-level response) is shown in Figures 3.32 - 3.39 for all eight bridge configurations and for excitation being 100% of the Kobe earthquake ground motion. As shown in Figures 3.32 and 3.33, the behavior of the elastomeric bearings is as expected - almost linear and with a low level of damping. Furthermore, the response of the system has some distinct differences depending on whether or not the piers are braced (since the presence of the bracings affects the dynamic of the structure and thus its response to the earthquake). Also, as can be seen from Figures 3.32 and 3.33, the total bearing force and base shear hysteresis loops are slightly different for each pier bracing condition due to the effects of the torsional restraint system (torsional restraints transfer a small shear force (via friction) from the deck to the piers and dissipate a small amount of energy (also via friction)).
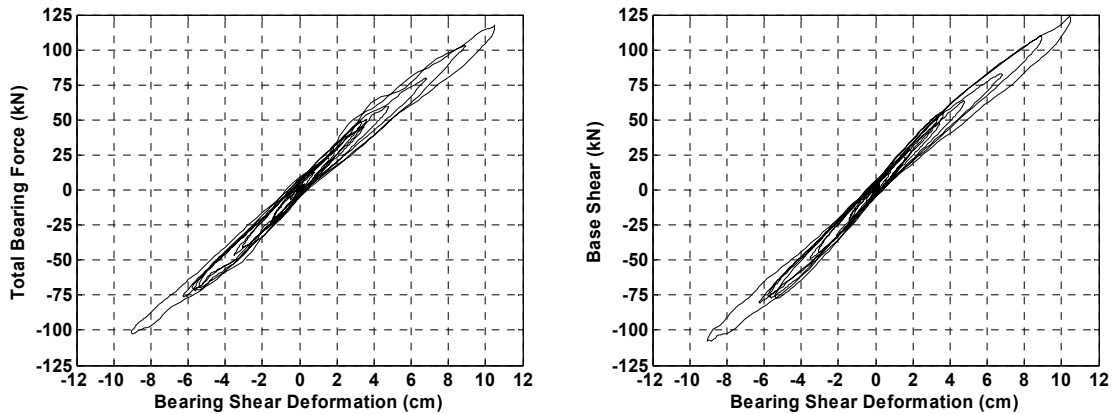
Figure 3.32. Hysteretic response of complete bridge structure and it components for the case of IB for the bridge with braced piers
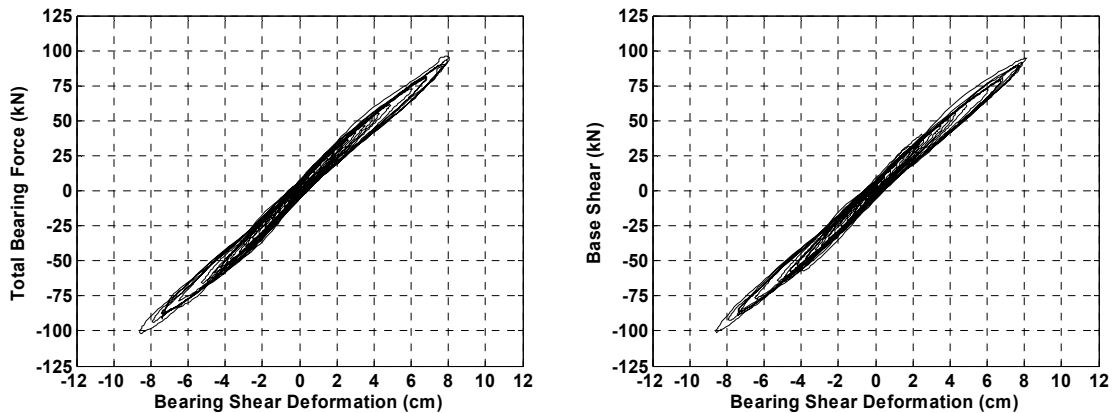
Figure 3.33. Hysteretic response of complete bridge structure and it components for the case of IB for the bridge with unbraced piers

The influence of the NSDs when added to the IB case is shown in Figures 3.34 and 3.35. As can be seen, the NSDs produce a substantial reduction in the forces as defined by the backbone curve of the complete system. From the figures, it is clear that the NSDs are designed in a way to create a virtual yield point followed by essentially zero stiffness regions in the hysteretic response of the bridge model. The bridge components remain elastic while the backbone curve of the complete system exhibits essentially elasto-plastic behavior. Note that the

width of the hysteretic loop for the complete system is mainly due to friction within the NSDs and their supporting assemblies. This friction is beneficial in that it provides energy dissipation that limits the deformations. If friction in the NSD system were reduced substantially, the forces in the structure would be reduced further but at the expense of increased deformations, thus requiring the addition of a damping mechanism. As can be seen in Figures 3.36 and 3.37, the addition of viscous dampers to the IB case results in significant energy dissipation via damping forces that are out-of-phase with the restoring forces, thereby reducing both peak forces and displacements relative to the IB case shown in Figures 3.32 and 3.33.

The hysteretic response for the case of IB+NSD+PD is shown in Figures 3.38 and 3.39. As can be seen, the addition of viscous dampers to the IB+NSD case results in a complete system response wherein the peak displacements are reduced by a small amount while the peak forces are increased appreciably. This may be explained by recognizing that, since the deformations have been decreased due to the high damping of the combined system, the NSDs generate relatively small forces during most of the response (due to the gap springs) but are still able to cancel out the positive stiffness of the elastomeric bearings, particularly at larger displacements. Furthermore, both the bearings and the NSDs have some level of damping associated with them but the largest contribution to damping comes from the viscous dampers which produce large forces near zero displacement (due to velocity dependence). Combining the hysteretic response for each of these three components (bearings, NSDs, and dampers) results in peak base shear forces occurring near zero displacement.
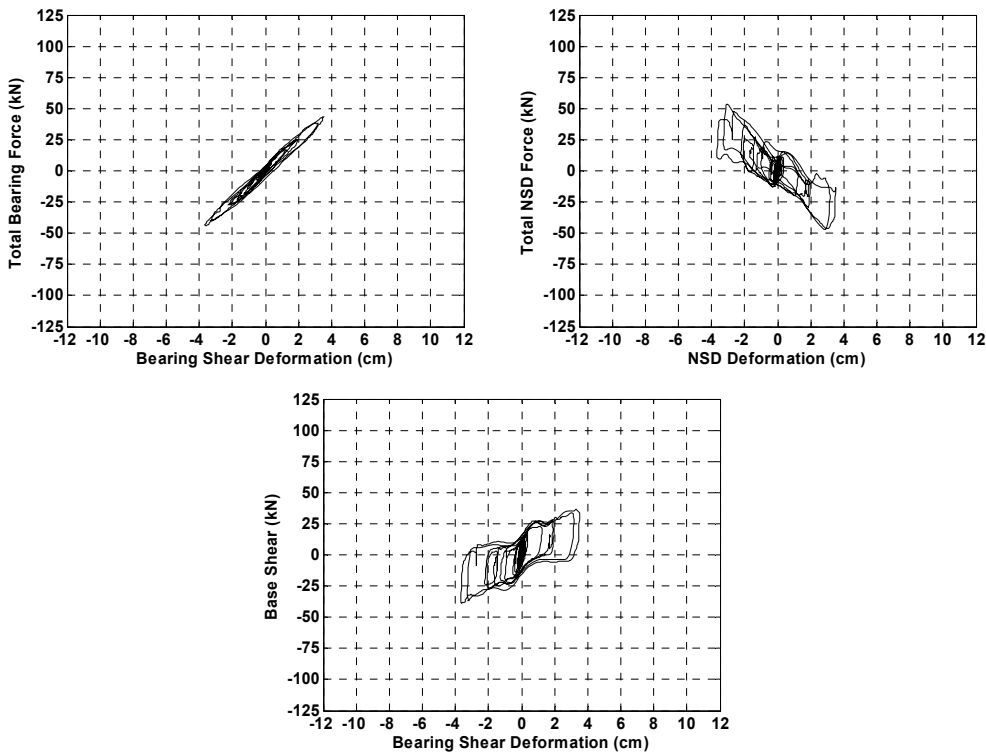
Figure 3.34. Hysteretic response of complete bridge structure and its components for the case of IB+NSD for the bridge with braced piers
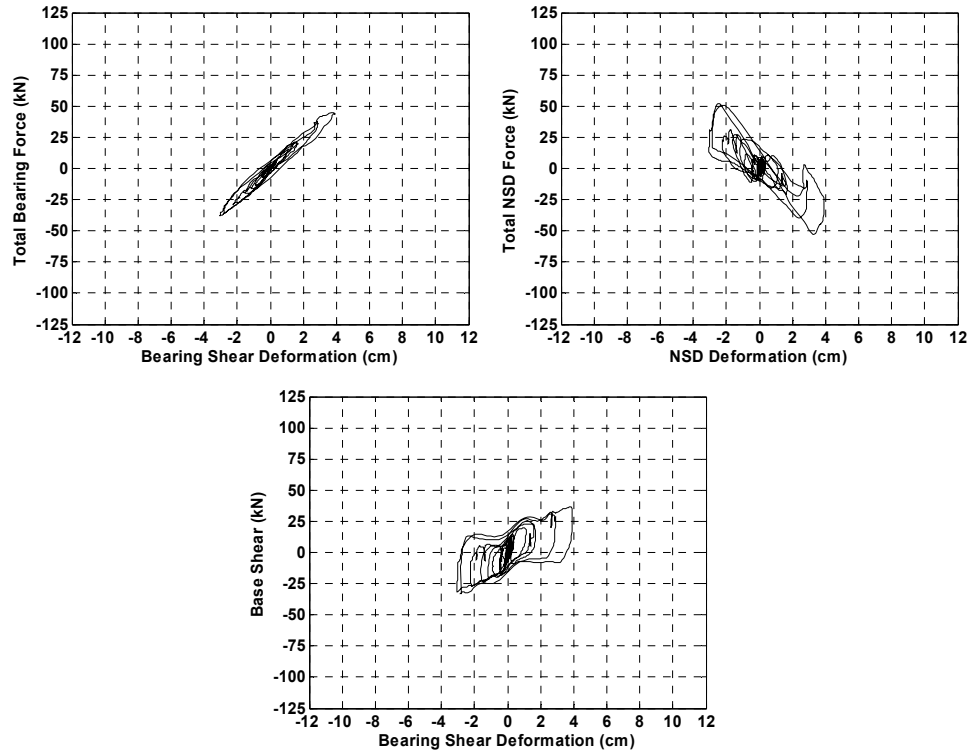
Figure 3.35. Hysteretic response of complete bridge structure and its components for the case of IB+NSD for the bridge with unbraced piers
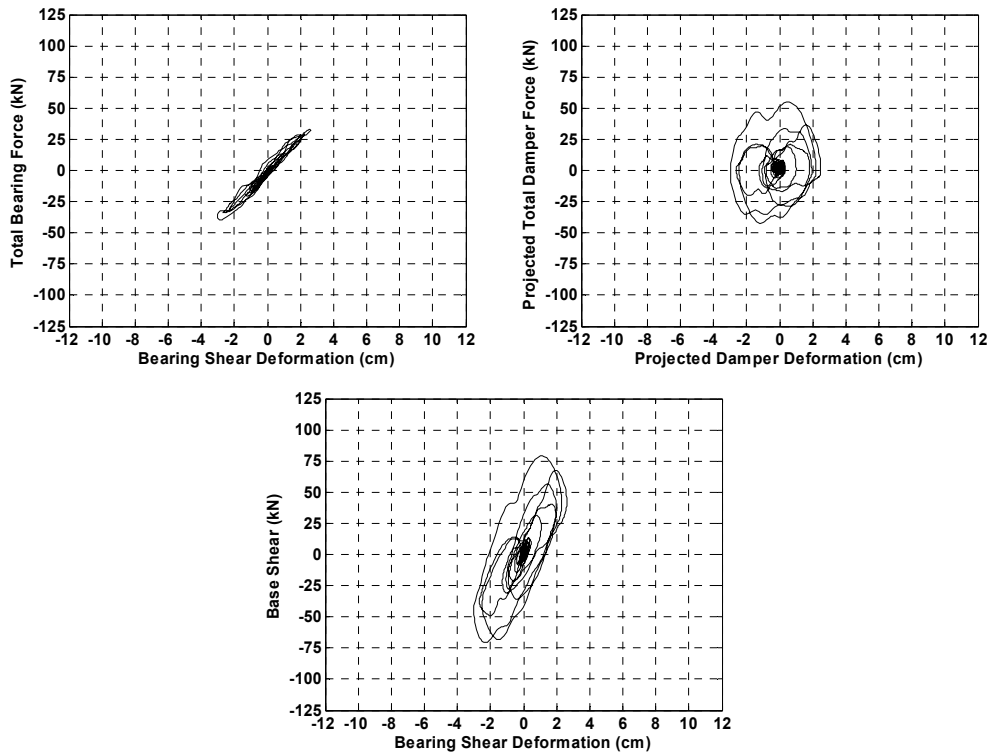
Figure 3.36. Hysteretic response of complete bridge structure and its components for the case of IB+PD for the bridge with braced piers
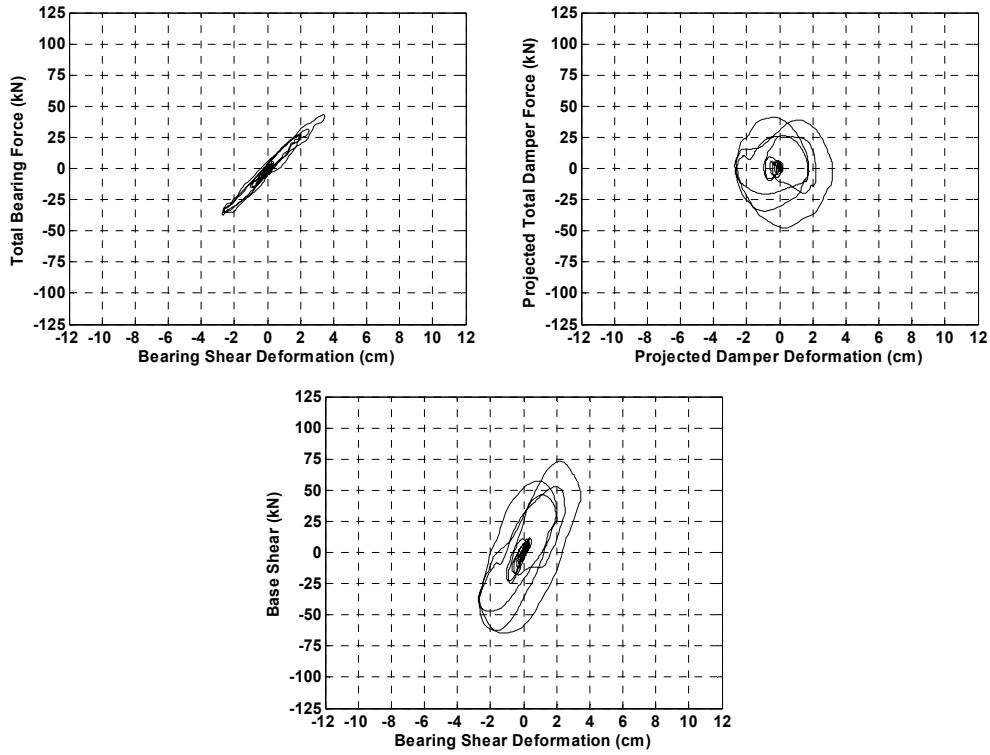
Figure 3.37. Hysteretic response of complete bridge structure and its components for the case of IB+PD for the bridge with unbraced piers
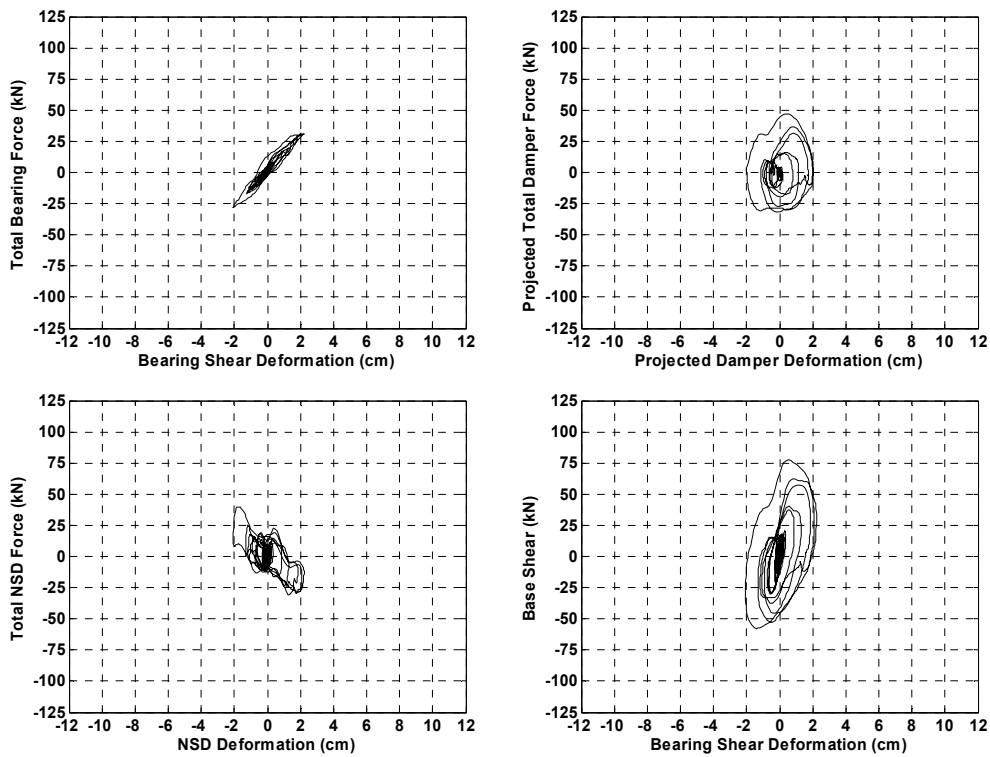
Figure 3.38. Hysteretic response of complete bridge structure and its components for the case of IB+NSD+PD for the bridge with braced piers
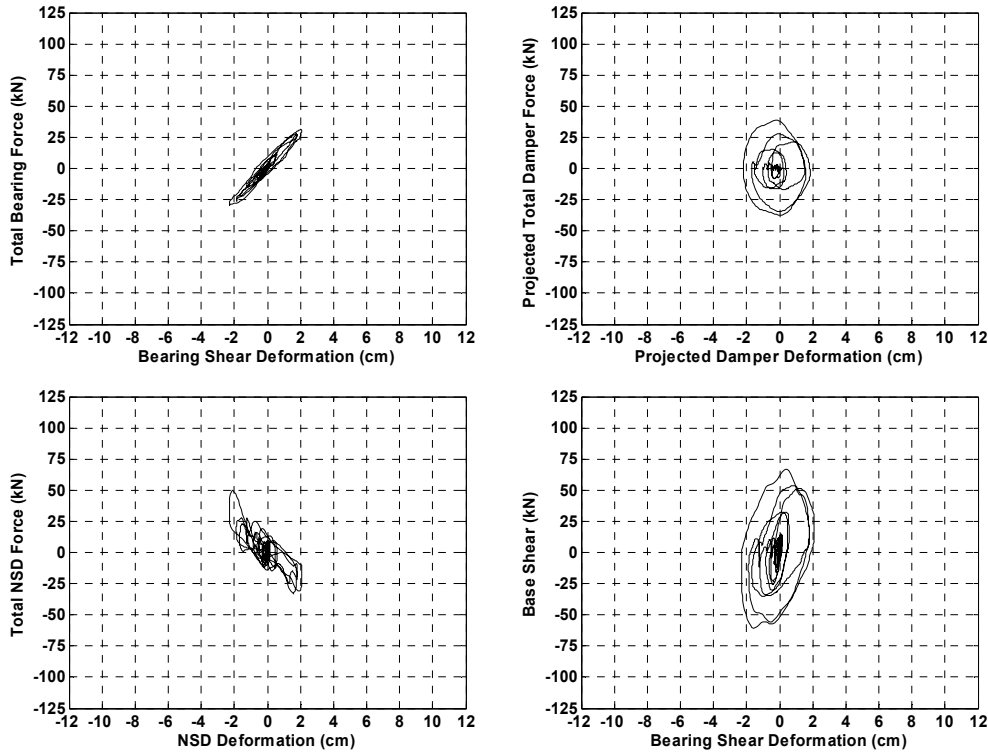
Figure 3.39. Hysteretic response of complete bridge structure and its components for the case of IB+NSD+PD for the bridge with unbraced piers

The effect of the isolation system on the deformation of the bridge piers (unbraced piers) is shown in Figure 3.40 for the case of 100% of the Kobe earthquake ground motion. Note that the two isolation systems that employ NSDs result in smaller peak pier drift than those systems without the NSDs. Furthermore, both the NSDs and viscous dampers are effective in reducing the pier drift with respect to the IB case. As shown in Figure 3.25, for this particular ground motion, viscous dampers are more effective than NSDs in reducing the isolation system deformation. However, the NSDs are more effective than viscous dampers in reducing pier deformation due to their method of applying force to the structure. During an earthquake, the NSDs push the deck in the same direction as the motion of the deck. In order to do that, the NSDs react against the piers and thus the force that the NSDs impose on the piers is 180 degrees out-of-phase with respect to the motion of the deck. This behavior results in overall reductions in pier deformation relative to that provided by viscous dampers.
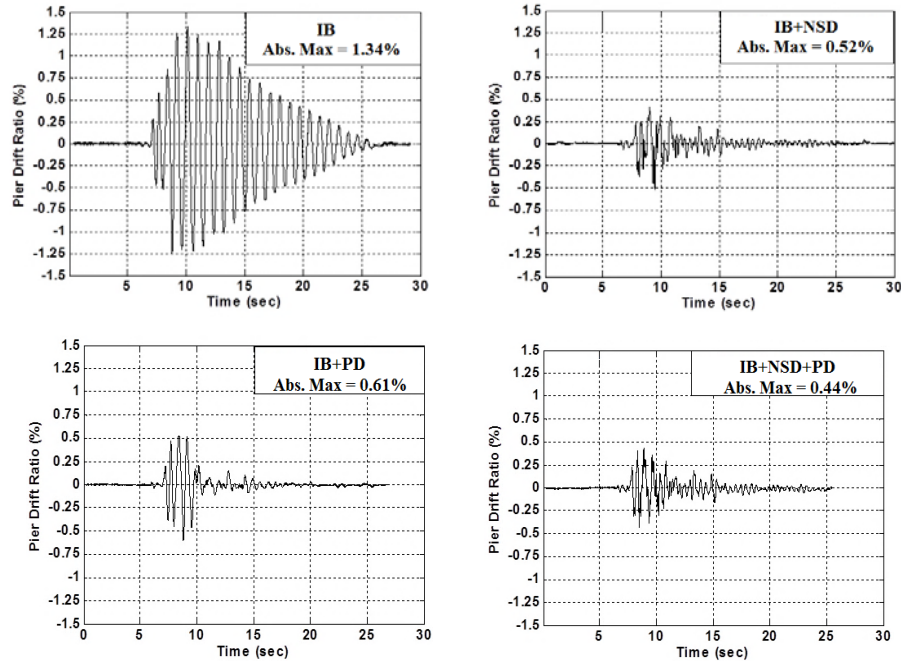
Figure 3.40. Lateral deformation of unbraced piers for different isolation system configurations (IB, IB+NSD, IB+PD and IB+NSD+PD)

3.8 Summary

A new seismic protection device that employs the concept of negative stiffness to limit the forces that develop in structures is presented herein along with its application to a scale-model highway bridge structure. The device is completely mechanical (passive) and features a pre-compressed spring that applies nonlinear displacement-dependent forces that are in-phase with the lateral displacement of the device. Thus, rather than applying a displacement-dependent restoring force, the device applies a destabilizing force that, when combined with the restoring force of the primary structure, results in an overall system that is stable. The negative stiffness device (NSD) was implemented in a quarter-scale highway bridge model and subjected to selected earthquake ground motions via a shake table located at the University at Buffalo. The tests were performed for the cases of a bridge with braced and unbraced piers and for four different bridge configurations: 1) Isolated Bridge (IB) using low damping elastomeric bearings, 2) Isolated bridge with NSDs (IB-NSD), 3) Isolated bridge with passive viscous dampers (IB-PD), and 4) Isolated bridge with NSDs and passive viscous dampers (IB-NSD-PD).

The experimental tests demonstrated that the use of NSDs within the isolation system can significantly reduce the peak base shear forces and accelerations of the deck with respect to the IB case for nearly all of the configurations and ground motions. Generally, it is expected that NSDs will increase deformations, due to the softening behavior of the system, but the deformations can be controlled by increasing the damping of the system. As discussed herein, the NSDs were inserted into a special support system which maintains their position within the isolation system located below the bridge deck. The support system was designed to dissipate energy through internal friction, resulting in sufficient damping to limit deformations during strong ground shaking. The experimental results showed that the deformation of the deck with

respect to the piers (isolation system deformation) for the IB+NSD case was reduced relative to the IB case for all of the ground motions that were considered. Thus, the combination of negative stiffness and friction provided by the NSDs and their support system resulted in a device that reduced force demands in the bridge while simultaneously limiting displacements.

A key outcome of the experimental tests is that they demonstrated that NSDs can be effective in cases where a flexible layer (i.e., the bridge piers) is inserted between the NSDs and the foundation of the structure (previous testing had been for the case of base-isolated buildings in which the NSDs were directly attached to a rigid foundation). In particular, the NSDs were as effective as viscous dampers in reducing peak pier drifts while at the same time reducing force demands on the structure. The shake table tests were performed for the case of the bridge with braced (modeling a bridge supported on abutments) and unbraced piers and results showed that the NSDs have reduced effectiveness in the case of the bridge with unbraced piers. This is due to the pre-compressed forces of the NSD springs acting to deform the piers and connecting elements rather than inducing negative stiffness in the structure.

Detailed results for all eight bridge configurations were presented herein for one particular strong ground motion, with attention given to evaluating peak base shear and isolation system deformation and examining the hysteretic response of the components that make up each bridge configuration, thus clarifying the influence of the NSDs on the response of the seismically isolated bridge. An important aspect of the bridge response with NSDs (IB+NSD) is that the positive stiffness of the bearings combined with the negative stiffness of the NSDs results in the creation of a virtual yield point in the hysteretic response of the bridge (due to the design of the nonlinear force-displacement relation for the NSDs which results in essentially zero stiffness regions in the hysteretic response of the bridge). Although the stiffness of the bridge system appears to be displacement-dependent, the bridge itself remains completely elastic while the backbone curve of the combined bridge-NSD system exhibits essentially elastic-perfectly plastic behavior, thereby reducing the forces in the system.

"This Page Intentionally Left Blank"

SECTION 4. PERFORMANCE EVALUATION OF NEGATIVE STIFFNESS DEVICES FOR SEISMIC RESPONSE CONTROL OF BRIDGE STRUCTURES VIA EXPERIMENTAL SHAKE TABLE TESTS AND ASSOCIATED NUMERICAL SIMULATIONS

4.1 Introduction

Since bridges often serve as critical lifelines after major seismic events, many seismic protection systems have been developed to protect such structures. These systems consist of passive, active or semi-active devices that change the properties (stiffness and/or damping) of the structure. Elastomeric bearings, sliding bearings, viscous dampers, and viscoelastic dampers, are common passive seismic protection devices for bridges. Passive devices that are effective in reducing the displacement of the bridge deck, such as viscous dampers, may not reduce the shear force in the piers and the acceleration of the bridge deck since these quantities have peak values that are dictated by the yield strength of the structure. To address the limitations of passive control devices, active and semi-active devices have been developed, tested, and in some cases, implemented in bridges. Iemura et al. (2006) described an application of pseudo-negative stiffness control in numerical simulations of a benchmark cable-stayed bridge, using controllable hydraulic damping devices, to reduce both the base shear of the bridge and the deck displacements. However, the variable damper required external power and a feedback signal to be able to generate negative stiffness, thus reducing its reliability relative to passive devices. Another method to reduce forces within structures during earthquakes was proposed by Reinhorn et al. (2005 and 2009) who introduced the concept of weakening of structures (reducing strength) to reduce seismic forces and added damping to reduce displacements. Although this method is capable of reducing both forces and deformations, it may lead to early yielding of the structural system, resulting in damage to the structure. Since 2008, our research team has been working on the development and experimental testing of a new passive seismic protection device that can develop "true" negative stiffness behavior (not pseudo-negative stiffness by means of hydraulic devices, as described previously) to substantially reduce earthquake forces in structures through "apparent weakening." The device produces negative stiffness behavior by using a pre-compressed spring within an arrangement of steel braces and levers. Nagarajaiah (2010) and Nagarajaiah et al. (2010) showed that using the negative stiffness device (NSD) in structures results in decreased dynamic forces. By engaging the NSD's at certain pre-defined displacements, the combined behavior of the primary structure and NSD's is one in which there is an apparent (or virtual) yield point at a small force level. The response is virtual in that the framing of the primary structural system does not actually yield; rather, the composite system appears to yield (i.e., apparent weakening).

In this project, two prototypes of the NSD were fabricated by a leading manufacturer of seismic protection devices and tested to evaluate their response to cyclic loading. In addition, the effects of the devices on the seismic response of two different three-story scale-model buildings was evaluated via shaking table tests (Sarlis et al, 2011 & 2012 and Pasala et al, 2011, 2013a and 2013b). In the final stage of the project, the NSD's were re-designed for implementation in a quarter-scale highway bridge model and tested on a shaking table (Attary et al., 2012a, 2012b, 2013). This chapter focuses on evaluation of the experimental shake table test results for each

bridge configuration, comparison of numerical simulations and experimental results, and performance assessment of the NSDs based on various performance measures.

4.2 Experimental tests results

The negative stiffness device that was developed and tested as part of this project is a completely mechanical device that develops a force that is in-phase with the motion of the device. This force is generated using a pre-compressed main spring, which is originally parallel to the sides of the NSD (see Fig. 4.1). When the NSD frame is subject to a shearing deformation, the main spring becomes inclined, creating a force in the same direction as the imposed motion. The deformed shape of the NSD is shown in Figure 4.1 along with an example of experimental test results in Figure 4.2 for three harmonic motions at different frequencies.

The bridge model, which is described in detail in previous chapter, consisted of a rigid steel deck (with additional concrete blocks on top of it) and two steel piers, which could be flexible or rigid (using four removable diagonal braces) (see Fig. 4.3). The bridge has a clear span of 4.8 m, a height of 2.7 m, and two custom-designed NSD support frames attached below the 5.4 m long bridge deck. The deck of the bridge is supported on a seismic isolation system consisting of four low damping elastomeric bearings and includes NSDs and/or viscous dampers within the isolation system (see Fig. 4.3).

Unlike the previous two phases of experimental testing of the NSDs within three-story buildings, in the third phase the NSDs react against a flexible component of the structure (the bridge piers) rather than being directly connected to the rigid foundation of the structure. The design of the NSDs was modified for implementation in the bridge model and thus system identification tests were performed to determine their hysteretic behavior (see Fig. 4.1). The experimental results clearly show the negative stiffness behavior along with some damping associated with internal friction (see Fig. 4.2).

Shake table testing of the bridge model was performed for four different bridge configurations: 1) Isolated Bridge with elastomeric bearings (IB), 2) Isolated bridge with NSDs (IB+NSD), 3) Isolated bridge with passive viscous dampers (IB+PD), and 4) Isolated bridge with NSDs and passive viscous dampers (IB+NSD+PD) (see Fig. 4.3). Each of these configurations was tested for the case of unbraced piers (mimicking the middle span of a multi-span bridge) and the case of braced piers (mimicking a single span bridge supported on abutments). Each of these eight cases was tested under seismic loading defined by the seven ground motions shown in Table 4.1.
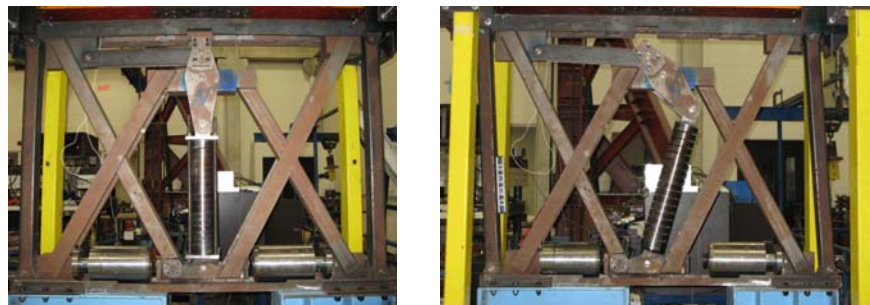
Figure 4.1. Undeformed and deformed shape of NSD inside load frame at University at Buffalo
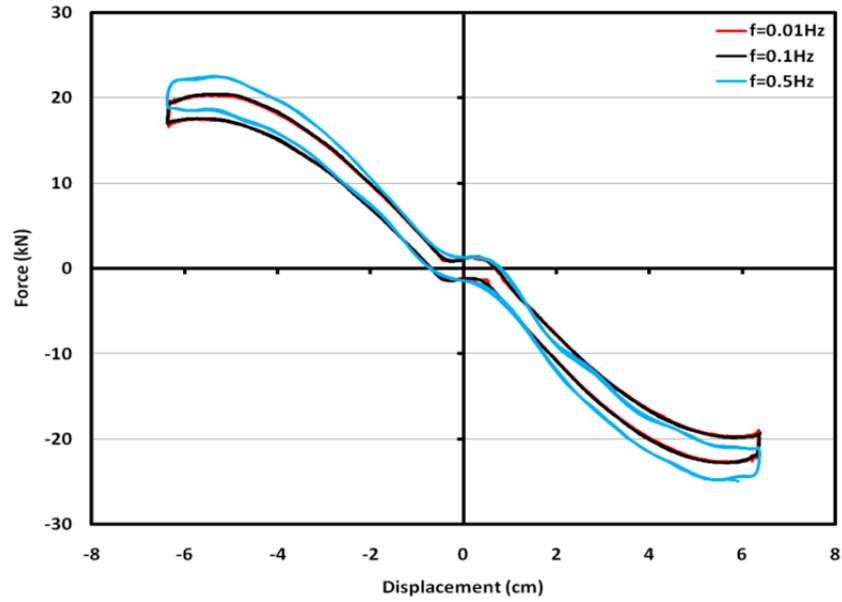
Figure 4.2. Hysteretic response of one of the NSDs from harmonic testing at three different frequencies
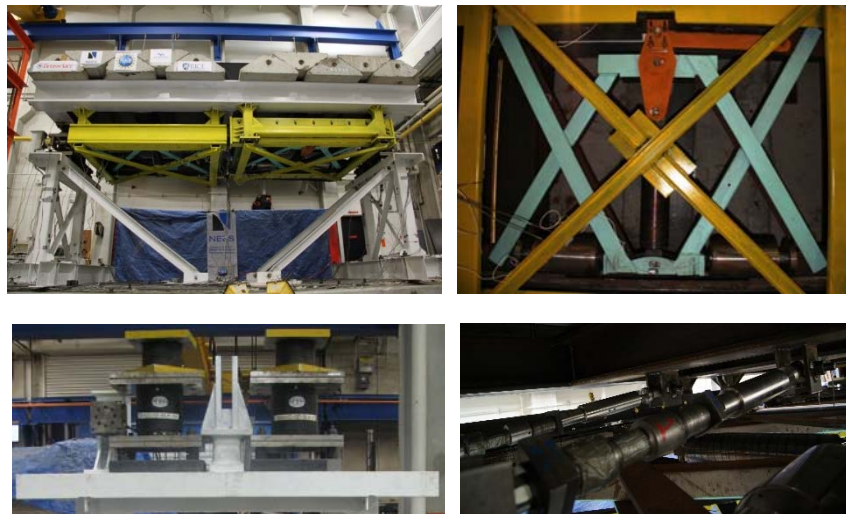
Figure 4.3. Bridge model and components used in some of the shake table tests (Top left: Bridge model with braced piers, Top right: NSD and its support system underneath the deck, Bottom left: Elastomeric bearings, Bottom right: Viscous dampers)

Table 4.1. Ground motions used in numerical simulations and experimental tests

No.	Earthquake	Record	Mw
1	Northridge, 1/17/1994	637-270	6.7
2	Loma Prieta, 10/18/1989	CAP-000	6.9
3	Cape Mendocino, 4/25/1992	PET-090	7.0
4	Kobe, 1/16/1995	KJM-000	6.9
5	Northridge, 1/17/1994	Sylmar-000	6.7
6	Landers, 6/28/1992	Yermo-000	7.3
7	Landers, 6/28/1992	Yermo-270	7.3

Typical damage that occurs in bridge structures subjected to earthquakes includes column failure and shear key failure (caused by the forces transferred from the deck to the piers) and deck collapse (falling off its supports) or damage to bearings and expansion joints (due to excessive displacement of the deck) (Chen and Duan, 2003). In addition, bridges that are seismically-isolated with elastomeric bearings may experience bearing damage due to excessive shear strain. Given the aforementioned types of damage, the performance of the bridge test specimen is evaluated herein based on two normalized response quantities (one related to peak forces and one related to peak deformations): 1) base shear coefficient (peak base shear normalized by weight of bridge model (173 kN) and 2) peak shear strain of the elastomeric bearings (displacement of bridge deck relative to the top of the piers normalized by total thickness of rubber in each bearing (5.7 cm). For each bridge configuration and for each ground motion, the measured base shear coefficient and bearing shear strain are shown in Figures 4.4 and 4.5, respectively. However, for the IB case, the isolation system was deemed to be highly vulnerable due to its low lateral stiffness combined with a small amount of damping. Furthermore, the piers of the bridge model were designed to yield at a base shear coefficient value of 0.5. Thus, for testing of the IB case, the KJM-000 and Sylmar-000 records were only run at a scaling of 50%. Therefore, the results shown in Figures 4.4 and 4.5 for these two records and the IB case are extrapolated from the values for the 50%-scaled motions. This allows for the comparison of different cases under a consistent level of ground shaking but with the understanding that in these particular cases, linear elastic behavior of the system is assumed to occur at levels of input larger than 50% of the full record.
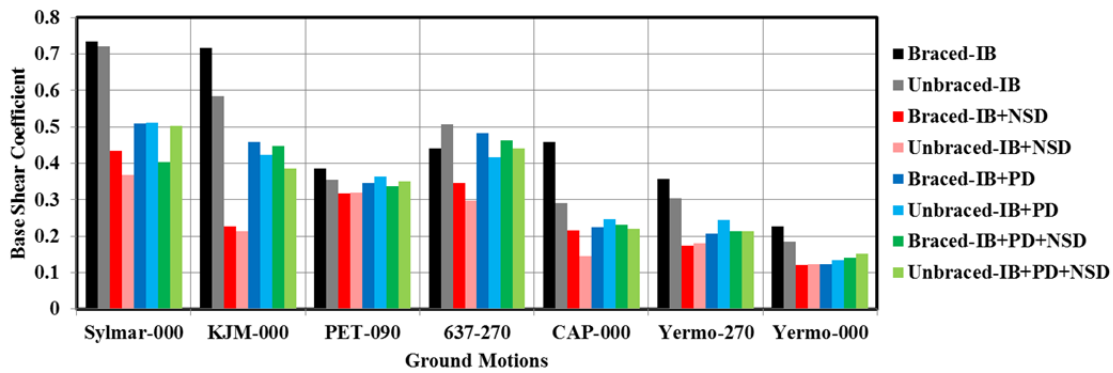
Figure 4.4. Base shear coefficient in bridge model with braced and unbraced piers for cases of isolated bridge (IB), isolated bridge with NSDs, isolated bridge with passive fluid viscous dampers (PD), and isolated bridge with NSDs and PDs for different ground motions
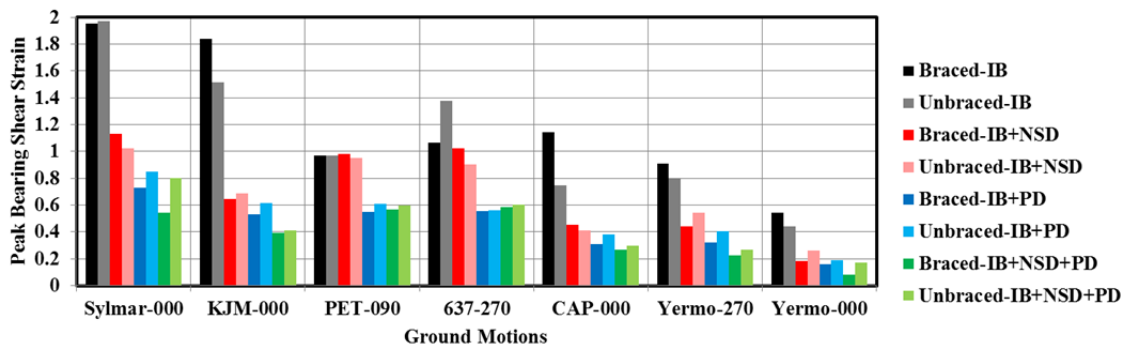
Figure 4.5. Peak bearing shear strain in bridge model with braced and unbraced piers for cases of isolated bridge (IB), isolated bridge with passive fluid viscous dampers (PD), and isolated bridge with NSDs and PDs for different ground motions

64

As shown in Figure 4.4 and 4.5, by adding NSDs to the IB case, the peak base shear coefficient and reduces substantially due to the development of a virtual yield point and a softening response beyond that yield point. Furthermore, the peak bearing shear strain reduces substantially due to friction damping that develops within the NSD itself and between the NSD and its support system. Similarly, as shown in Figure 4.5, the case with highest damping (IB+NSD+PD) exhibits the lowest peak bearing shear strain for most of the ground motions. In this case the combined system has two major sources of damping (viscous damping from the fluid dampers and friction damping from the NSDs and their supporting system), resulting in a system with high damping and thus low deformations. Comparing these two cases shows that the addition of PDs to the case of IB+NSD further decreases the deformations of the isolation system relative to the IB case (due to the high damping provided by the dampers) but increases the base shear force for almost all of the ground motions. Thus, the NSDs are primarily effective in limiting forces in the system while the viscous dampers are primarily effective in limiting deformations.

The hysteretic response of the bridge for the eight different bridge configurations is illustrated in Figures 4.6 and 4.7 for the KJM-000 and PET-090 ground motions, respectively. The KJM-000 ground motion is selected for presentation since, for this motion, the NSDs were most effective in reducing forces. The PET-090 motion was selected since the effect of the NSDs on the response of the bridge was very minor. Note that each of the four plots shown in Figure 4.6 are plotted to different scales so that the hysteresis loops are clearly visible along with their comparison between braced and unbraced cases.
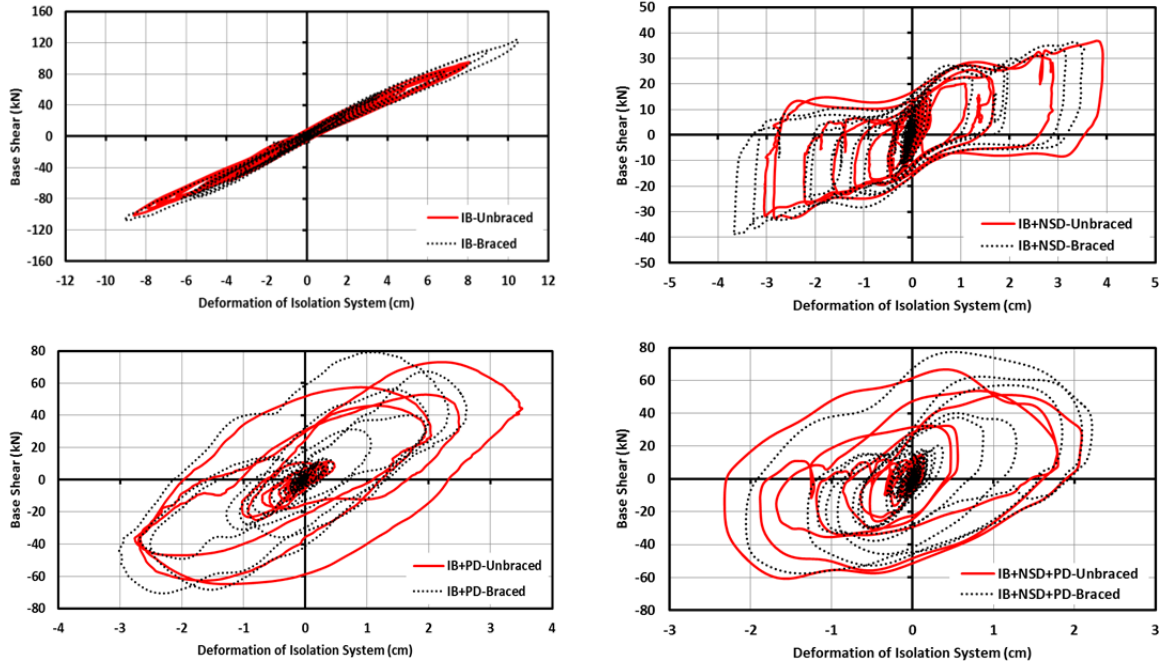
Figure 4.6. Hysteretic response of bridge model with braced and unbraced piers for the cases of IB, IB+NSD, IB+PD and IB+NSD+PD for KJM-000 ground motion
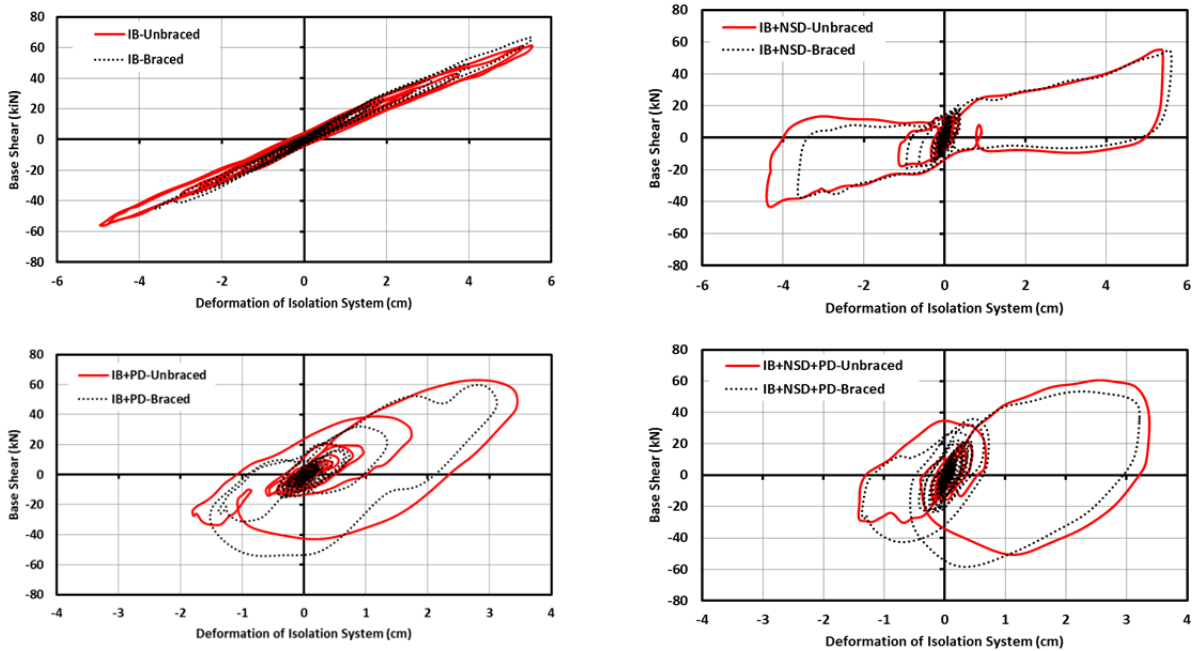
Figure 4.7. Hysteretic response of bridge model with braced and unbraced piers for the cases of IB, IB+NSD, IB+PD and IB+NSD+PD for PET-090 ground motion

As can be seen in Figures 4.6 and 4.7, for the case of IB+NSD, the hysteretic response indicates low stiffness combined with significant energy dissipation (large areas within hysteresis loops). The low stiffness is mainly due to the combination of the positive stiffness from the bearings and the negative stiffness from the NSDs and the energy dissipation is due to friction within the NSDs and their supporting system. Due to the nonlinear nature of the friction

66

effects, the width of the loop in the vertical direction increases as the displacement increases, resulting in an increase in force levels at the maximum displacement. The opposite behavior occurs for the case of IB+PD where the hysteresis loops indicate moderate stiffness combined with significant energy dissipation where the loops are wide at small displacements and narrow at large displacements. The moderate stiffness is due mainly to the positive stiffness of the bearings and the energy dissipation is due to the viscous damping. The variation in the shape of the loop is consistent with linear viscous damping (i.e., the viscous damping forces are 90 degrees out-of-phase with respect to the displacement of the isolation system). Combining the NSDs and PDs (IB+NSD +PD) results in hysteresis loops that are a combination of the two aforementioned cases (i.e., low stiffness combined with significant energy dissipation) wherein the loops are wide both at the extreme deformations and near zero deformation, thus providing significant energy dissipation per cycle.

A comparison of the hysteretic response of the bridge model with braced and unbraced piers for the KJM000 ground motion, and for the cases of IB, IB+NSD and IB+NDS+PD, is shown in Figure 4.8. This figure clearly demonstrates the effectiveness of the NSDs in reducing the stiffness, peak force and peak deformation with respect to the IB case. It is also provides a direct comparison between the hysteretic response of the system with NSDs and with viscous dampers, illustrating the fundamental difference between the effect of these protective devices on the response of the system (the NSDs and viscous dampers produce similar reductions in peak displacement but the NSDs are more effective in reducing peak force - the peak base shear of the IB+PD case is almost twice that of the IB+NSD case).
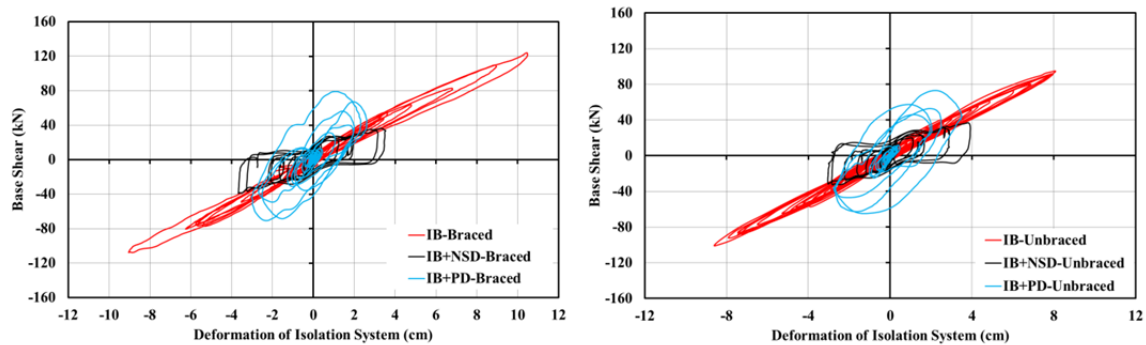
Figure 4.8. Comparison of hysteretic response of isolation system for cases of IB, IB+NSD and IB+PD for the bridge model with unbraced (left) and braced (right) piers for the KJM000 ground motion

As mentioned previously, for the PET090 ground motion, the NSDs are not able to improve the seismic performance of the structure. This is shown in Figure 4.9 via the hysteretic response of the bridge model for this particular ground motion. Although the NSDs result in a system with reduced effective stiffness and a virtual yield point, the characteristics of this ground motion (strong near-field velocity pulse) are such that the friction damping (which is not rate-dependent) provided by the NSDs is insufficient to control the deformation of the system, resulting in the NSDs passing through the negative stiffness region of their behavior and into the positive stiffness region (see Fig. 4.2 where the NSDs can be seen to begin developing positive tangent stiffness at approximately 6 cm of deformation). Since the NSDs and their support system provide significant friction damping, the hysteretic response of the bridge model with NSDs exhibits a large range of forces at large displacements, and thus the peak force is nearly as much as the IB case. For the case of IB+PD, since the viscous dampers are rate-dependent

67

devices and this particular motion exhibits a strong velocity pulse, the viscous dampers are very effective in reducing the peak deformation but, due to the associated large damping force, caused by high velocity motion, the dampers have a minor effect on the peak force of the system.
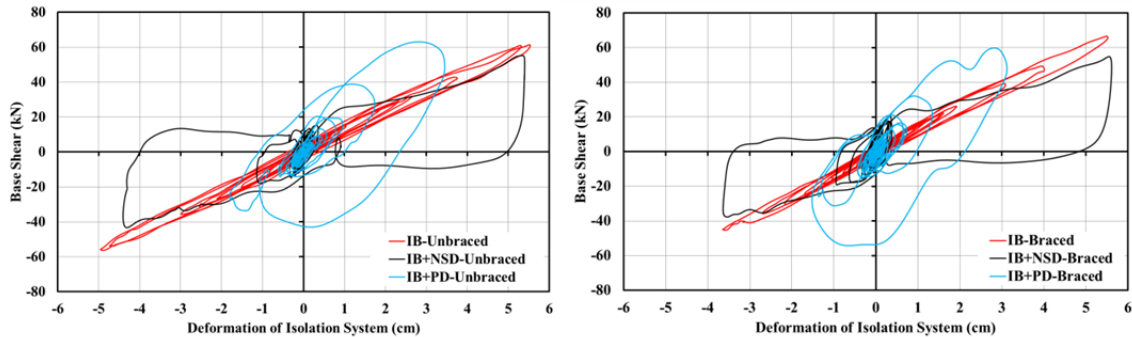
Figure 4.9. Comparison of hysteretic response of isolation system for cases of IB, IB+NSD and IB+PD for the bridge model with unbraced (left) and braced (right) piers for the PET090 ground motion

Since the behavior of the NSDs is displacement-dependent (see Fig. 4.2), it is expected that their effect on the response of the bridge model may depend on the intensity of the ground motion. To evaluate the influence of different levels of ground motion intensity on the effects of the NSDs, the ground motions were incremented during the test program. As one example, Figure 4.10 shows the hysteretic response of the bridge model with braced piers for the case of IB+NSD and for a range of intensities of the Sylmar ground motion. Since the hysteretic response of the IB case is almost linear, the IB case under 50% of the same motion is also shown in Figure 4.10 as a reference. As can be seen in Figure 4.10, one of the characteristics of the NSD assembly is that, due to friction, the hysteresis loops become wider (vertical width) as the intensity of the ground motion increases. This phenomenon can also be seen in Figure 4.11, which shows the hysteretic response of the NSDs for the case of IB+NSD with braced piers and for harmonic excitation at a frequency of 0.5 Hz (shake table motion is harmonic but NSD response exhibits a transient component during the first cycle, which is represented by the outermost loop in Figure 4.11, which is larger than the inner loops that are associated with steady-state response). To explain the increasing width of the hysteresis loops for increasing seismic intensity, a plan view of the bridge model, taken at the level of the NSDs and their support system, is shown in Figure 4.12. One side of each NSD is rigidly attached to the deck and the other side is supported by the deck (weight is supported by deck) but is attached to the piers through a sliding rail system. This railing system allows one side of the NSD to slide relative to the bridge deck and thus to develop shear deformation in the NSD. As the NSD deforms, a component of the forces developed within the NSDs acts along the direction of the rail while another component acts perpendicular to the contact surface of the rail. The perpendicular component represents a normal force that results in friction along the sliding surface of the rail. As the shearing deformation of the NSD increases, these force component increase and therefore friction force in the direction of the rail also increases. Thus, the width of the hysteresis loops increases as the shearing deformation increases (i.e., as the ground motion intensity increases).
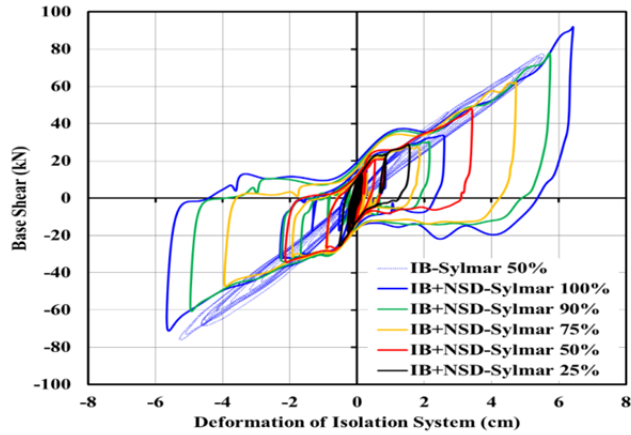
Figure 4.10. Hysteretic response of isolation system for the case of IB+NSD for the bridge model with braced piers for various intensities of the Sylmar ground motion in comparison with the case of IB for 50% of the same motion
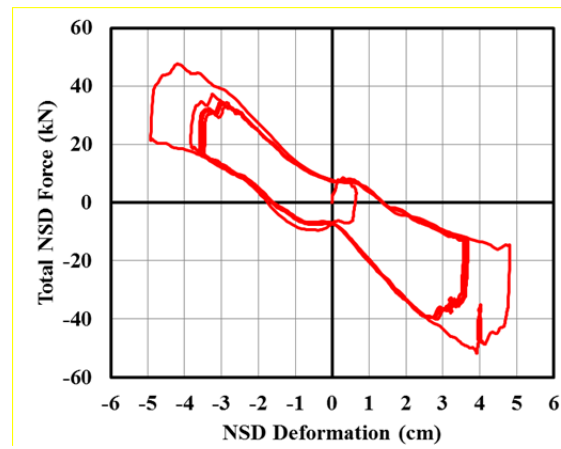
Figure 4.11. Hysteretic response of NSDs for the case of IB+NSD with braced piers and with harmonic excitation at a frequency of 0.5 Hz
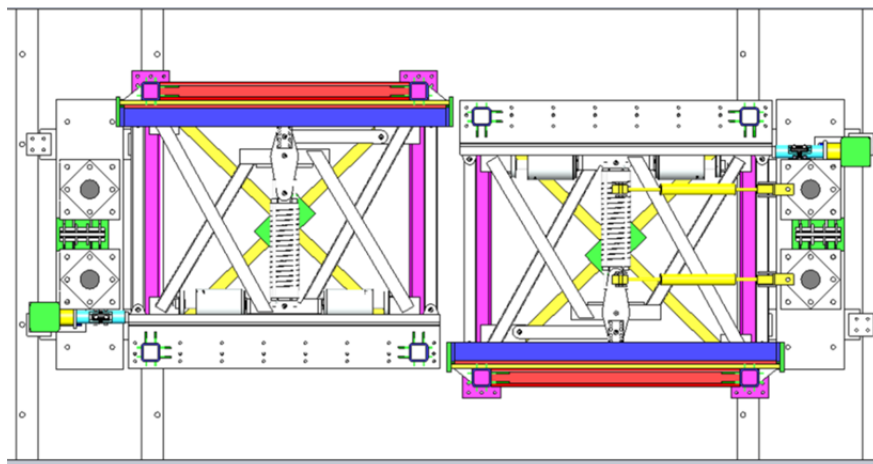
Figure 4.12. Plan view of bridge model at NSD level

The effectiveness of the NSDs for a range of ground motion intensities is illustrated in Figures 4.13 and 4.14 in terms of peak deck acceleration and peak isolation system deformation, respectively, for the cases of IB, IB+PD and IB+NSD and with either braced or unbraced piers. The KJM000 and PET090 ground motions are selected for Figures 4.13 and 4.14, respectively, since, for one of them (KJM000), the NSDs were shown to provide the maximum peak base shear reduction relative to the IB case (see Fig. 4.4) and, for the other (PET090), the NSDs had a minor effect on the peak base shear (see Fig. 4.4). For the Kobe earthquake, it can be seen in Figure 4.13 that both the forces (proportional to acceleration) and deformations increase approximately linearly with increasing intensity, indicating that the effectiveness of the NSDs in reducing accelerations and deformations does not change with the intensity of the motion. Furthermore, it is evident that, over the entire range of ground motion intensities considered, the NSDs were able to reduce forces much more than the viscous dampers and the NSDs were as effective as the viscous dampers in reducing the deformations of the isolation system. Finally, both the NSDs and viscous dampers are more effective in reducing forces and displacements for the case of the bridge model with braced piers as compared to that with unbraced piers, particularly for large ground motion intensities.
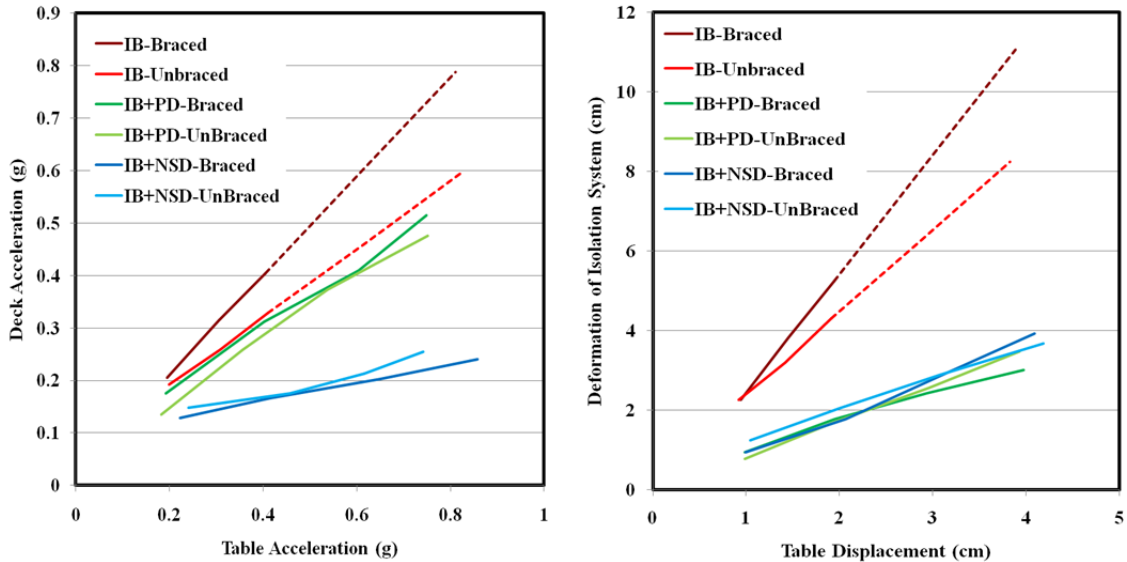
Figure 4.13. Effect of ground motion intensity (KJM000 record) on peak acceleration of bridge deck (left) and peak deformation of the isolation system (right)

For the case of the PET090 ground motion, the response for increasing seismic intensity is markedly different from that for the KJM000 ground motion. As shown in Figure 4.14, for the full range of seismic intensities, the viscous dampers have a relatively minor effect on the peak acceleration. Also, for the case of braced piers, the peak accelerations are increased relative to the IB case for nearly all of the intensities. However, as seen in Figure 4.14, the viscous dampers have a strong effect on the peak deformation over the full range of seismic intensities. On the other hand, for this particular ground motion, NSDs have minimal effect on accelerations at low intensities (since they have minimal engagement), reduce accelerations as the intensity increases, and then have reduced effectiveness at higher intensities. In addition, the effect of the NSDs on the peak deformations of the isolation system are relatively minor with their effect decreasing as the intensity of the motion increases.

70
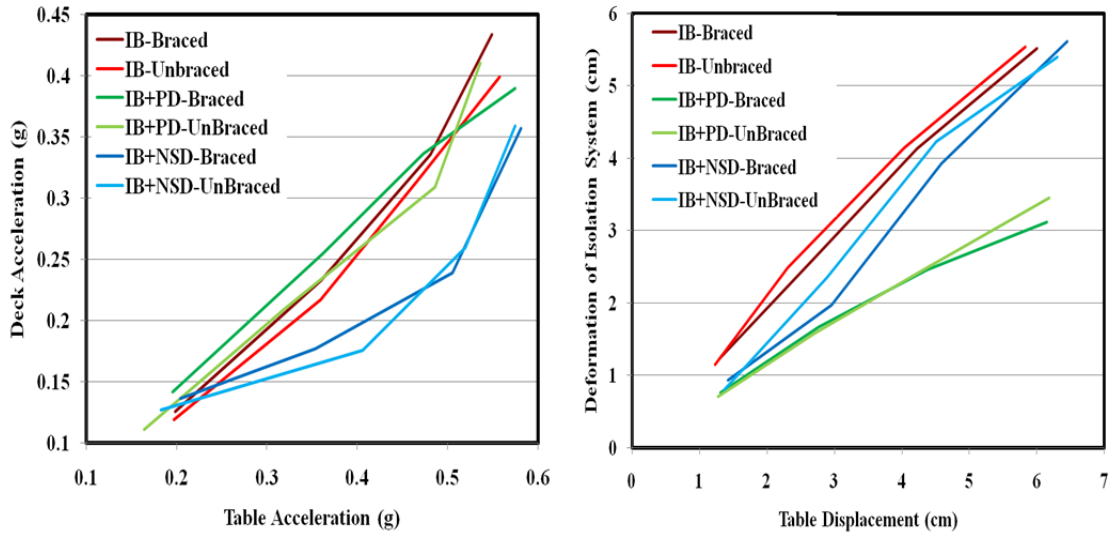
Figure 4.14. Effect of ground motion intensity (PET090 record) on peak acceleration of bridge deck (Left) and peak deformation of the isolation system (Right)

4.3 Evaluation of experimental results in frequency domain

As discussed above, the bridge model was tested for many different input motions and for different bridge/isolation system configurations. Among those input motions, sine sweeps and white noise signals were used for system identification. For the case of the bridge model with braced piers, the structure primarily behaves as a single-degree-of-freedom system with the degree of freedom being the deformation of the elastomeric bearings. Pseudo-static cyclic testing of the elastomeric bearings showed that the effective stiffness of the combination of four elastomeric bearings is approximately 1068 kN/m. With four bearings supporting the bridge deck and the deck weighing approximately 158 kN, the natural frequency for the case of braced piers is estimated to be 1.30 Hz. Experimental testing using a sine sweep input motion (0 - 5 Hz with amplitude of 1.78 cm.) indicated that the natural frequency was 1.32 Hz (see Fig. 4.15 which shows the Fourier amplitude of the deck acceleration). Thus, the estimated natural frequency is very close to the measured value and therefore the simplified SDOF representation of the structure is reasonable.

When the NSDs are added to the isolation system, it is expected that the acceleration of the deck, and thus the forces within the system, will decrease. However, the nonlinear behavior of the NSDs is such the bridge no longer exhibits any distinct natural frequencies (i.e., the natural frequency continuously changes based on the deformation at the isolation level). Therefore, a resonant condition cannot be achieved and thus distinct spikes in the Fourier amplitude spectrum are not expected. This behavior is clearly shown in the Fourier amplitude of the deck acceleration (normalized by the peak ground acceleration) (see Fig. 4.15) where the dominant spike for the linear case (isolated bridge deck) is completely absent in the nonlinear case (isolated bridge with NSDs). In Figure 4.15, the excitation is a sine sweep from 0.1-2.0 Hz with an amplitude of 0.508 cm for the IB case and 1.778 cm for the IB+NSD case.

71
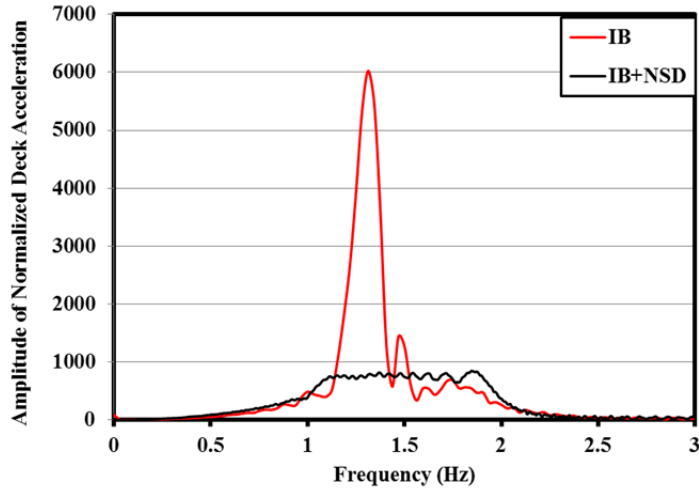
Figure 4.15. Fourier amplitude of deck acceleration (braced piers and cases of IB and IB+NSD)

4.4 Computational Model of Bridge Test Specimen

For conducting numerical simulations of the seismic response of the bridge test specimen for each of the configurations described previously, analytical models for each component of the bridge (bearings, viscous dampers, NSDs, and bridge piers) were developed and calibrated using data from cyclic tests.

Modeling of Bridge Piers

The bridge piers were modeled as linear elastic beam-column elements with properties based on data from fabrication drawings and the work of Tsopolas et al. (1994) wherein the same bridge piers were used in seismic testing.

Modeling of Elastomeric Bearings

The behavior of the elastomeric bearings can be simulated using a variety of models of varying complexity. As described in chapter two, the bearings are made of natural rubber of grade 5 and Shore durometer Type A hardness of 50. The effective shear stiffness of each of the bearings can be determined as follows (Naeim and Kelly, 1999):

$$K_{eff} = \frac{G A_r}{T_r}$$

(4.1)

where G is the shear modulus of the rubber, A_r is the bonded rubber area and T_r is the total rubber thickness. Assuming a typical shear modulus of 0.7 MPa for this type of material and using the known total rubber thickness and bonded area (5.7 cm and 243 cm^2, respectively), the effective shear stiffness of each bearing is calculated to be 2.98 kN/cm.

One simple model of the bearings employs a linear spring in parallel with a linear viscous dashpot wherein the aforementioned effective stiffness defines the properties of the linear spring and an equivalent viscous damping ratio is used to account for the effect of the dashpot. Another approach is to utilize a linear spring (having the aforementioned effective stiffness) in parallel with an elasto-plastic element to account for energy dissipation. Such models may be adequate

72

for capturing the global behavior of the bearings. However, experimental cyclic testing of the bearings showed that the bearing stiffness reduces at displacements larger than about 2.5 cm (exact value is different for each bearing) and then increases at displacements larger than about 5 cm (these values correspond to rubber shear strains of about 50% and 100%, respectively) (see Fig. 4.16).
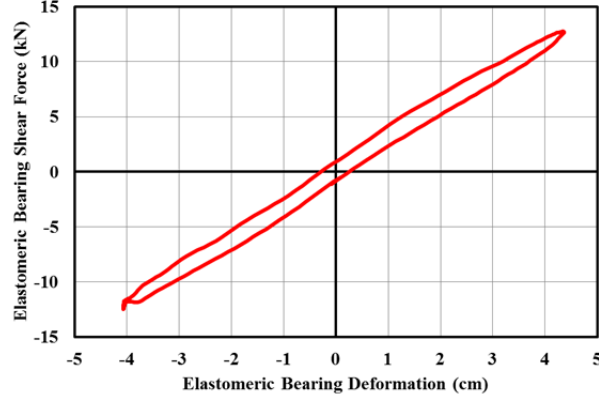
Figure 4.16. Hysteretic response of elastomeric bearings subjected to harmonic motion

To account for the displacement-dependencies of the bearings, two additional elements can be added in parallel with the aforementioned spring and elasto-plastic elements (Sarlis et al. 2013) (see Fig. 4.17). These two elements have a dead zone at small displacements. Beyond some displacement, one of the elements exhibits negative stiffness, thus generating a softening behavior. Increasing the displacement further engages the second element, which exhibits positive stiffness, thus generating hardening behavior. Combining these four elements together results in hysteretic behavior that captures well the behavior of the bearings (see Fig. 4.18). Sarlis et al. (2013) used such a method for modeling the same elastomeric bearings that were utilized in testing of the bridge model and thus the same model parameter values obtained by Sarlis et al. (2013), via cyclic testing and an associated model calibration process, are used herein (see Table 4.2). The resulting prediction of the hysteretic response of the bearing under harmonic loading conditions compares well with experimental test data (see Fig. 4.18).

Modeling of Negative Stiffness Devices
The basic behavior of the NSDs can be simulated using the following nonlinear elastic force-displacement relation as defined in chapter two (and obtained using the free-body diagrams shown in Fig. 4.19):

$$F_{NSD} = -F_S \left(\frac{L_1}{L_2} \right) \left(2 + \frac{L_2}{L_1} + \frac{L_p + L_1}{\sqrt{L_2^2 - u^2}} \right) + F_g \tag{4.2}$$

where L_p is the initial length of the main spring, L_1 and L_2 are the lengths of the two sides of the pivot plate, u is the shear deformation of the NSD, and F_s is the force in the pre-compressed main spring as given by

$$F_S = \left(\frac{F_{pc} + K_s L_p}{L_s} - K_s \right) u \tag{4.3}$$

where F_{pc} is the initial force in the pre-compressed main spring, K_s is the stiffness of the main spring and L_s is the length of the deformed shape of the main spring. The force F_g is the force in the gap-spring assembly and is given by

$$F_g = \begin{cases} k_{stiff}\, u & |u| < d_g \\ \left[F_{comp} + \dfrac{k_{stiff}\, k_{soft}}{k_{stiff} + k_{soft}}\left(|u| - d_g\right)\right]\mathrm{sgn}\left(u\right) & |u| > d_g \end{cases} \tag{4.4}$$

where k_{stiff} is the stiffness of the outer spring of the GSA (stiffer spring), k_{soft} is the stiffness of the inner spring of the GSA (softer spring), d_g is the amount of shear deformation of the negative stiffness device prior to initiation of global negative stiffness behavior (i.e., the combined effect of the GSAs and the main spring produces negative stiffness for displacements larger than d_g), F_{comp} is the pre-compressed force in the soft spring (which prevents its engagement until the displacement d_g is reached), and the signum function returns the sign of the displacement.
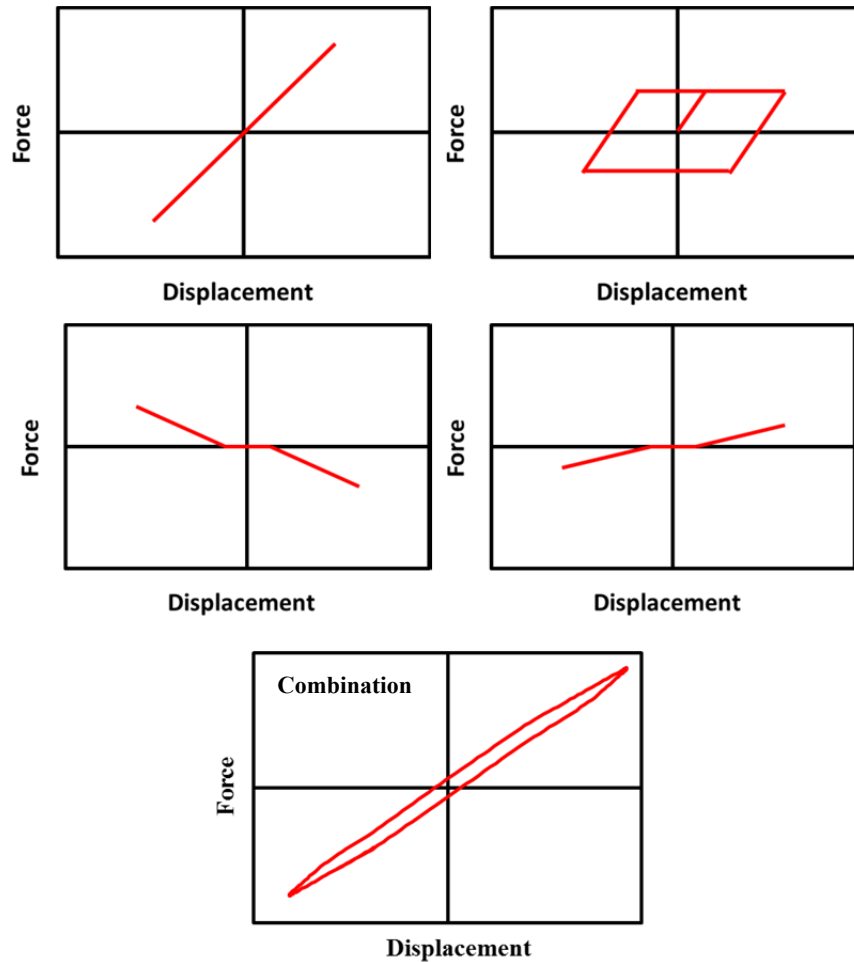
Figure 4.17. Force-Displacement relations for components used to model elastomeric bearings and resultant hysteresis loop

74
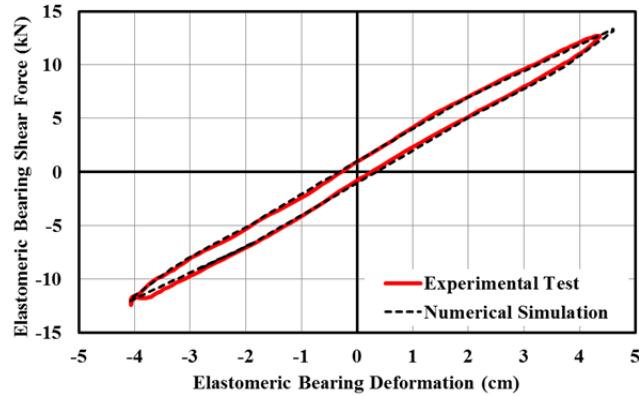
Figure 4.18. Simulated hysteretic response of elastomeric bearings overlaid with corresponding experimental test data

Table 4.2. Values of parameters used to define hysteretic response of each elastomeric bearing

Element	Parameter	Bearing			
		1	2	3	4
Linear Spring	Effective stiffness (kN/cm)	2.87	3	3.08	3.15
Wen-Bilinear	Elastic Stiffness (kN/cm)	1.52	1.52	1.52	1.52
	Yield Force (kN)	1.35	1.43	2.32	1.29
Softening Element	Starting Displacement (cm)	2.36	1.6	1.37	1.83
	Added Negative Stiffness (kN/cm)	-0.51	-0.53	-0.65	-0.56
Hardening Element	Starting Displacement (cm)	5.56	5.84	6.1	5.72
	Added Positive Stiffness (kN/cm)	0.58	0.39	1.24	0.77
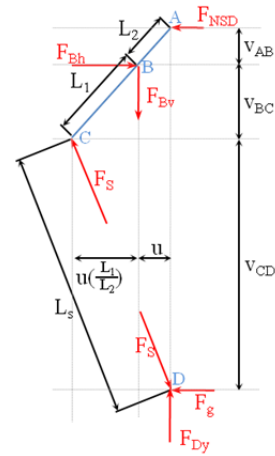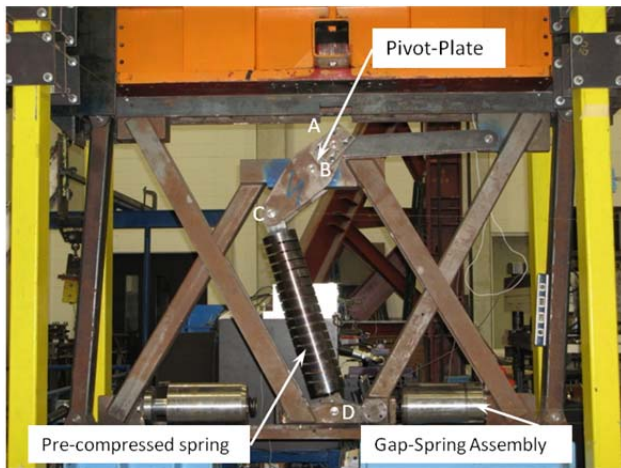
Figure 4.19. Prototype NSD undergoing cyclic testing and free-body diagrams for evaluation of lateral force

Since the design of the NSDs was modified for application to the bridge model, cyclic testing of the re-designed NSDs was performed to determine their properties. The cyclic tests (harmonic motion over a range of amplitudes and frequencies) were conducted at the University at Buffalo using a load frame that could impose shearing deformation to the NSD. Using the

cyclic test data, values of the parameters that define the device behavior can be calibrated by overlaying the backbone curve of the experimental data on the analytical solution. Performing this calibration resulted in the parameter values shown in Table 4.3.

Table 4.3. Values of parameters used to define NSD behavior

Parameter	Values
Distance from spring pin to fixed pin (L_1)	0.254 m
Distance from lever pin to fixed pin (L_2)	0.127 m
Initial length of main spring (L_p)	0.762 m
Stiffness of main spring (K_s)	140 kN/m
Preload of main spring (F_{pc})*	21.13 kN
NSD engagement displacement (d_g)	0.5 cm
Stiffness of soft spring (K_{soft})*	6.59 kN/m
Stiffness of stiff spring (K_{stiff})*	491.2 kN/m
Pre-compressed force of soft spring (F_{comp})	2.8 kN

* Parameters used for calibration (other parameters are measured or nominal values)

As an example of the predictive capability of the model, Figure 4.20 shows the response of the NSD under cyclic loading conditions (using the analytical model for one of the NSDs where calibration was performed using three of the parameters shown in Table 4.3). As can be seen, the experimental data is influenced by the presence of friction in the device (discussed below). In Figure 4.20, the friction effect is removed in an approximate way by taking the average of the test data. This average data compares very well with the nonlinear elastic analytical model, suggesting that the basic behavior of the NSD is modeled well by the analytical model.
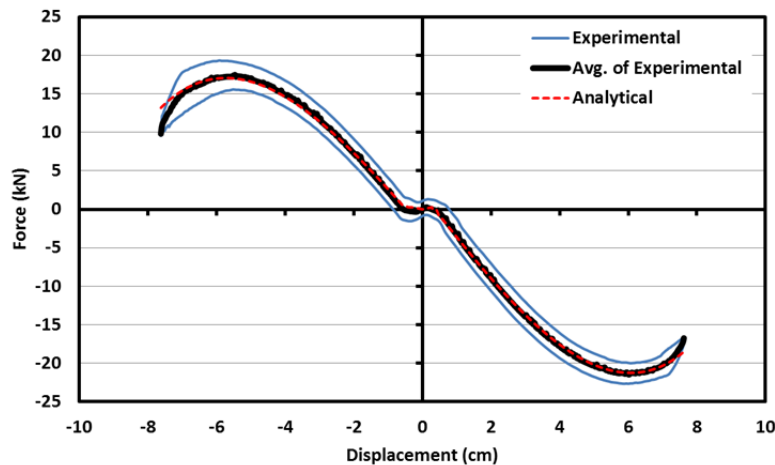
Figure 4.20. Comparison of predicted response and experimental test data

Since the NSDs are mechanical devices that are constructed of steel, friction develops at any sliding interfaces. In addition, when the NSDs are placed inside the support system that is attached to the underside of the bridge deck, additional friction forces develop due to sliding between the NSDs and the sliding rail of the support system. Figure 4.21 shows a comparison of the hysteretic response of one of the NSDs within the bridge model and the same device within

the load frame for a harmonic motion at the same frequency; the additional damping from the NSD support system is evident.
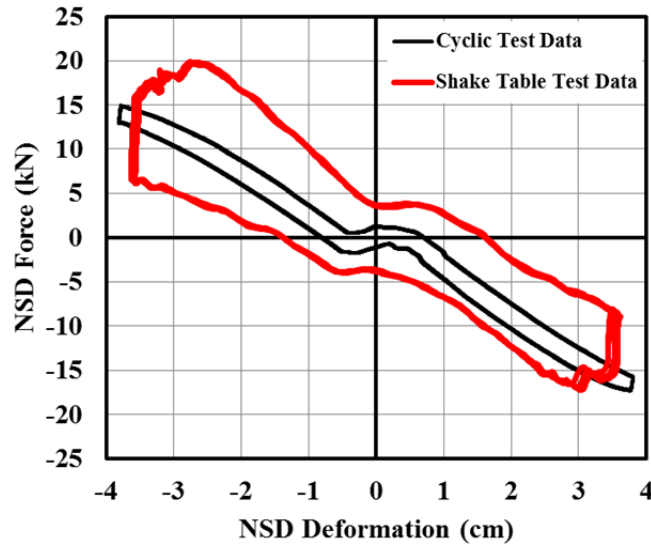
Figure 4.21. Comparison of hysteretic response of in-situ NSD (North) and NSD in load frame for harmonic motion at a frequency of 0.5 Hz

The additional friction forces in the NSD's arise from sliding at two different interfaces. As shown in Figure 4.22, the railing system included two types of roller plates, ones that were horizontal and thus allowed sliding on horizontal surfaces, and ones that were vertical and thus allowed sliding on vertical surfaces. The normal force on the horizontal roller plates is equal to a portion of the weight of the NSDs and thus the friction force at the associated horizontal surfaces is constant and therefore can be modeled with the aforementioned elasto-plastic element with high elastic stiffness (i.e., an equivalent Coulomb friction element). For small NSD deformations, there are no normal forces on the vertical roller plates and thus the friction force is zero. As the NSD deformations increase, the sliding rail comes into contact with the vertical roller plates and thus normal forces develop. These normal forces continue to increase as the NSD shearing deformation increases, thereby increasing the friction forces. Thus, an additional element is needed in which friction increases with displacement. Such an element is common in mechanical devices that have frictional components (as an example, such a model has been used by Nagarajaiah et al. (1991) to capture the behavior of frictional isolators in which the normal force on the contact surface is variable).
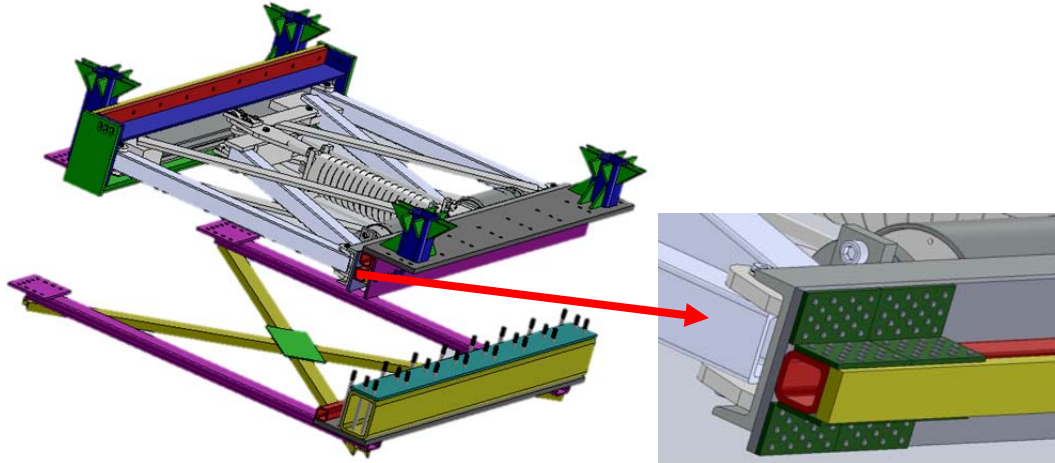
Figure 4.22. Details of NSD support system and close-up view of rail and rollers

The three sources of friction (one from internal friction in the NSD and two from the interaction of the NSD with its support system) were modeled using a combination of two elasto-plastic elements with zero post-yield stiffness (Coulomb friction elements) and one variable friction element. The friction force associated with internal friction in the NSD is defined by

$$F_1 = \alpha_1 \, sgn\left(\dot{u}\right) \tag{4.5}$$

and the friction force associated with interaction between the NSD and its support system is given by

$$F_2 = \alpha_2 \, sgn\left(\dot{u}\right) \tag{4.6}$$

where α_1 is the magnitude of the friction force generated within the NSD (measured from cyclic testing of the NSD alone; see Fig. 4.20) and α_2 is the magnitude of the friction force due to interaction between the NSD and its support system (measured from cyclic testing of the NSD and support system within the bridge model; see Fig. 4.21 where force near zero displacement was utilized). The friction force associated with the variable friction element (having a friction force magnitude proportional to displacement) is defined by

$$F_3 = \beta |u| \, sgn\left(\dot{u}\right) \tag{4.7}$$

where β is the magnitude of the slope of the hysteresis loop (measured from cyclic testing of the NSD and support system within the bridge model; see Fig. 4.21 where forces over a range of displacements was utilized). In all three cases, the signum function returns the sign of the velocity. The values of the aforementioned parameters are provided in Table 4.4 where the values correspond to a single NSD.

Table 4.4. Values of parameters used to define friction forces of the NSD and supporting system

Parameter	Value
α_1	1 kN
α_2	3 kN
β	1.1 kN/cm

The final model of each of the NSD's consists of four elements (see Fig. 4.23); a nonlinear elastic element (from Eq. 4.2), two Coulomb friction elements (from Eq. 4.5 and 4.6), and a variable friction element with displacement-dependent friction (from Eq. 4.7). The resultant NSD force, including the effects of friction, is given by:

$$F_{NSD}^F = F_{NSD} + F_1 + F_2 + F_3 = -F_S \left(\frac{L_1}{L_2} \right) \left(2 + \frac{L_2}{L_1} + \frac{L_p + L_1}{\sqrt{L_2^2 - u^2}} \right) + F_g + \alpha_1\, sgn(\dot{u}) + \alpha_2\, sgn(\dot{u}) + \beta|u|sgn(\dot{u}) \quad (4.8)$$

where all parameters have been defined previously. A comparison of the predicted hysteretic response with experimental test data for harmonic loading conditions is shown in Figure 4.24 where it can be seen that the model provides a good reproduction of the experimental data.

Modeling of Fluid Viscous Dampers
The hysteretic response of the fluid dampers under cyclic loading (see Fig. 4.25) reveals that the dampers primarily provide energy dissipation but also provide some stiffness. Thus, the dampers were modeled as linear viscous damper elements in parallel with linear elastic spring elements (Kelvin model of viscoelasticity). The damping coefficient of the linear damper elements was determined from system identification test data (direct measurement of the damper force and displacement) from harmonic shake table tests for the case of IB+PD (e.g., see Fig. 4.25). The resulting damping coefficient of the viscous damper element was 0.60 kN-s/cm (value specified by manufacturer was 0.63 kN-s/cm) and the resulting stiffness of the spring element was 1.0 kN/cm. Note that two fluid dampers were used in the bridge model testing and thus two viscous damper elements and two linear spring elements were used in the model for numerical simulations. A comparison of the predicted hysteretic response with experimental test data for harmonic loading conditions is shown in Figure 4.26 where it can be seen that the model provides good reproduction of the experimental data.
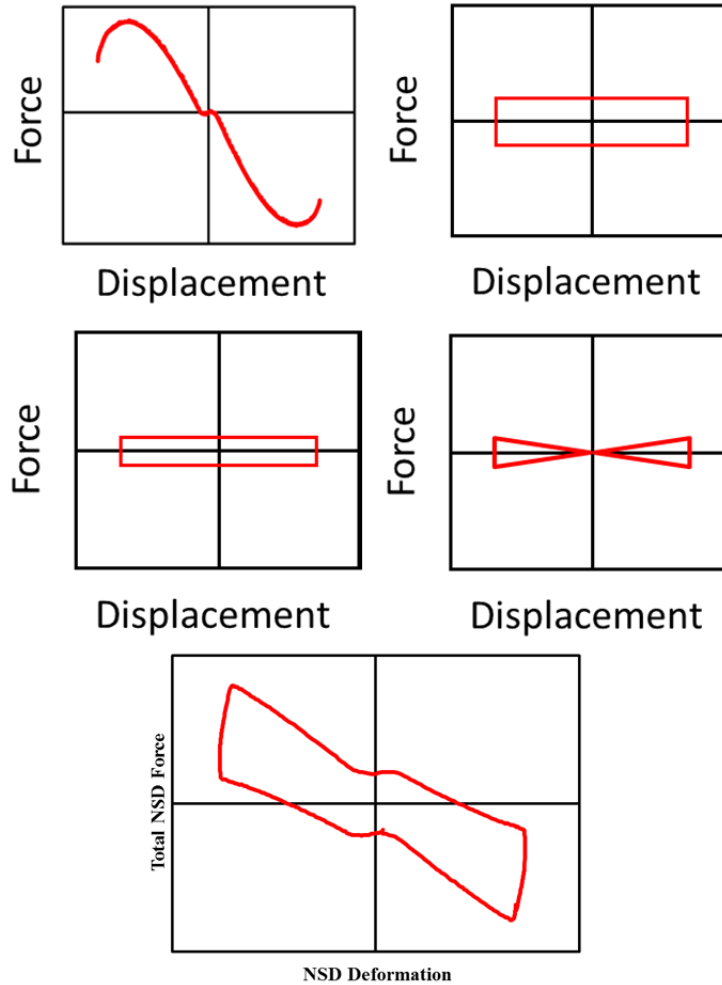
Figure 4.23. Force-displacement relation for four elements used to simulate the behavior of the NSDs and the resultant hysteresis loop
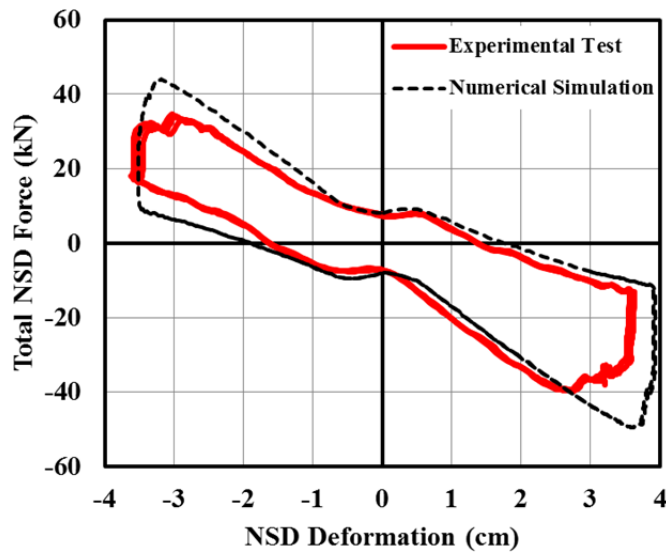
Figure 4.24. Comparison of predicted and measured hysteretic response of the NSDs for the bridge with braced piers (IB + NSD case) and subjected to harmonic ground motion (frequency of 0.5 Hz and amplitude of 4.5 in.)
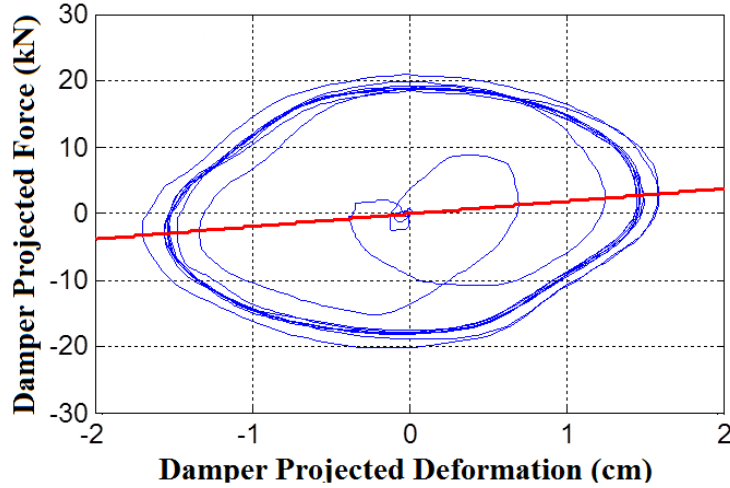
Figure 4.25. Hysteretic response (combined force from two dampers) for bridge with braced piers (IB + PD case) subjected to harmonic ground motion (frequency of 1.7 Hz and amplitude of 1.27 cm)
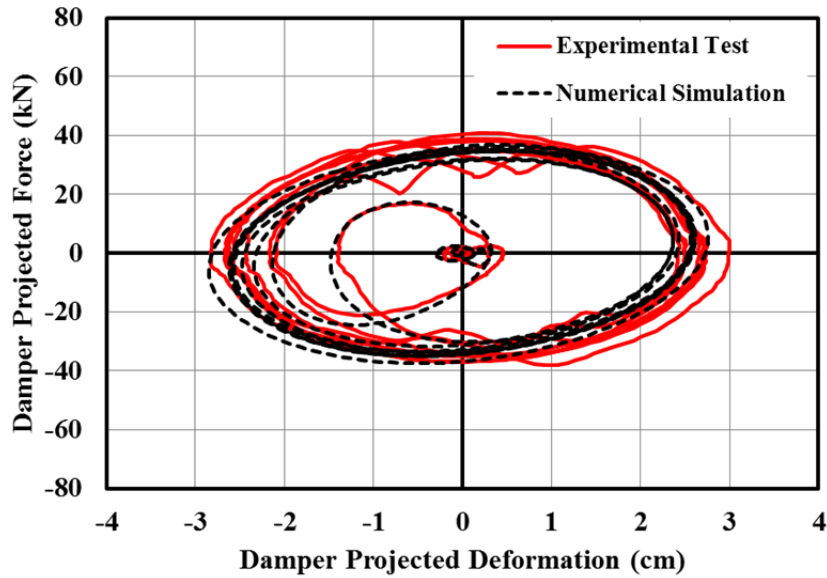
Figure 4.26. Comparison of predicted and measured hysteretic response of viscous dampers for the bridge with braced piers (IB + PD case) and subjected to harmonic ground motion (frequency of 1.7 Hz and amplitude of 2.54 cm)

Equation of Motion for Bridge Model

Using the analytical models described above for each component of the bridge model, the equation of motion may be written as

$$[M]\{\ddot{u}\} + [C]\{\dot{u}\} + [K]\{u\} + \{f(u,\dot{u})\} = -[M]\{l\}\ddot{u}_g(t) \tag{4.9}$$

where $[M]$ is the mass matrix, $[C]$ is the damping matrix associated with inherent damping in the bridge (Rayleigh damping model used with 2% damping in the first and second modes), $[K]$ is the elastic stiffness matrix associated with the bridge piers and deck, $\{u\}, \{\dot{u}\}$ and $\{\ddot{u}\}$ are the displacement, velocity and acceleration vectors along the degrees of freedom, $\ddot{u}_g$ is the

81

horizontal ground acceleration (acceleration of shake table) and $\{l\}$ is the ground motion influence vector. The forces within the isolation system are defined by

$$\{f(u,\dot{u})\} = \{f_{EB}(u,\dot{u})\} + \{f_{PD}(u,\dot{u})\} + \{f_{NSD}(u,\dot{u})\} \tag{4.10}$$

where $\{f_{EB}(u,\dot{u})\}$ is the elastomeric bearing force vector, $\{f_{PD}(u,\dot{u})\}$ is the viscous damper force vector and $\{f_{NSD}(u,\dot{u})\}$ is the NSD force vector. The velocity dependence of the isolation system forces is associated with either a dependence on the velocity itself or its sign.

4.5 Numerical predictions of seismic test results

The analytical model of the bridge test specimen was used to develop a finite-element model of the bridge using the software SAP2000. The bridge deck was modeled as a system of beam elements supporting concrete slabs, the piers were modeled as linear elastic beam-column elements, the viscous dampers were modeled as linear link elements (linear elastic spring element in parallel with linear viscous damping element), the elastomeric bearings were modeled as a combination of four link elements in parallel (one linear elastic element, one elasto-plastic element, and two dead-zone elements), and the NSDs were modeled as four link elements in parallel (one nonlinear elastic element, two Coulomb friction elements, and one variable friction element). The computational model of the bridge test specimen was used to conduct various numerical simulations to predict the response of the bridge under dynamic loading conditions.

Prior to fabrication of the bridge model, a series of preliminary numerical simulations were performed wherein the design properties of each bridge component were utilized to define the values of various parameters. These simulations were conducted to estimate the response of the bridge model for each configuration that was to be tested on the shaking table. The complete bridge test specimen was then mounted on the seismic shaking table and system identification tests were performed to verify the properties of each component when installed within the bridge model. These tests revealed that there was a need to update the models of each component (particularly the need to include friction damping associated with the NSDs and their support system). Thus, the numerical simulations were repeated to provide final predictions of the bridge response for the pending seismic tests.

An evaluation of the ability of the numerical model (finite-element model using parameter values obtained from system identification tests) to simulate the seismic response of the test specimen is presented below for seismic loading corresponding to the PET090 ground motion (selected due to its unique effects on the bridge). In Figure 4.27, a comparison of experimental results and numerical simulations is provided for the case of IB with both braced and unbraced piers and for 100% of the PET090 ground motion. The responses are presented both in the force-displacement plane (hysteretic response) and as a force response-history. In spite of the moderately complex behavior of the isolation bearings, the predictions match well with the experimental data.
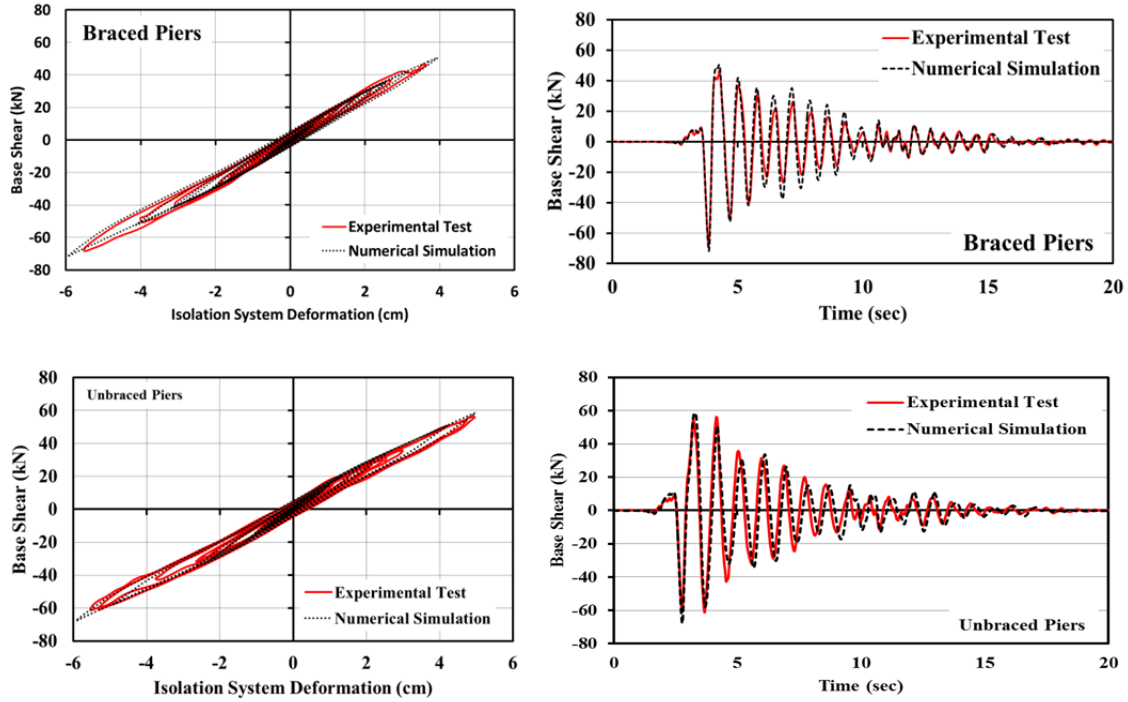
Figure 4.27. Experimental results and numerical simulations of bridge model for the case of IB with braced (top) and unbraced (bottom) piers for 100% of PET090 ground motion

As described previously, for numerical modeling of the behavior of each of the NSDs, four elements were used in parallel. These components are combined to obtain the numerically computed hysteretic response of the isolation system. As an example, the hysteretic response along with the base shear response-history for the IB +NSD case of the bridge model with braced piers and subjected to the PET090 ground motion is shown in Figure 4.28 (top plots). The case with unbraced piers is shown in the bottom plots of Figure 4.28. As can be seen in Figure 4.28, in spite of the strong nonlinearities in the numerical model, the model is able to predict the experimental results with high fidelity (peak forces are accurately predicted; peak deformation from numerical simulations is somewhat larger than from experimental data). Figure 4.29 shows the same type of results for the case of IB+PD. Again, it can be seen that the numerical model provides a very good prediction of the experimental test results.
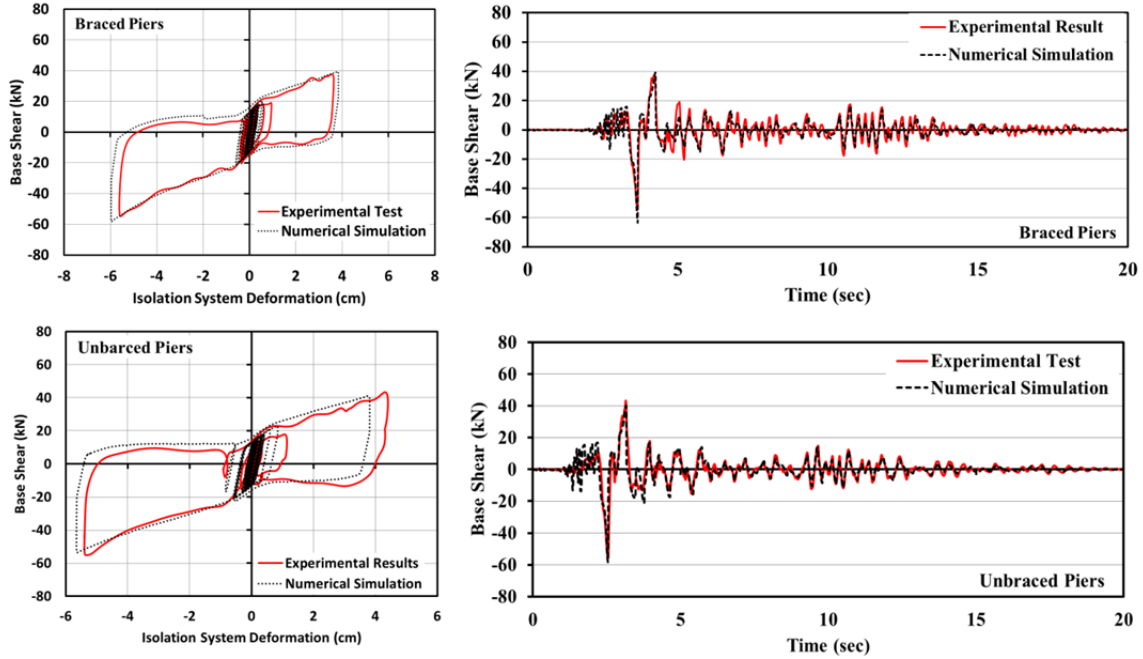
Figure 4.28. Experimental results and numerical simulations of bridge model for the case of IB+NSD with braced (top) and unbraced (bottom) piers for 100% of PET090 ground motion
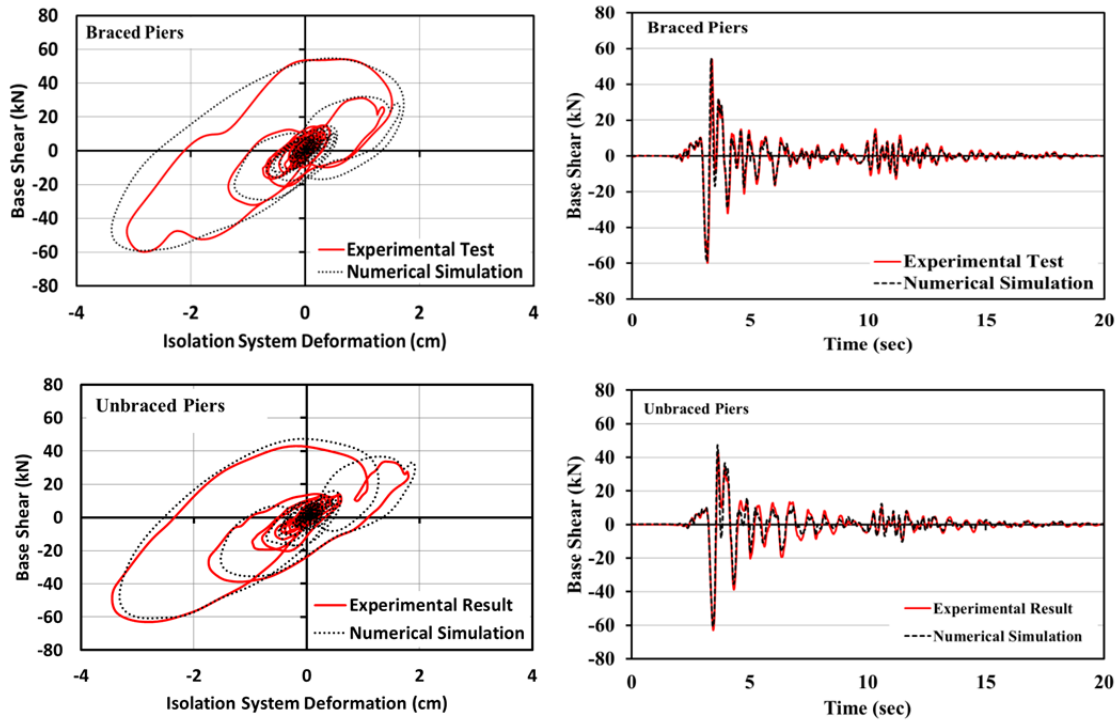
Figure 4.29. Experimental results and numerical simulations of bridge model for the case of IB+PD with braced (top) and unbraced (bottom) piers for 100% of PET090 ground motion

4.6 Performance measures

To systematically evaluate the effectiveness of the NSDs, the following Performance Measures (PM) (Reigles and Symans, 2005) are defined (provide comparisons of the force and displacement response of the system with NSDs relative to that without the NSDs (subscript 1 below) and relative to that with viscous dampers (subscript 2 below)):

$$PM_{V1} = \frac{Max\,|V^{IB+NSD}(t)|}{Max\,|V^{IB}(t)|} \tag{4.11}$$

$$PM_{V2} = \frac{Max\,|V^{IB+NSD}(t)|}{Max\,|V^{IB+PD}(t)|} \tag{4.12}$$

$$PM_{D1} = \frac{Max\,|D^{IB+NSD}(t)|}{Max\,|D^{IB}(t)|} \tag{4.13}$$

$$PM_{D2} = \frac{Max\,|D^{IB+NSD}(t)|}{Max\,|D^{IB+PD}(t)|} \tag{4.14}$$

where $Max\,|V^{IB}(t)|$, $Max\,|V^{IB+NSD}(t)|$ and $Max\,|V^{IB+PD}(t)|$ are the peak base shear for the cases of IB, IB+NSD, and IB+PD, respectively and $Max\,|D^{IB}(t)|$, $Max\,|D^{IB+NSD}(t)|$, and $Max\,|D^{IB+PD}(t)|$ are the peak shear deformation of the isolation system for the cases of IB, IB+NSD, and IB+PD, respectively.

A summary of the PM values for each ground motion is shown in Figure 4.30 and 4.31. Note that a PM value smaller than unity indicates that the NSDs were effective in reducing a particular response quantity. As expected, the effect of the NSDs is to reduce the shear forces for all cases with respect to the isolation system without the NSDs and also with respect to the case with viscous dampers. In general, the NSDs are more effective in reducing the response of the bridge model with braced piers (since they are reacting against rigid abutments rather than flexible piers). Due to the friction that develops within the NSDs and their support system, the NSDs were effective in reducing the displacements relative to the system without NSDs but were not as effective as the viscous dampers.
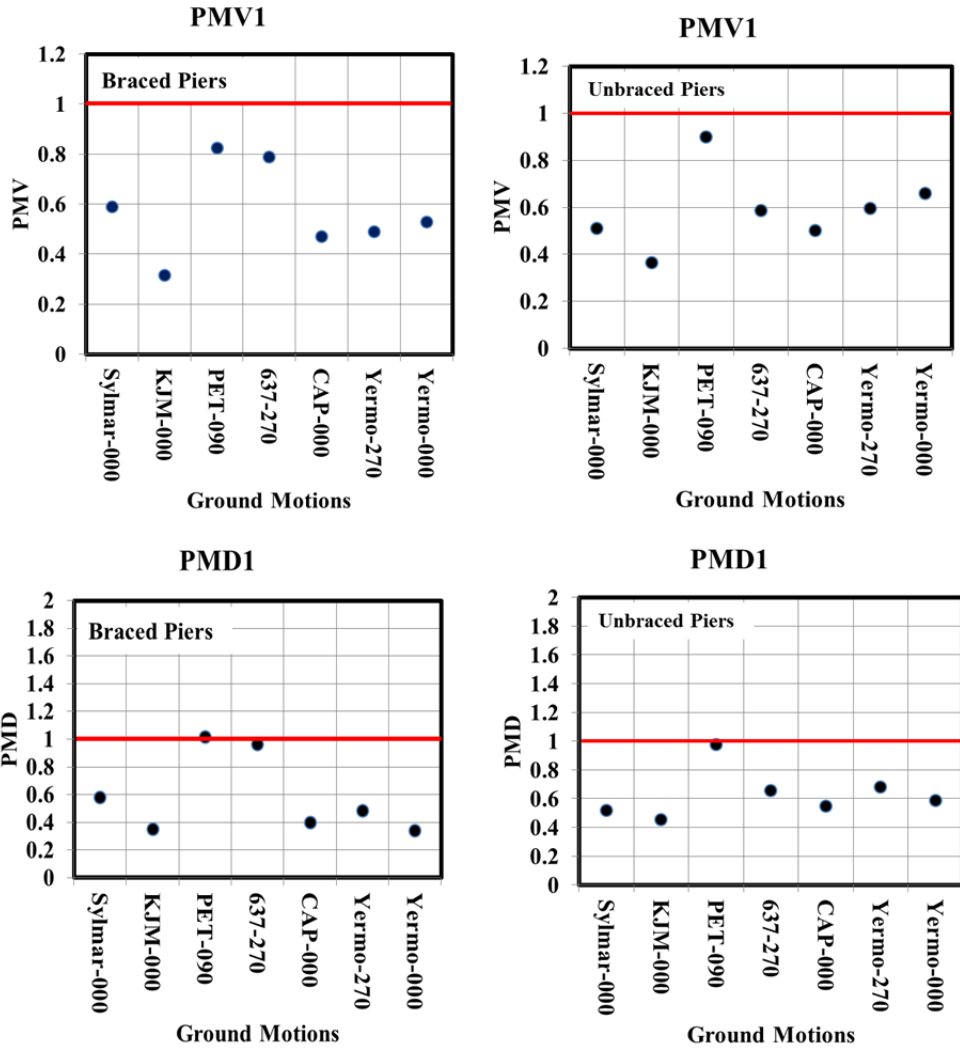
Figure 4.30. Evaluation of performance of bridge model with NSDs relative to that without NSDs for various ground motions and with braced (left) and unbraced (right) piers

Figure 4.31. Evalution of performance of bridge model with NSDs relative to that with viscous damper for various ground motions and for braced (left) and unbraced (right) piers

In general, it is difficult to simultaneously reduce forces and displacements in an isolated bridge structure. As a means of illustrating the effectiveness of the various isolation systems in simultaneously reducing both of these quantities, the shear force and displacement performance measures can be combined in a single plot (see Fig. 4.32). In such a plot, the best systems are those, which remain under unity for both axes. As shown in Figure 4.32, for both the cases of braced and unbraced piers, the NSDs simultaneously reduced the forces and the displacements in the structure relative to the case without the NSDs but increased the displacements relative to the case with viscous dampers.
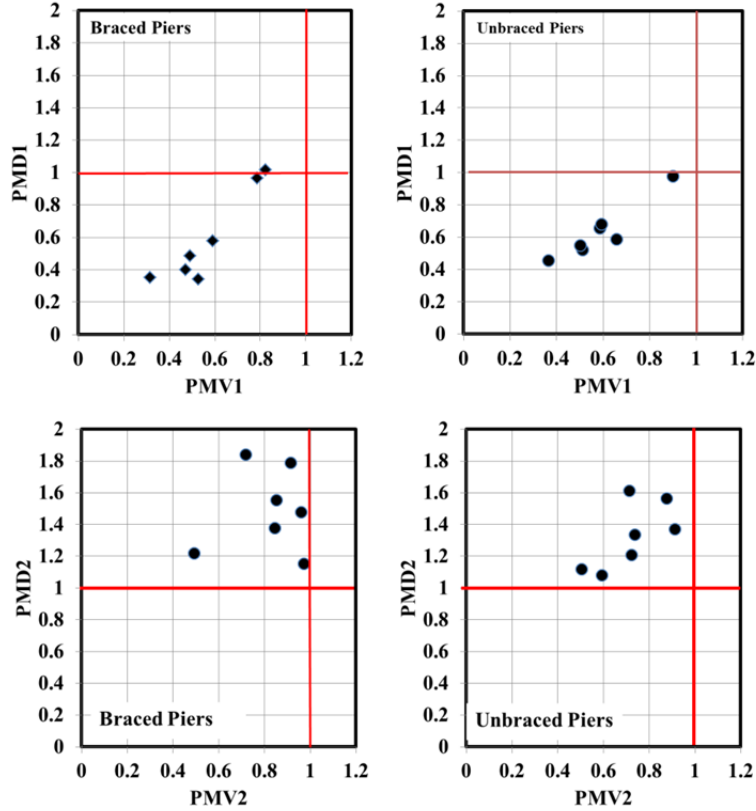
Figure 4.32. Simultaneous evaluation of force- and displacement-related performance measures for the case of the bridge model with braced piers (left) and unbraced piers (right)

Another approach to quantifying the performance of the NSDs in terms of simultaneous consideration of force and displacement response is via a Combined Performance Measure (CPM) (Reigles and Symans, 2005):

$$CPM_1 = \frac{Max\,|V^{IB+NSD}(t)| - Max\,|V^{IB}(t)|}{Max\,|V^{IB}(t)|} + \frac{Max\,|D^{IB+NSD}(t)| - Max\,|D^{IB}(t)|}{Max\,|D^{IB}(t)|} \qquad (4.15)$$

$$CPM_2 = \frac{Max\,|V^{IB+NSD}(t)| - Max\,|V^{IB+PD}(t)|}{Max\,|V^{IB+PD}(t)|} + \frac{Max\,|D^{IB+NSD}(t)| - Max\,|D^{IB+PD}(t)|}{Max\,|D^{IB+PD}(t)|} \qquad (4.16)$$

With these particular definitions, equal weight is given to the effects that the NSDs have displacements and forces. Note that, if the value of CPM is less than zero, the system with NSDs produces an overall improvement in performance relative to the system without NSDs. As shown in Figure 4.33, the NSDs reduce the shear forces and displacements in the bridge model significantly as compared to the isolated bridge without the NSDs. Although the NSDs were more effective in reducing the shear forces in comparison with viscous dampers for all of the ground motions, in some cases the CPM2 values are positive indicating better overall performance of the system with viscous dampers. This is due to the viscous dampers being more effective in reducing displacements (see Fig. 4.33).

In summary, the performance measures show that the NSDs reduce shear forces significantly while reducing displacements in some cases (the displacement reduction being

dependent on the friction damping within the NSD and its support system) and increasing it in others (i.e., when compared to the case with viscous dampers). Thus, it may be argued that the NSDs provide good overall performance with regard to both forces and displacements (displacements are reduced relative to the case without NSDs but not by as much as for the case with viscous dampers).
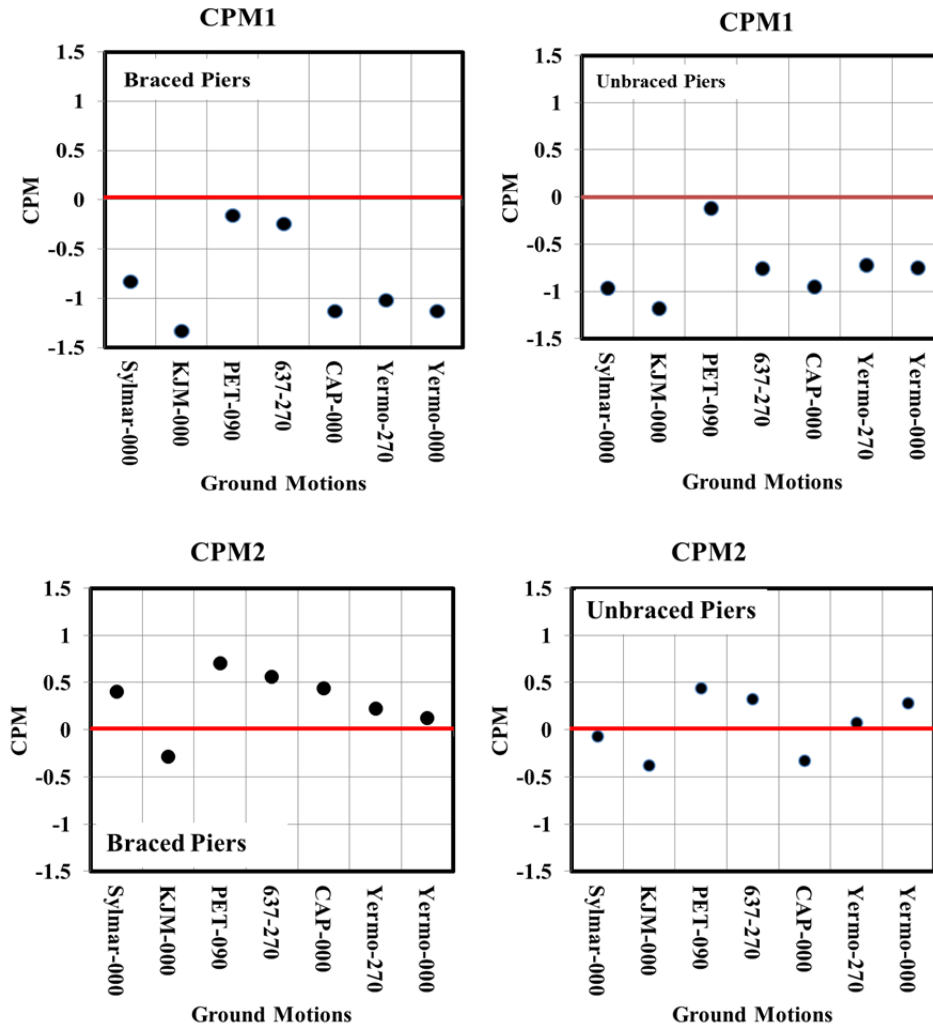
Figure 4.33. CPM values for various ground motions and for bridge model with braced piers (left) and unbraced piers (right)

4.7 Effects of high damping on performance measures

As indicated previously, one of the bridge configurations that was used in the shake table tests was one in which the isolation system contained both NSDs and viscous dampers. The original intent of this configuration was to use the dampers to provide energy dissipation and thus to limit the deformations of the isolation system. However, the experimental testing showed that the NSDs and their support system provided a large amount of damping via friction. In addition, due to the softening effect of the NSDs, the effective stiffness of the complete system is reduced such that the ability of the system to dissipate energy, as characterized by a damping ratio, is increased significantly. Thus, adding the viscous dampers in parallel with the NSDs resulted in a system

which had excessive damping, resulting in significant increases in forces. As an example, Figure 4.34 shows the hysteresis loops for the case of IB+NSD+PD for the bridge with braced piers and subjected to three harmonic load cases (frequency of 1.7 Hz but different amplitudes). As can be seen in the figure, as the deformation of the isolation system increases, the effective stiffness of the system decreases (due to the softening behavior induced by the NSDs). The equivalent viscous damping ratio of the system for each hysteresis loop was determined (using the dissipated energy per cycle and the peak elastic strain energy as defined by the force at the maximum displacement) and is shown in Figure 4.35 with the effective stiffness of the system (plotted against the average peak displacement for each test). As can be seen, the softening effect of the NSDs, which is more pronounced as displacements increase, leads to significant increases in equivalent viscous damping.
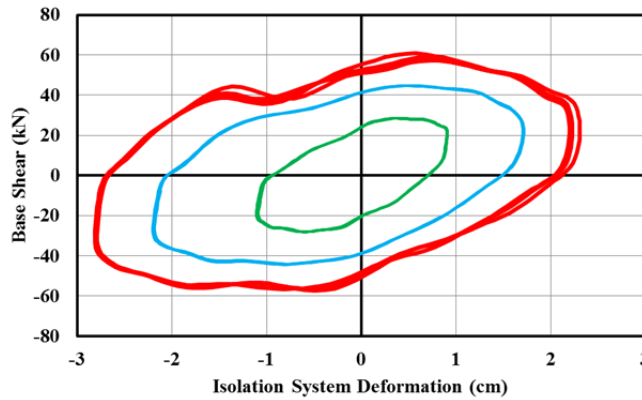
Figure 4.34. Hysteresis loops for the case of IB+NSD+PD for the bridge with braced piers and subjected to three harmonic loads having different amplitudes and a frequency of 1.7 Hz
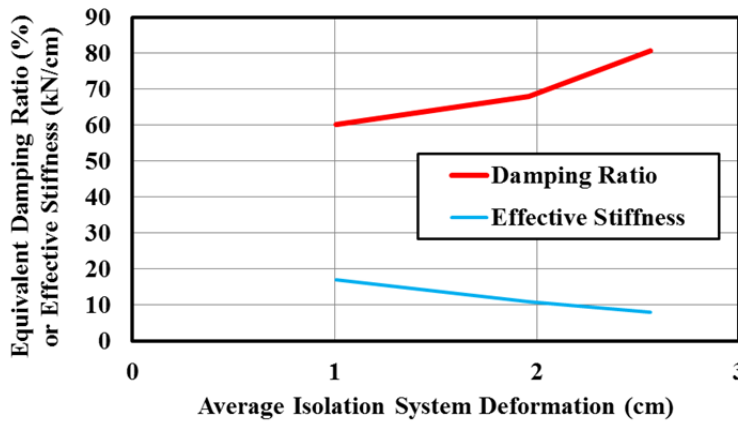
Figure 4.35. Influence of NSD behavior on stiffness and damping in bridge model for case of IB+NSD+PD and braced piers

The following performance measures, which are similar to those described previously, can be used to evaluate the performance of the bridge with NSDs (IB+NSD) relative to that that includes both NSDs and viscous dampers (IB+NSD+PD), and thus to evaluate the influence of high levels of damping:

$$PM_{V3} = \frac{Max \left| V^{IB+NSD+PD}(t) \right|}{Max \left| V^{IB+NSD}(t) \right|} \tag{4.17}$$

90

$$PM_{D3} = \frac{Max\ |D^{IB+NSD+PD}(t)|}{Max\ |D^{IB+NSD}(t)|} \tag{4.18}$$

$$CPM_3 = \frac{Max\ |V^{IB+NSD+PD}(t)|-Max\ |V^{IB+NSD}(t)|}{Max\ |V^{IB+NSD}(t)|} + \frac{Max\ |D^{IB+NSD+PD}(t)|-Max\ |D^{IB+NSD}(t)|}{Max\ |D^{IB+NSD}(t)|} \tag{4.19}$$

where $Max\ |V^{IB+NSD+PD}(t)|$ is the peak base shear for the case of IB+NSD+PD and $Max\ |D^{IB+NSD+PD}(t)|$ is the peak shear deformation of the isolation system for the same case. The performance measure values are shown in Figure 4.36 where the increase in forces is evident for both the braced and unbraced cases. It should be noted that one of the reasons for the increase in peak forces is that the friction damping within the system is a type of rate-independent damping that produces peak forces at the same time as peak displacements, thus maximizing the width (vertical height) of the hysteresis loops at their extreme displacements. As an example, for the case of IB+NSD, if it is assumed that the NSDs and their support system have frictionless interfaces and a viscous damper is installed in parallel with the NSDs (i.e., the friction is removed from the NSDs and accounted for via equivalent viscous damping), the hysteresis loop would have their maximum height at zero displacement with zero force contribution from the dampers at the extreme displacements. In such an idealized system, the peak force would be less than that that develops in the actual system that has friction and thus would be more effective in terms of reducing forces. To illustrate this, Figure 4.37 shows the hysteretic response for this idealized case, based on numerical simulations for the PET-090 ground motion. The idealized case produces peak forces that are about 15% less than those associated with the actual system, which had frictional damping.
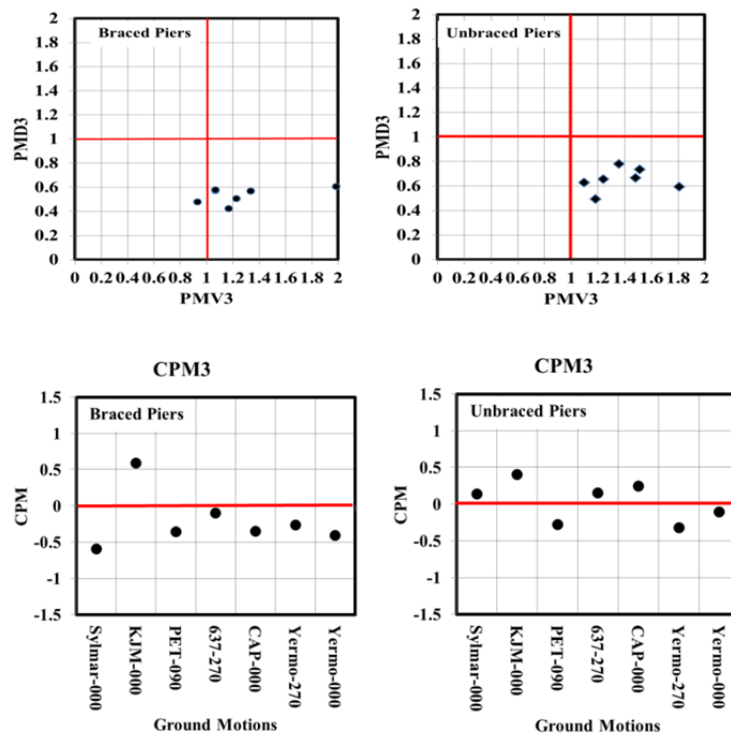
Figure 4.36. Performance measures for evaluating influence of damping on bridge model response for case of braced piers (left) and unbraced piers (right)
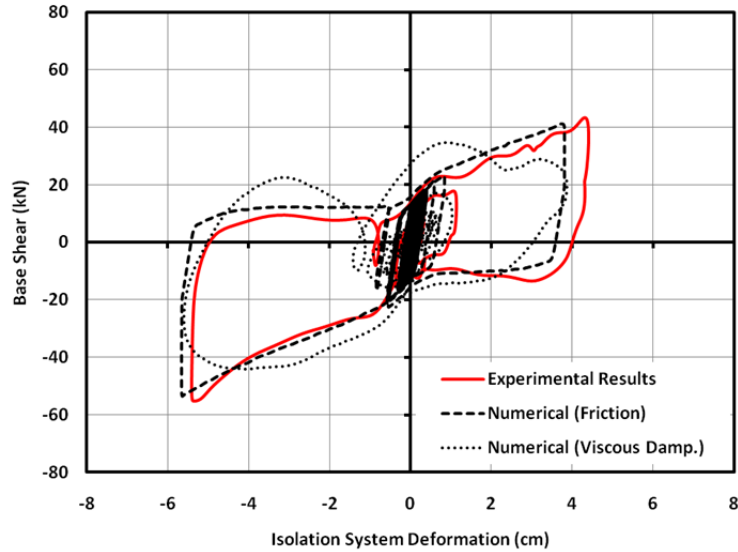
Figure 4.37. Comparison of hysteretic response for idealized conditions (frictionless NSDs with friction accounted for via equivalent viscous damping) and for realistic conditions (NSDs with friction) for bridge model without bracing and for PET-090 ground

4.8 Alternative Device Configuration for Development of Negative Stiffness

An alternative approach to developing negative stiffness, and one that could result in more compact NSDs, is to convert the translational motion of the bridge to rotational motion. Within this project, a new concept for rotation-based NSDs was developed but remains at a preliminary stage. The newly developed devices are able to modify stiffness and/or damping of a structure mechanically using mechanical feedback from the structure to which it is attached. In general the devices work by transforming the linear motion of a structure into rotation and then using rotational elements (e.g, gears) to control the behavior of the structure during seismic loading events. Using such rotational elements, many adaptive passive seismic protection devices can be configured, each having unique capabilities. It is expected that detailed information on the behavior of rotation-based NSD devices will be presented in future publications.

4.9 Summary

Experimental tests of a seismically-isolated bridge model demonstrated that the use of NSDs within the isolation system can significantly reduce the peak base shear. It is expected that the NSDs will generally increase the deformation of the isolation level, which can be limited by providing damping within the isolation system. For the tests described herein, the NSDs and their support system, included sliding rails, provided significant damping via friction. This combination of negative stiffness and friction resulted in good performance with regard to both forces and displacements. Furthermore, the experimental tests demonstrated that NSDs can be effective in cases where a flexible layer (i.e., the bridge piers) is inserted between the NSDs and the foundation of the structure (previous testing had been performed for the case of base-isolated buildings in which the NSDs were directly attached to the foundation).

The hysteretic response of the bridge model for two particular ground motions (KJM-000 and PET-090) were presented in this report to provide a detailed evaluation of the effects of the

NSDs on the response of the bridge. Comparing the cases of IB and IB+NSD, the NSDs produced the maximum base shear reduction for the KJM-000 ground motion (between the seven motions selected for the test program) but had only a minor effect on both the peak force and displacement for the PET-090 ground motion. Since the behavior of the NSDs is dependent on various parameters which can be readily modified (e.g., by changing the device geometry via alteration of the NSD lever arms and/or by changing the stiffness values for each spring), the device can be designed such that it is most effective for the particular characteristics of the ground motions expected at a site (e.g., based on site-specific ground motion records). Such modifications could have been made to the NSDs such that they would have been effective in reducing the bridge model response for the PET-090 ground motion.

One of the main effects of the NSDs is to modify the dynamics of a structure such that there is no resonant condition. For example, by adding the NSDs to the bridge model, the effective stiffness and natural frequency of the combined system continuously changes, thus avoiding resonance. This effect of the NSDs was clearly demonstrated by examining the response of the bridge model when subjected to a sine-sweep harmonic excitation (response in frequency domain was essentially flat indicating no resonant frequency). Another major effect of the NSD is to soften the behavior of the combined system, resulting in reduced bridge deck accelerations and thus reduced base shear forces. In addition, the softening behavior increases the effective damping ratio, thus providing some ability to control the deformations of the system.

Finally, a numerical model of the bridge test specimen was described in detail along with numerical simulation results for excitation being the PET090 ground motion. The predicted hysteretic response of the bridge model for different bridge model configurations were compared with those from experimental tests with the good comparisons indicating that the model of the bridge and its components is adequate for predicting the response to general seismic loading.

"This Page Intentionally Left Blank"

SECTION 5.   CONCLUSIONS

A new control device has been developed and implemented for seismic response control of highway bridges. The device produces negative stiffness in a completely passive manner via a mechanical mechanism. Numerical simulations and experimental shaking table tests have demonstrated the effectiveness of the device in limiting the seismic demands on bridge structures. The main feature of the negative stiffness device is a pre-compressed spring, which can push the structure away from its center position and thus induce negative stiffness. When implemented in parallel with a structure having positive stiffness, the combined system appears to have substantially reduced stiffness while remaining stable. Thus, there is an "apparent weakening" of the structure that results in an "apparent yield point," reduced forces and increased displacements. The increase in displacement response can be limited by incorporating a damping device in parallel with the negative stiffness device or by adding friction to the device assembly.

In this report, the negative stiffness devices are described along with their hysteretic behavior as obtained from a series of cyclic tests which were utilized to calibrate the parameters of a numerical model. In addition, results from numerical simulations and seismic testing of a quarter-scale bridge model are presented wherein the bridge was configured with various isolation system components (isolation bearings, negative stiffness devices, and viscous dampers). In addition, the bridge was designed to mimic either a single-span bridge supported on abutments or an interior span of a multi-span bridge. The comprehensive results of the investigation, obtained from both numerical simulations and experimental shaking table tests, clearly demonstrate the effectiveness of the negative stiffness devices in limiting the seismic response of the bridge for multiple bridge configurations.

As a result of this research, the following conclusions can be stated:

- One of the main effects of the NSDs is to modify the dynamics of a structure such that there is no resonant condition. For example, by adding the NSDs to the bridge model, the effective stiffness and natural frequency of the combined system continuously changes, thus avoiding resonance.

- A major effect of the NSD is to soften the behavior of the combined structure/NSD system, resulting in reduced accelerations and thus reduced base shear forces. In addition, the softening behavior increases the effective damping ratio of the system, thus providing some ability to control the deformations of the system.

- Numerical simulations and experimental tests demonstrated that the use of NSDs within a bridge isolation system can significantly reduce the peak base shear forces and accelerations of the deck with respect to the IB case (isolated bridge - elastomeric bearings only) for nearly all of the ground motions considered in this study.

- NSDs are effective in cases where the isolation system that incorporates the NSDs is reacting against a flexible layer (i.e., the bridge piers) and deforming based on the relative deformation between two degrees of freedom rather than being directly connected to the foundation of the structure.

- Although NSDs are highly effective for a wide range of ground motions, they may not be effective in reducing forces for some ground motions due to the unique characteristics of those ground motions relative to the dynamics of the structure.

- The shake table tests results for the case of the bridge with braced and unbraced piers showed that the NSDs have reduced effectiveness in the case of the bridge with unbraced piers.

- For the IB+NSD case (isolated bridge with NSDs), the positive stiffness of the bearings combined with the negative stiffness of the NSDs results in the creation of an apparent yield point in the hysteretic response of the bridge, thus controlling the peak force demand in the bridge.

- The NSDs and their support system, including sliding rails, provided significant damping via friction. This combination of negative stiffness and friction resulted in good performance with regard to both the force and displacement response of the bridge.

- The predicted hysteretic response of the bridge model for eight different bridge model configurations was compared with those from experimental tests with the good comparisons indicating that the analytical/numerical model of the bridge and its components is adequate for predicting the response to general seismic loading.

SECTION 6.   REFERENCES

Attary, N., Symans, M.D., Nagarajaiah, S., Reinhorn, A.M., Constantinou, M.C., Taylor, D., Pasala, D.T.R. & Sarlis, A.A. (2013). "Performance assessment of a highway bridge structure employing adaptive negative stiffness for seismic protection." *Proceeding of 2013 ASCE Structures Congress* (pp. 1736-1746). Pittsburgh, PA. doi: 10.1061/9780784412848.152

Attary, N., Symans, M.D., Nagarajaiah, S., Reinhorn, A.M., Constantinou, M.C., Taylor, D., Pasala, D.T.R. & Sarlis, A.A. (2012a). "Performance evaluation of a seismically-isolated bridge structure with adaptive passive negative stiffness." *Proceeding of Fifteenth World Conference on Earthquake Engineering* (pp. 1-10), (Paper Number: 4310). Lisbon, Portugal.

Attary, N., Symans, M.D., Nagarajaiah, S., Reinhorn, A.M., Constantinou, M.C., Taylor, D., Sarlis, A.A. & Pasala, D.T.R. (2012b). "Application of negative stiffness devices for seismic protection of bridge structures." *Proceeding of 2012 ASCE Structures Congress* (pp. 506-515). Chicago, IL. doi: 10.1061/9780784412367.045

Chen, W.F. and Duan, L. (2003). "*Bridge engineering: Seismic design.*" Boca Raton, FL: CRC Press.

Han, J., Shishu, X, and Shaowen, L. (2010). "Isolation effect analysis of the bridge with the negative stiffness damping device." *International Conference of Mechanic Automation and Control Engineering* (pp. 1052-1056). Wuhan, China. doi:10.1109/MACE.2010.5536760

Iemura, H. and Pradono, M.H. (2003). "Application of pseudo-negative stiffness control to the benchmark cable-stayed bridge." *Journal of Structural Control, 10,* 187–203. doi:10.1002/stc.25

Iemura, H., Igarashi, A., Pradono, M.H. and Kalantari, A. (2006). "Negative stiffness friction damping for seismically isolated structures." *Structural Control and Health Monitoring, 13,* 775–791. doi:10.1002/stc.111

Iemura, H. and Pradono, M.H. (2009). "Advances in the development of pseudo-negative-stiffness dampers for seismic response control." *Structural Control and Health Monitoring, 16,* 784–799. doi:10.1002/stc.345

Kawashima, K. and Unjoh, S. (1994). "Seismic response control of bridges by variable dampers." *Journal of Structural Engineering, 9,* 2583-2601.

Nagarajaiah, S., Riley, M. A., and Reinhorn, A. M. (1993). "Control of sliding isolated bridges with absolute acceleration feedback." *Journal of Engineering Mechanics, ASCE, 119*(11), 2317-2332.

Nagarajaiah, S., and Reinhorn, A. M. (1994). "Applicability of pseudo-force method to highly nonlinear dynamic problems," *Proceedings of 1994 ASCE Structures Congress*, ASCE, Atlanta, Georgia, 165-172.

Nagarajaiah, S. (2010). "Adaptive stiffness systems: Recent developments in structural control using semiactive/smart variable stiffness and adaptive passive stiffness." *Proceedings of 5th World Conference on Structural Control and Monitoring* (pp. 1-30), (Paper Number: 007). Tokyo, Japan.

Nagarajaiah, S., Reinhorn, A.M., Constantinou, M.C., Taylor, D., Pasala, D.T.R. & Sarlis, A.A. (2010). "Adaptive negative stiffness: A new structural modification approach for seismic protection." *Proceedings of 5th World Conference on Structural Control and Monitoring* (pp. 1-15), (Paper Number: 103). Tokyo, Japan.

Naeim, F. and Kelly, J.M. (1999). *"Design of seismic isolated structures."* New York, NY: J. Wiley & Sons.

Pasala, D. T. R., Sarlis, A. A. S., Nagarajaiah, S., Reinhorn, A. M., Constantinou M. C. & Taylor, D., (2011). "Adaptive negative stiffness: A new structural modification approach for seismic protection." *Proceedings of 2011 ASCE Structures Congress,* (pp. 2892-2904). Las Vegas, NV. doi: 10.1061/41171(401)251

Pasala, D.T.R., Sarlis, A.A., Nagarajaiah, S., Reinhorn, A.M., Constantinou, M.C. and Taylor D. (2013a). "Adaptive negative stiffness: A new structural modification approach for seismic protection." *Journal of Structural Engineering, Special Issue: NEES 1: Advances in Earthquake Engineering, 139*(7), 1112-1123. doi:10.1061/(ASCE)ST.1943-541X.0000615

Pasala, D.T.R., Sarlis, A.A., Nagarajaiah, S., Reinhorn, A.M., Constantinou, M.C. and Taylor D. (2013b). "Simulated bilinear-elastic behavior in a SDOF elastic structure using negative stiffness device: Experimental and analytical study." *Journal of Structural Engineering*, 1-13. doi:10.1061/(ASCE)ST.1943-541X.0000830

Ray, T., Reinhorn, A. M. and Nagarajaiah, S. (2013). "Nonlinear elastic and inelastic spectra with inherent and supplemental damping." *Earthquake Engineering and Structural. Dynamics*, *42*: 2151–2165. doi: 10.1002/eqe.2318

Reinhorn, A.M., Viti, S. & Cimellaro G.P. (2005). "Retrofit of structures: Strength reduction with damping enhancement." *37th Technical Panel Meeting on Wind and Seismic Effects*, (pp. 158-171). Tsukuba, Japan.

Reinhorn, A.M., Lavan, O. & Cimellaro, G.P. (2009). "Design of controlled elastic and inelastic structures." *Earthquake Engineering and Engineering Vibration-Special issue on "Advances in Seismic Response Control of Structures, 8*(4), 469-479.

Sahasrabudhe, S.S. and Nagarajaiah, S. (2005a). "Semi-active control of sliding isolated bridges using MR dampers: An experimental and numerical study." *Earthquake Engineering and Structural Dynamics, 34*, 965-983.

Sahasrabudhe, S.S. and Nagarajaiah, S. (2005b). "Effectiveness of variable stiffness systems in base-isolated bridges subjected to near-fault earthquakes: An experimental and analytical study." *Journal of Intelligent Material Systems and Structures, 16*, 743-756.

Sarlis, A.A, Pasala, D.T.R, Constantinou, M.C, Reinhorn, A.M, Nagarajaiah, S., and Taylor, D. (2011). "Negative stiffness device for seismic protection of structures – An analytical and experimental study." *Proc. of 3rd ECCOMAS Thematic Conference on Computational Methods in Structural Dynamics and Earthquake Engineering* (pp. 1-23), (Paper Number: 536). Corfu, Greece.

Sarlis, A.A, Pasala, D.T.R, Constantinou, M.C, Reinhorn, A.M, Nagarajaiah, S. and Taylor, D. (2012). "Negative stiffness device for seismic protection of structures." *Journal of Structural Engineering, Special Issue: NEES 1: Advances in Earthquake Engineering*, 1124–1133. doi:10.1061/(ASCE)ST.1943-541X.0000616.

Sarlis, A.A, Pasala, D.T.R, Constantinou, M.C, Reinhorn, A.M, Nagarajaiah, S. and Taylor, D. (2013). "Negative stiffness device for seismic protection of structures." *Technical Report MCEER-13-0005, Multidisciplinary Center for Earthquake Engineering Research.* State University of New York at Buffalo, Buffalo, NY.

Shen, J., Ysai M.H., Chang, K.C. and Lee, G.C, (2004). "Performance of a seismically isolated bridge under near-fault earthquake ground motions." *Journal of Structural Engineering ASCE, 130*(6), 861-868.

Tsopelas, P. and Constantinou, M.C. (1994). "NCEER-Taisei Research program on sliding seismic isolation systems for bridges: Experimental and analytical study of a system consisting of sliding bearings and fluid restoring force/damping devices." *Technical Report NCEER-94-0014, National Center for Earthquake Engineering Research.* State University of New York, Buffalo, NY.

Tsopelas, P., Constantinou, M.C., S. Okamoto, Fujii S. and Ozaki D. (1996). "Experimental study of bridge seismic sliding isolation systems." *Engineering Structures, 18*(4), 301-310.

Wolff, E.D. and Constantinou, M.C. (2004). "Experimental study of seismic isolation systems with emphasis on secondary system response and verification of accuracy of dynamic response history analysis methods." *Technical Report MCEER-04-0001, Multidisciplinary Center for Earthquake Engineering Research.* State University of New York at Buffalo, Buffalo, NY.

"This Page Intentionally Left Blank"

APPENDICES

A. Hysteretic Response of NSDs for Harmonic Loading

A.1. Hysteretic Response of North NSD

Amplitudes: 0.15 - 3.0 in.
Frequencies: 0.01, 0.1, and 0.5 Hz
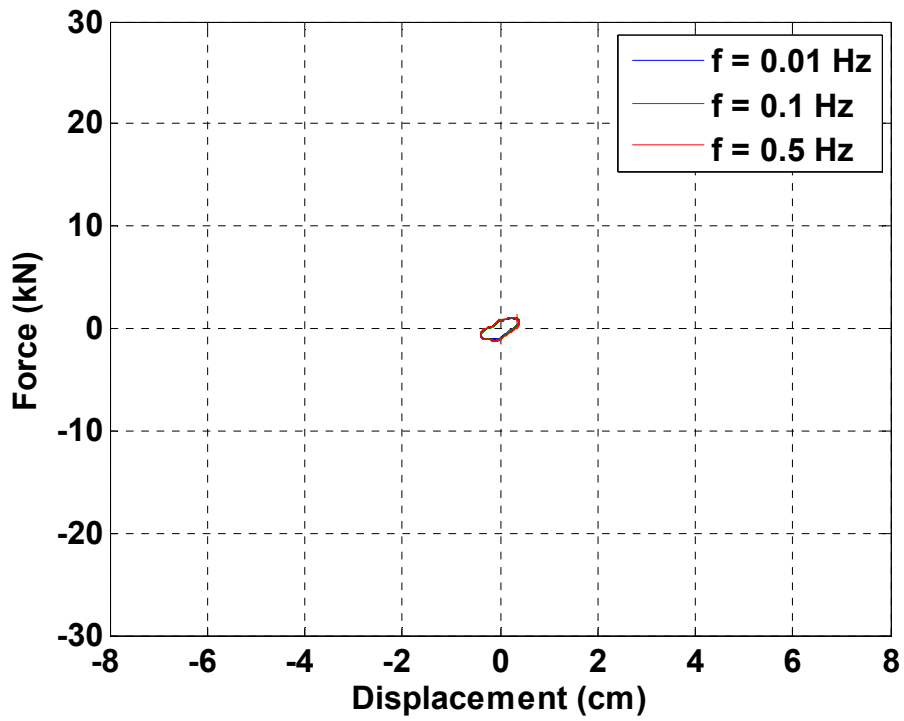
Figure A.1. Hysteretic response of North NSD for harmonic loading at different frequencies and 0.38 cm amplitude
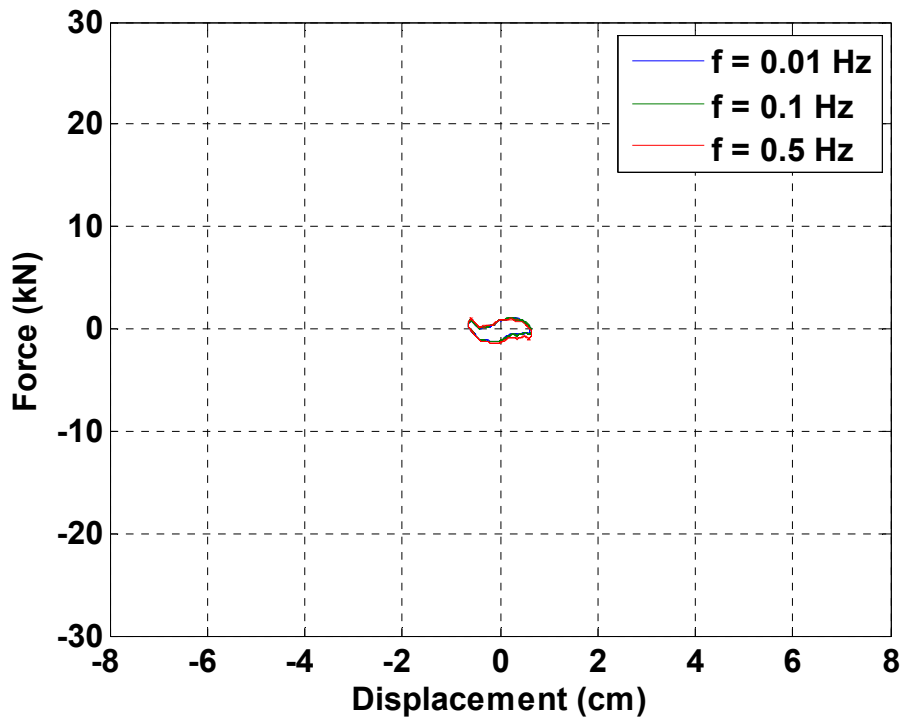
Figure A.2. Hysteretic response of North NSD for harmonic loading at different frequencies and 0.64 cm amplitude
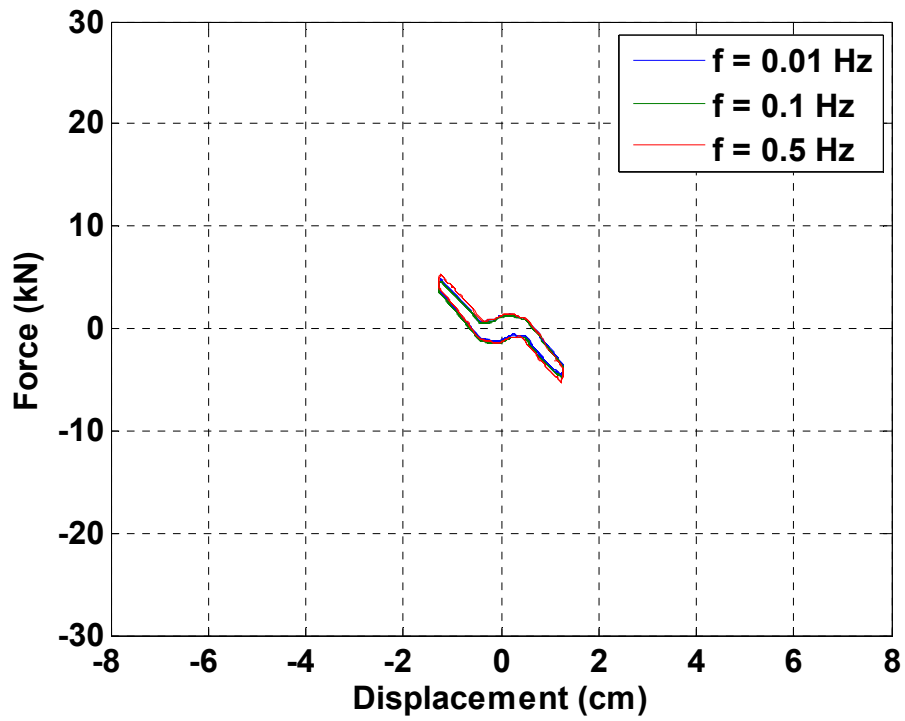
Figure A.3. Hysteretic response of North NSD for harmonic loading at different frequencies and 1.27 cm amplitude
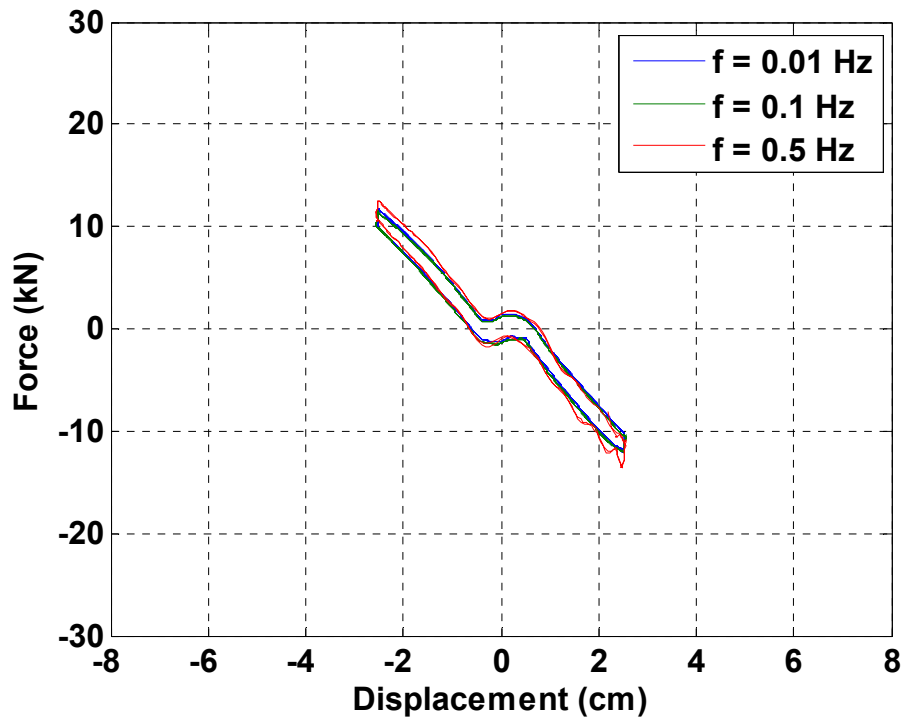
Figure A.4. Hysteretic response of North NSD for harmonic loading at different frequencies and 2.54 cm amplitude
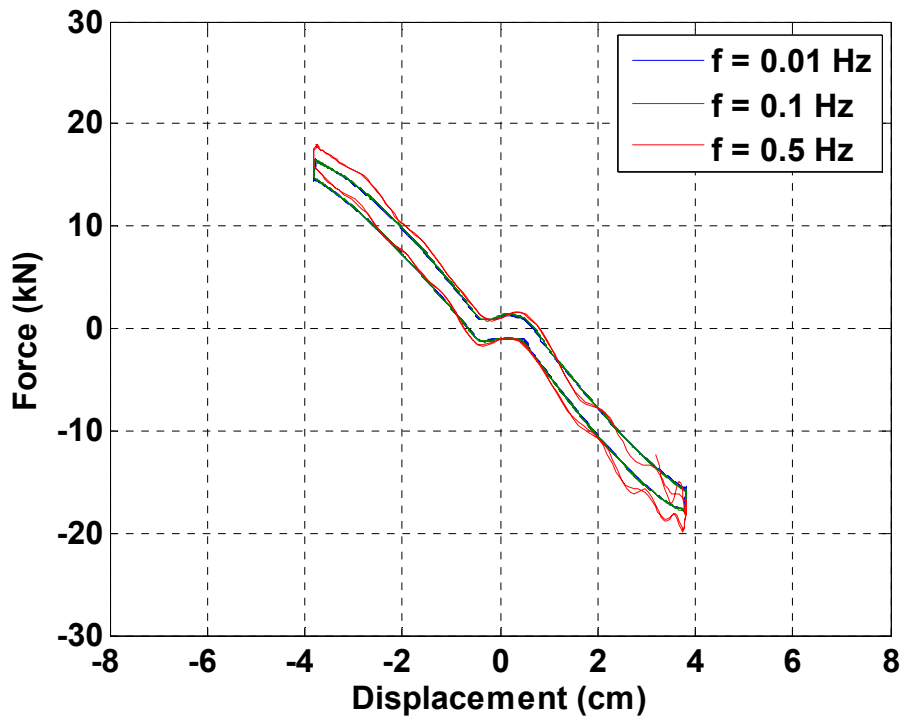
Figure A.5. Hysteretic response of North NSD for harmonic loading at different frequencies and 3.81 cm amplitude
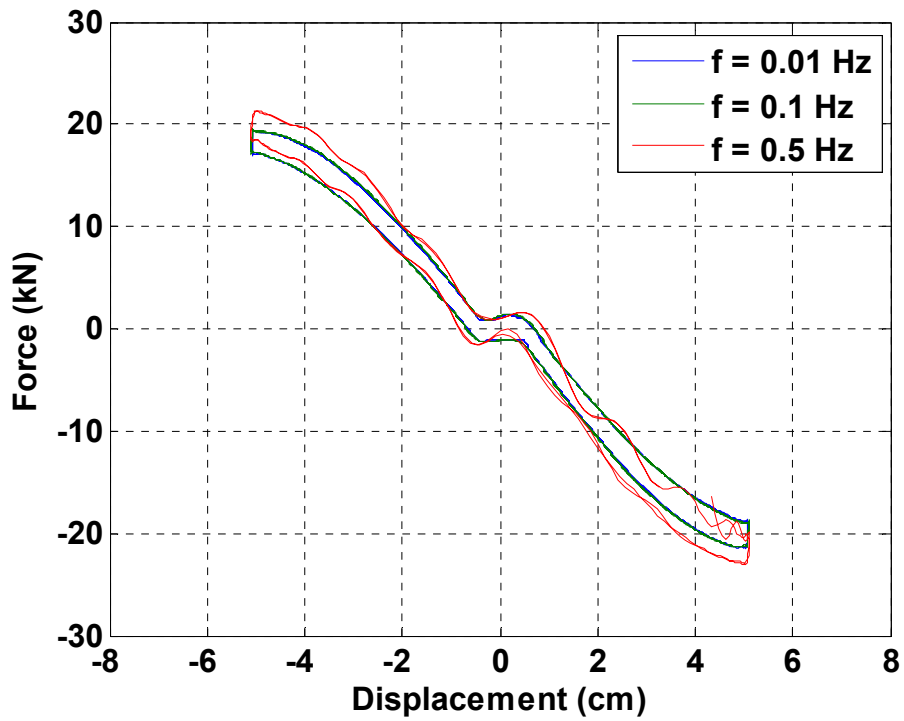
Figure A.6. Hysteretic response of North NSD for harmonic loading at different frequencies and 5.08 cm amplitude
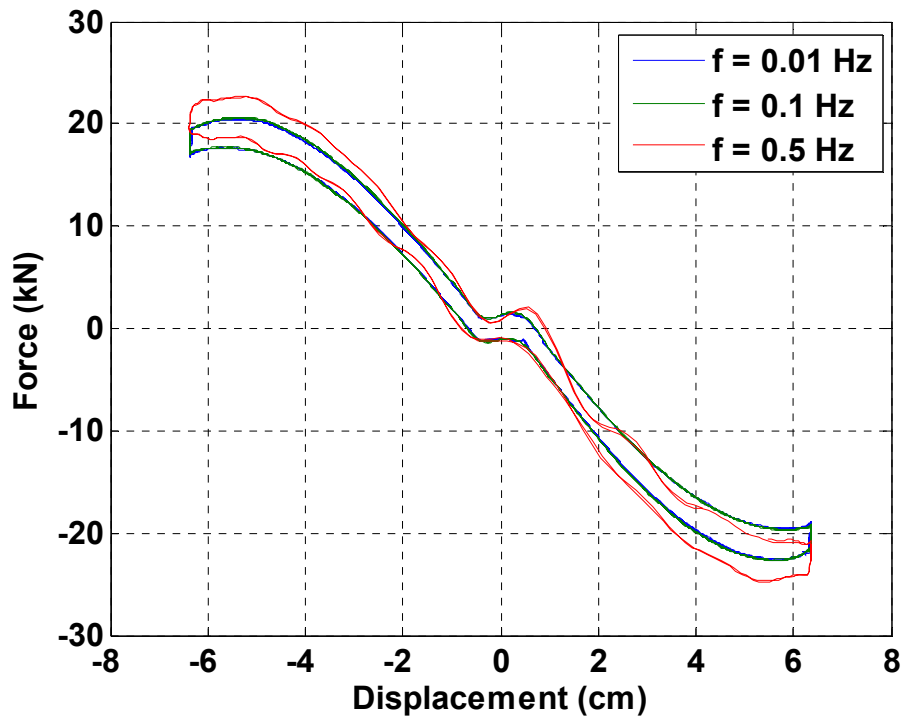
Figure A.7. Hysteretic response of North NSD for harmonic loading at different frequencies and 6.35 cm amplitude
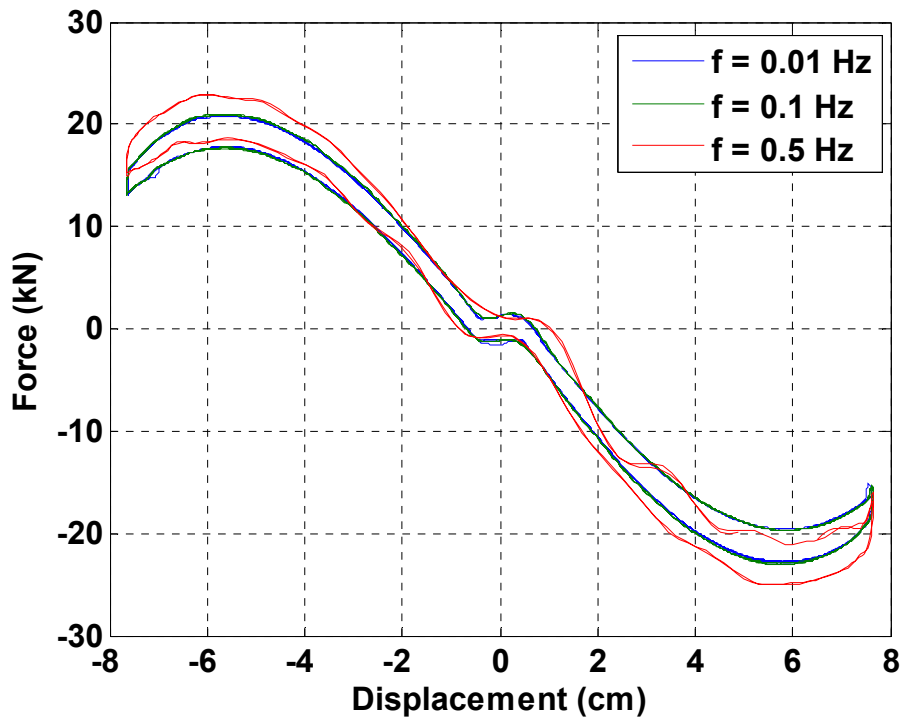
Figure A.8. Hysteretic response of North NSD for harmonic loading at different frequencies and 7.62 cm amplitude

A.2. Hysteretic Response of South NSD

Amplitudes: 0.15 - 3.0 in.
Frequencies: 0.01, 0.1, and 0.5 Hz
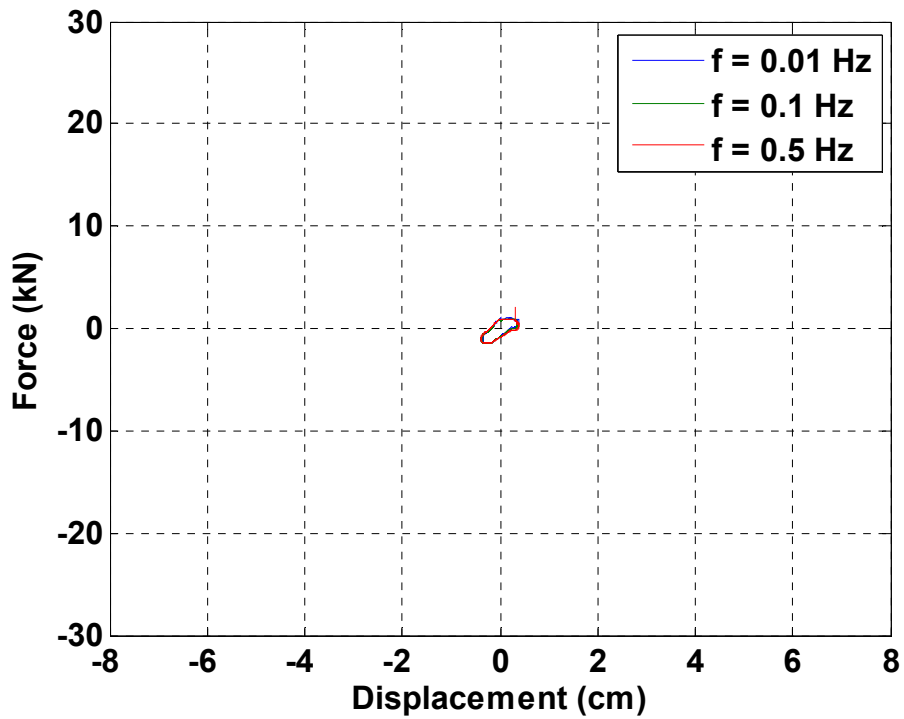
Figure A.9. Hysteretic response of South NSD for harmonic loading at different frequencies and 0.38 cm amplitude
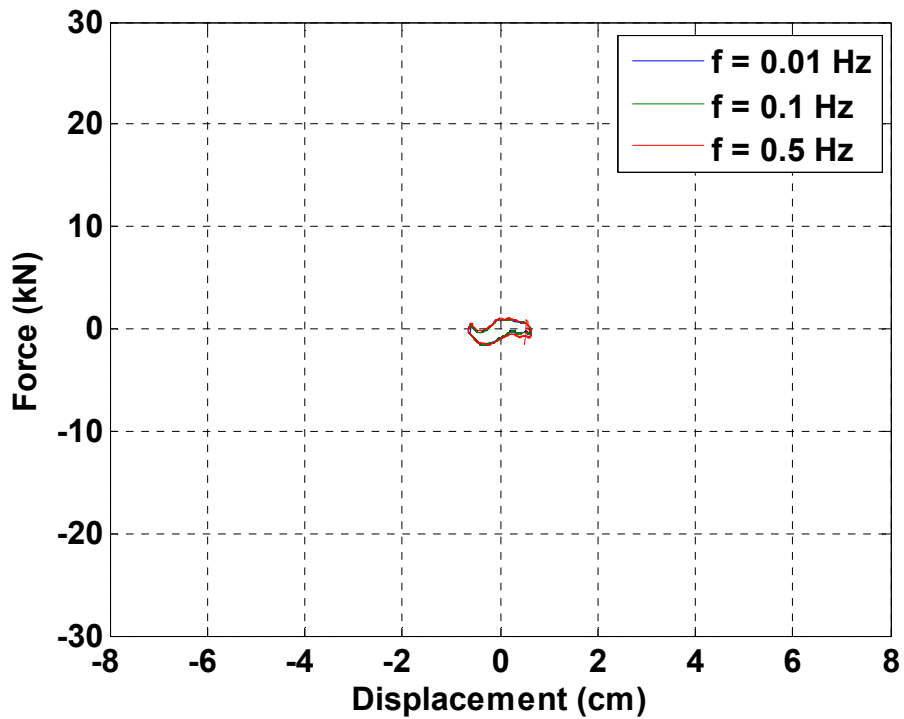
Figure A.10. Hysteretic response of South NSD for harmonic loading at different frequencies and 0.64 cm amplitude
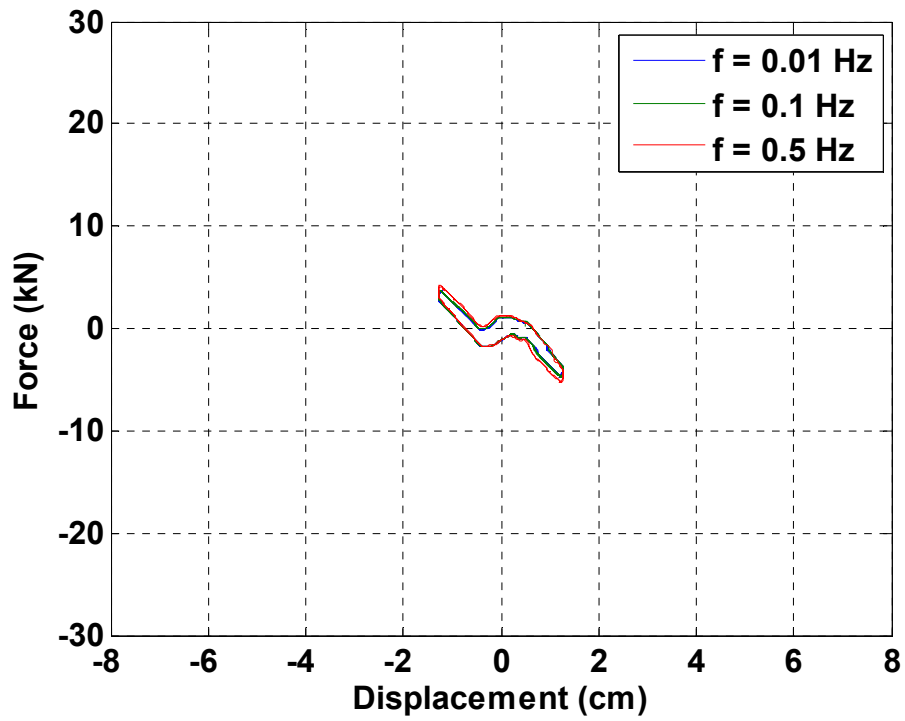
Figure A.11. Hysteretic response of South NSD for harmonic loading at different frequencies and 1.27 cm amplitude
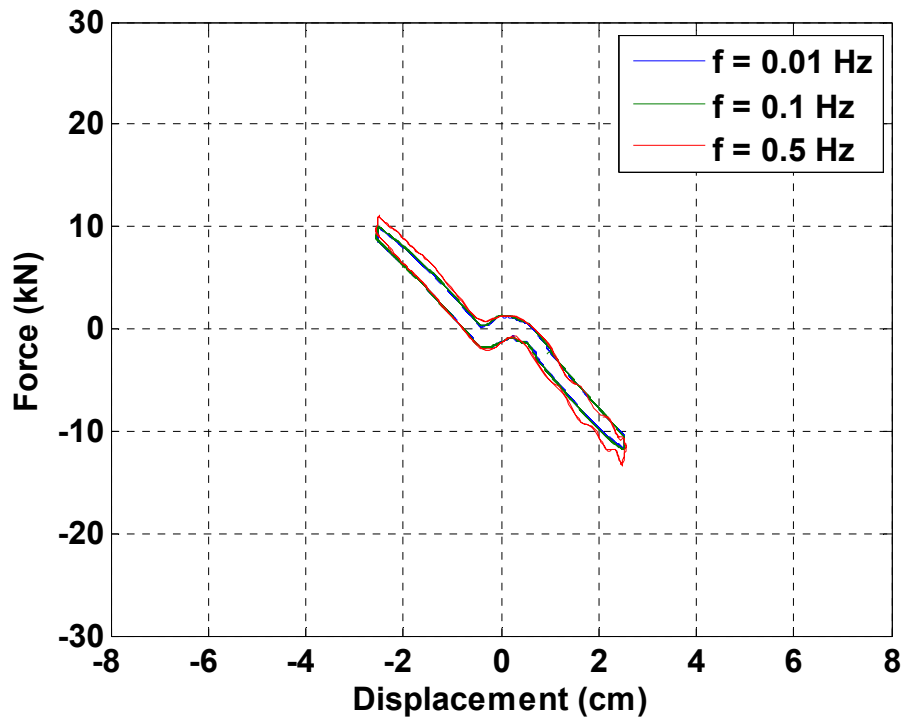
Figure A.12. Hysteretic response of South NSD for harmonic loading at different frequencies and 2.54 cm amplitude
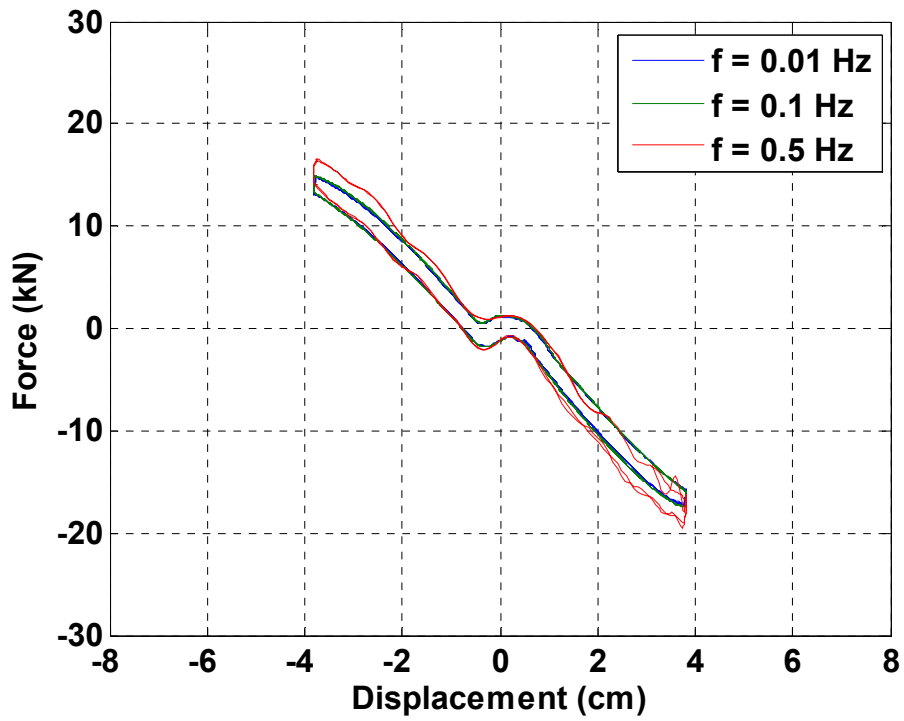
Figure A.13. Hysteretic response of South NSD for harmonic loading at different frequencies and 3.81 cm amplitude
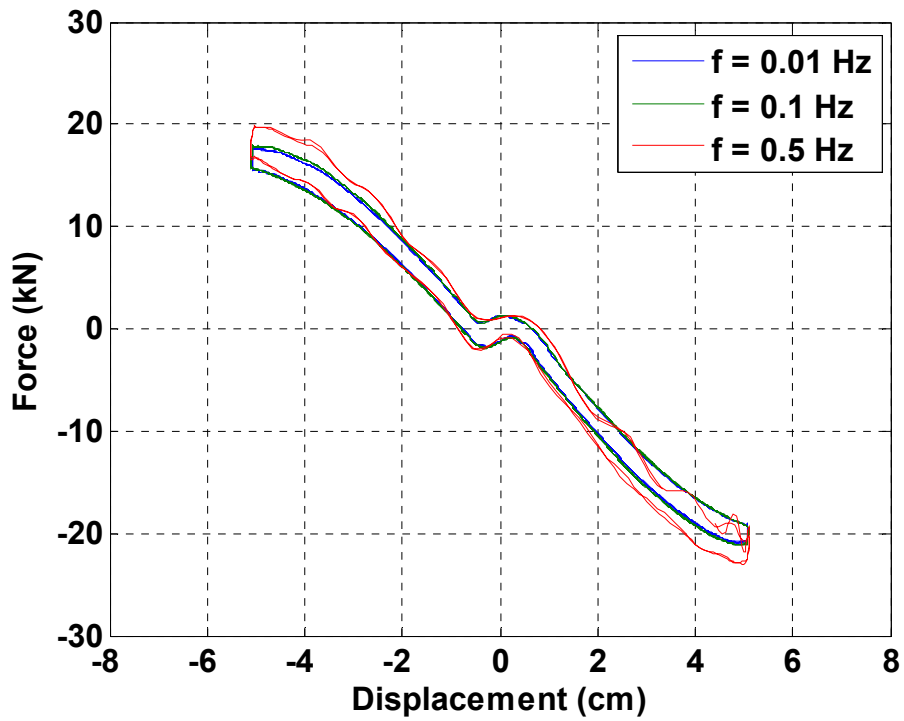
Figure A.14. Hysteretic response of South NSD for harmonic loading at different frequencies and 5.08 cm amplitude
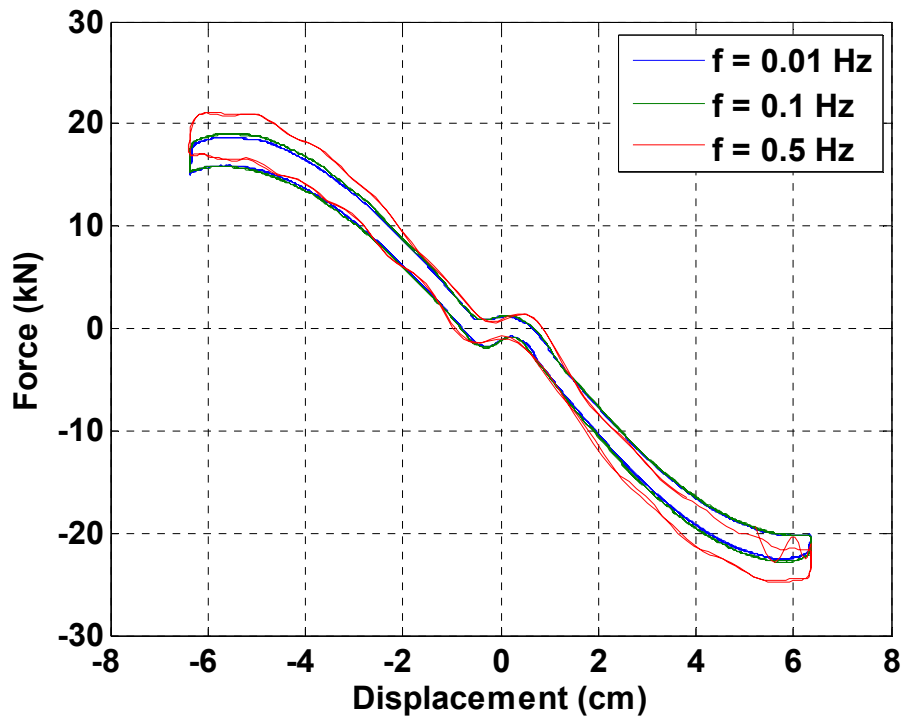
Figure A.15. Hysteretic response of South NSD for harmonic loading at different frequencies and 6.35 cm amplitude
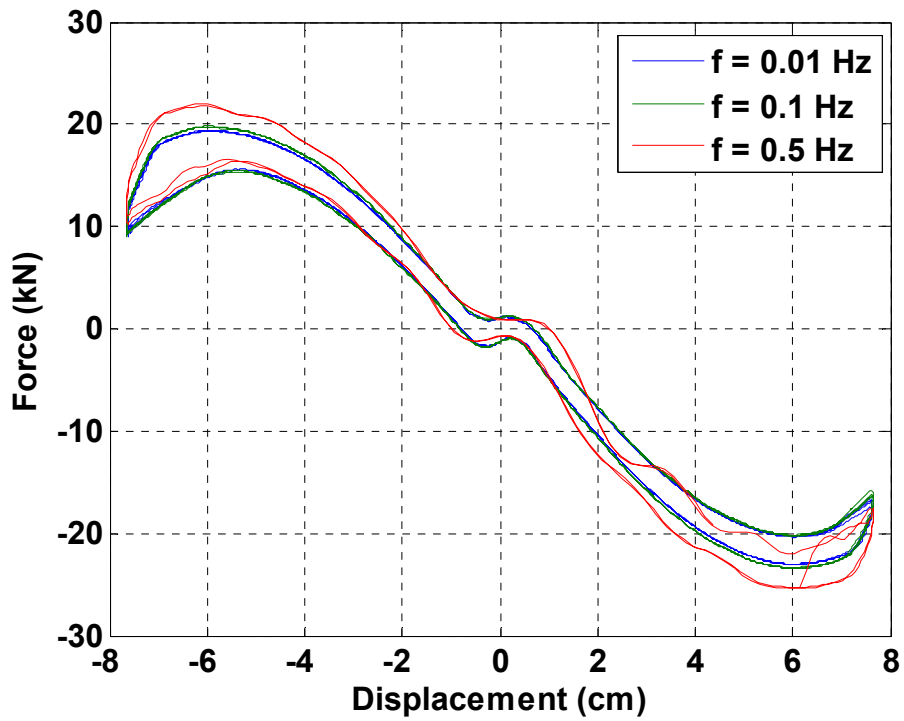
Figure A.16. Hysteretic response of South NSD for harmonic loading at different frequencies and 7.62 cm amplitude

112

B. Seismic Test Results for Bridge Structure Subjected to Various Ground Motions

B.1. Experimental Results for Bridge Model with Braced Piers for the Case of Isolated Bridge (IB)
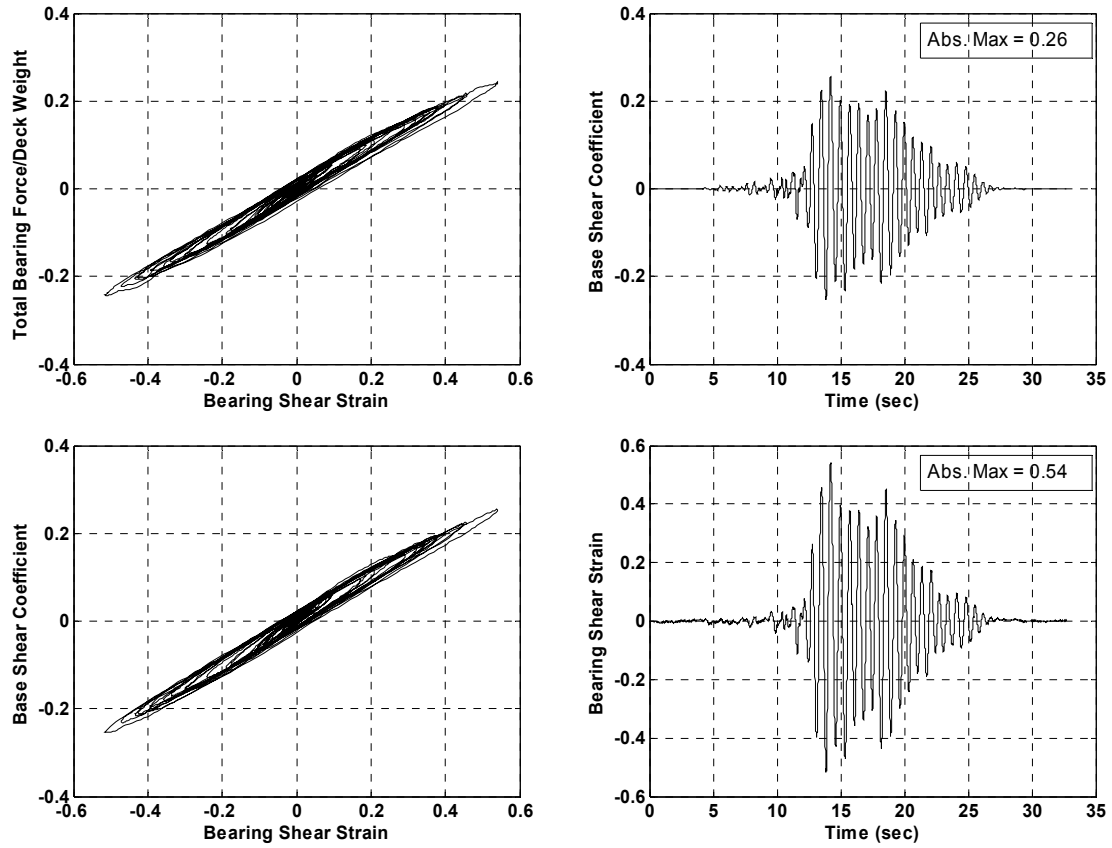
Figure B.1. Experimental results for bridge model with braced piers for the case of IB and 100% of YER-000 ground motion
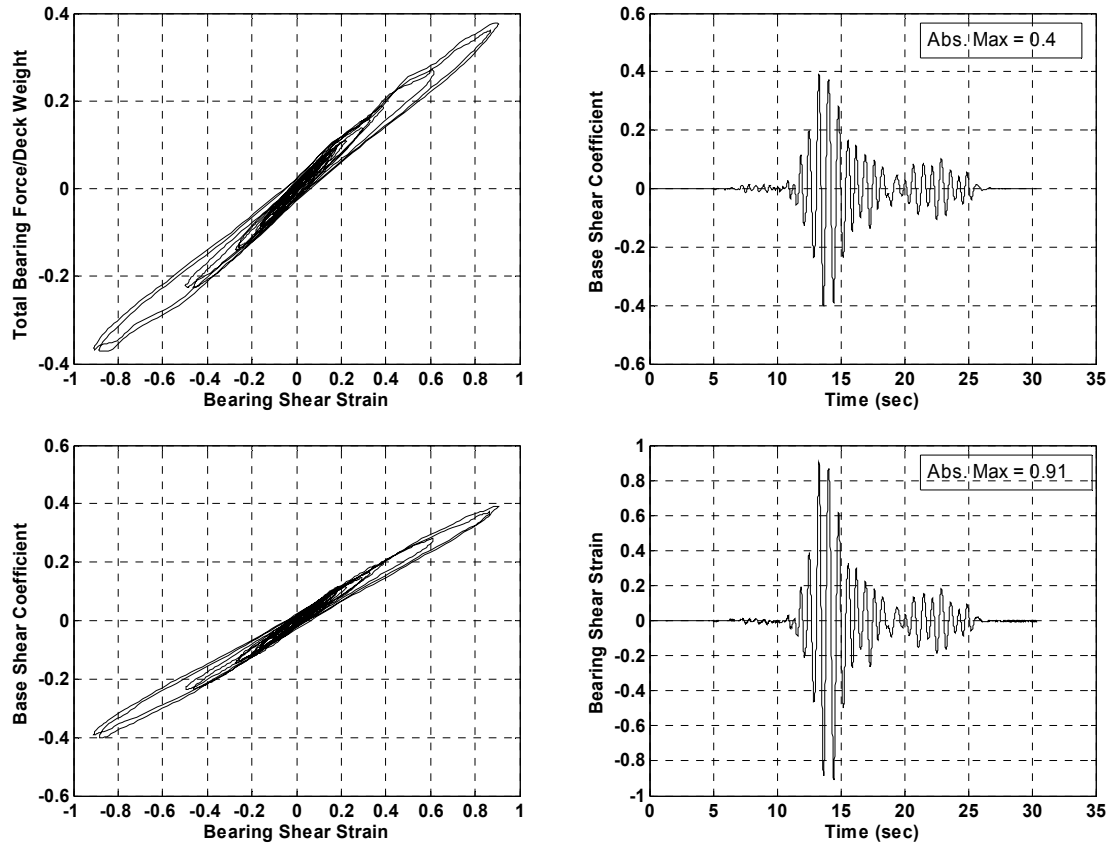
Figure B.2. Experimental results for bridge model with braced piers for the case of IB and 100% of YER-270 ground motion

116
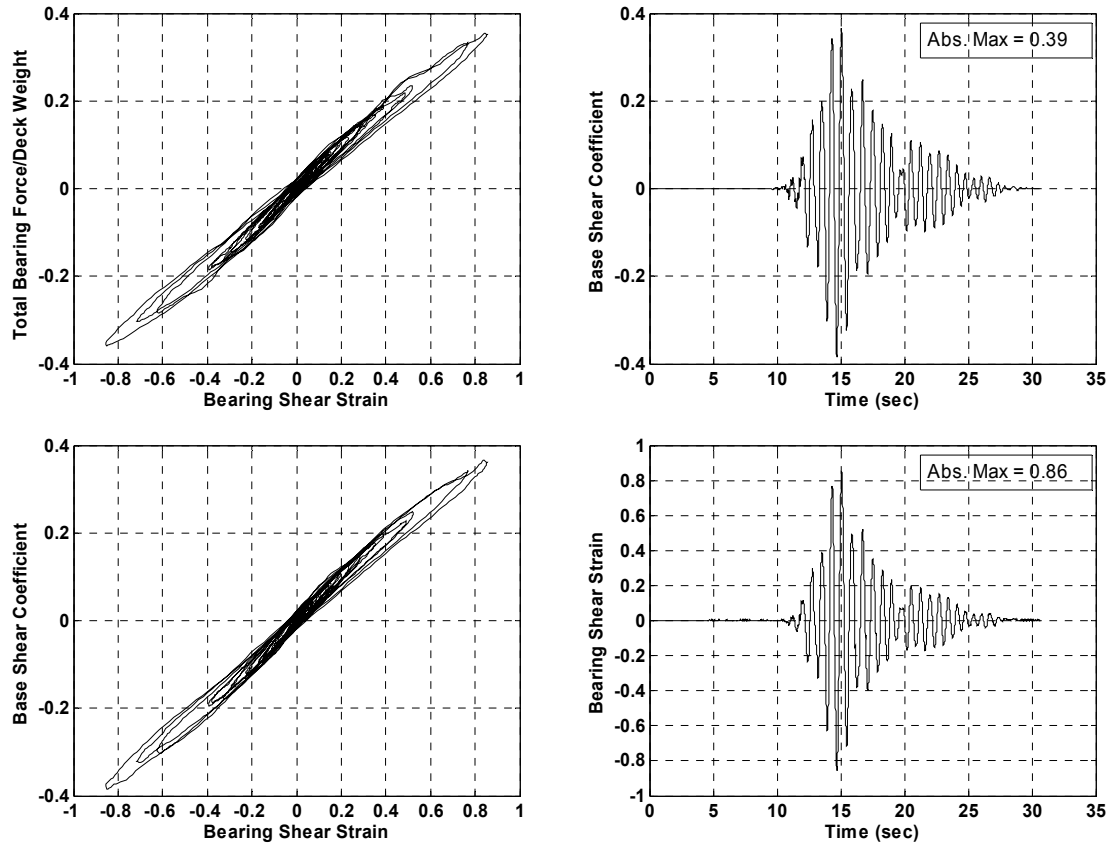
Figure B.3. Experimental results for bridge model with braced piers for the case of IB and 75% of CAP-000 ground motion
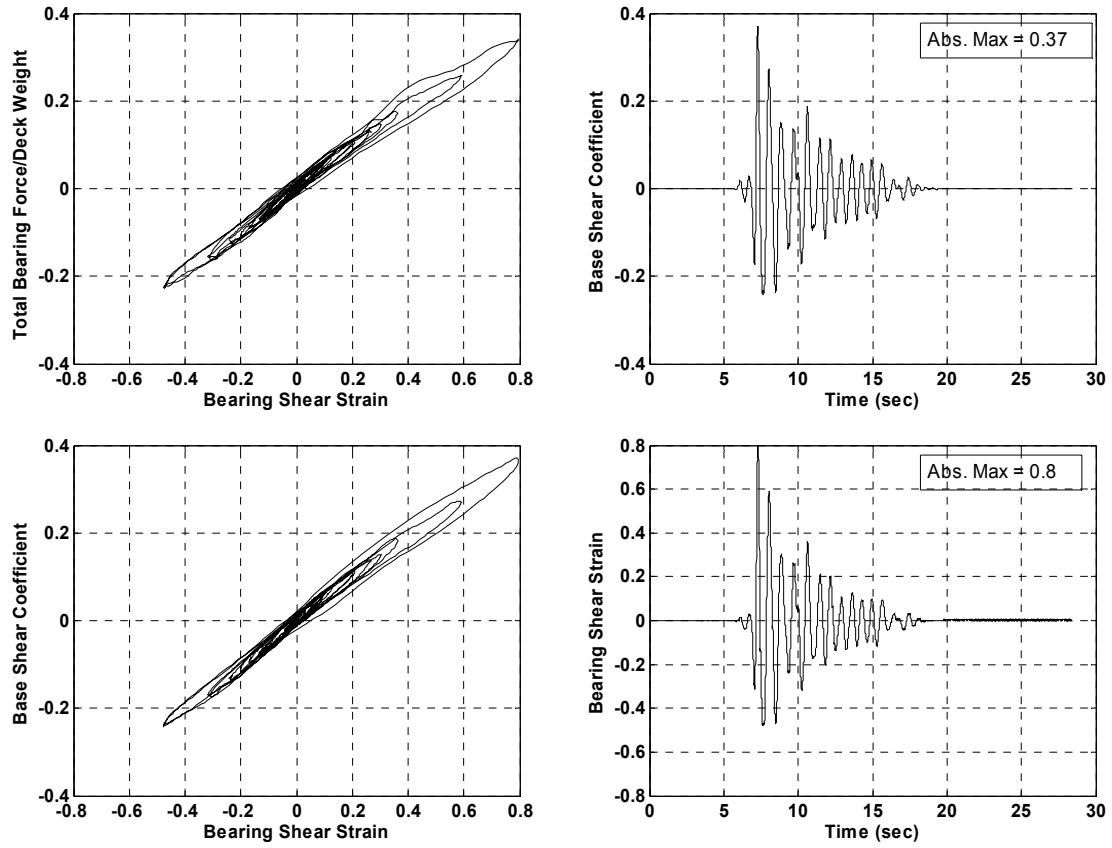
Figure B.4. Experimental results for bridge model with braced piers for the case of IB and 75% of 637-270 ground motion
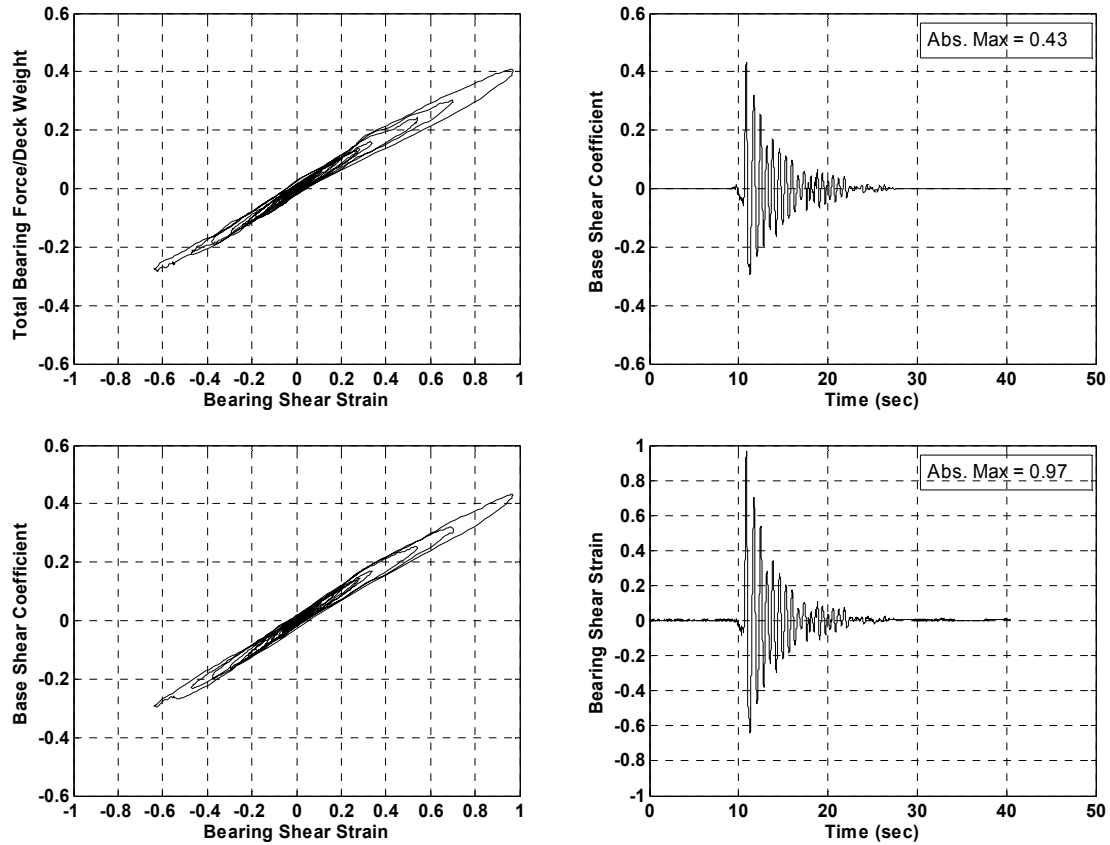
Figure B.5. Experimental results for bridge model with braced piers for the case of IB and 100% of PET-090 ground motion
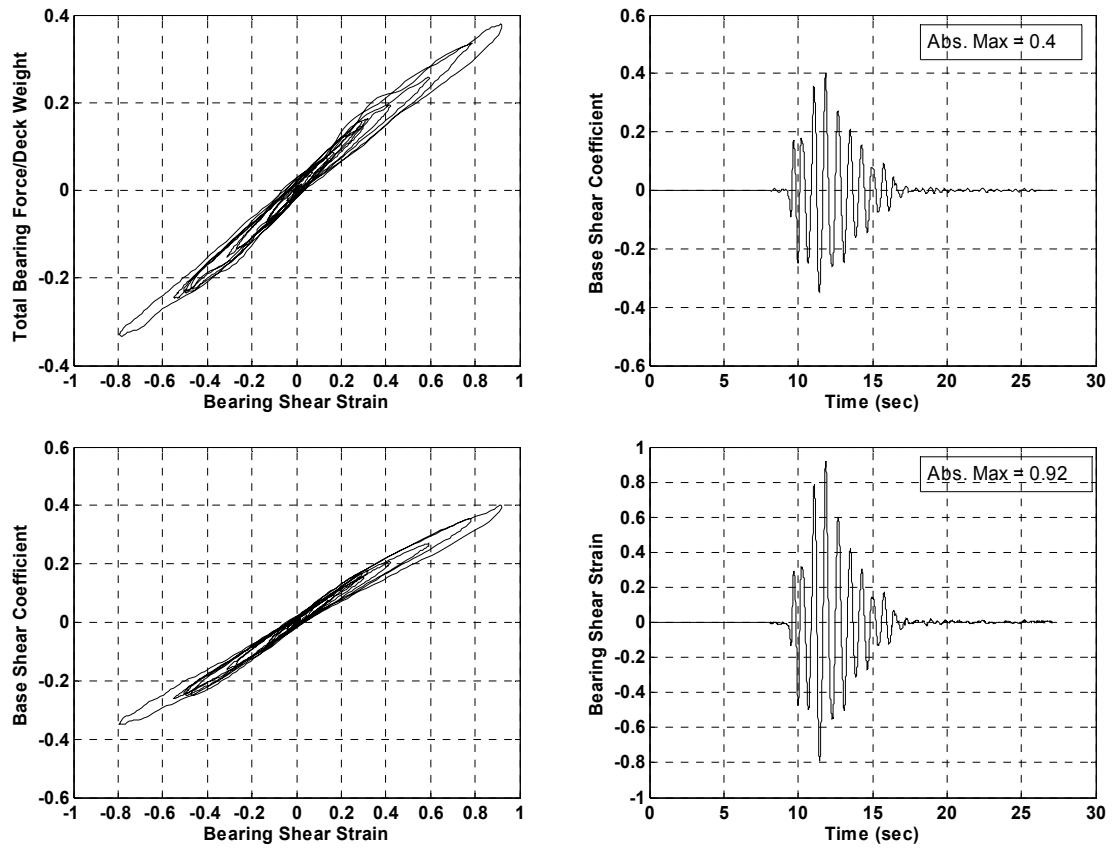
Figure B.6. Experimental results for bridge model with braced piers for the case of IB and 50% of KJM-000 ground motion
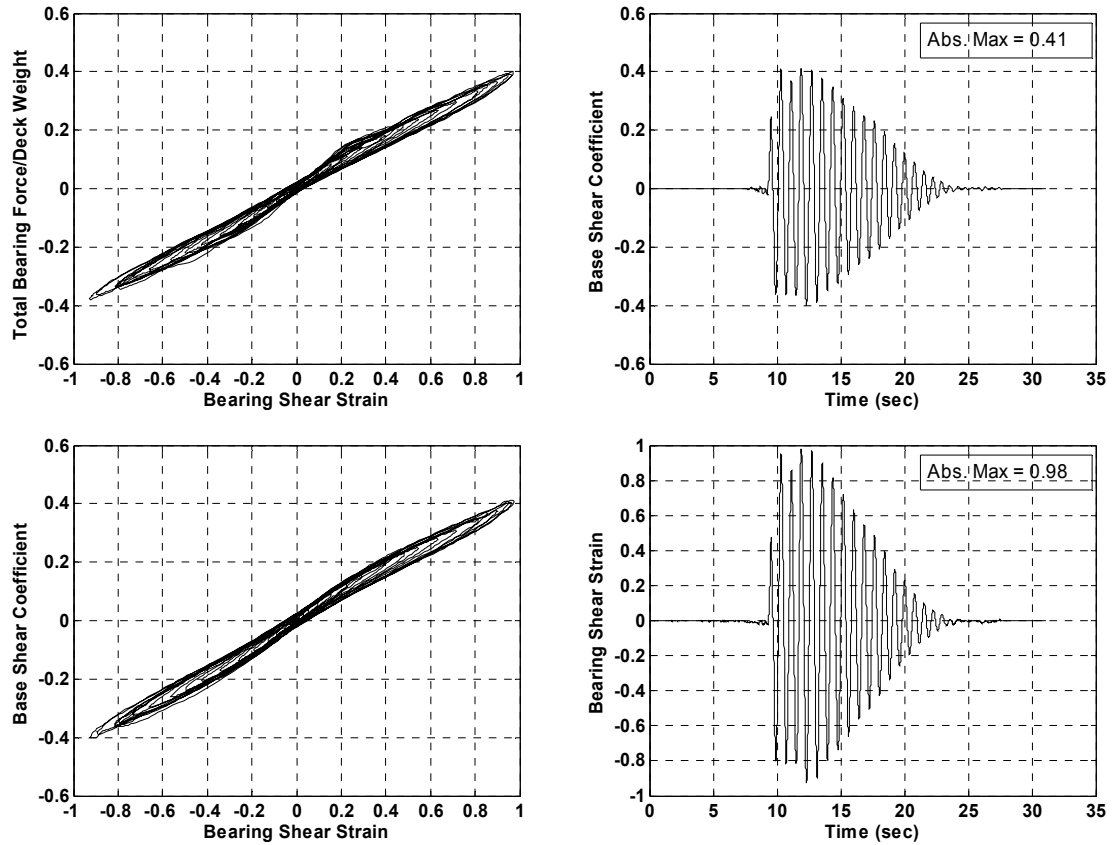
Figure B.7. Experimental results for bridge model with braced piers for the case of IB and 50% of SYL-000 ground motion

B.2. Experimental Results for Bridge Model with Unbraced Piers for the Case of Isolated Bridge (IB)
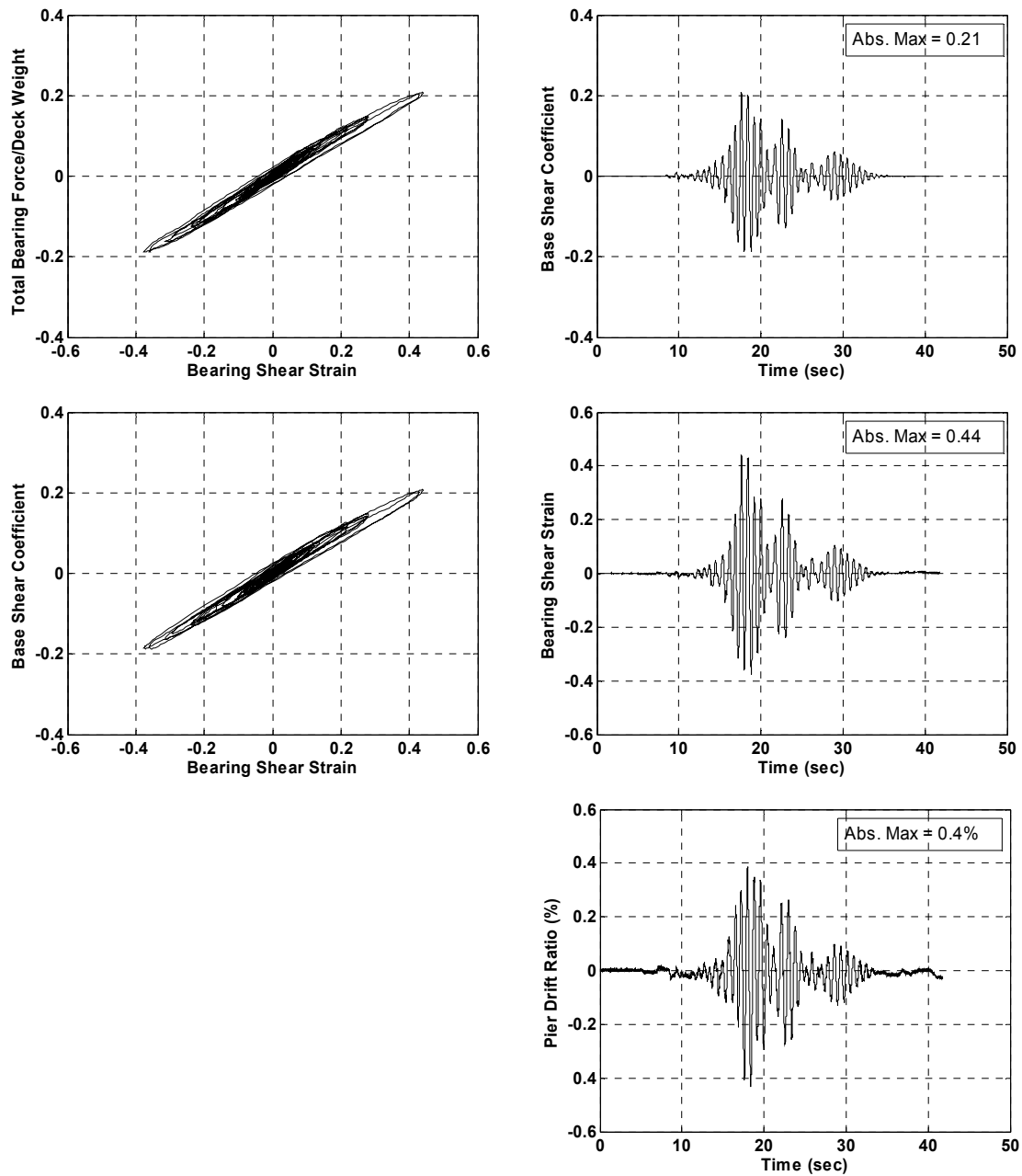
Figure B.8. Experimental results for bridge model with unbraced piers for the case of IB and 100% of YER-000 ground motion

123
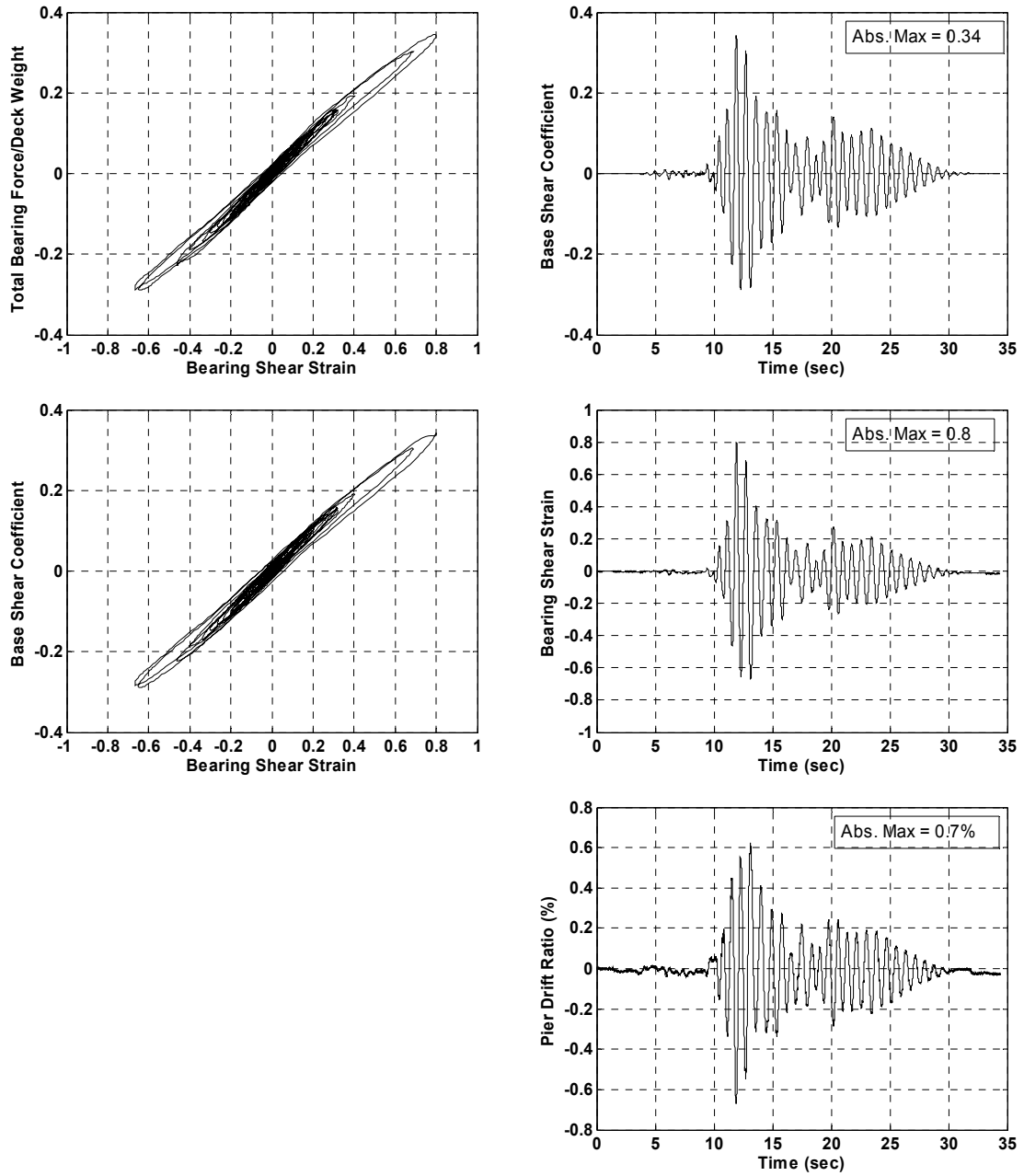
Figure B.9. Experimental results for bridge model with unbraced piers for the case of IB and 100% of YER-270 ground motion
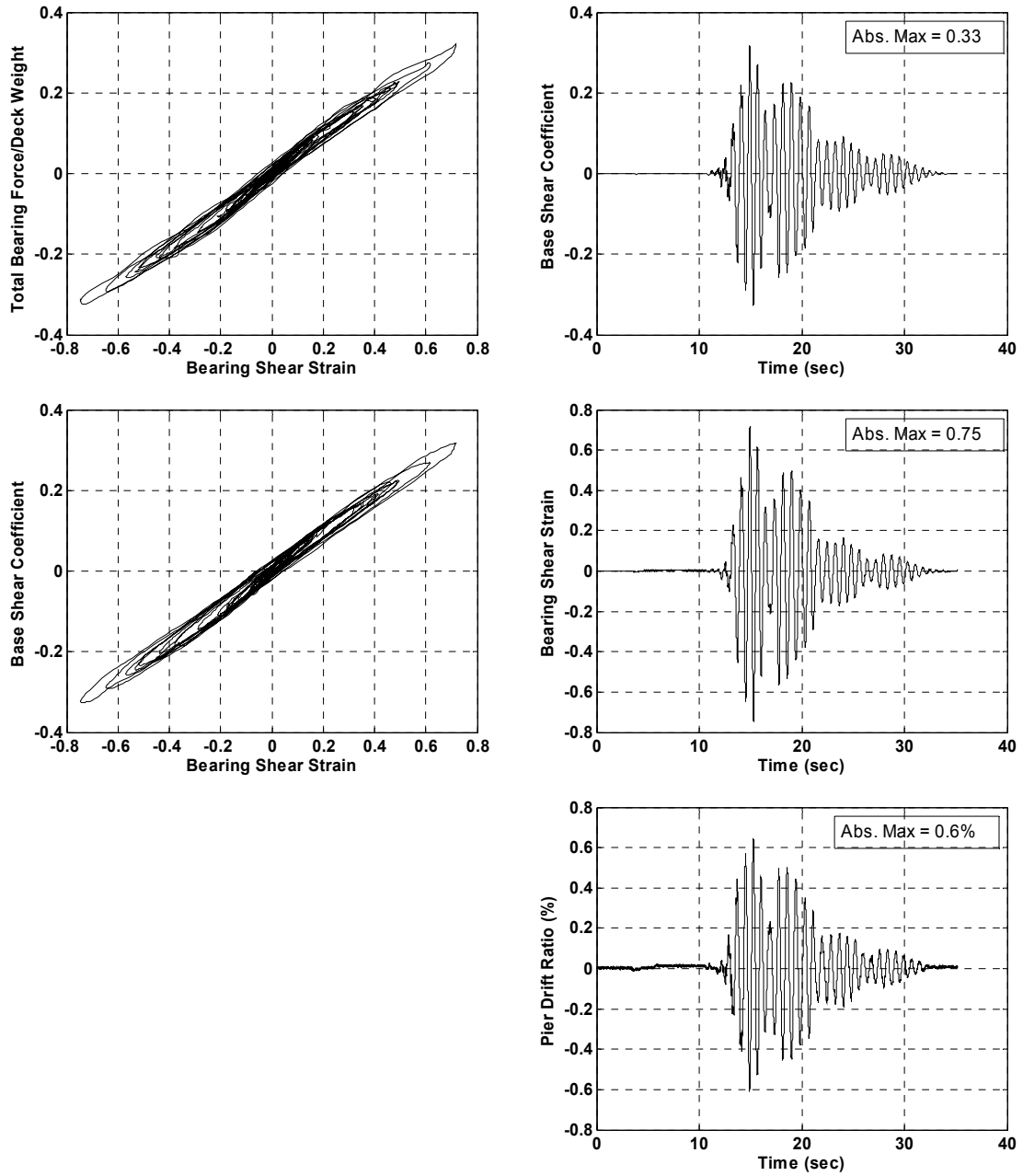
Figure B.10. Experimental results for bridge model with unbraced piers for the case of IB and 100% of CAP-000 ground motion
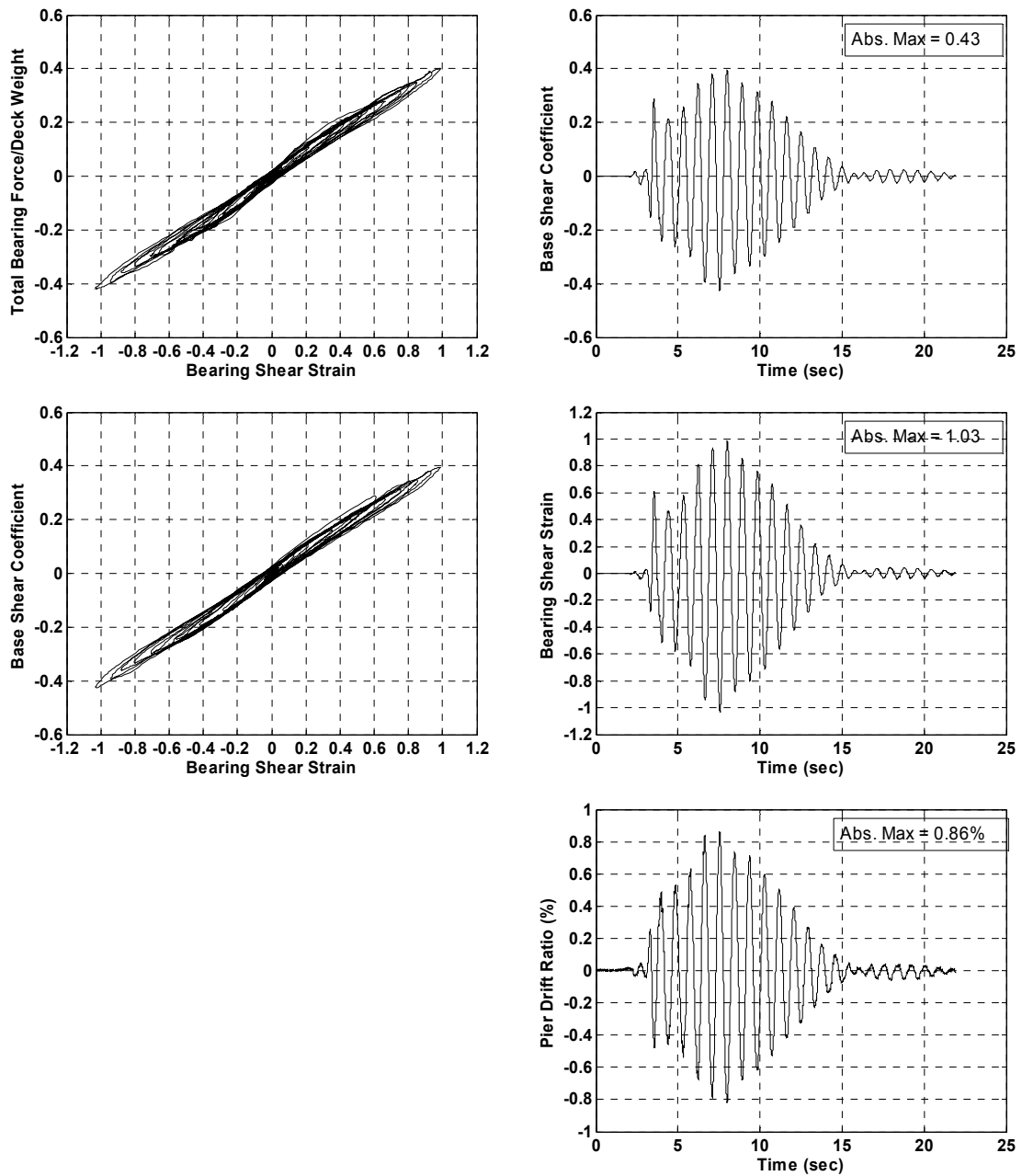
Figure B.11. Experimental results for bridge model with unbraced piers for the case of IB and 75% of 637-270 ground motion
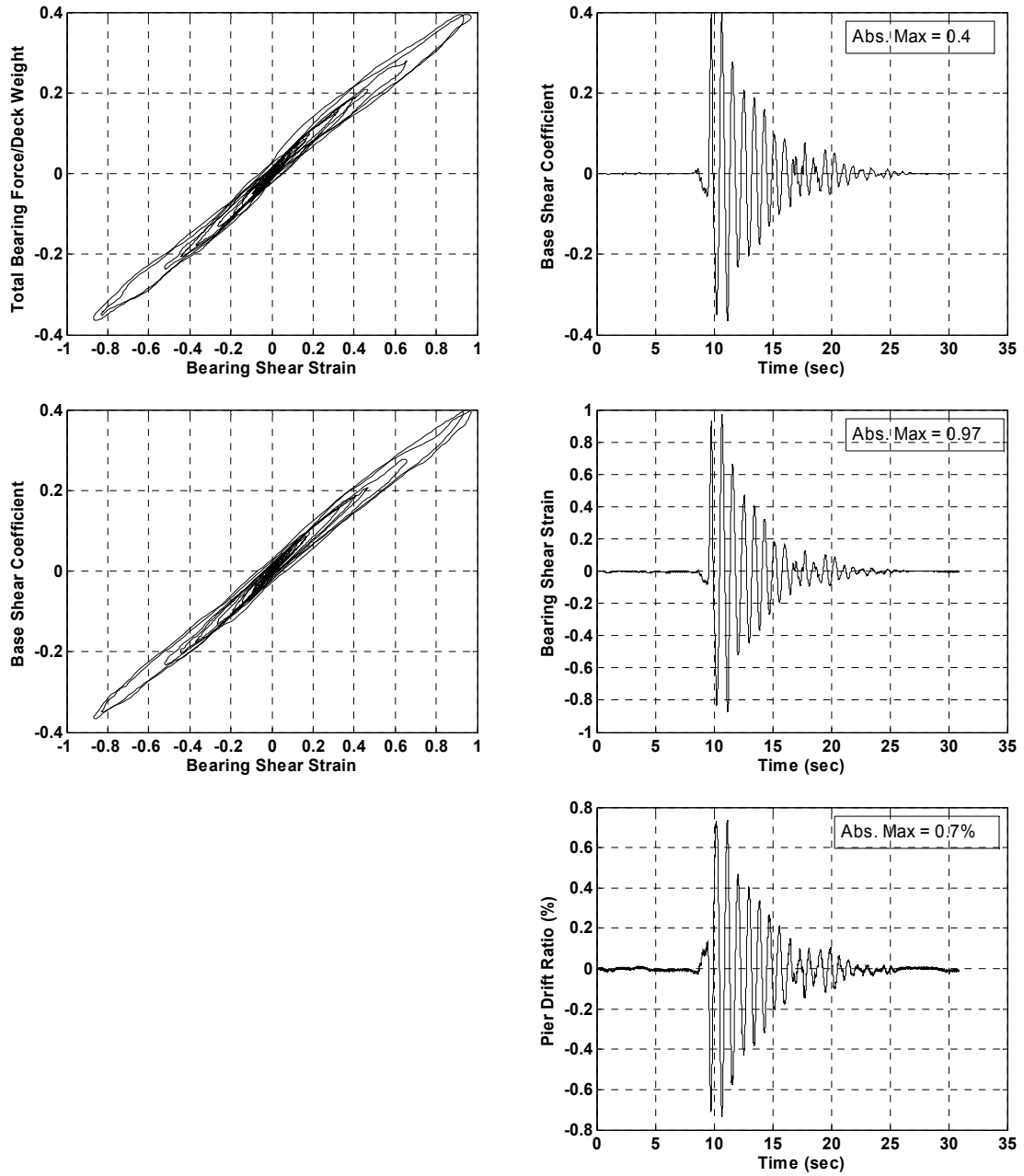
Figure B.12. Experimental results for bridge model with unbraced piers for the case of IB and 100% of PET-090 ground motion
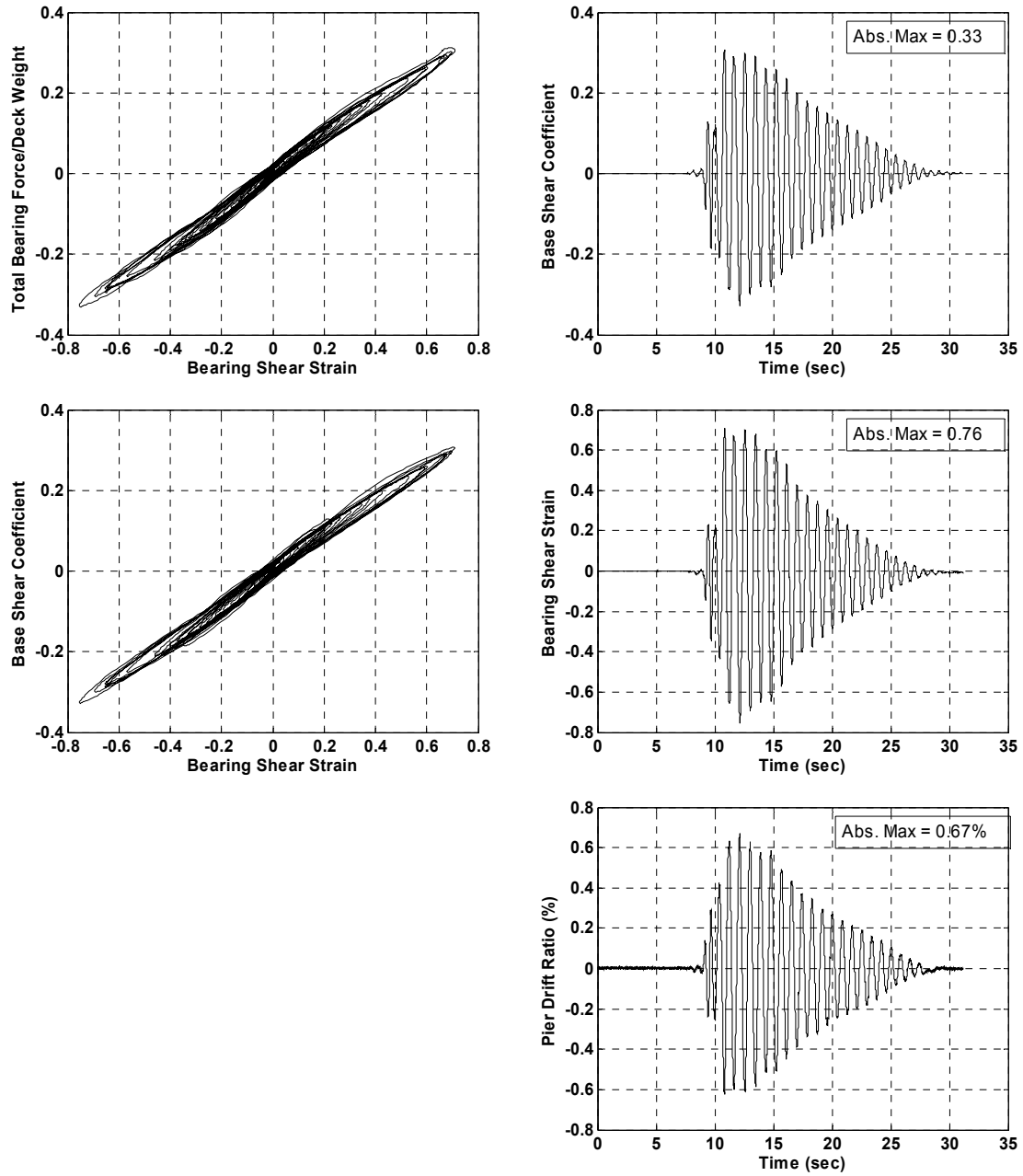
Figure B.13. Experimental results for bridge model with unbraced piers for the case of IB and 50% of KJM-000 ground motion
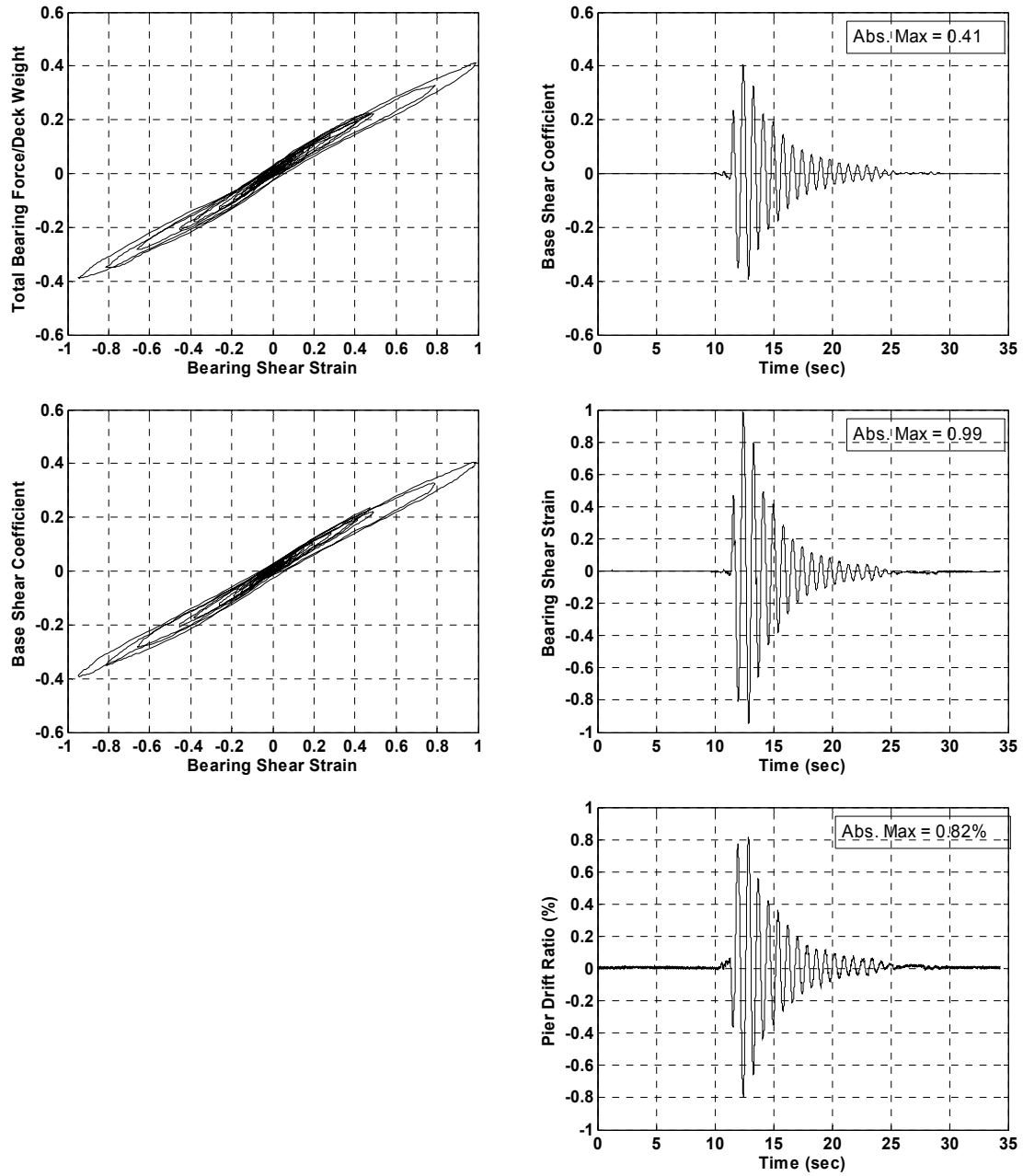
Figure B.14. Experimental results for bridge model with unbraced piers for the case of IB and 50% of SYL-000 ground motion

B.3. Experimental Results for Bridge Model with Braced Piers for the Case of Isolated Bridge with Passive Damper (IB+PD)
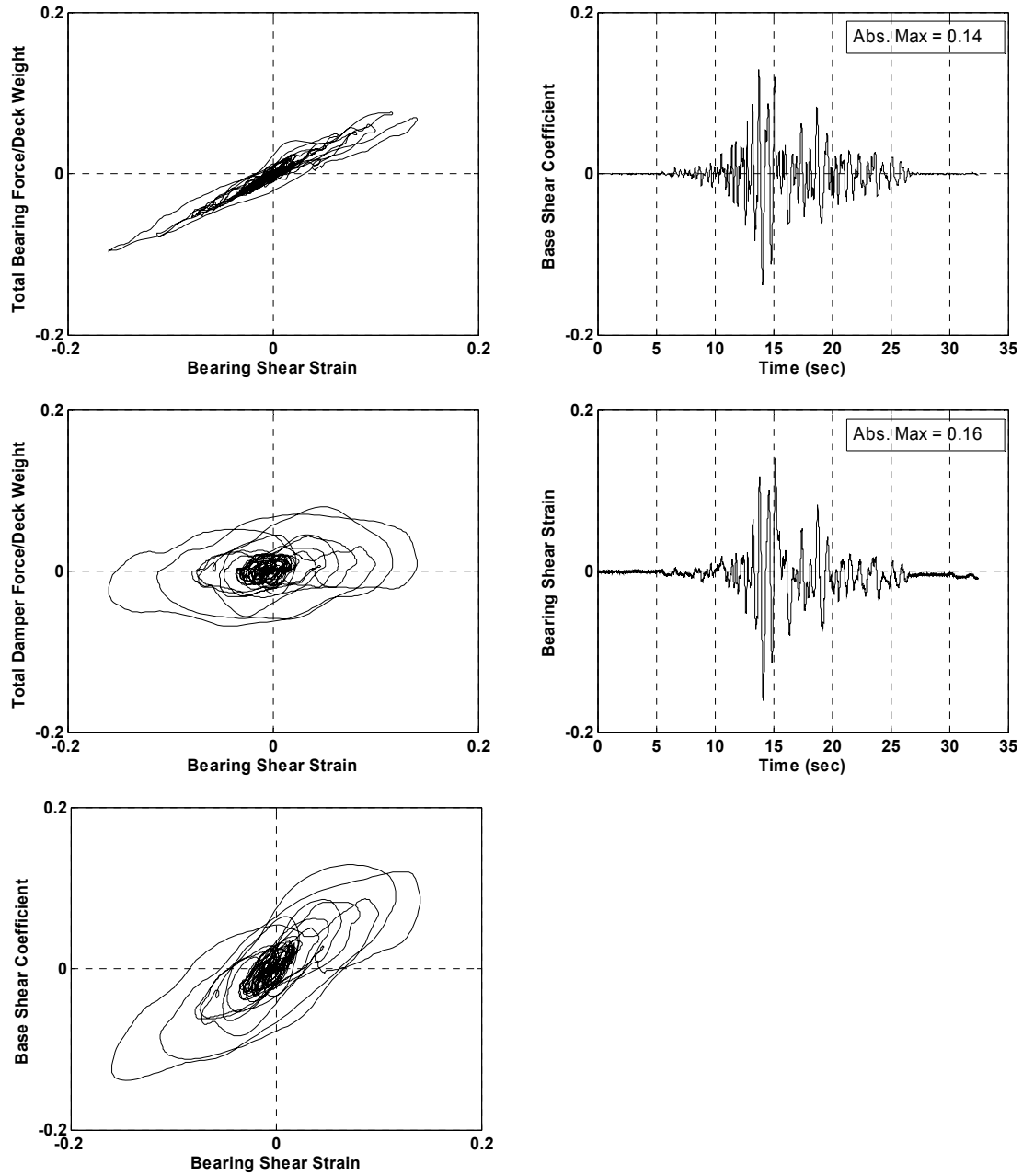
Figure B.15. Experimental results for bridge model with braced piers for the case of IB+PD and 100% of YER-000 ground motion
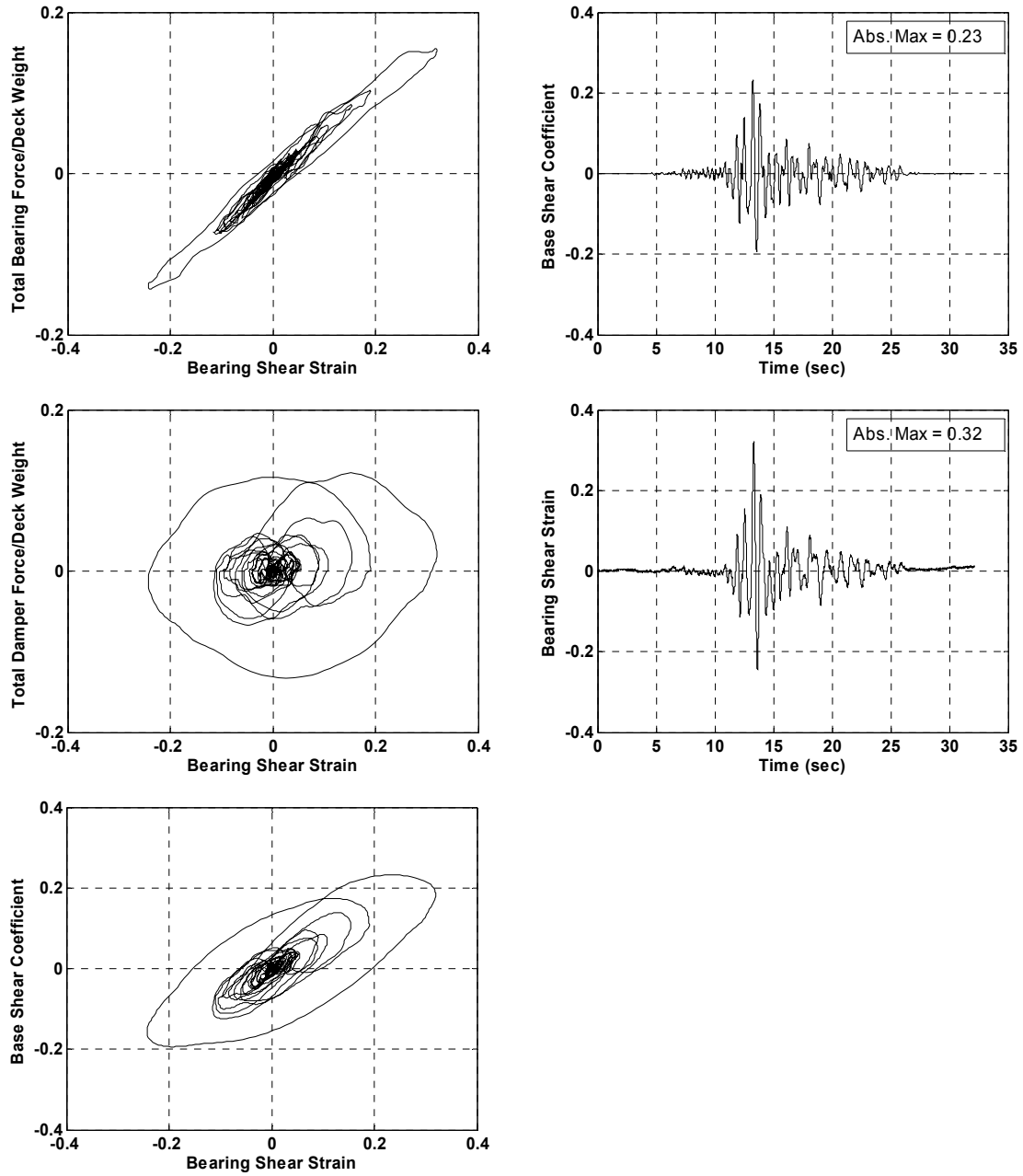
Figure B.16. Experimental results for bridge model with braced piers for the case of IB+PD and 100% of YER-270 ground motion

132
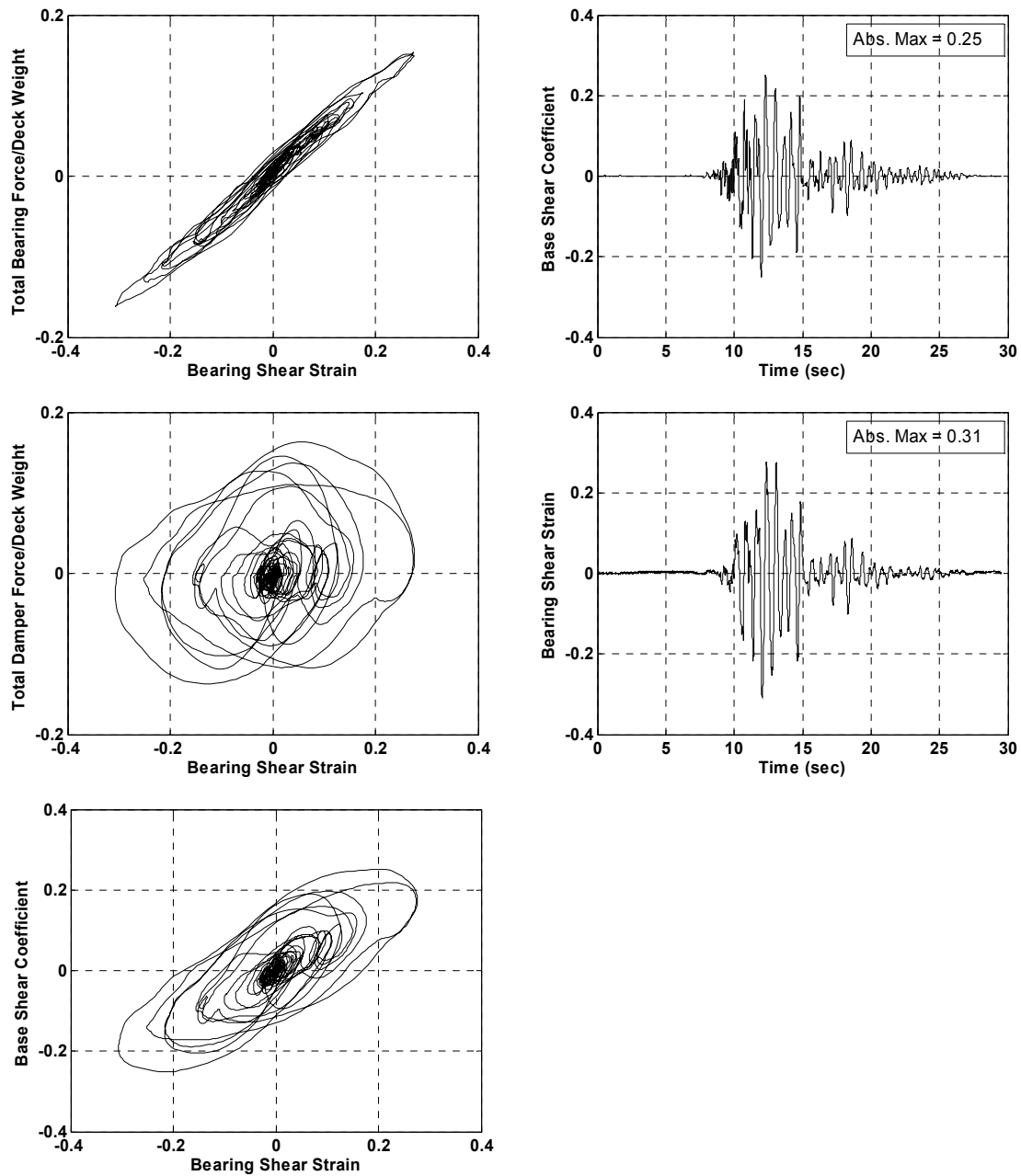
Figure B.17. Experimental results for bridge model with braced piers for the case of IB+PD and 100% of CAP-000 ground motion

133
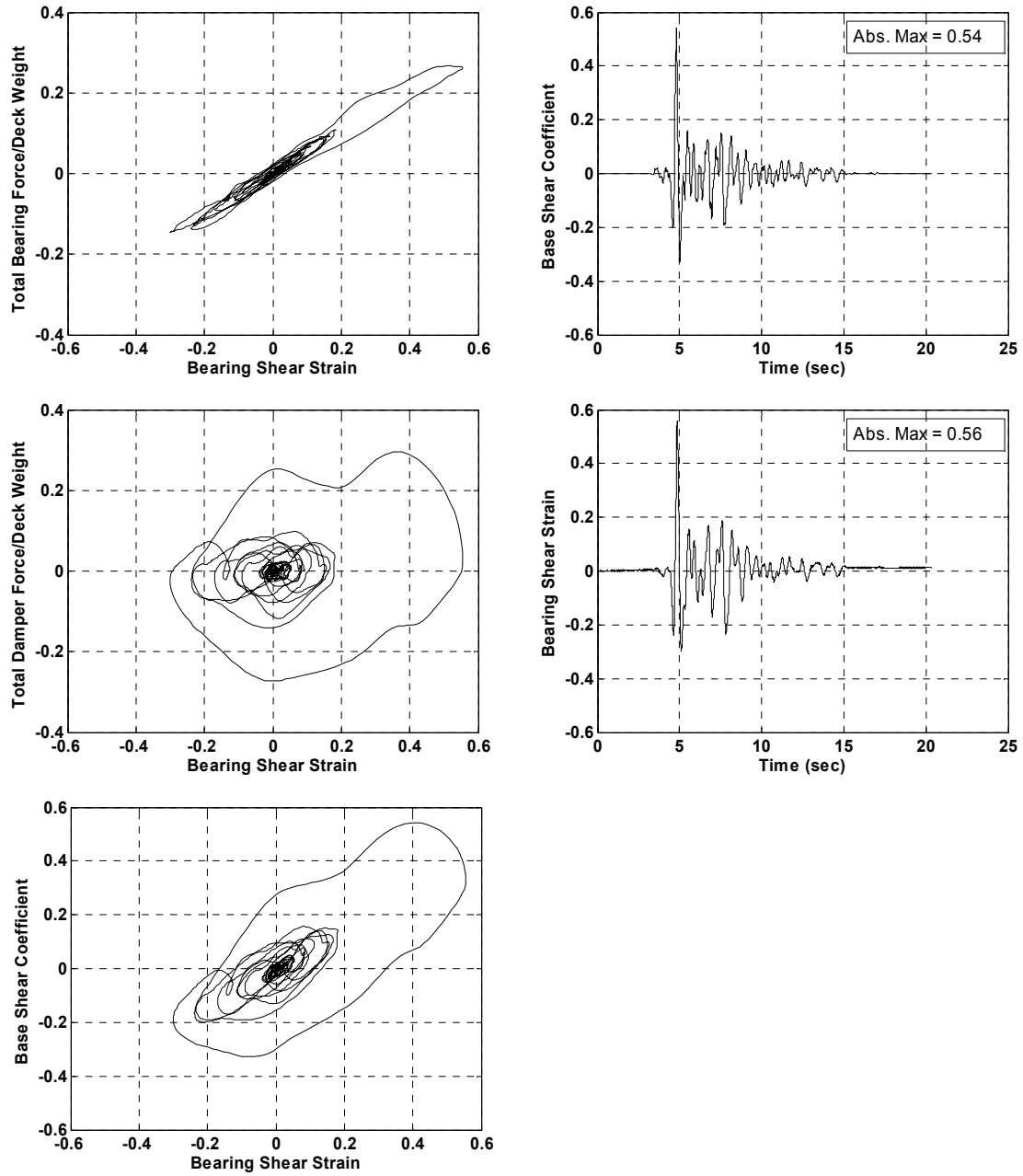
Figure B.18. Experimental results for bridge model with braced piers for the case of IB+PD and 100% of 637-270 ground motion
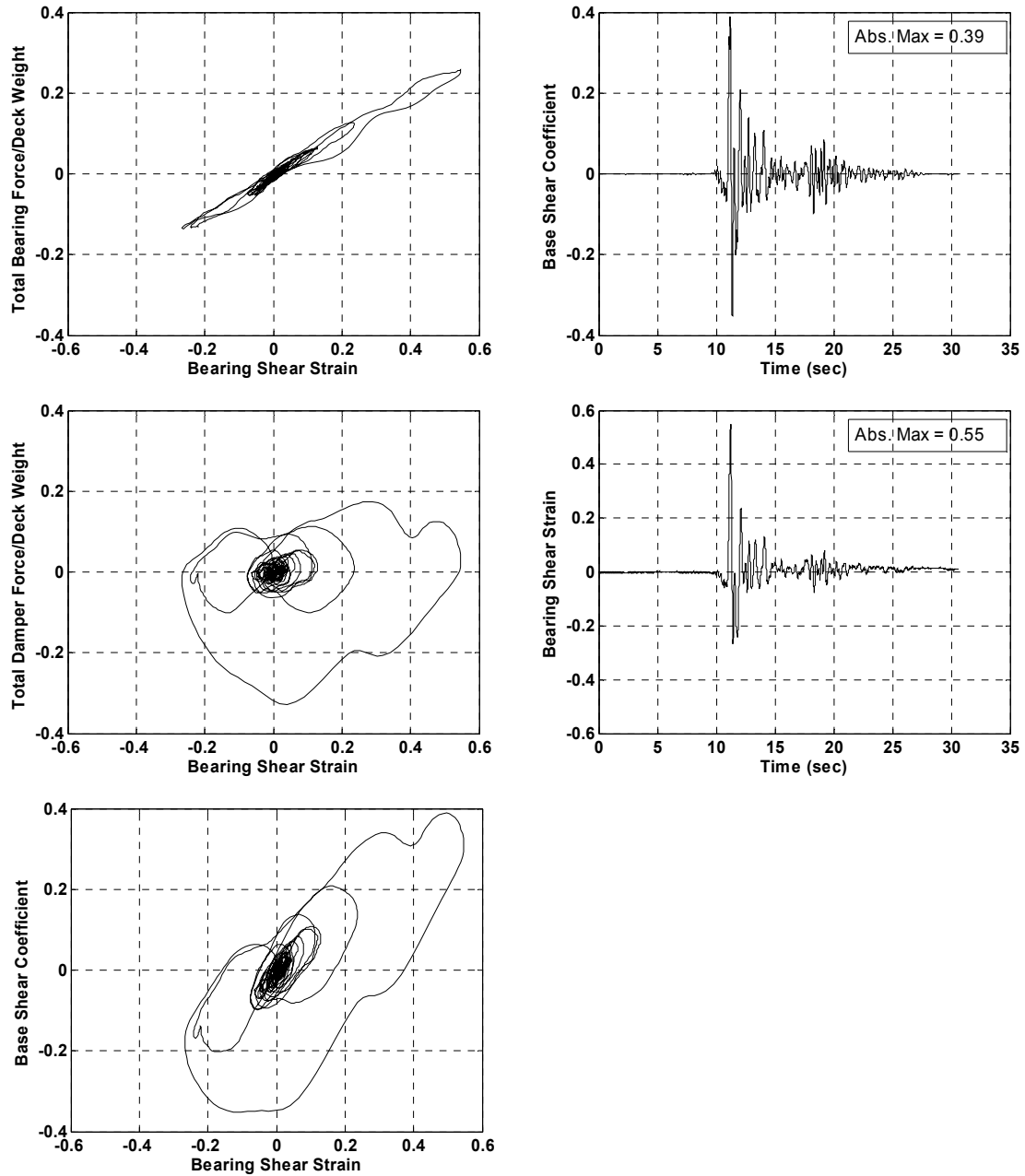
Figure B.19. Experimental results for bridge model with braced piers for the case of IB+PD and 100% of PET-090 ground motion

135
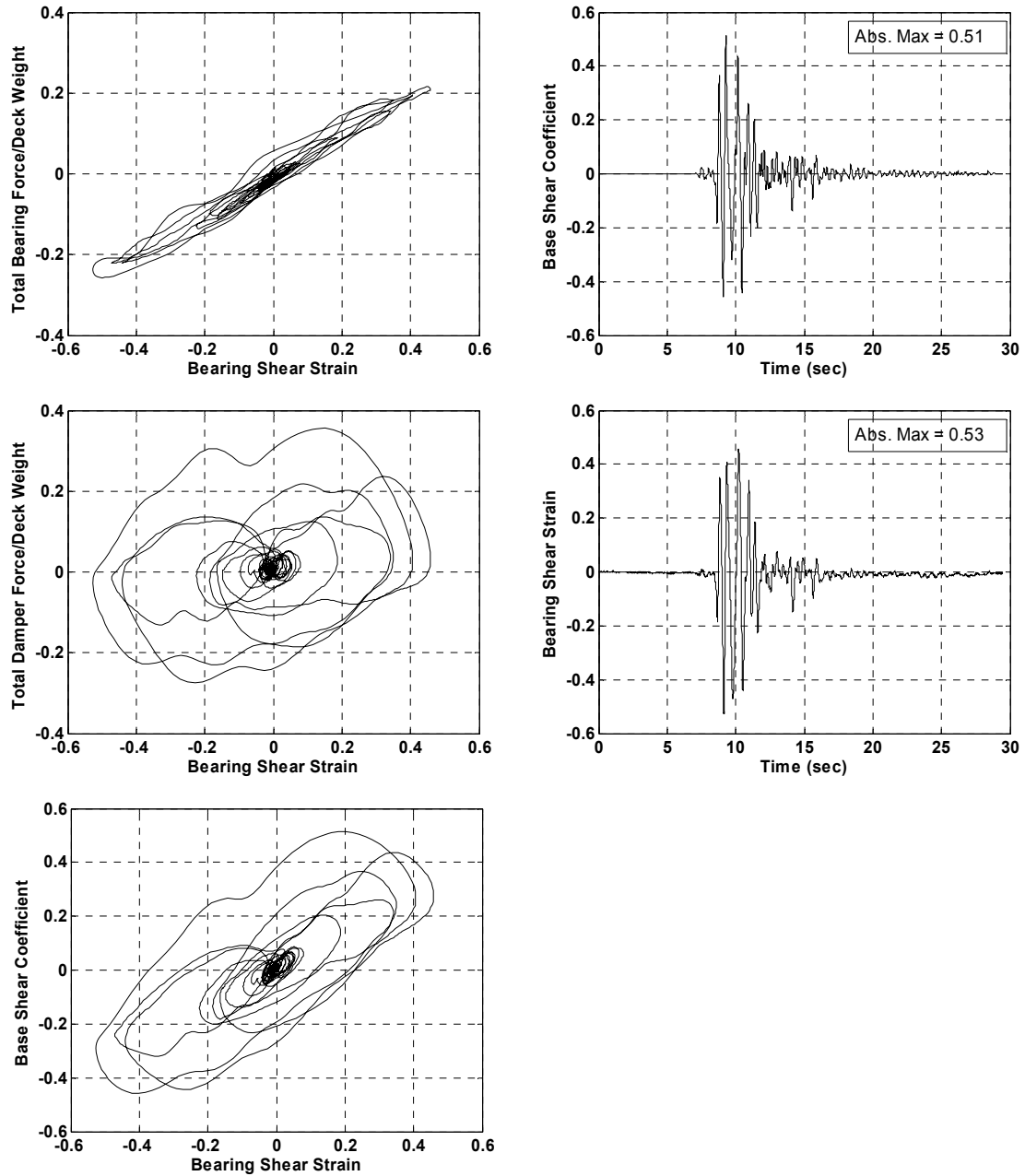
Figure B.20. Experimental results for bridge model with braced piers for the case of IB+PD and 100% of KJM-000 ground motion

136
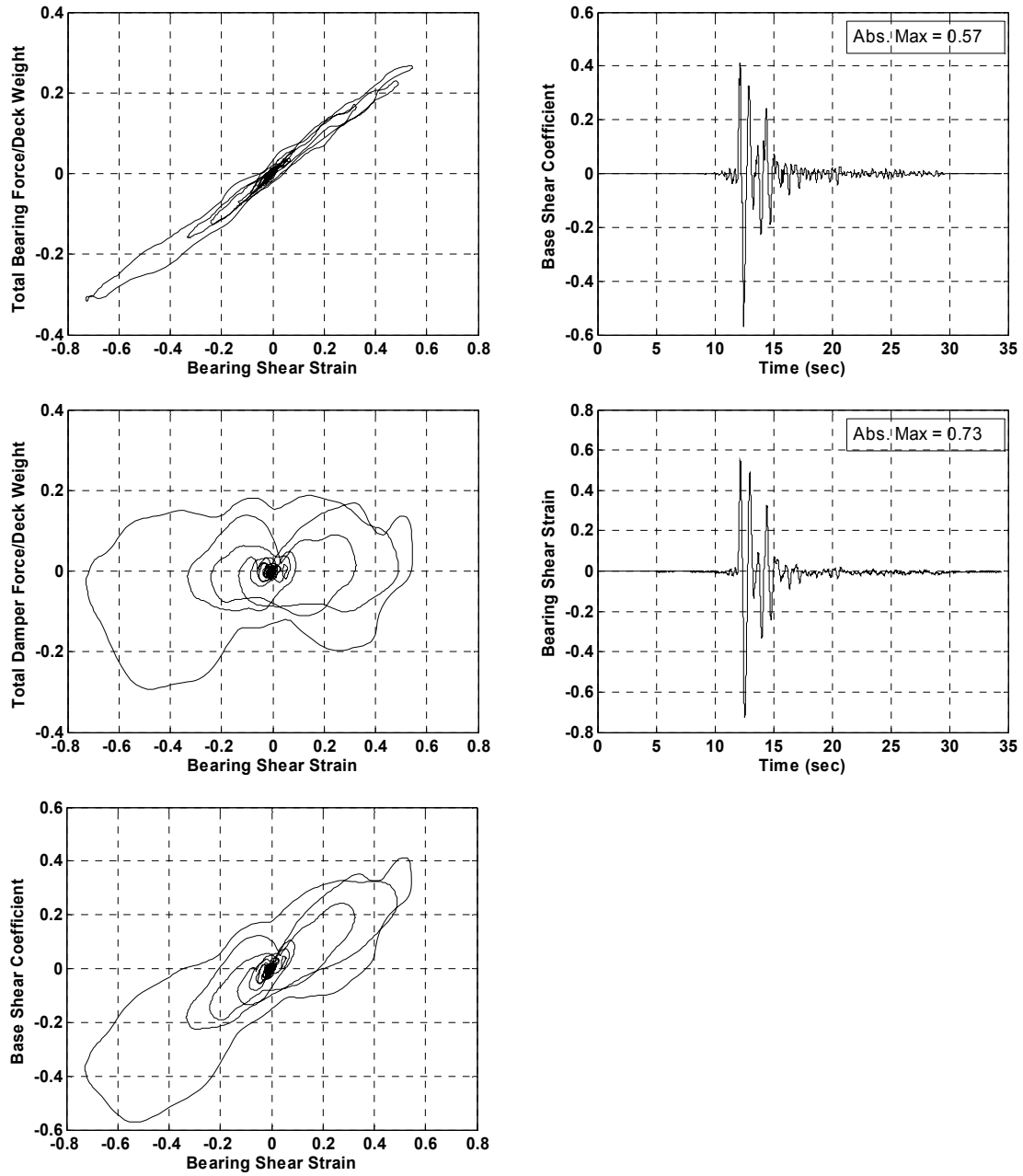
Figure B.21. Experimental results for bridge model with braced piers for the case of IB+PD and 100% of SYL-000 ground motion

137

B.4. Experimental Results for Bridge Model with Unbraced Piers for the Case of Isolated Bridge with Passive Damper (IB+PD)
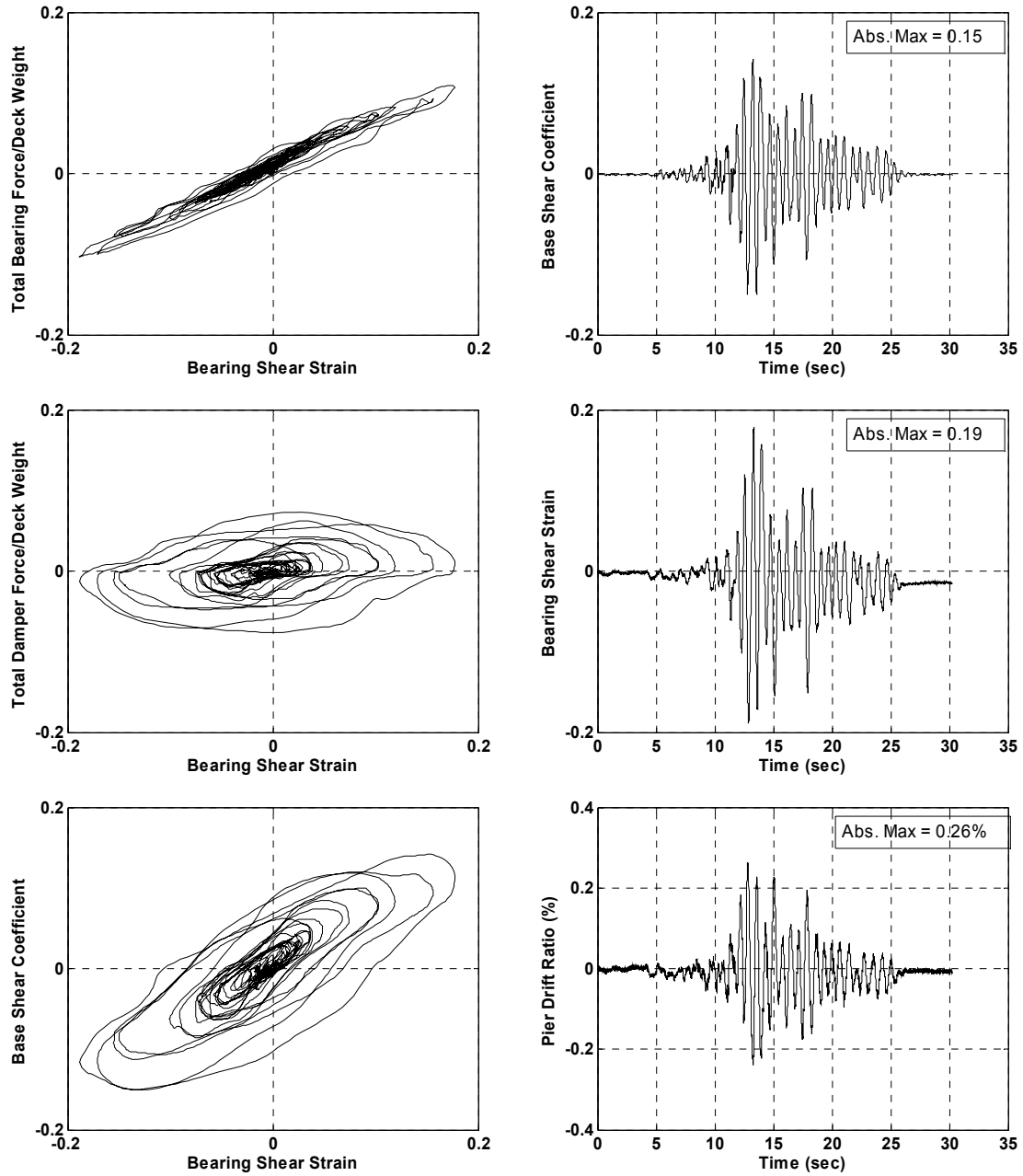
Figure B.22. Experimental results for bridge model with unbraced piers for the case of IB+PD and 100% of YER-000 ground motion

139
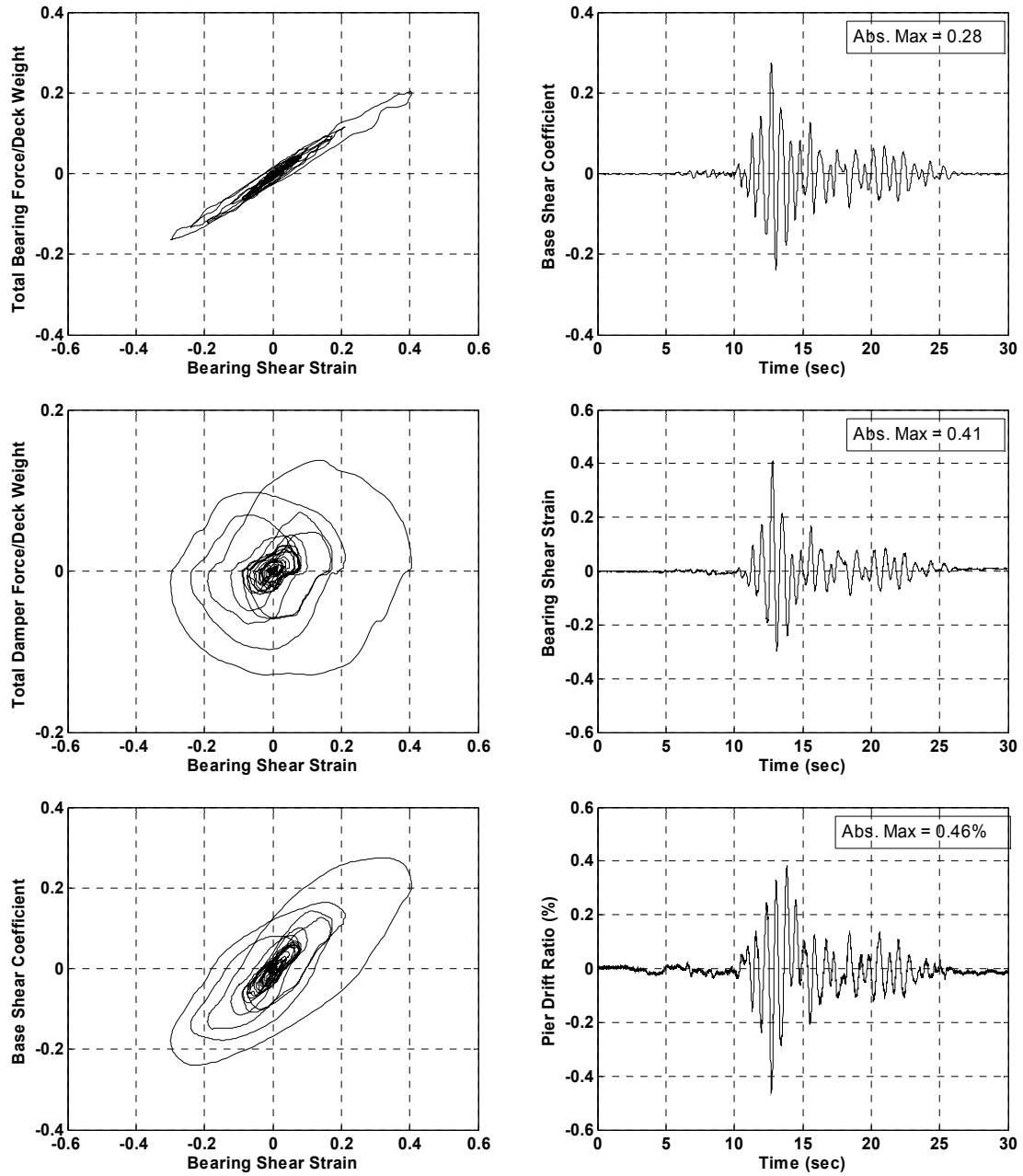
Figure B.23. Experimental results for bridge model with unbraced piers for the case of IB+PD and 100% of YER-270 ground motion

140
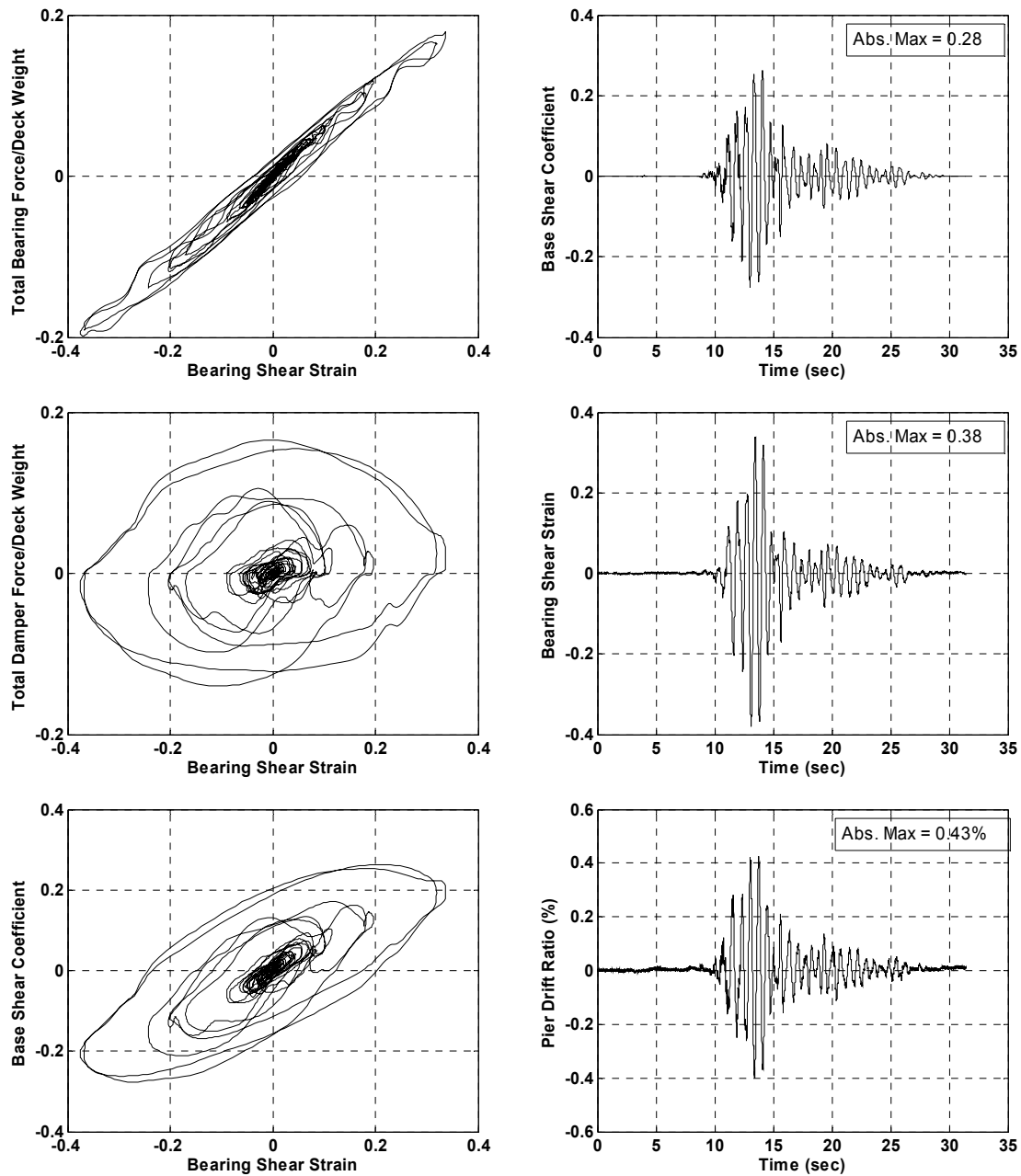
Figure B.24. Experimental results for bridge model with unbraced piers for the case of IB+PD and 100% of CAP-000 ground motion

141
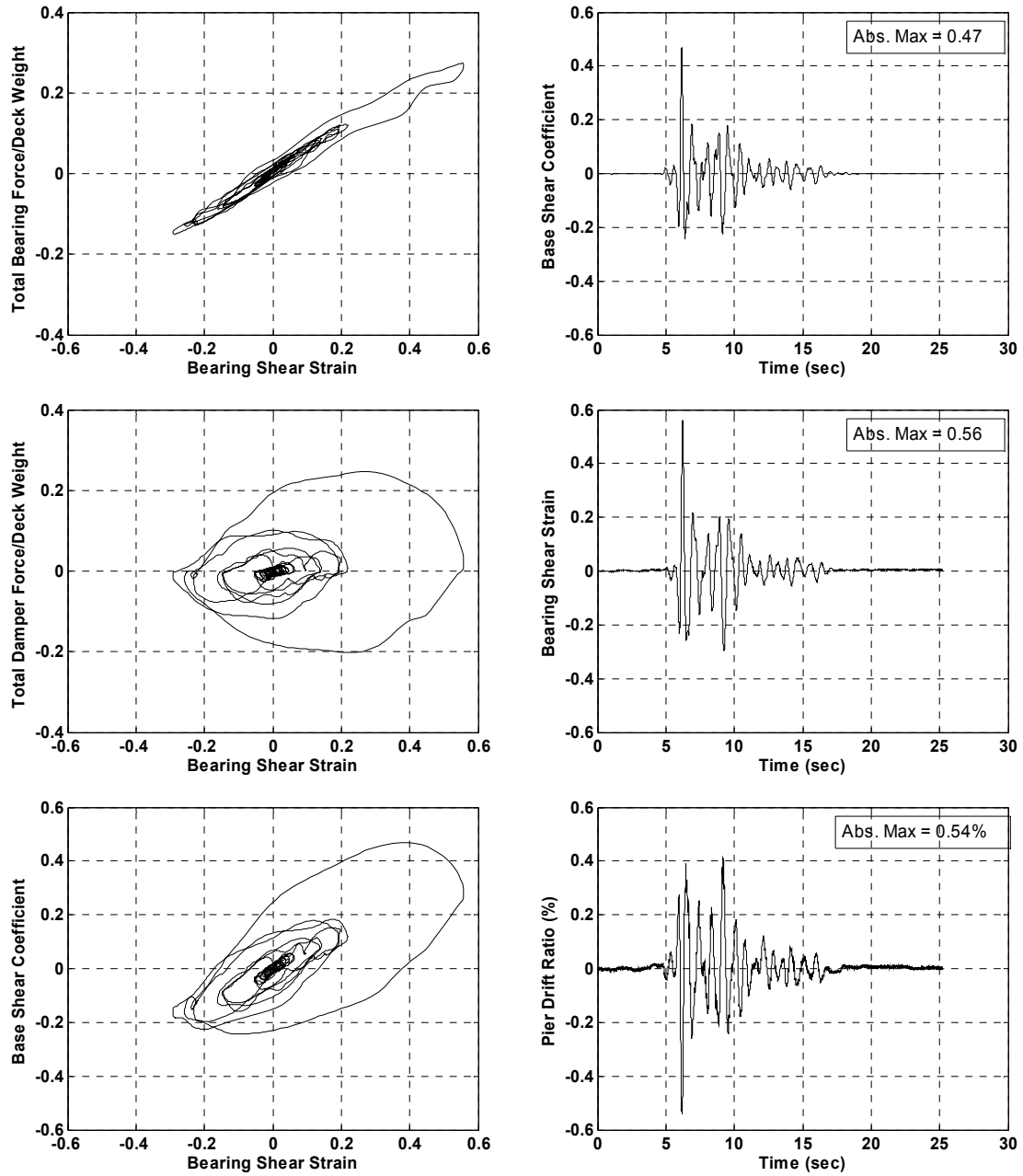
Figure B.25. Experimental results for bridge model with unbraced piers for the case of IB+PD and 100% of 637-270 ground motion

142
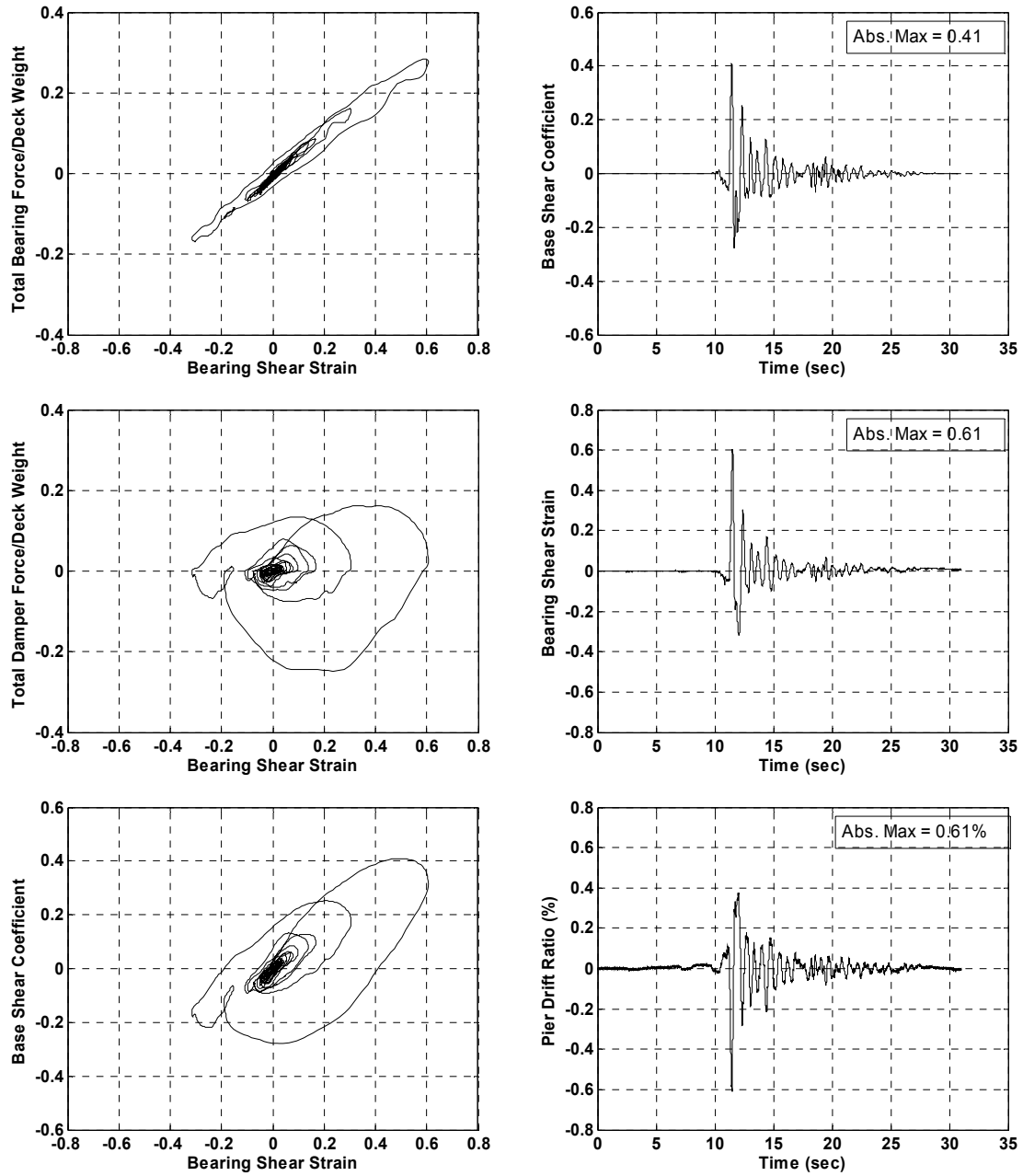
Figure B.26. Experimental results for bridge model with unbraced piers for the case of IB+PD and 100% of PET-090 ground motion

143
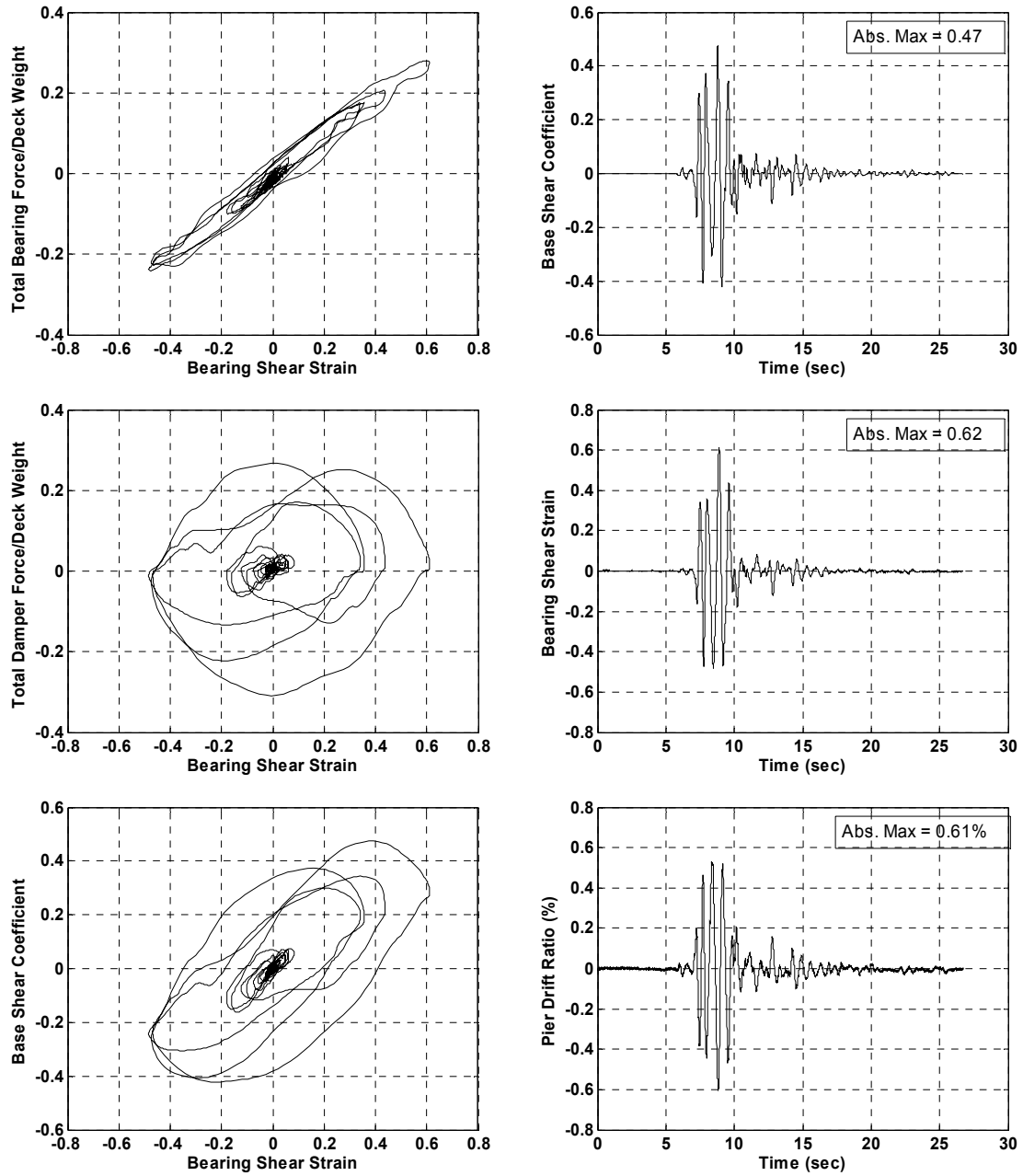
Figure B.27. Experimental results for bridge model with unbraced piers for the case of IB+PD and 100% of KJM-000 ground motion
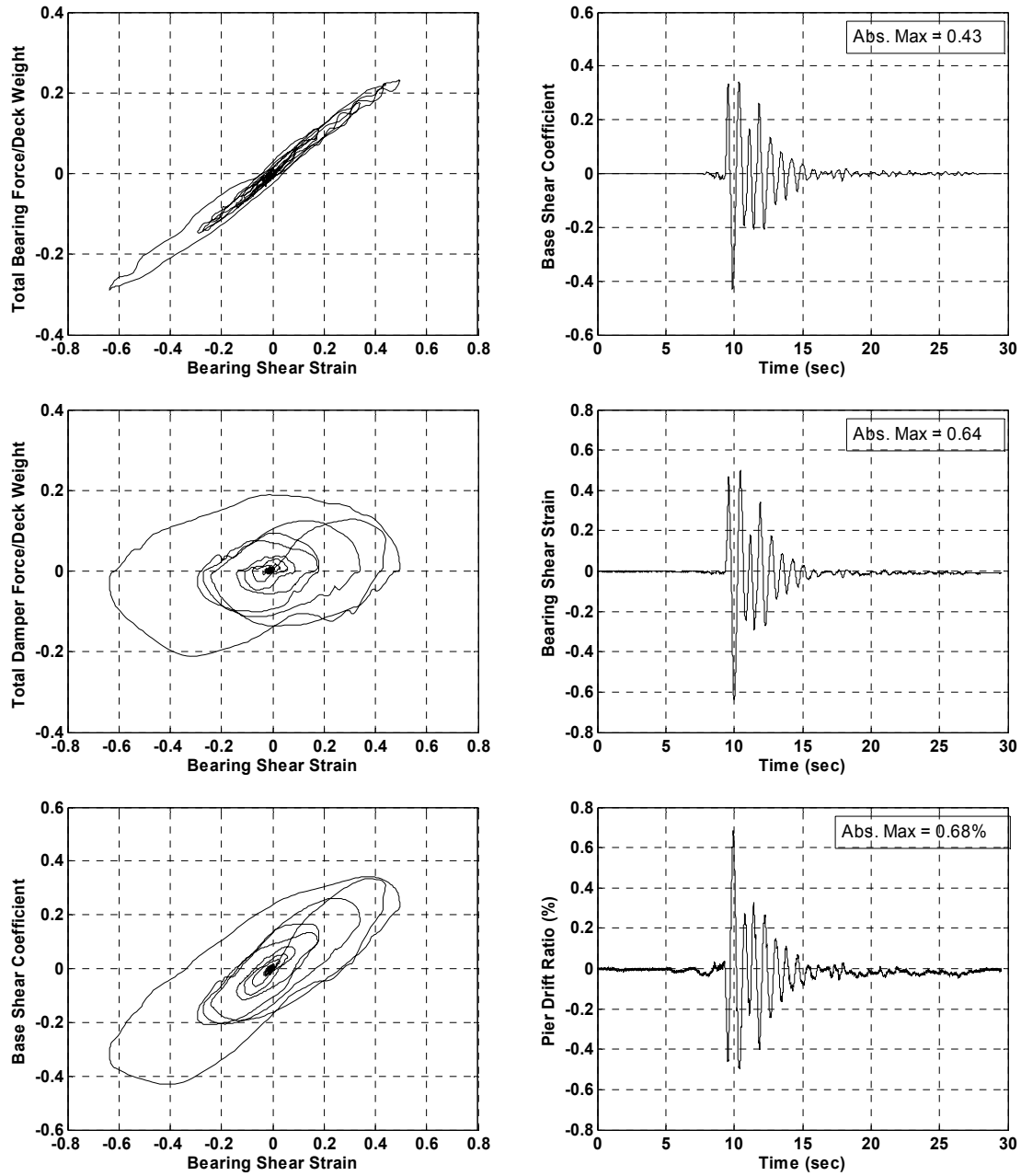
Figure B.28. Experimental results for bridge model with unbraced piers for the case of IB+PD and 75% of SYL-000 ground motion

145

B.5. Experimental Results for Bridge Model with Braced Piers for the Case of Isolated Bridge with Negative Stiffness Device (IB+NSD)
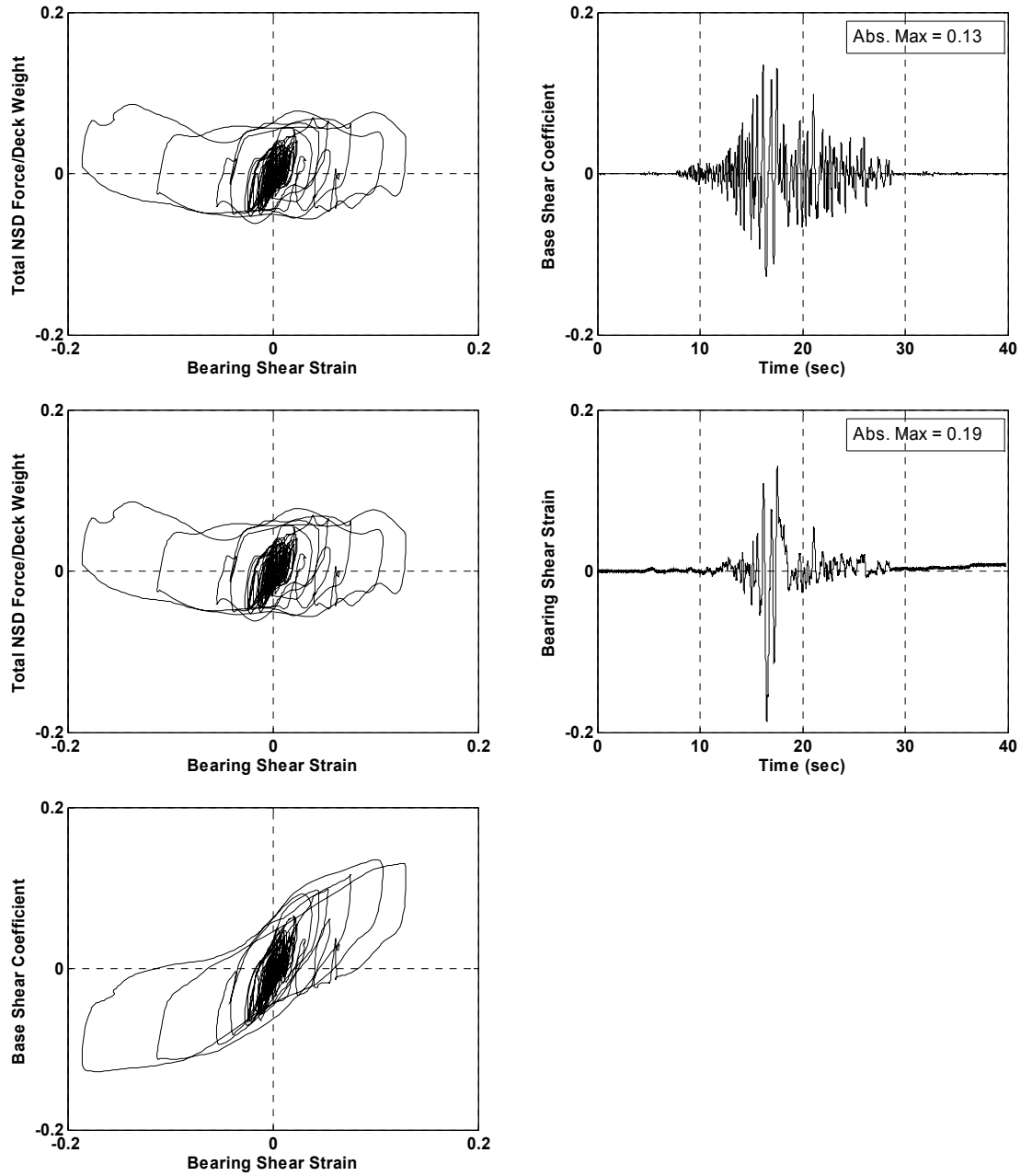
Figure B.29. Experimental results for bridge model with braced piers for the case of IB+NSD and 100% of YER-000 ground motion
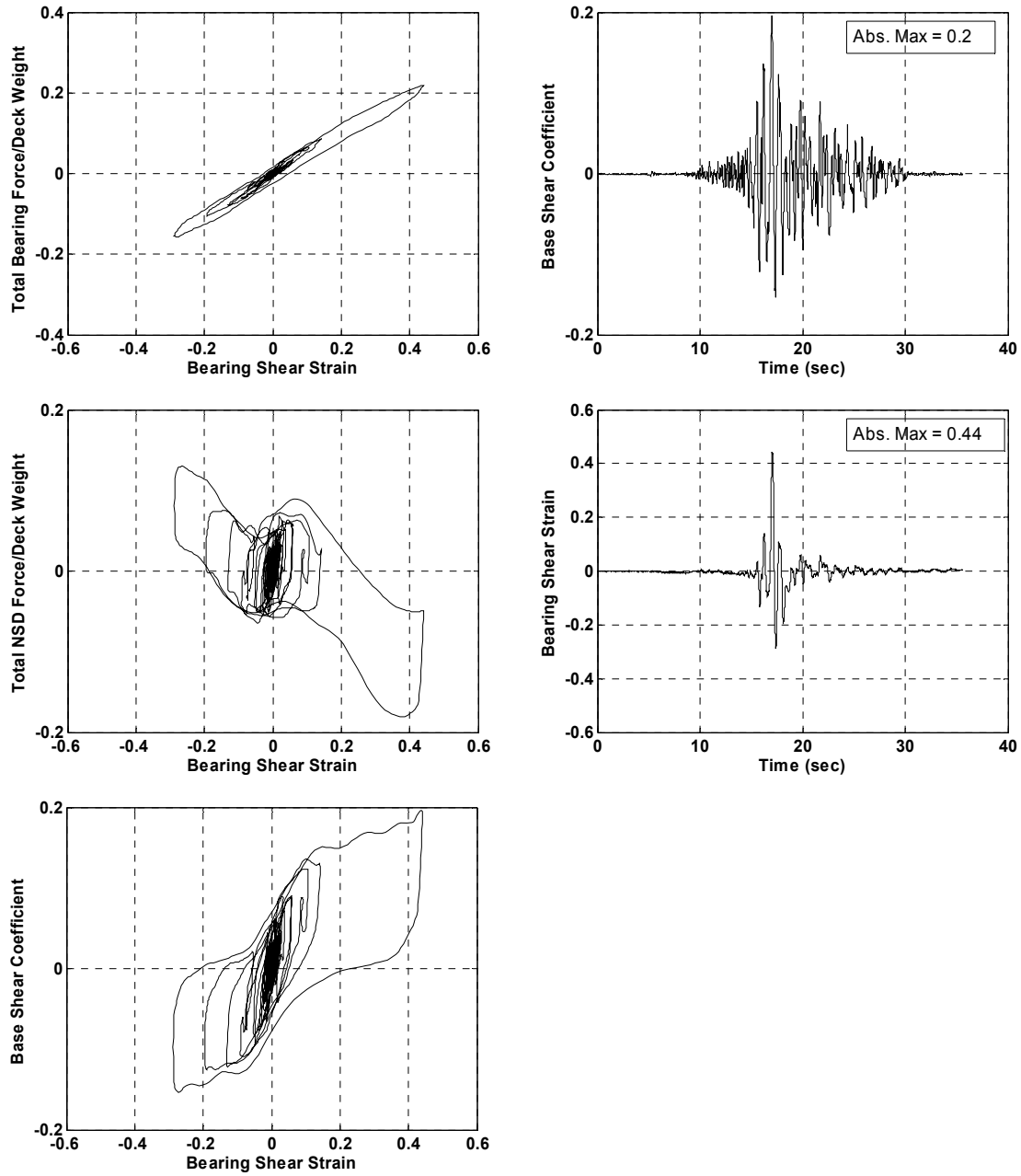
Figure B.30. Experimental results for bridge model with braced piers for the case of IB+NSD and 100% of YER-270 ground motion

148
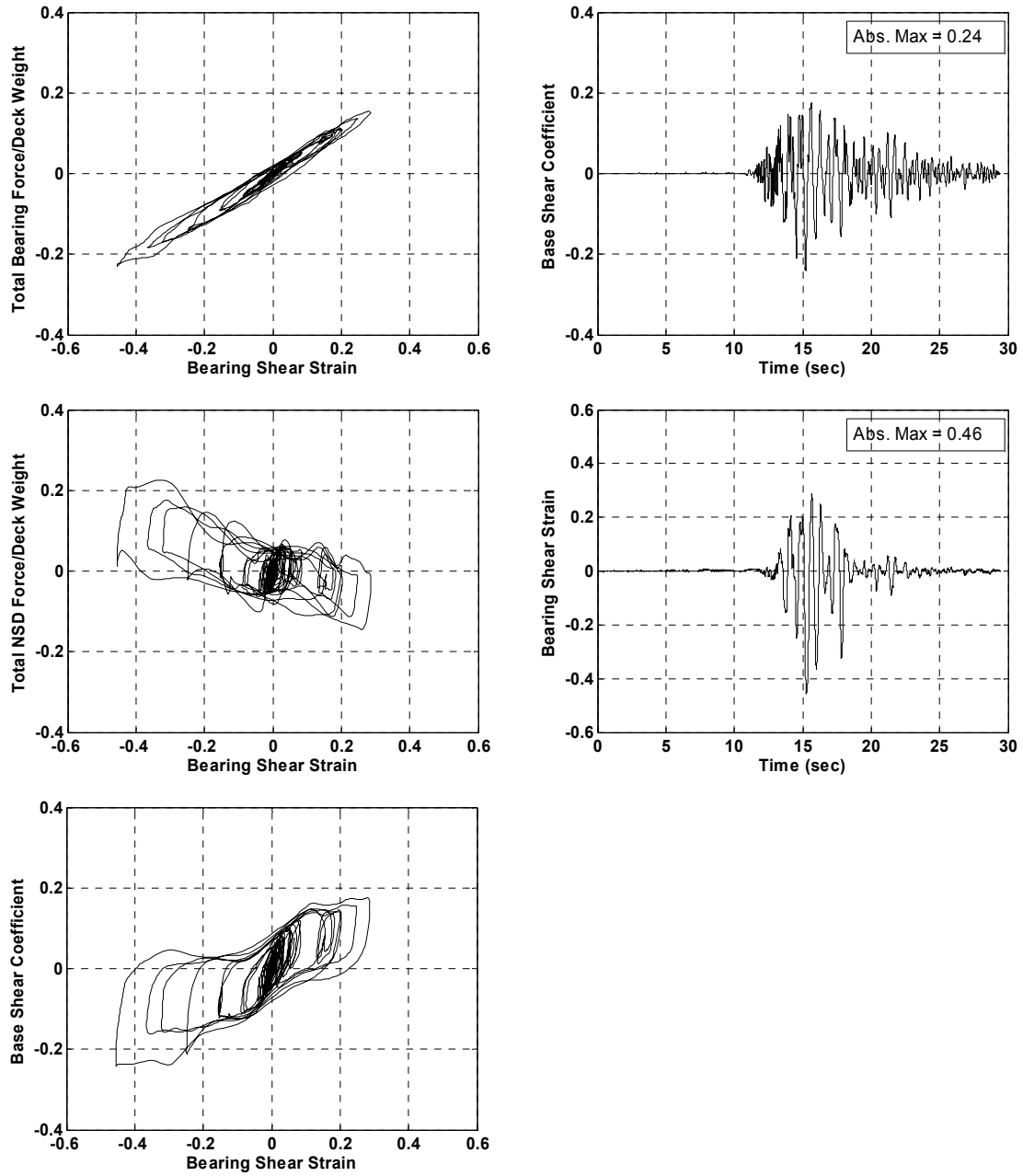
Figure B.31. Experimental results for bridge model with braced piers for the case of IB+NSD and 100% of CAP-000 ground motion

149
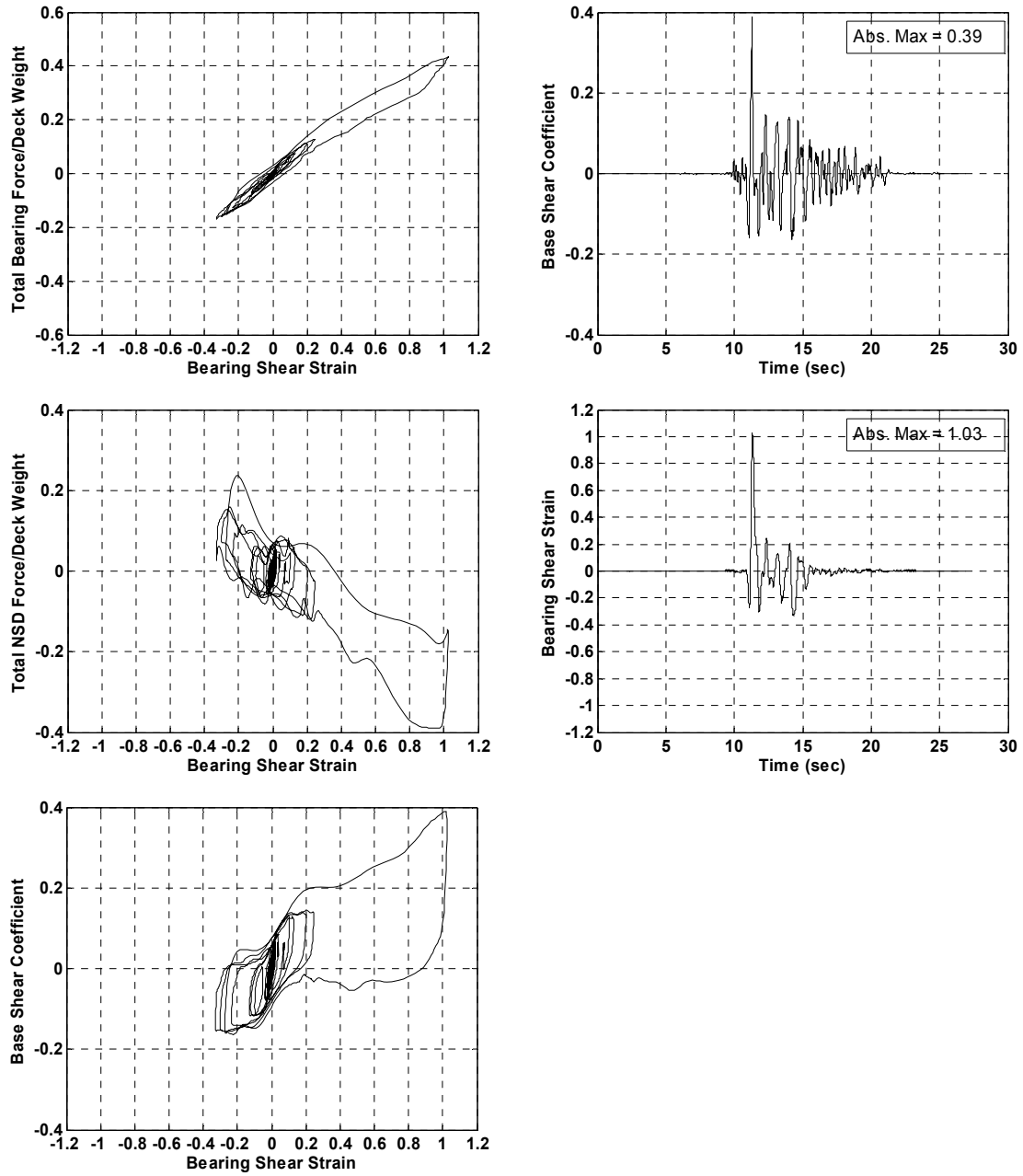
Figure B.32. Experimental results for bridge model with braced piers for the case of IB+NSD and 100% of 637-270 ground motion

150
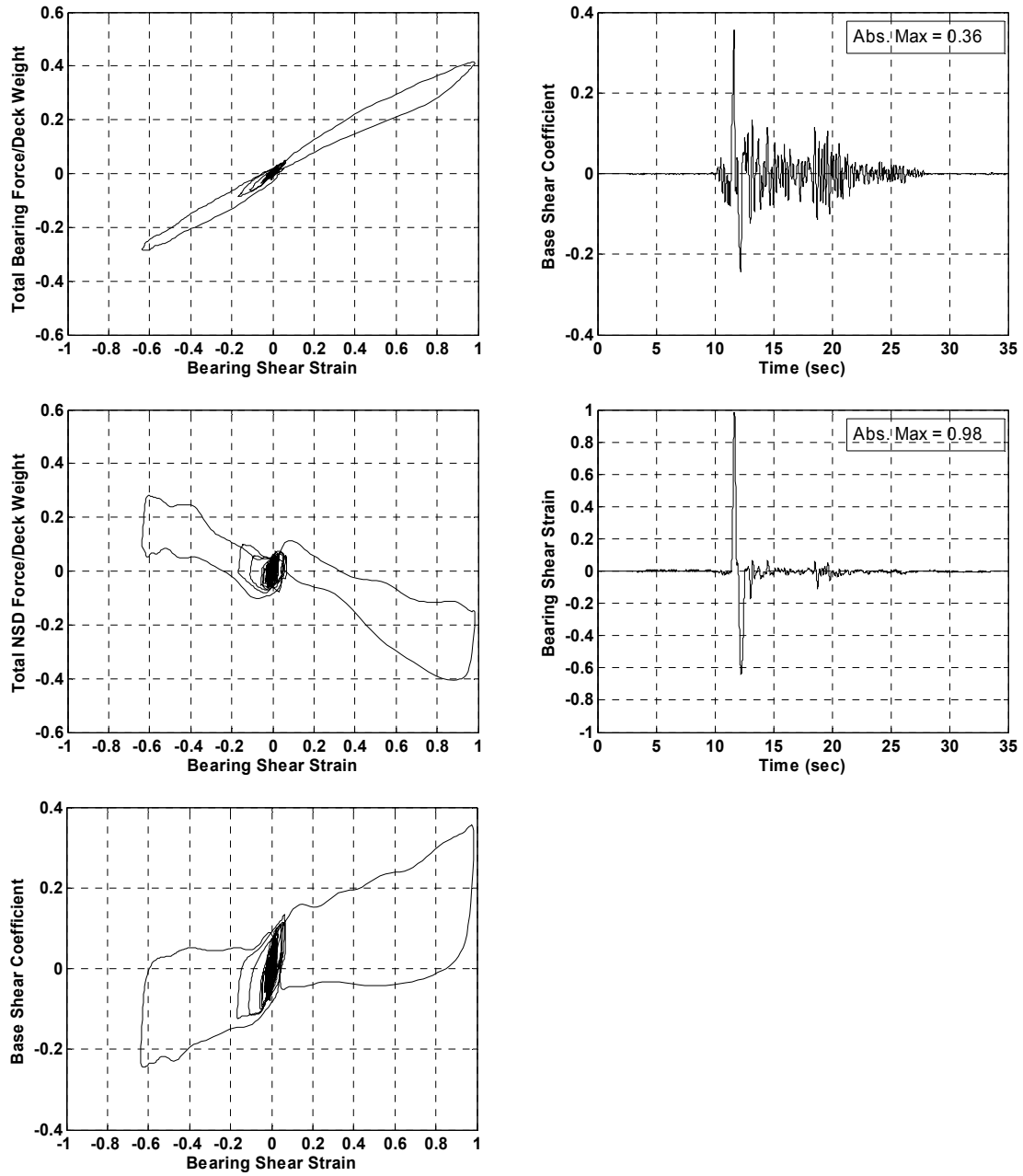
Figure B.33. Experimental results for bridge model with braced piers for the case of IB+NSD and 100% of PET-090 ground motion

151
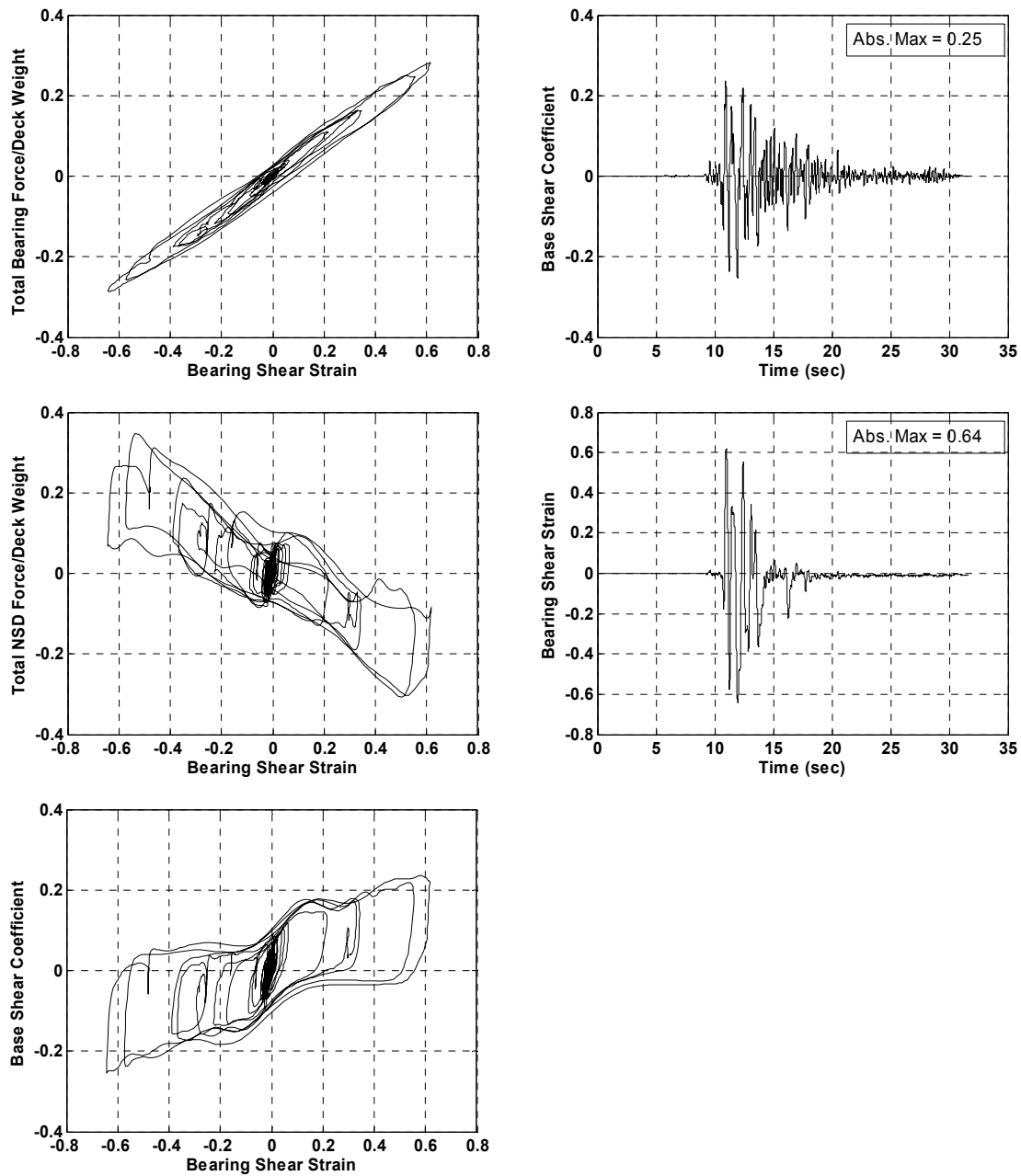
Figure B.34. Experimental results for bridge model with braced piers for the case of IB+NSD and 100% of KJM-000 ground motion
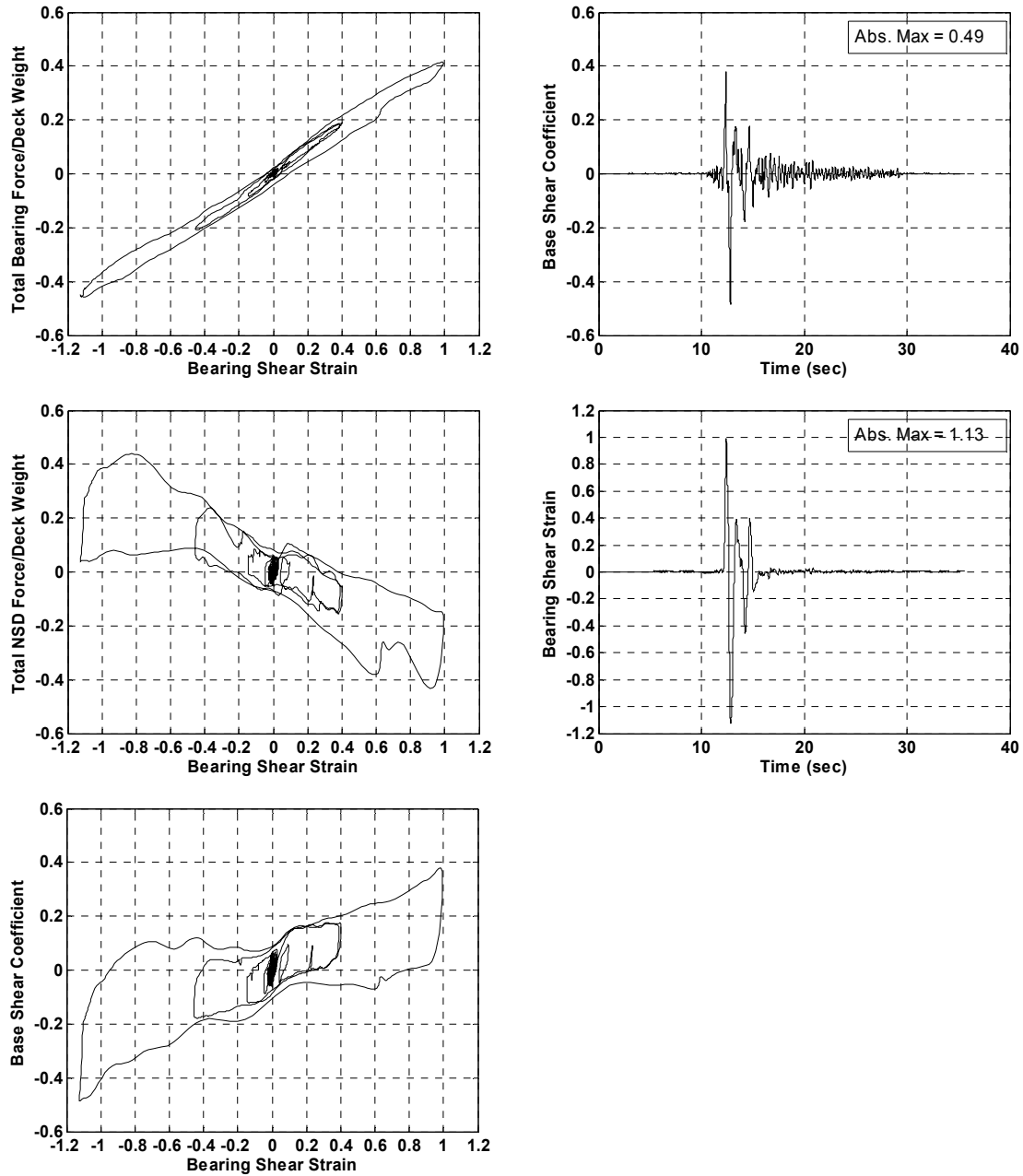
Figure B.35. Experimental results for bridge model with braced piers for the case of IB+NSD and 100% of SYL-000 ground motion

153

B.6. Experimental Results for Bridge Model with Unbraced Piers for the Case of Isolated Bridge with Negative Stiffness Device (IB+NSD)
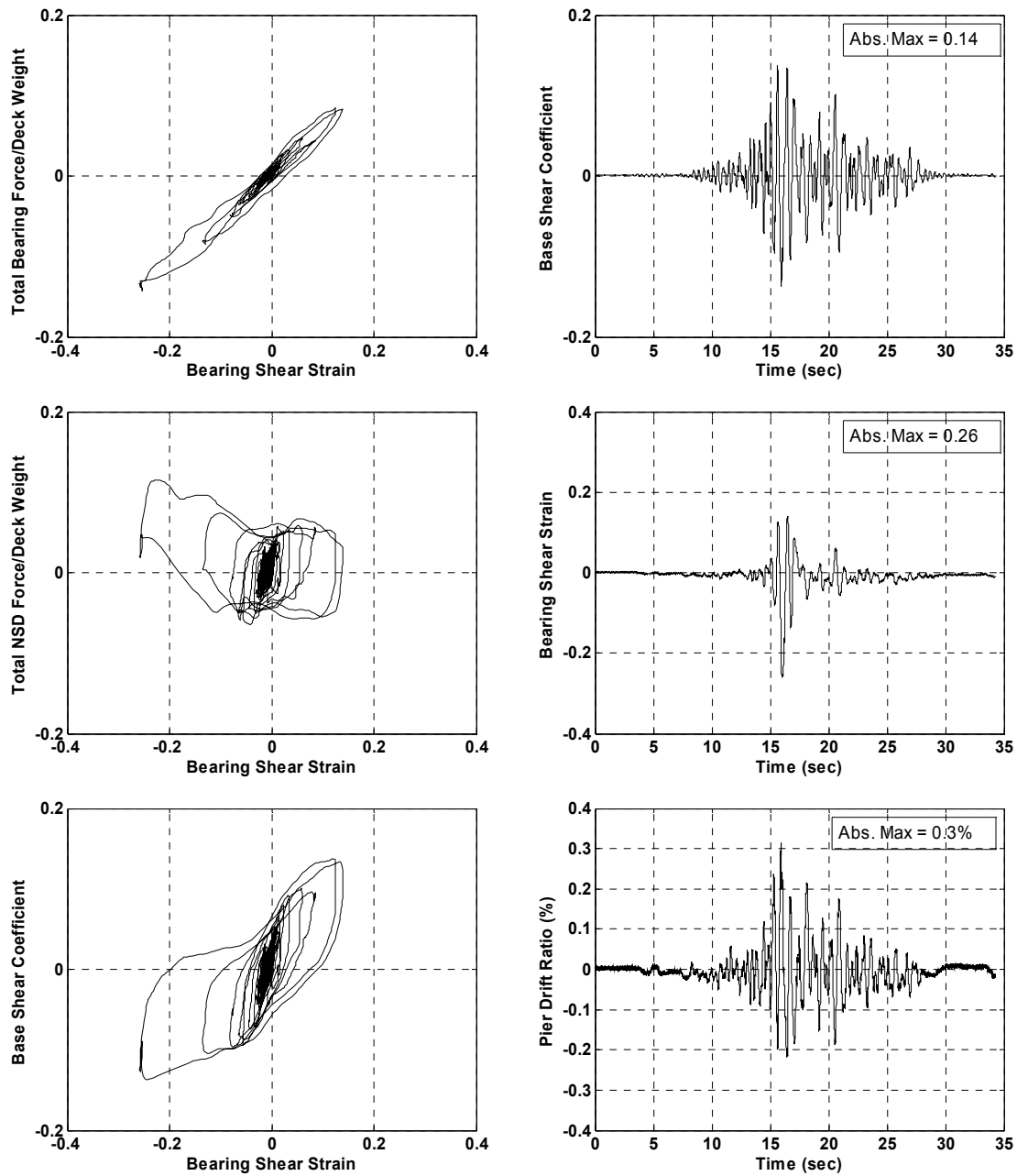
Figure B.36. Experimental results for bridge model with unbraced piers for the case of IB+NSD and 100% of YER-000 ground motion
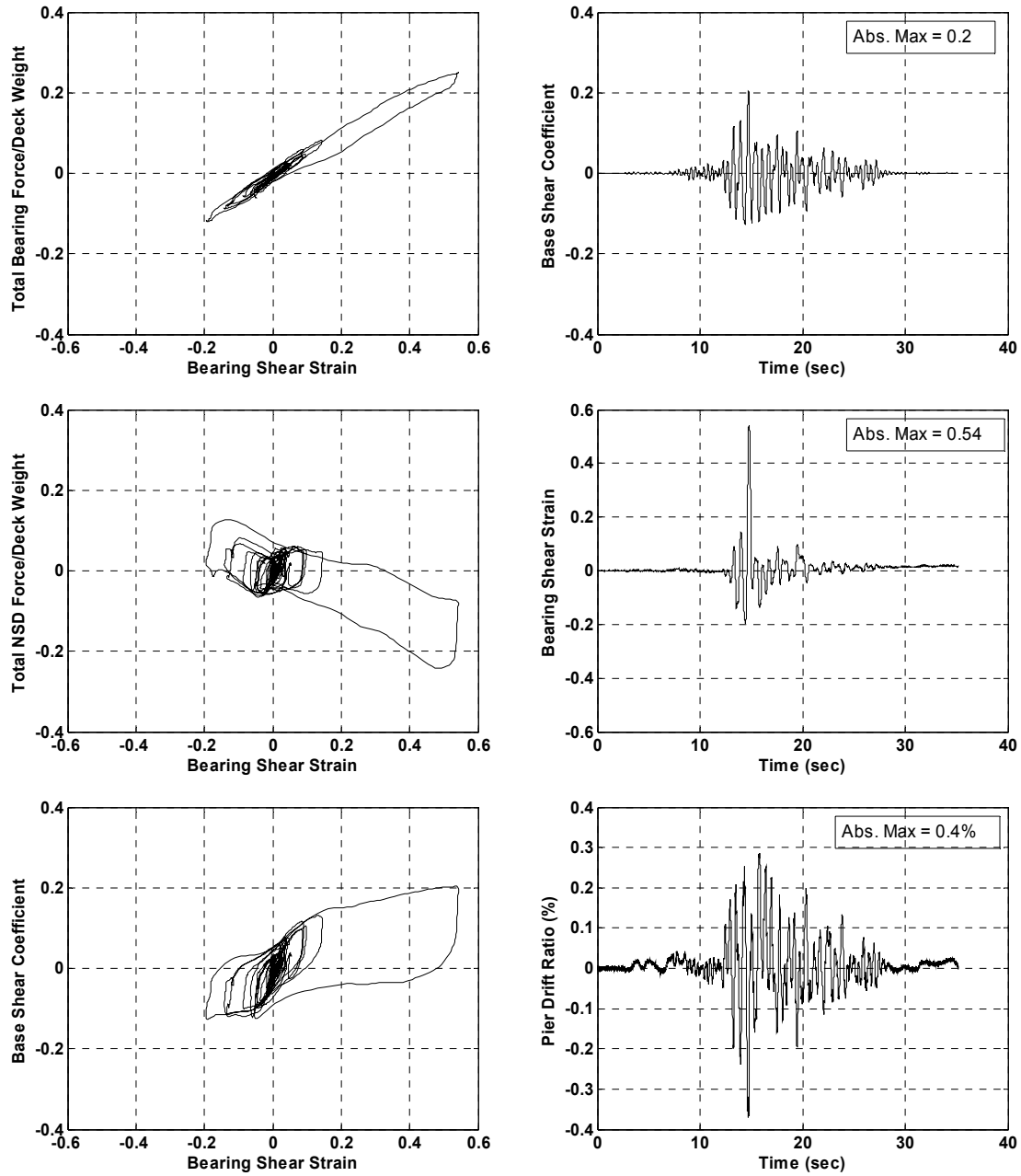
Figure B.37. Experimental results for bridge model with unbraced piers for the case of IB+NSD and 100% of   YER-270 ground motion
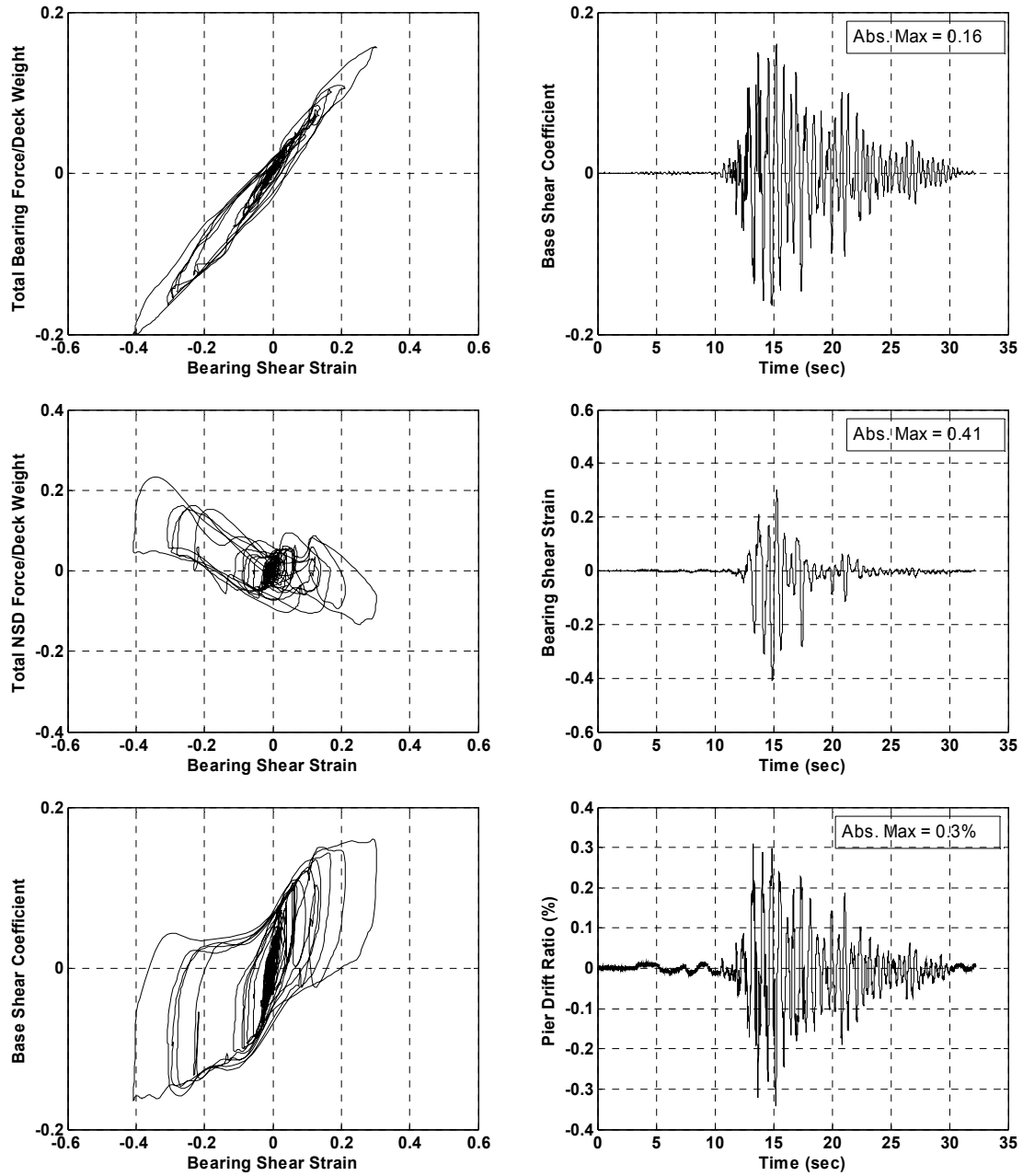
Figure B.38. Experimental results for bridge model with unbraced piers for the case of IB+NSD and 100% of CAP-000 ground motion
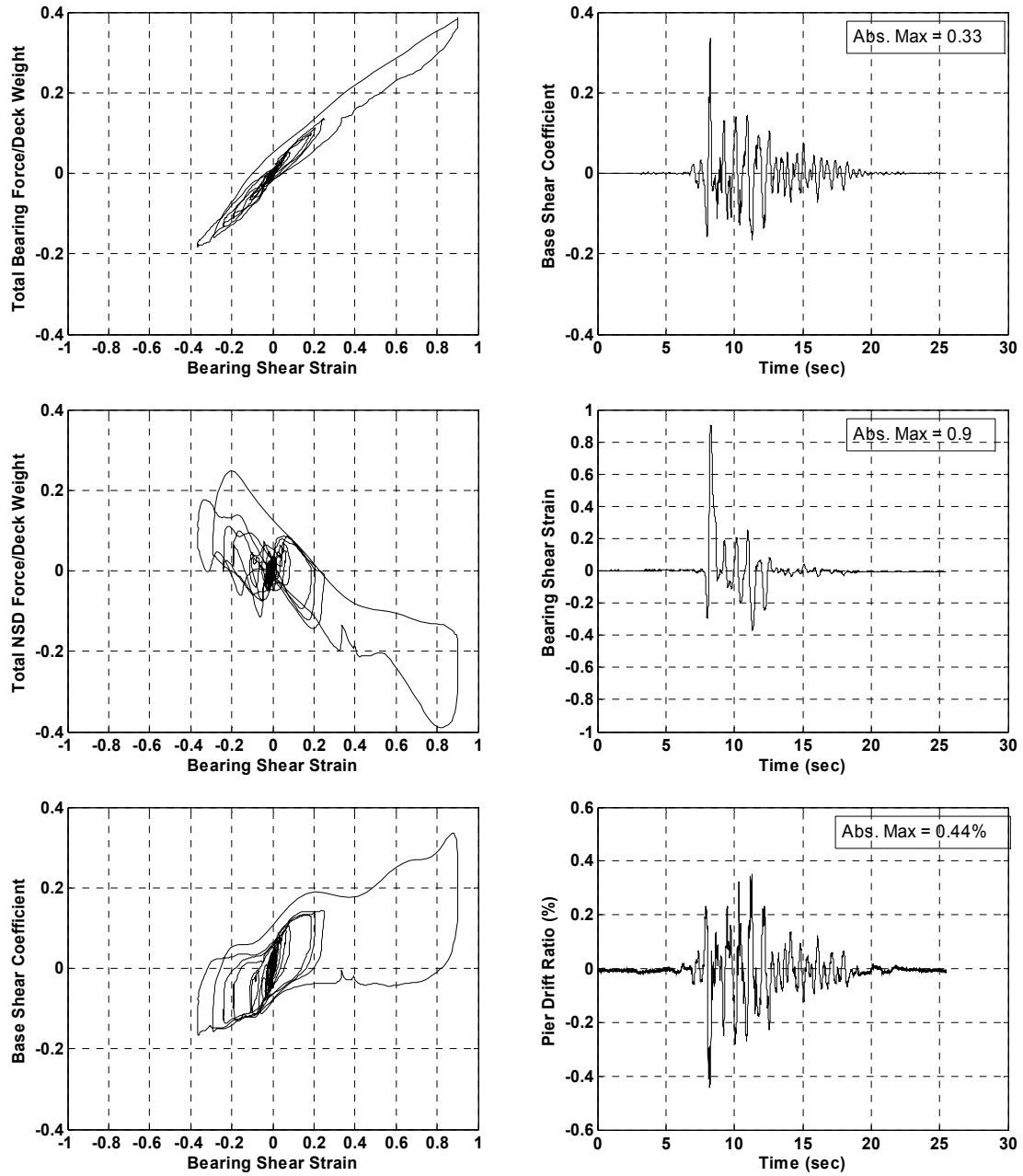
Figure B.39. Experimental results for bridge model with unbraced piers for the case of IB+NSD and 100% of 637-270 ground motion
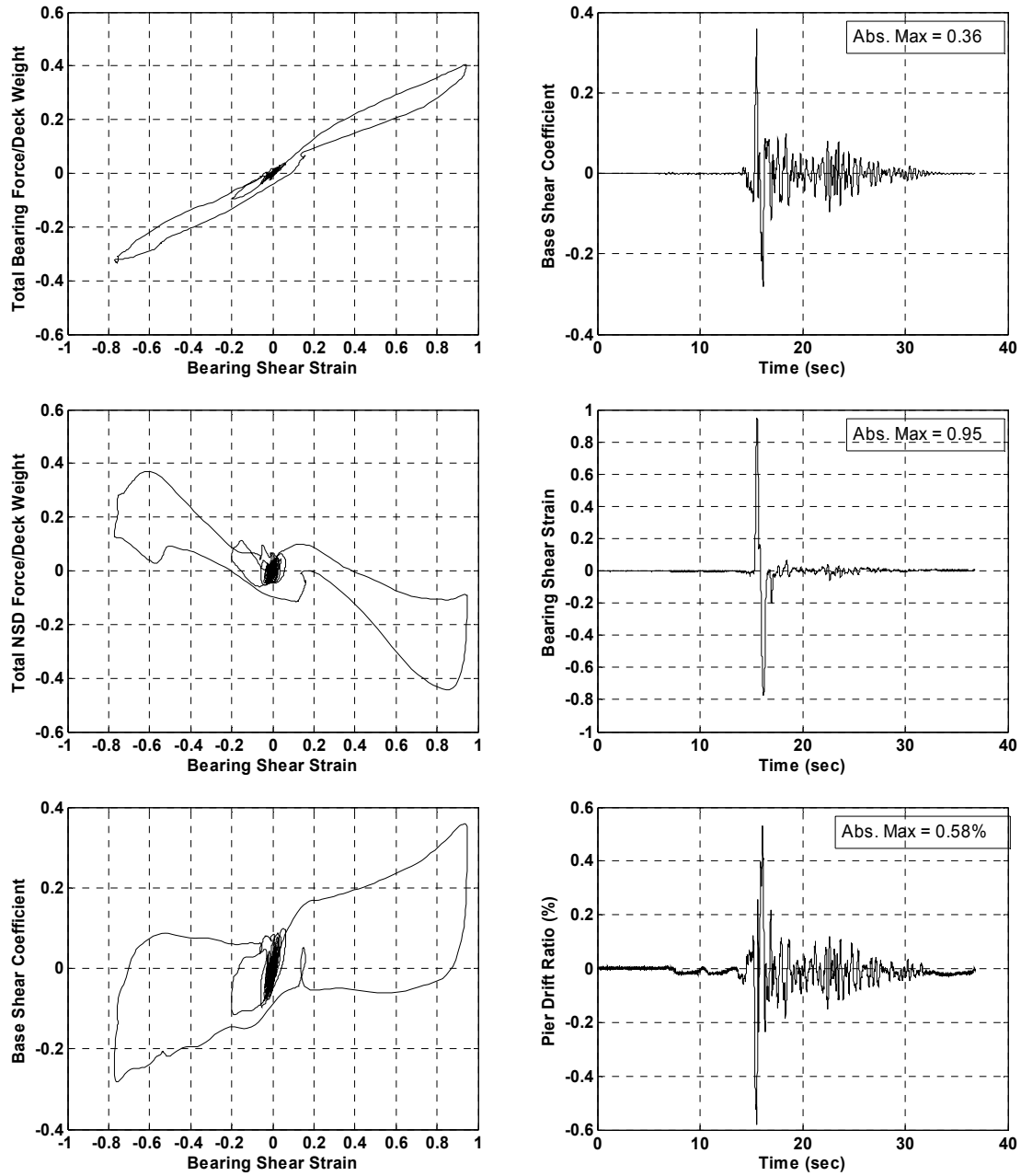
Figure B.40. Experimental results for bridge model with unbraced piers for the case of IB+NSD and 100% of PET-090 ground motion
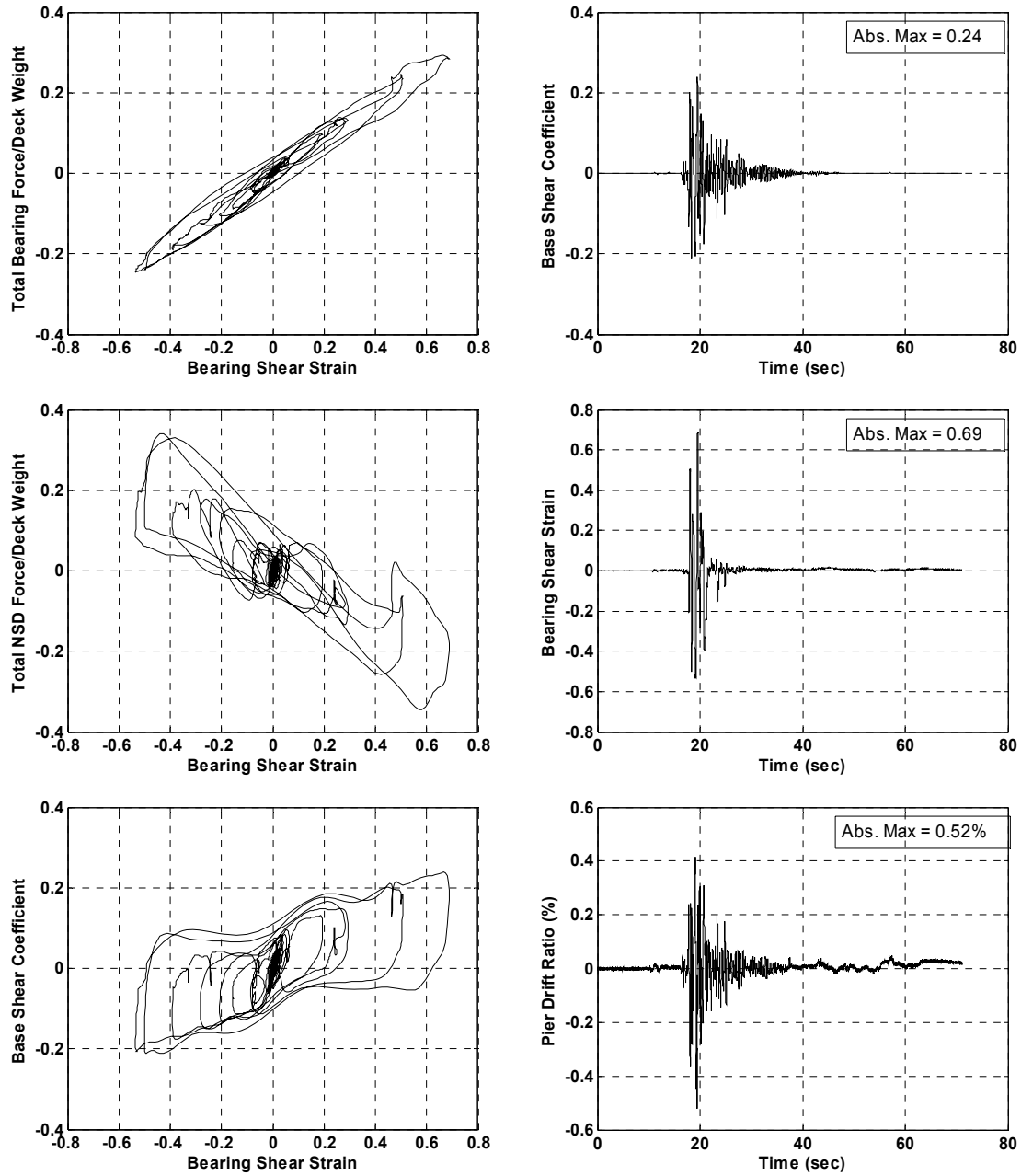
Figure B.41. Experimental results for bridge model with unbraced piers for the case of IB+NSD and 100% of   KJM-000 ground motion
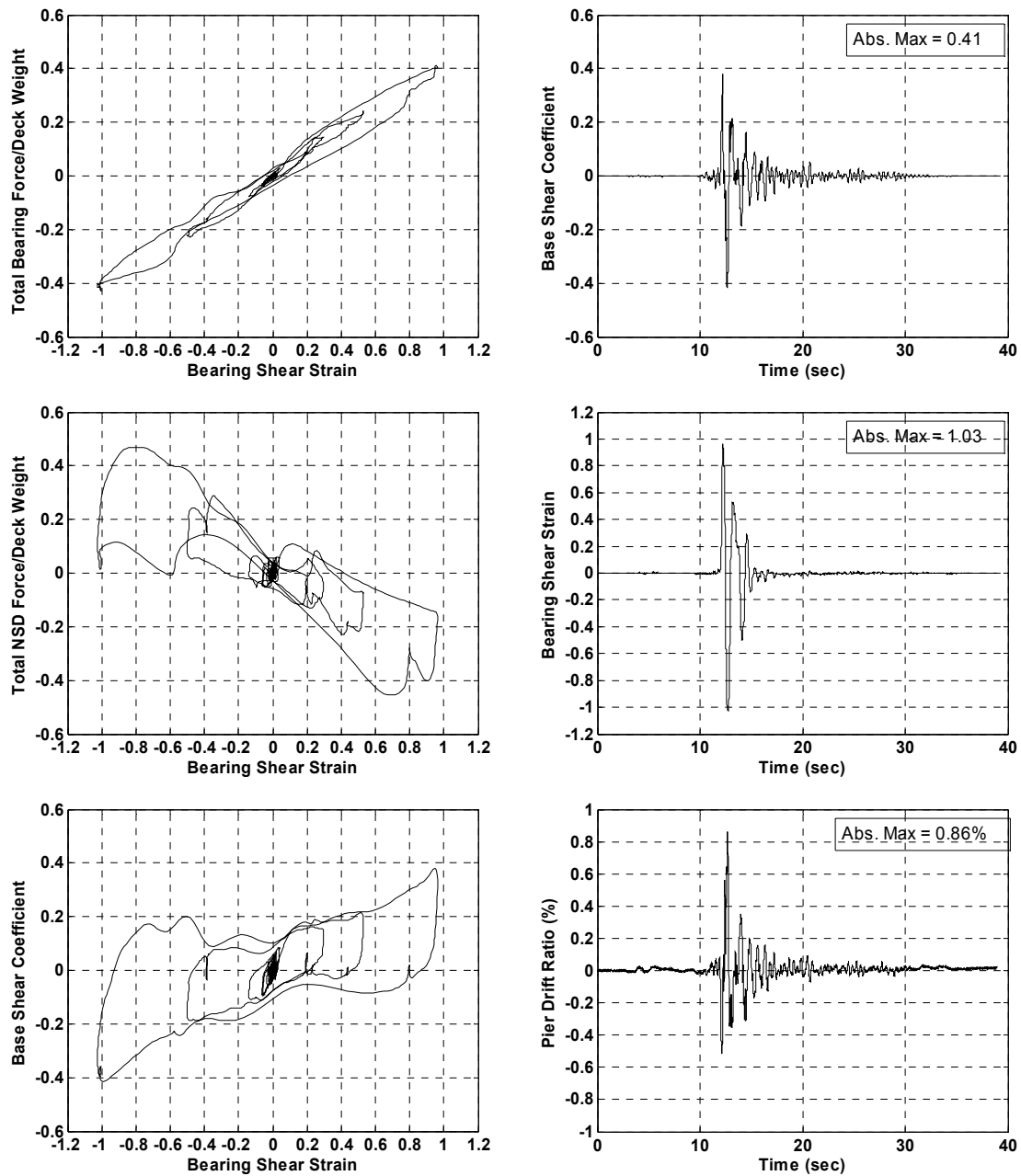
Figure B.42. Experimental results for bridge model with unbraced piers for the case of IB+NSD and 100% of SYL-000 ground motion

B.7. Experimental Results for Bridge Model with Braced Piers for the Case of Isolated Bridge with Negative Stiffness Device and Passive Damper (IB+NSD+PD)
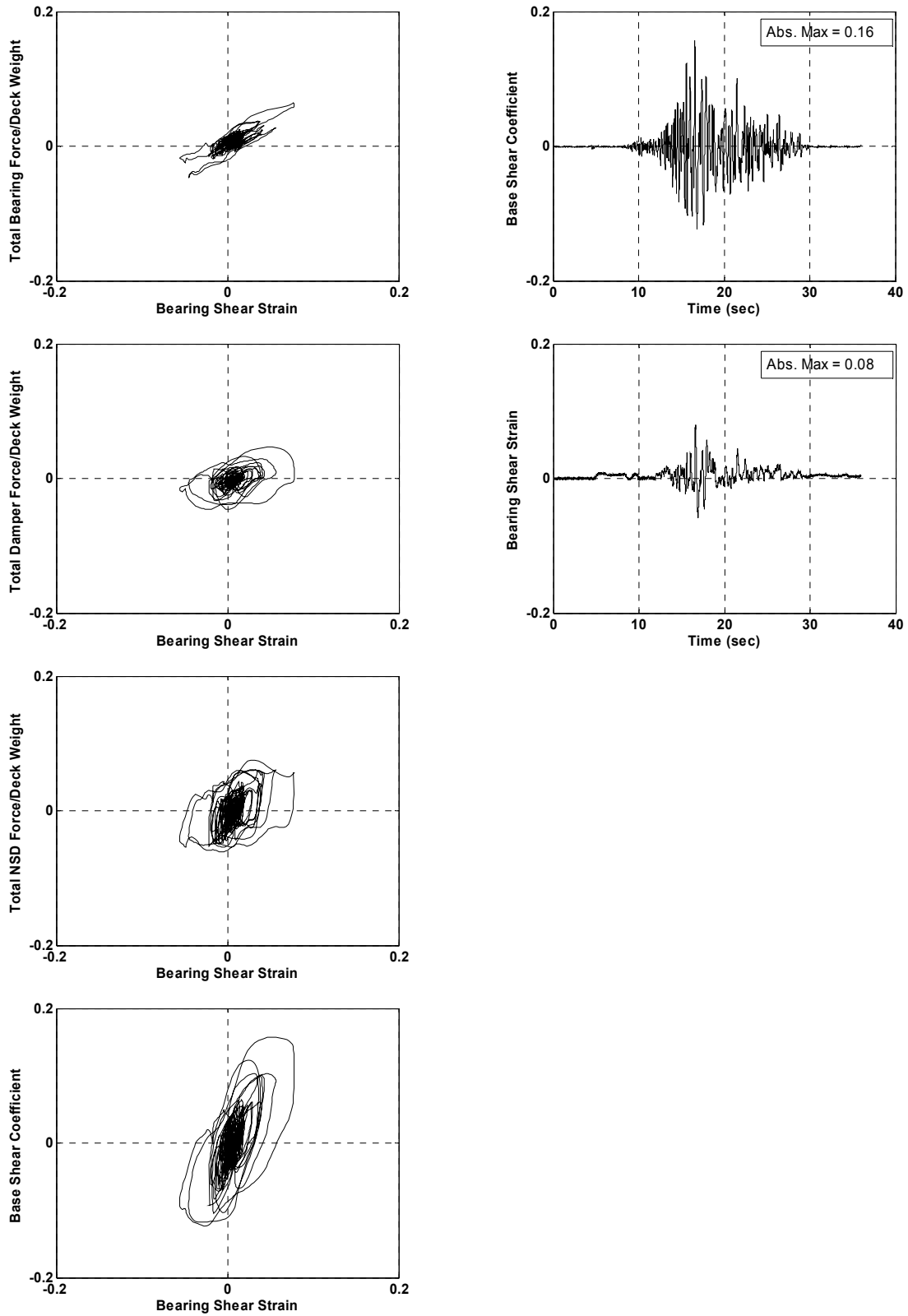
Figure B.43. Experimental results for bridge model with braced piers for the case of IB+NSD+PD and 100% of YER-000 ground motion
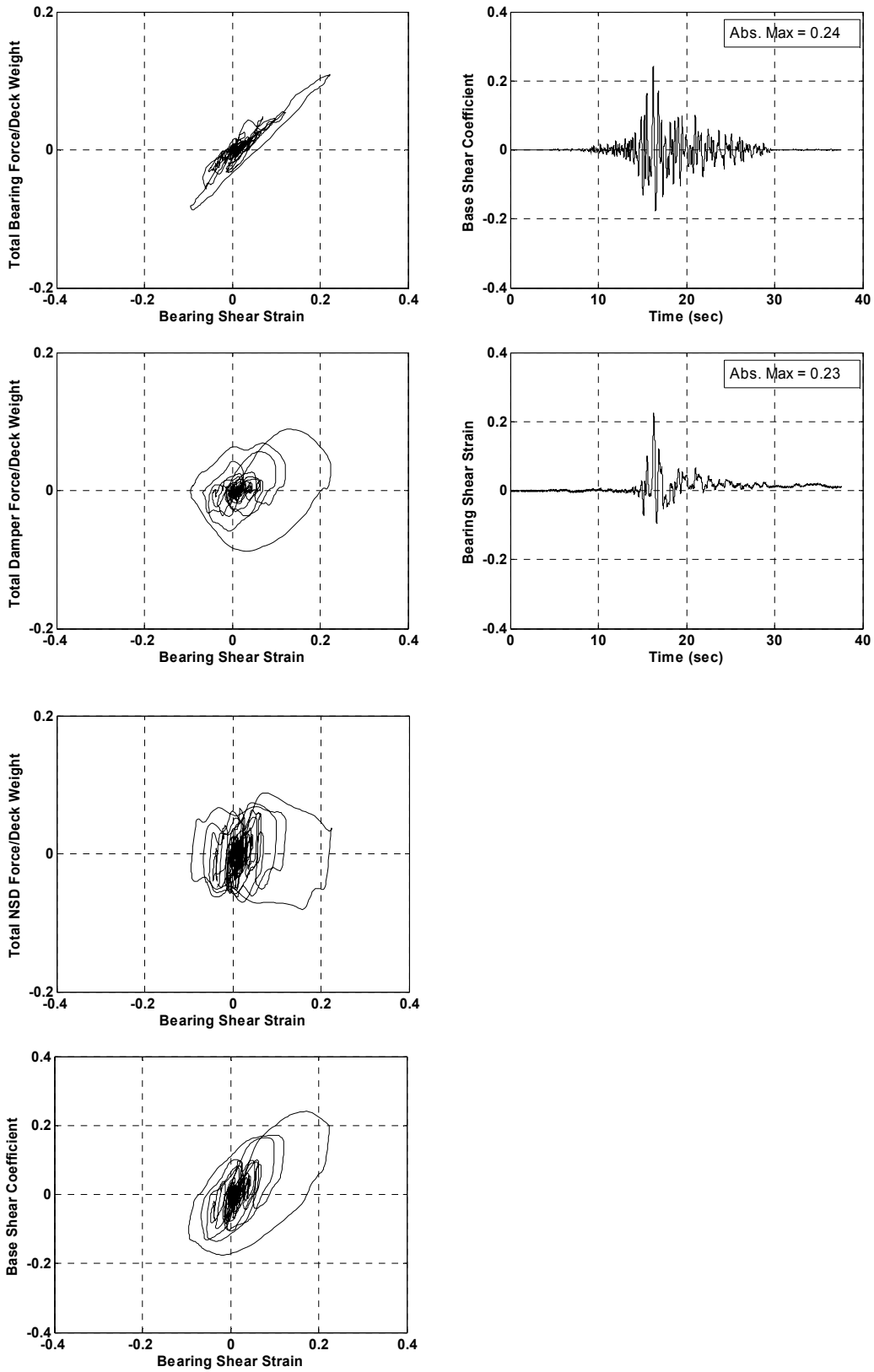
Figure B.44. Experimental results for bridge model with braced piers for the case of IB+NSD+PD and 100% of YER-270 ground motion
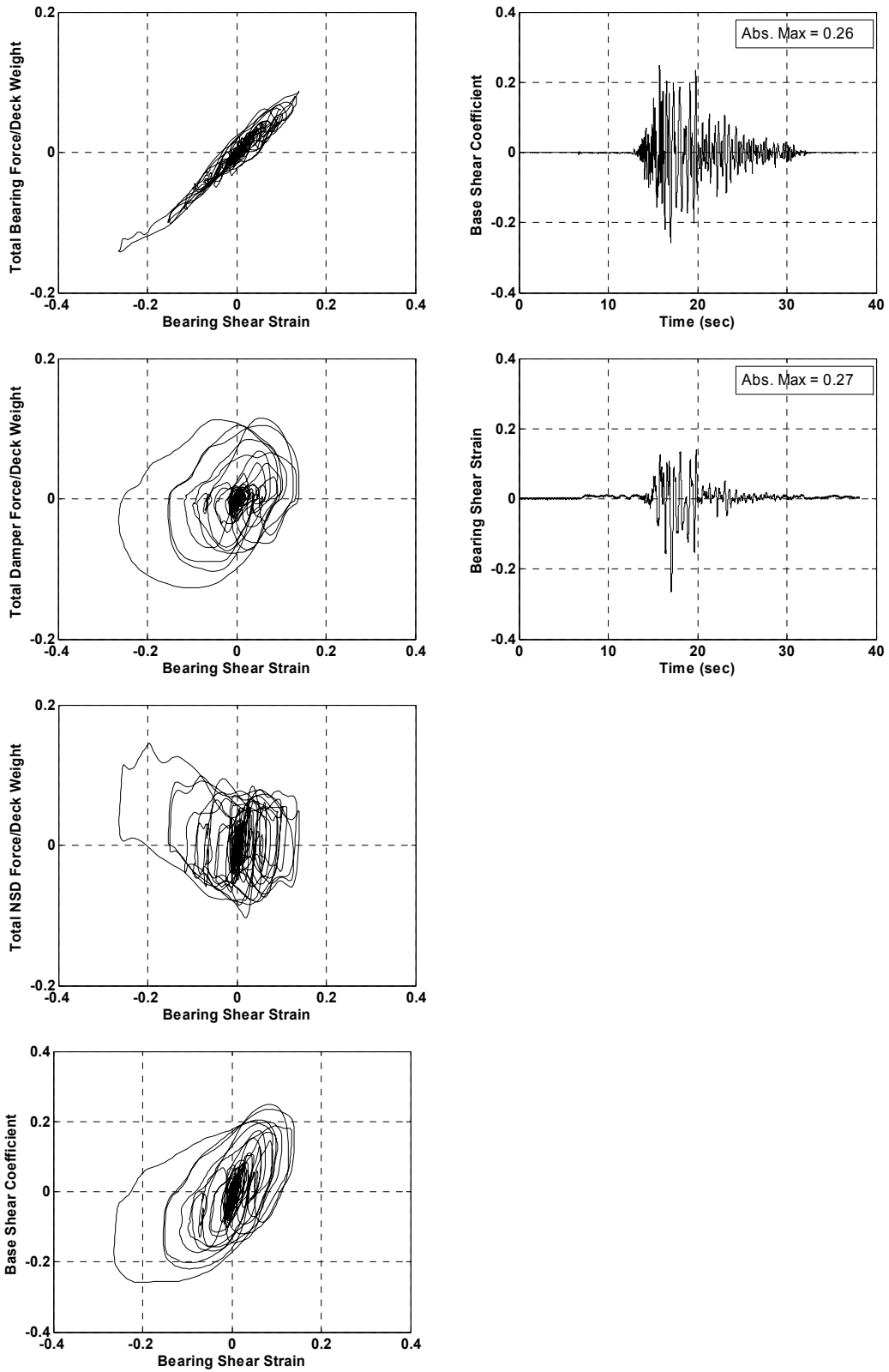
Figure B.45. Experimental results for bridge model with braced piers for the case of IB+NSD+PD and 100% of CAP-000 ground motion
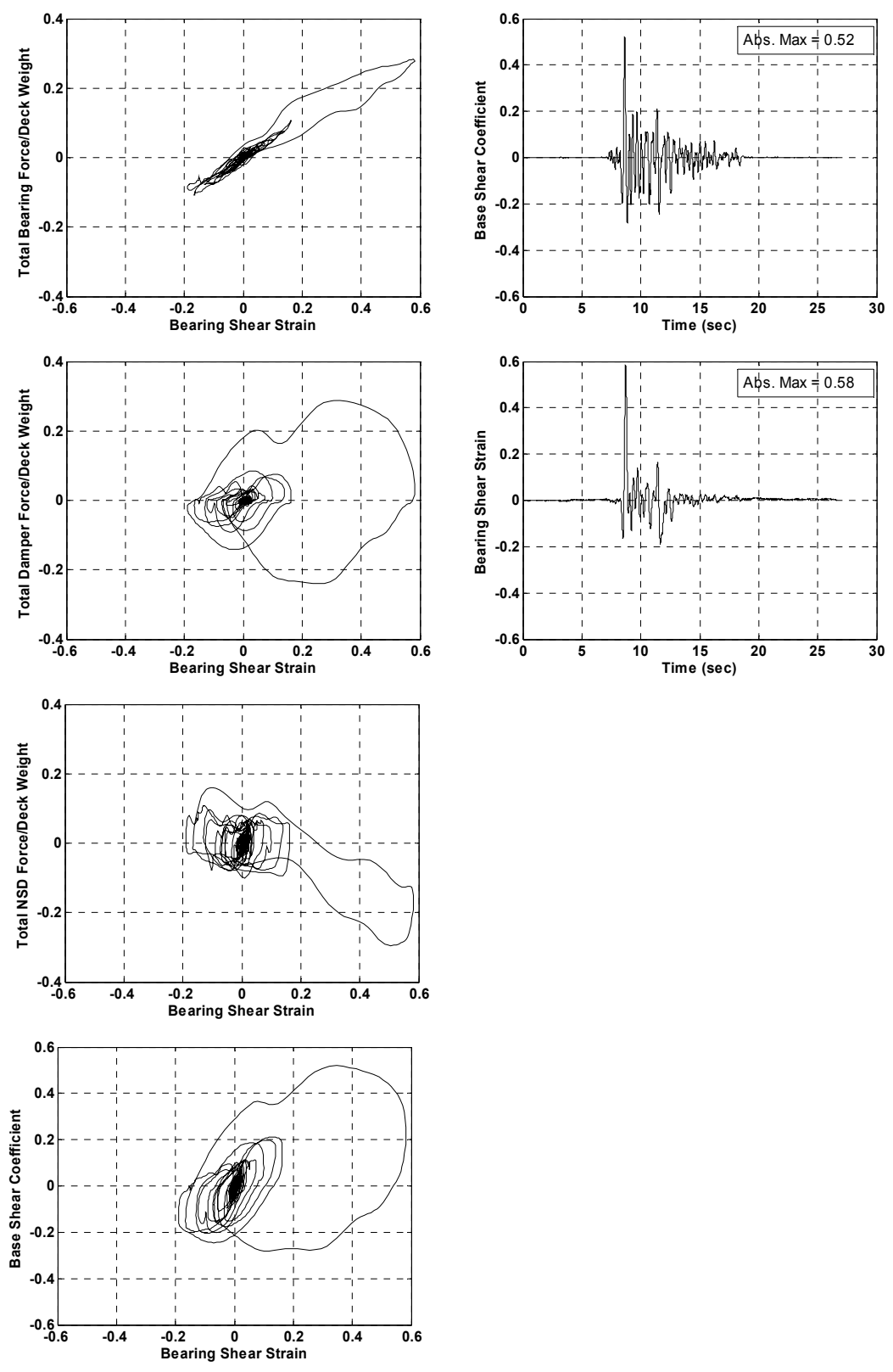
Figure B.46. Experimental results for bridge model with braced piers for the case of IB+NSD+PD and 100% of 637-270 ground motion
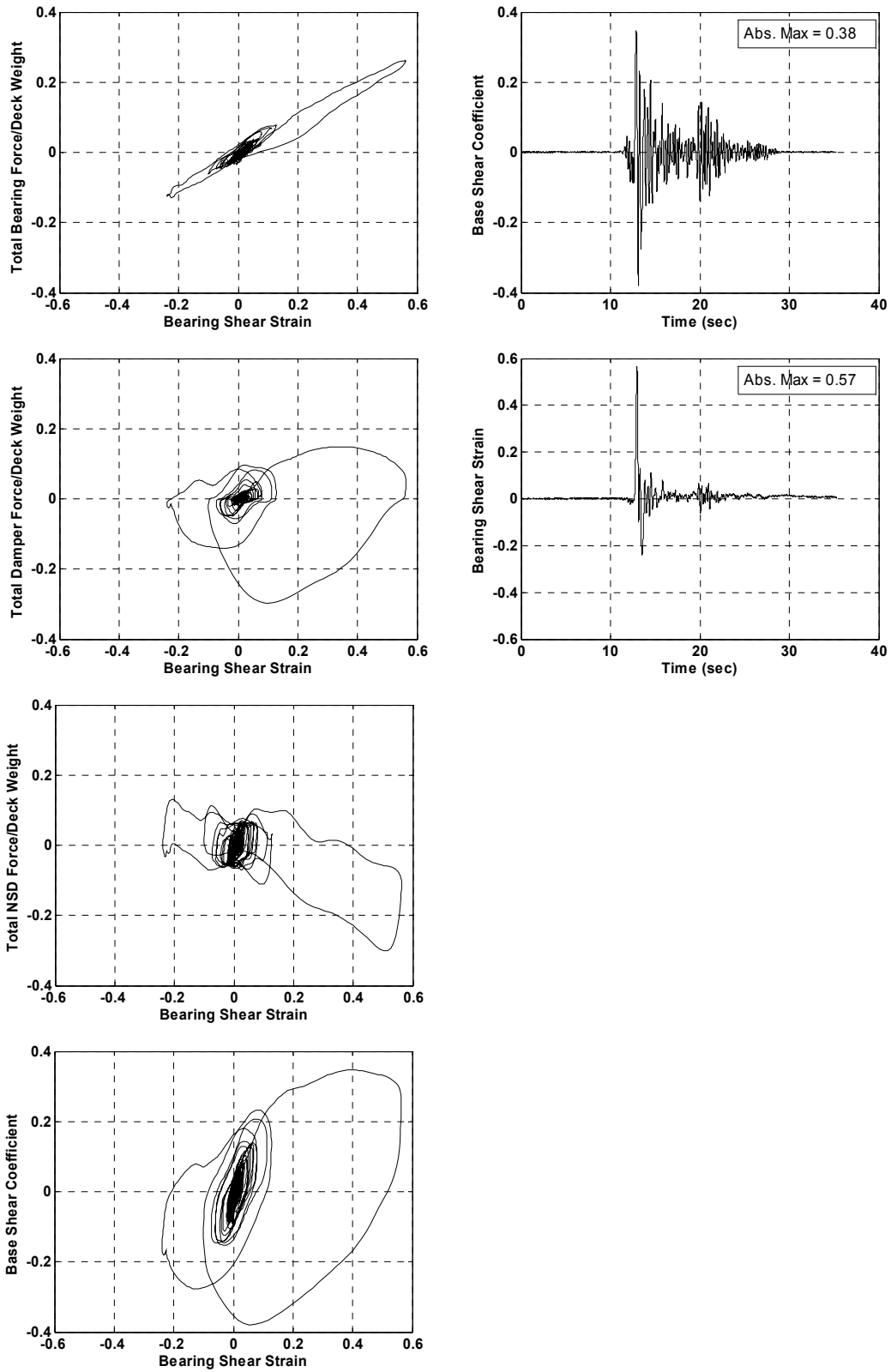
Figure B.47. Experimental results for bridge model with braced piers for the case of IB+NSD+PD and 100% of PET-090 ground motion
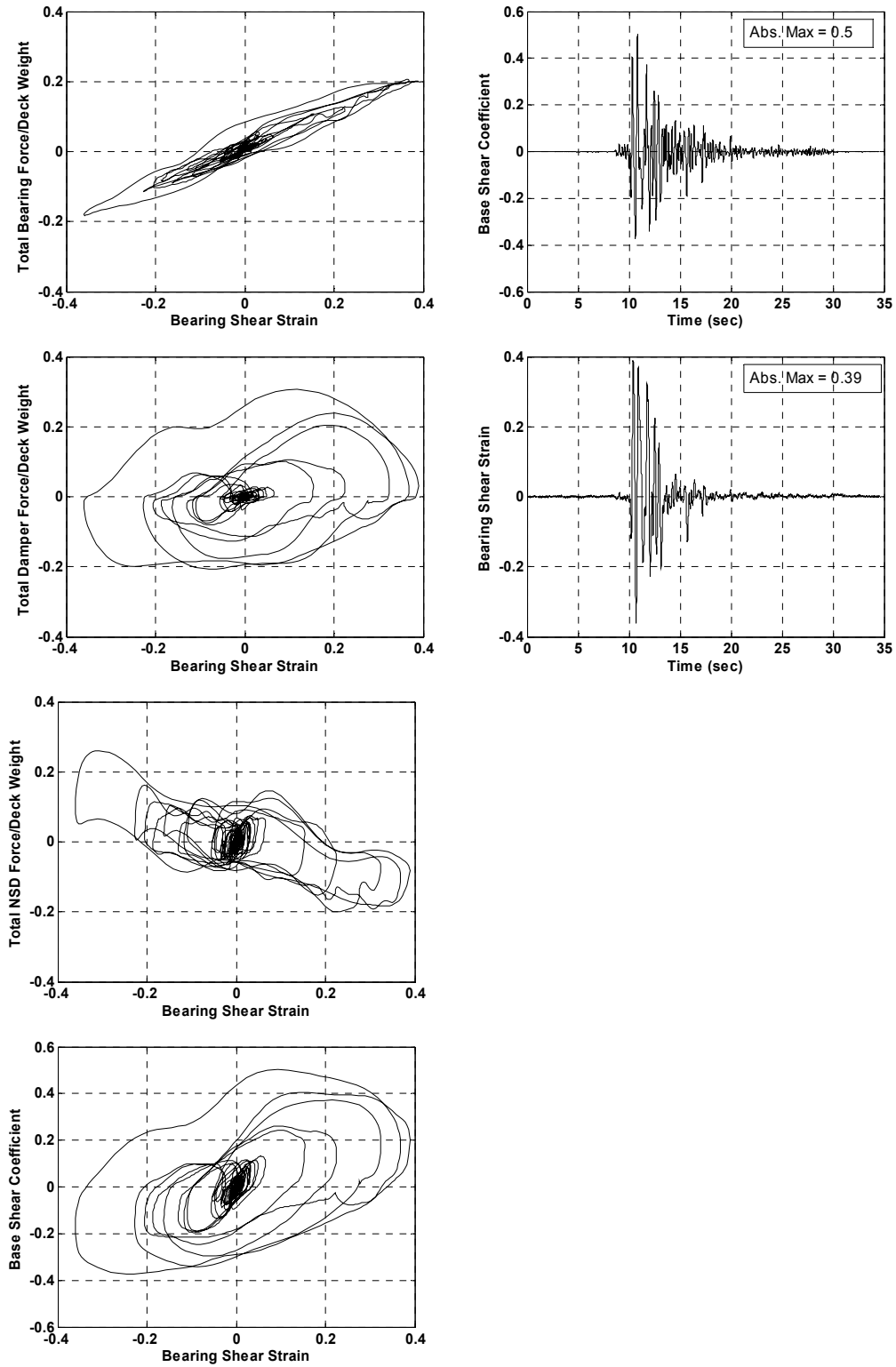
Figure B.48. Experimental results for bridge model with braced piers for the case of IB+NSD+PD and 100% of KJM-000 ground motion
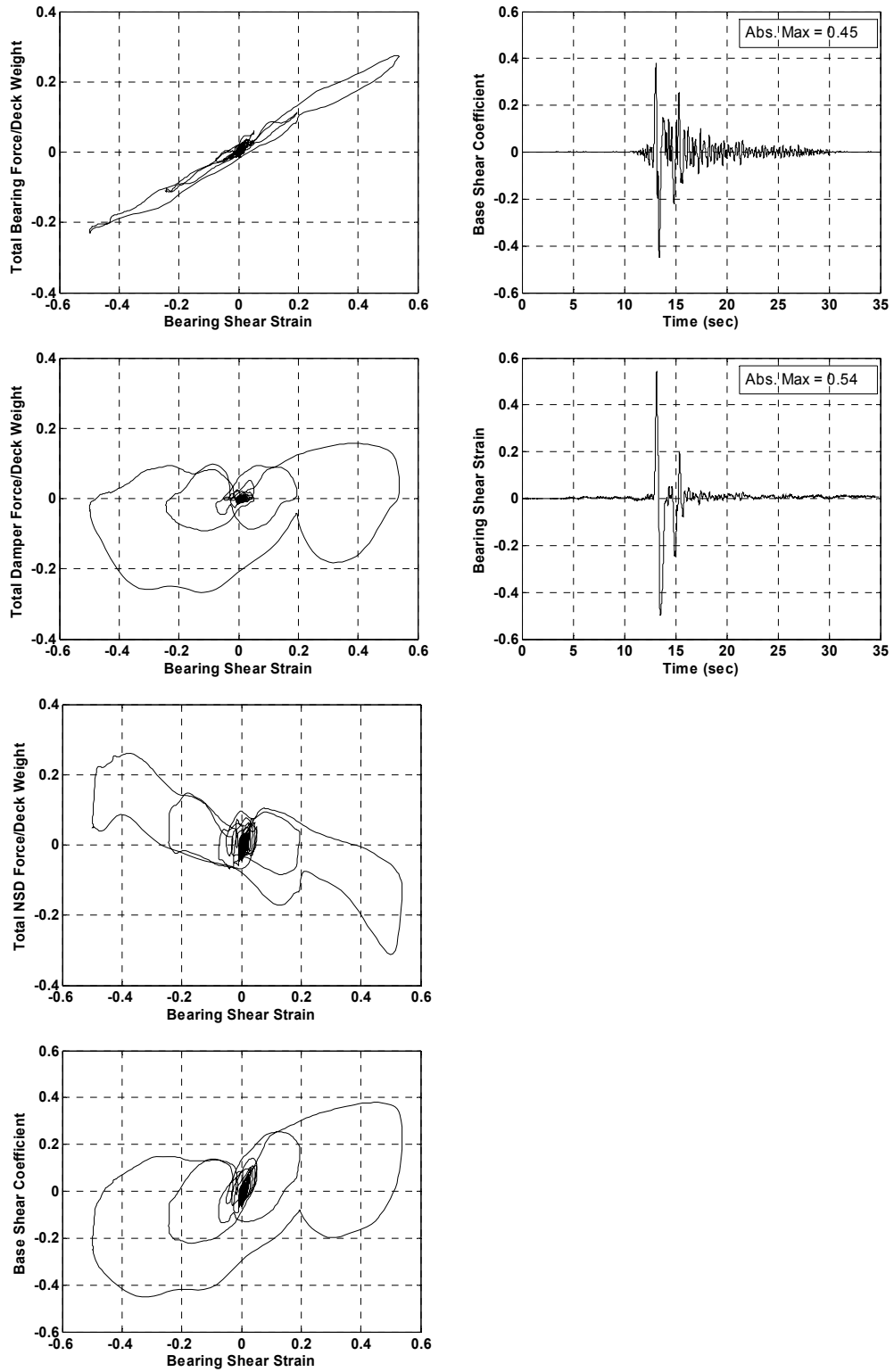
Figure B.49. Experimental results for bridge model with braced piers for the case of IB+NSD+PD and 100% of SYL-000 ground motion

B.8. Experimental Results for Bridge Model with Unbraced Piers for the Case of Isolated Bridge with Negative Stiffness Device and Passive Damper (IB+NSD+PD)
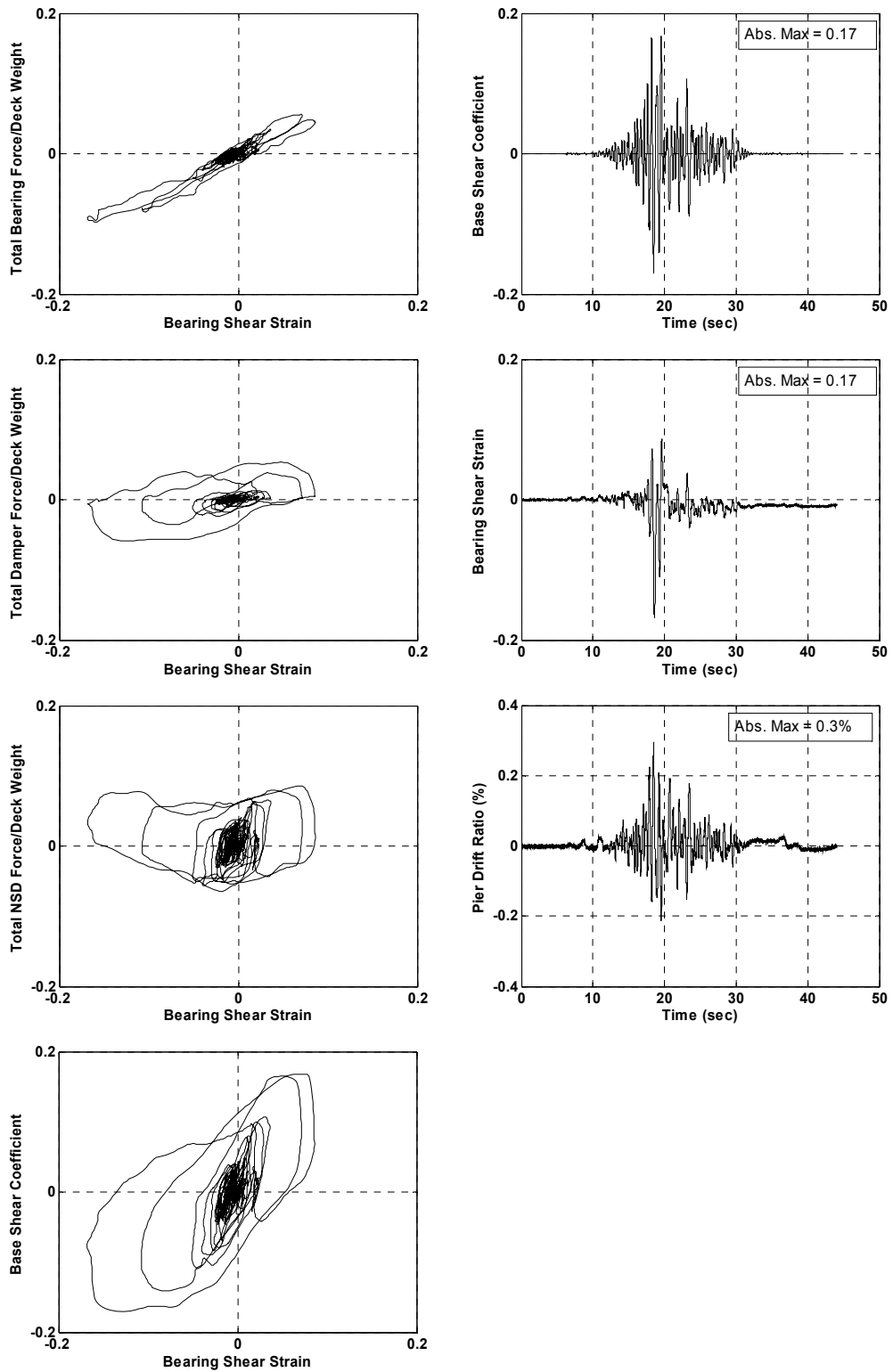
Figure B.50. Experimental results for bridge model with unbraced piers for the case of IB+NSD+PD and 100% of YER-000 ground motion
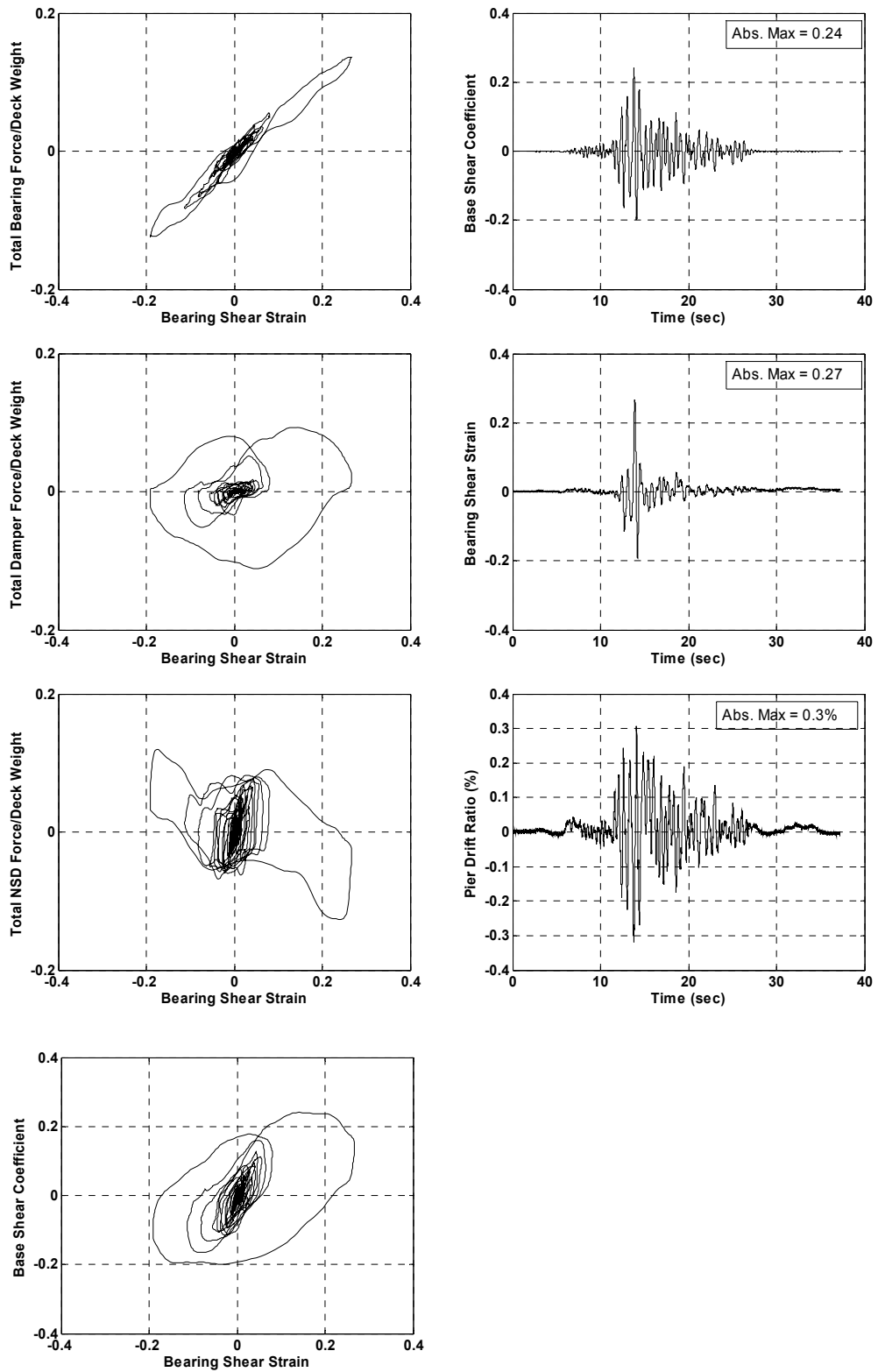
Figure B.51. Experimental results for bridge model with unbraced piers for the case of IB+NSD+PD and 100% of YER-270 ground motion
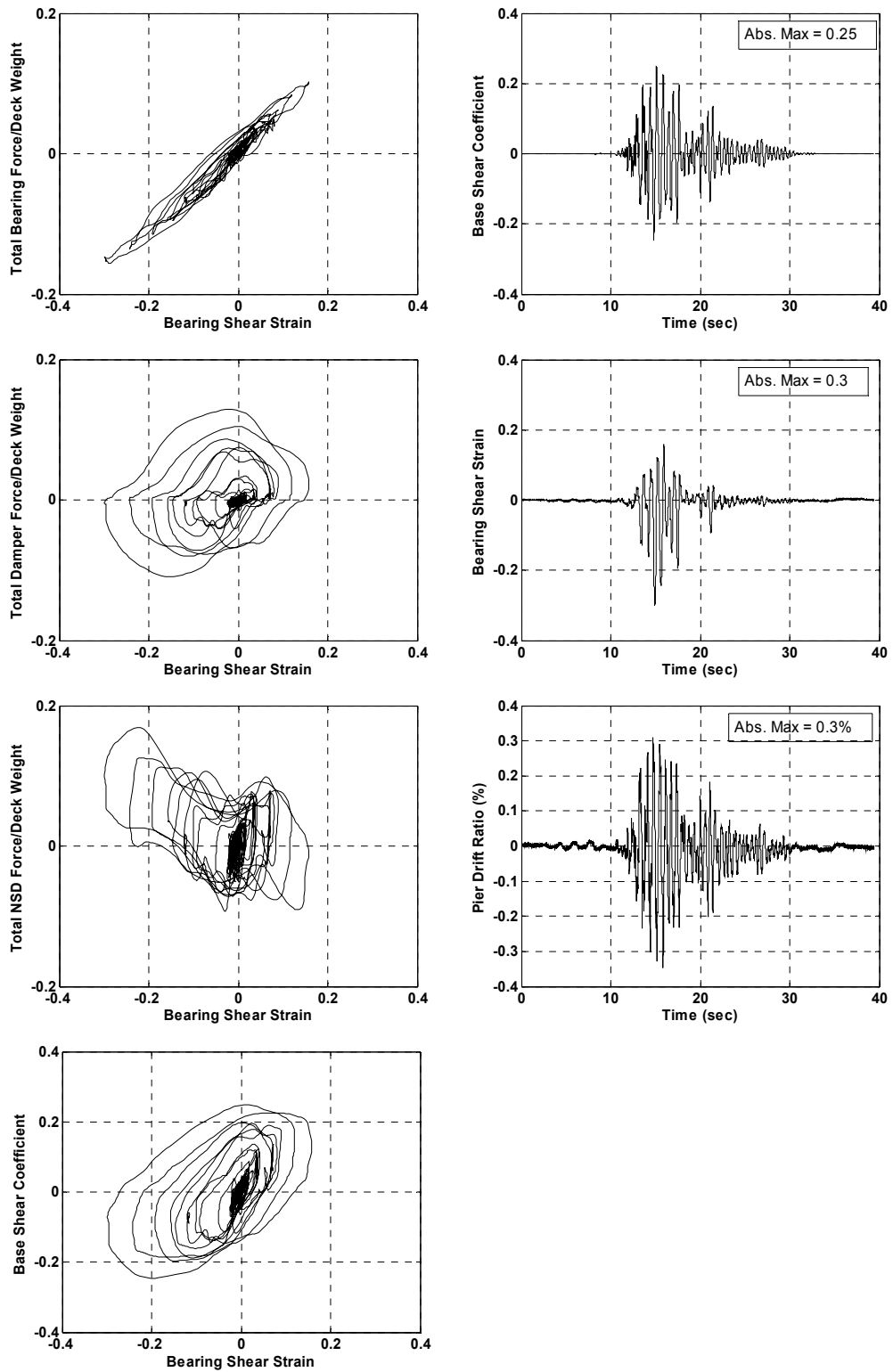
Figure B.52. Experimental results for bridge model with unbraced piers for the case of IB+NSD+PD and 100% of CAP-000 ground motion
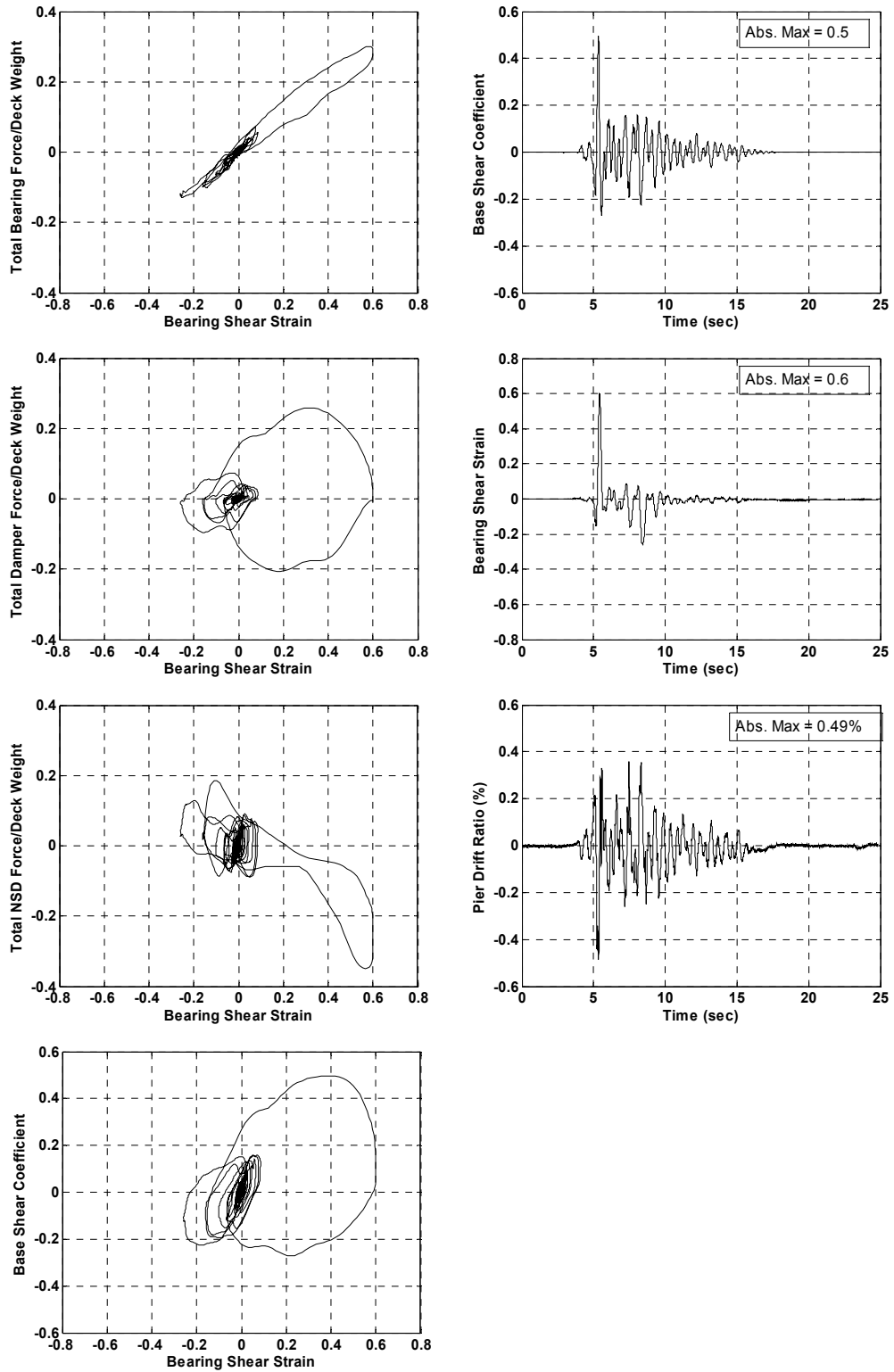
Figure B.53. Experimental results for bridge model with unbraced piers for the case of IB+NSD+PD and 100% of 637-270 ground motion

174
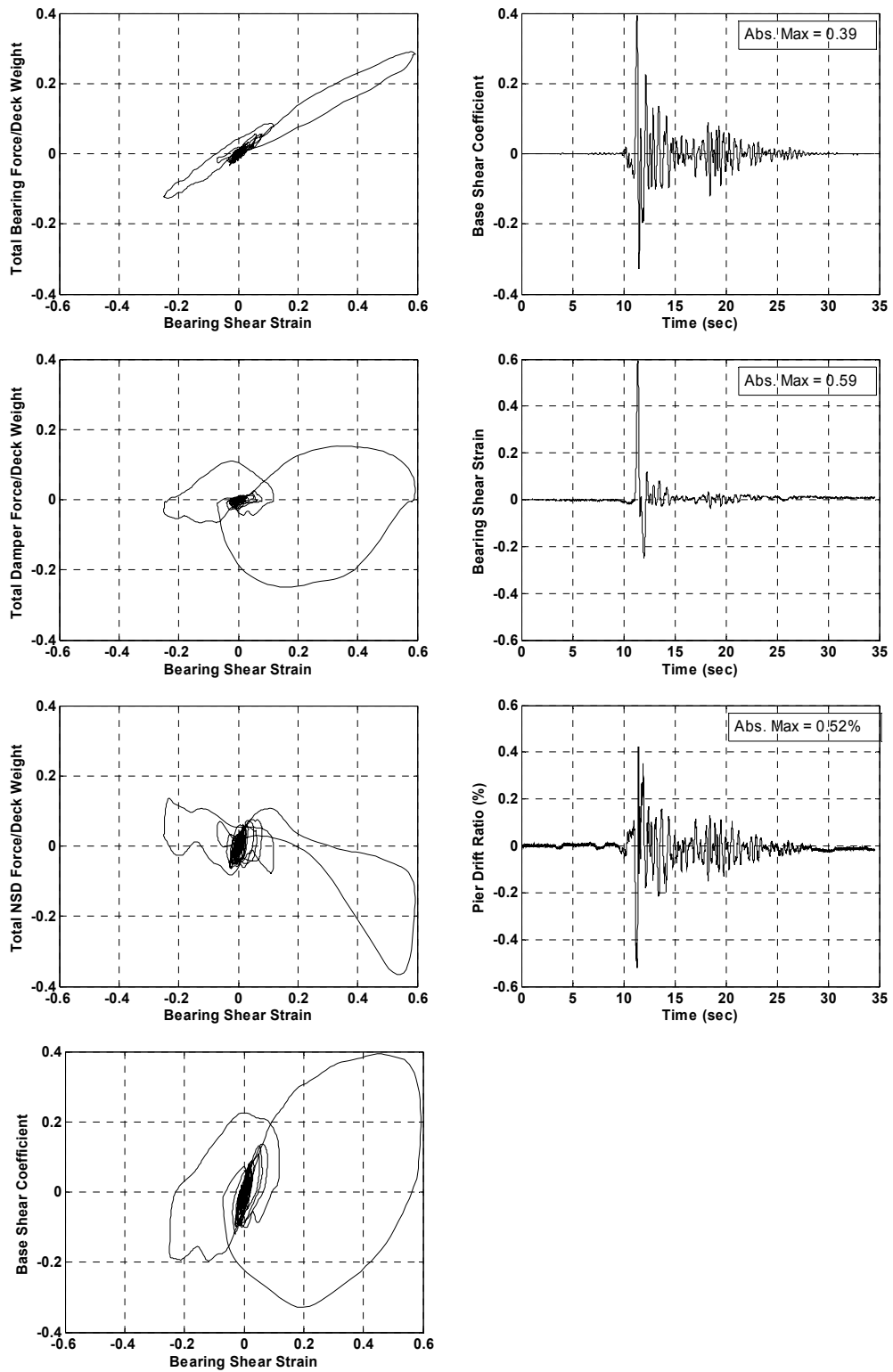
Figure B.54. Experimental results for bridge model with unbraced piers for the case of IB+NSD+PD and 100% of PET-090 ground motion
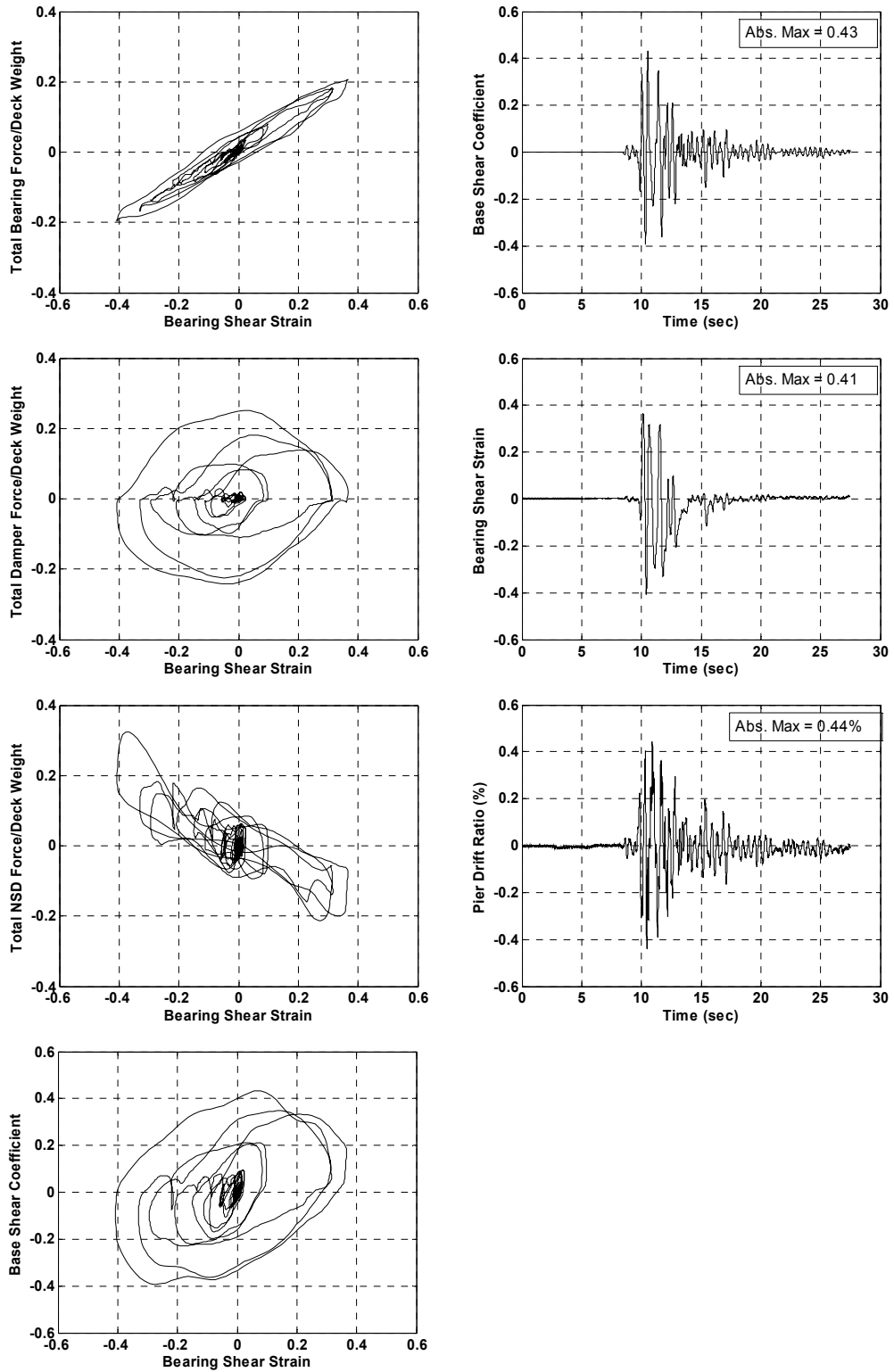
Figure B.55. Experimental results for bridge model with unbraced piers for the case of IB+NSD+PD and 100% of KJM-000 ground motion
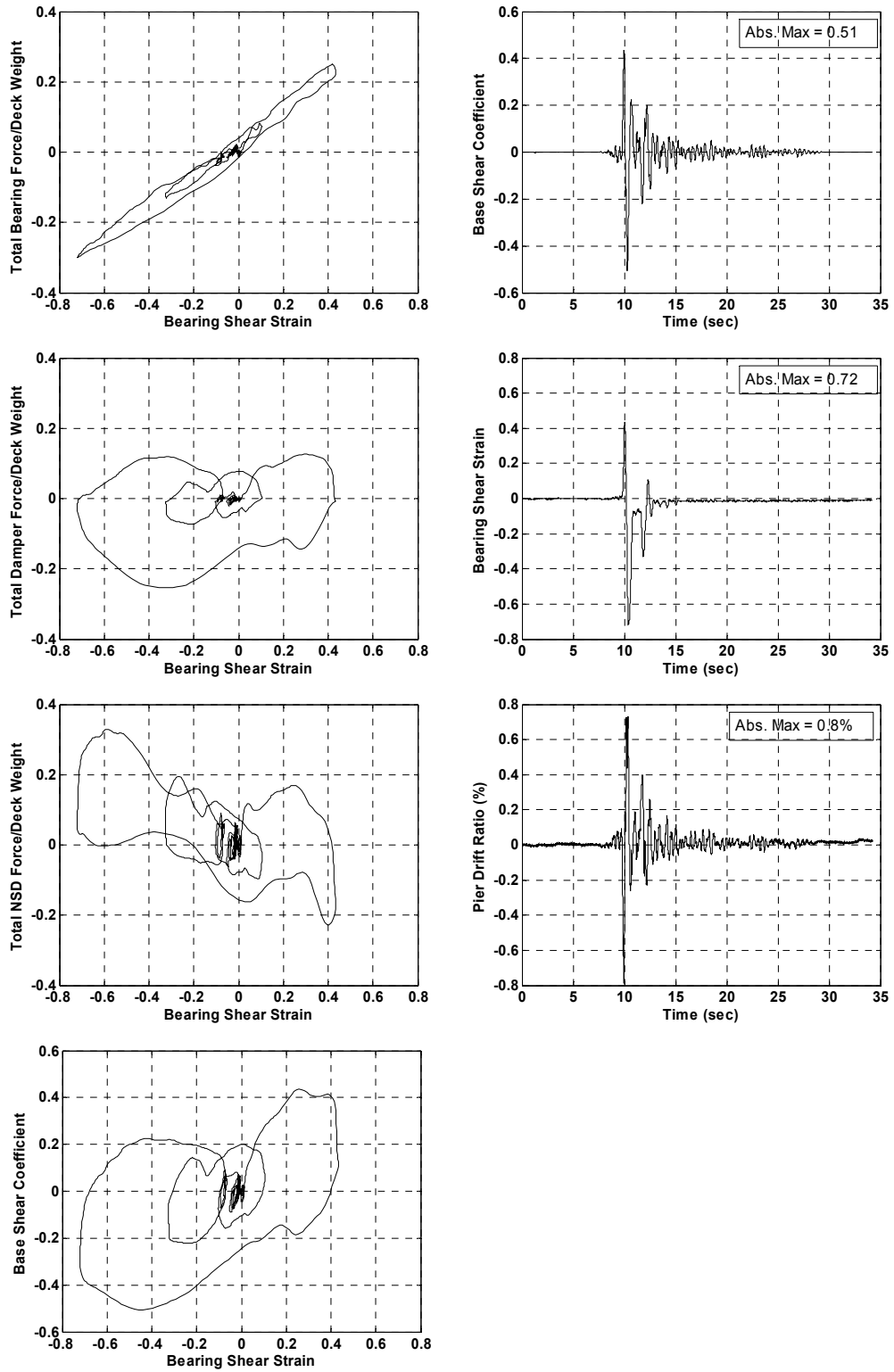
Figure B.56. Experimental results for bridge model with unbraced piers for the case of IB+NSD+PD and 100% of SYL-000 ground motion

"This Page Intentionally Left Blank"

C.   Instrumentation of the Bridge model

Instrumentation Plan

✦	Longitudinal Accelerometer	=11
✦	Transverse Accelerometer	=5
✚	Longitudinal String Pot	=16
✚	Transverse String Pot	=4
✦	Vertical Accelerometer	=13
●↔●	Relative String Pot	=2
✖	Strain Gauges	=16
	Black Loadcells	=4
	Yellow Loadcells	=2

Number of channels:
Total String Pots=22, Total Accelerometer=29, Black loadcells=20,
Yellow Loadcells=10, Strain Gages=4
Total Channels =85 - (Available Channels = 128)

Figure C.1. Instrumentaion summary and definition of the icons used in the drawings
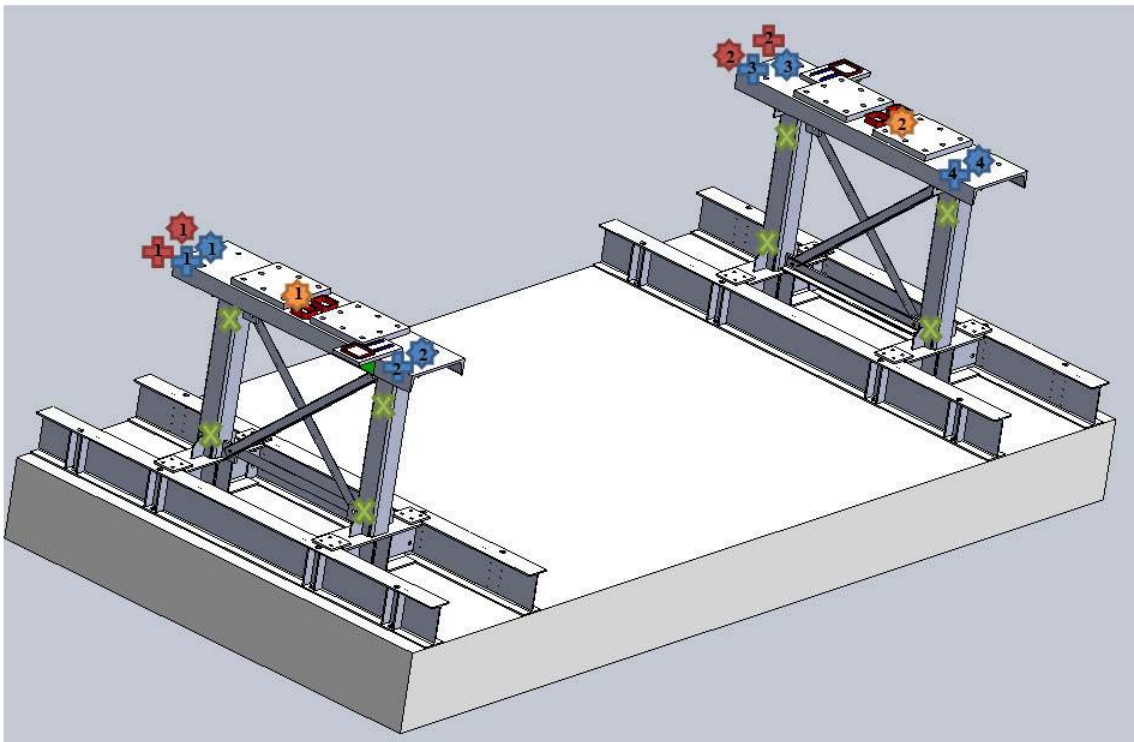
Figure C.2. Instrumentions placed on the piers
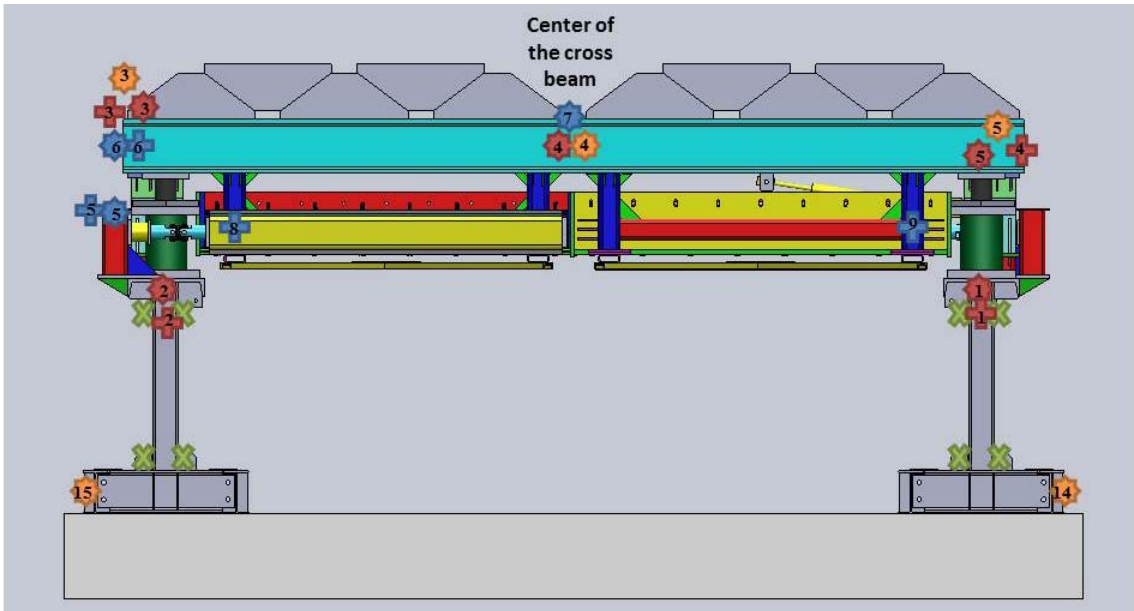
Figure C.3. View from the west of the specimen showing the sensors on the bridge model
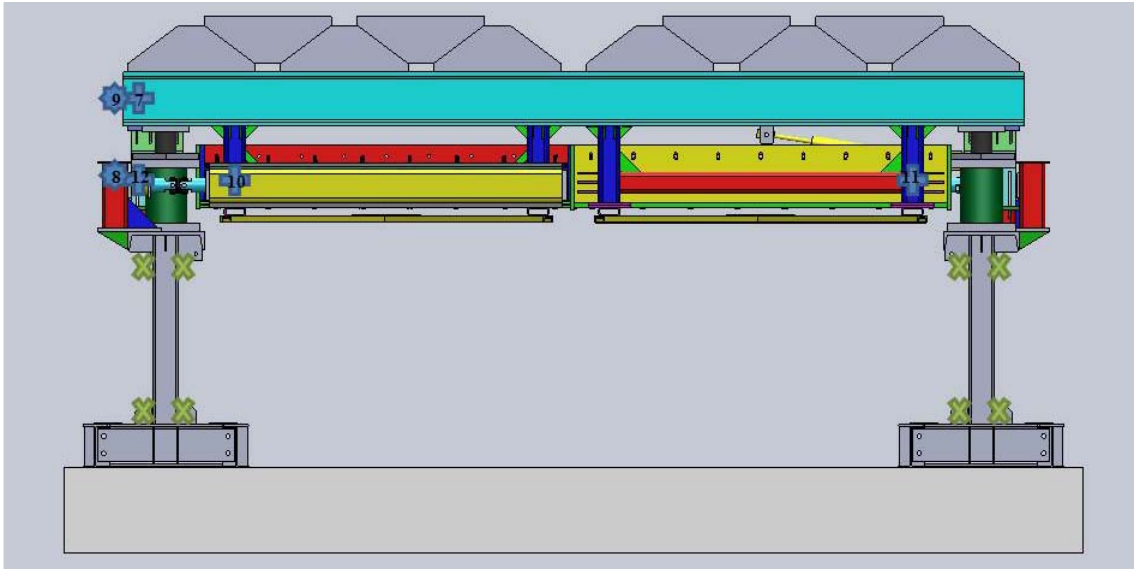
Figure C.4. View from the east of the specimen showing the sensors on the bridge model
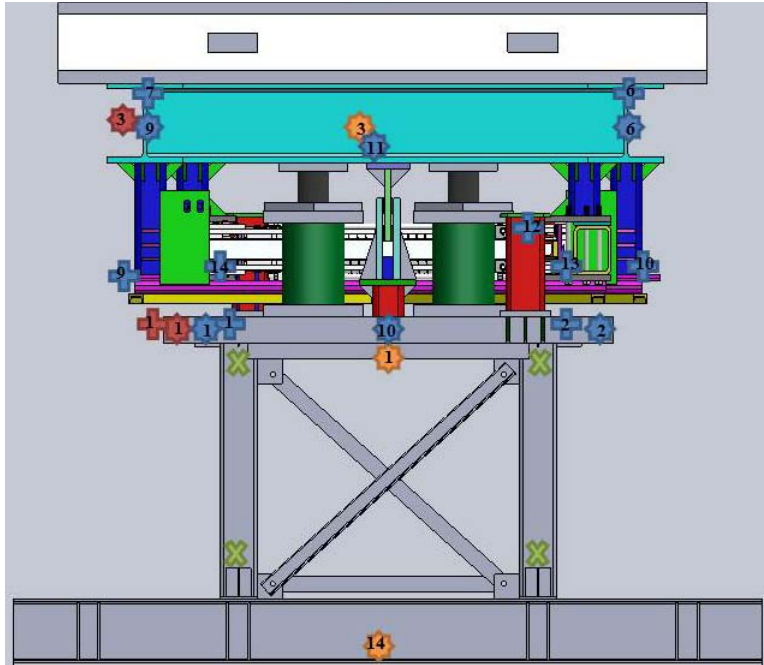
Figure C.5. View from the south of the specimen showing the sensors on the bridge model
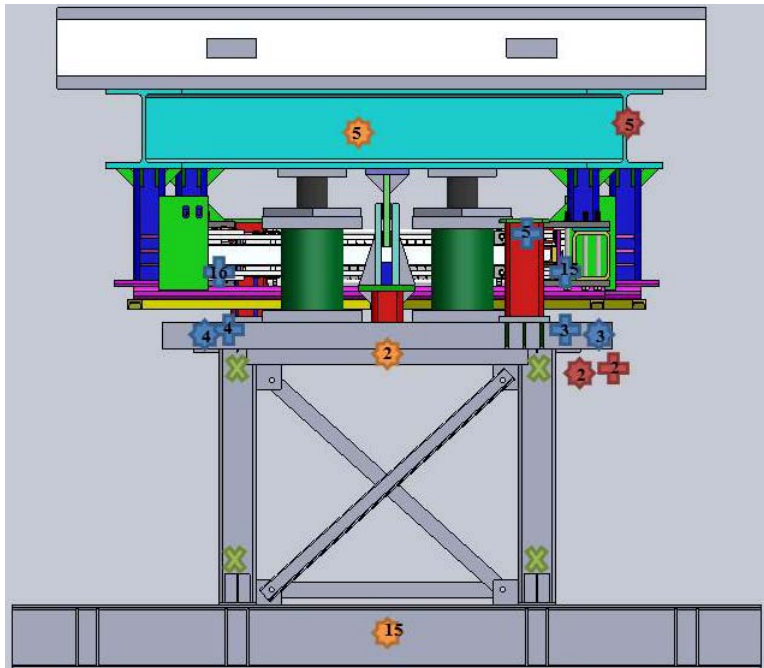
Figure C.6. View from the north of the specimen showing the sensors on the bridge model
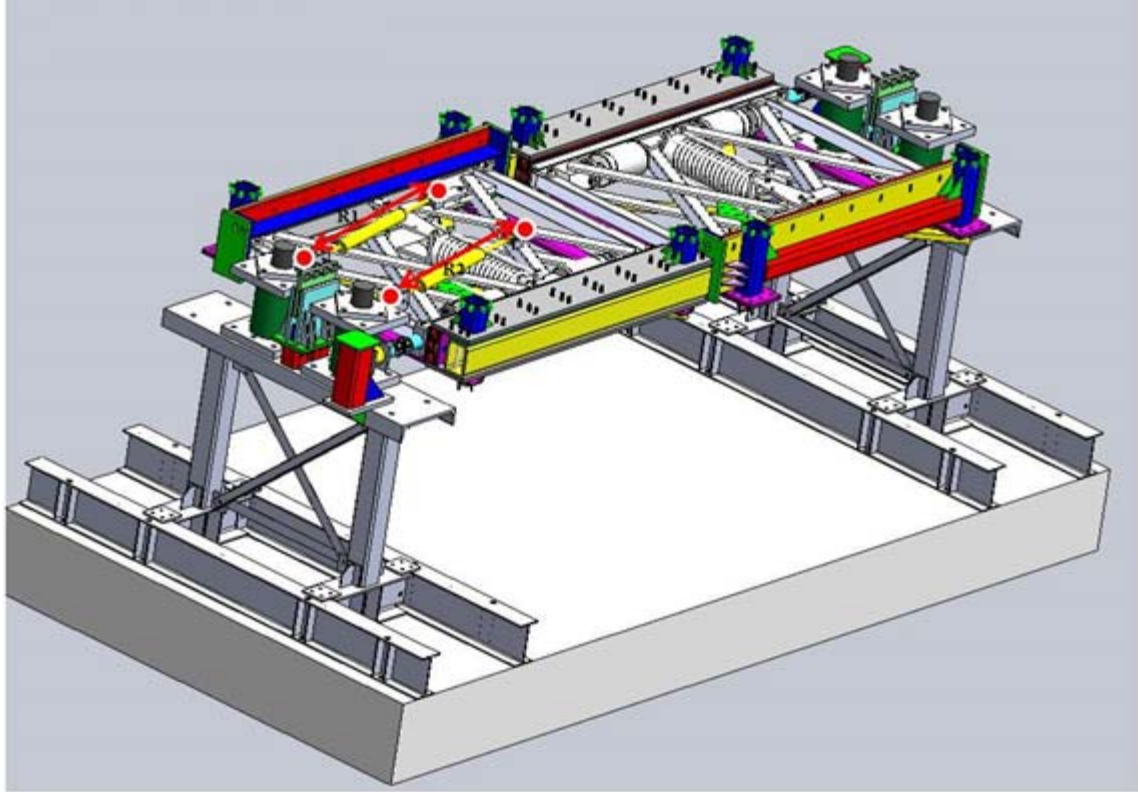
Figure C.7. Relative string potentiometers on the viscous dampers
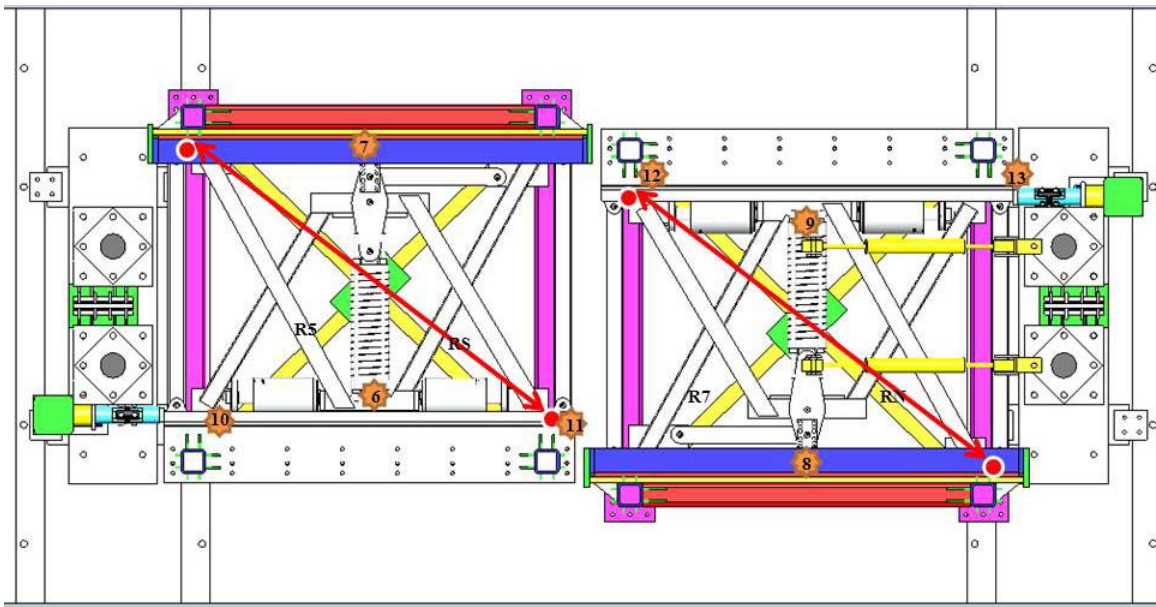
Figure C.8. Relative String potentiometers and vertical sensors on the NSDs

Table C.1. List of the accelerometers and their properties

Sensor Label	Sensor Type	Serial Number	DA Channel Number	Channel Name	Calibration Constant		Zero Offset
					Value	Units	Value
A-L1	Accelerometer	739-112-113	35	36	-0.001116734	g/mV	0.004885709
A-L2	Accelerometer	786-113-114	36	37	-8.99E-04	g/mV	0.006462489
A-L3	Accelerometer	1114187	37	38	0.001099656	g/mV	0.003436426
A-L4	Accelerometer	1032352	38	39	0.001138587	g/mV	-0.00249066
A-L5	Accelerometer	1057930	39	40	9.31E-04	g/mV	-0.001746471
A-L6	Accelerometer	1125336	40	41	0.001088621	g/mV	0.00170097
A-L7	Accelerometer	1031992	41	42	0.001132343	g/mV	-0.001061571
A-L8	Accelerometer	1048882	42	43	0.001209601	g/mV	-0.001134001
A-L9	Accelerometer	180-116-117	43	44	0.001061888	g/mV	-0.00232288
A-L10	Accelerometer	1110894	97	98	0.001024328	g/mV	0.005121639
A-L11	Accelerometer	1124556	98	99	9.81E-04	g/mV	-0.005823755
A-T1	Accelerometer	1124881	63	64	-8.12E-04	g/mV	5.08E-04
A-T2	Accelerometer	1058802	99	100	-0.001169591	g/mV	3.65E-04
A-T3	Accelerometer	1104116	65	66	-0.001068269	g/mV	0.003338341
A-T4	Accelerometer	1124112	66	67	-0.001023836	g/mV	0.001279795
A-T5	Accelerometer	1125343	67	68	-0.001101359	g/mV	0.001720874
A-V1	Accelerometer	1031989	84	85	0.001068983	g/mV	-6.68E-04
A-V2	Accelerometer	1124542	85	86	0.001074006	g/mV	-0.003356268
A-V3	Accelerometer	102016	86	87	0.001187384	g/mV	0.003339518
A-V4	Accelerometer	124576	87	88	0.001064892	g/mV	-0.001663894
A-V5	Accelerometer	1124877	88	89	-7.66E-04	g/mV	-2.40E-04
A-V6	Accelerometer	1124880	89	90	8.13E-04	g/mV	-5.08E-04
A-V7	Accelerometer	1125344	90	91	-0.001125968	g/mV	0.003518649
A-V8	Accelerometer	1124545	91	92	-9.82E-04	g/mV	-0.00399079
A-V9	Accelerometer	1104912	92	93	0.001011058	g/mV	-0.002527646
A-V10	Accelerometer	1125348	93	94	8.18E-04	g/mV	-7.67E-04
A-V11	Accelerometer	1124539	94	95	0.001048149	g/mV	9.83E-04
A-V12	Accelerometer	1032350	95	96	0.001147776	g/mV	0.00143472
A-V13	Accelerometer	1032348	96	97	0.001193807	g/mV	3.73E-04
A-V14	Accelerometer	9811011	102	103	-8.04E-04	g/mV	0.00175769
A-V15	Accelerometer	1124118	103	104	-0.00115921	g/mV	-0.003622532

Table C.2. List of the loadcells and their properties

Sensor Label	Sensor Type	Serial Number	DA Channel Number	Channel Name	Calibration Constant		Zero Offset	
					Value	Units	Value	Units
COL-LC-NE	Load cell	739	0	1	0.00552908	kips/mV	-0.1313156	kips/mV
COL-LC-NW	Load cell	786	1	2	0.00522041	kips/mV	-0.0081569	kips/mV
COL-LC-SE	Load cell	787	2	3	0.00542342	kips/mV	-0.0118637	kips/mV
COL-LC-SW	Load cell	711	3	4	0.0055448	kips/mV	-0.034655	kips/mV
BLK-1-N	Load cell	LC-BLK-1	4	5	22.002996	kips/mV	2.448019	kips/mV
BLK-1-SX	Load cell	LC-BLK-1	5	6	-6.584772	kips/mV	0.208812	kips/mV
BLK-1-SY	Load cell	LC-BLK-1	6	7	-6.809928	kips/mV	-0.0310939	kips/mV
BLK-1-MX	Load cell	LC-BLK-1	7	8	-21.319446	kips/mV	-1.512816	kips/mV
BLK-2-N	Load cell	LC-BLK-2	8	9	-20.553646	kips/mV	-1.093621	kips/mV
BLK-2SX	Load cell	LC-BLK-2	9	10	-6.836721	kips/mV	-1.093621	kips/mV
BLK-2-SY	Load cell	LC-BLK-2	34	35	6.726059	kips/mV	-0.129182	kips/mV
BLK-2-MX	Load cell	LC-BLK-2	11	12	20.742839	kips/mV	3.738809	kips/mV
BLK-2-MY	Load cell	LC-BLK-2	12	13	21.508372	kips/mV	-1.093079	kips/mV
BLK-3-N	Load cell	LC-BLK-3	13	14	-20.211947	kips/mV	-21.285154	kips/mV
BLK-3-SX	Load cell	LC-BLK-3	14	15	-10.324547	kips/mV	0.616528	kips/mV
BLK-3-SY	Load cell	LC-BLK-3	15	16	-6.277443	kips/mV	0.192593	kips/mV
BLK-3-MX	Load cell	LC-BLK-3	16	17	-23.153778	kips/mV	-12.448732	kips/mV
BLK-3-MY	Load cell	LC-BLK-3	17	18	-21.285154	kips/mV	1.08064	kips/mV
BLK-4-N	Load cell	LC-BLK-4	18	19	-20..470585	kips/mV	-1.337208	kips/mV
BLK-4-SX	Load cell	LC-BLK-4	19	20	-6.906288	kips/mV	-0.354161	kips/mV
BLK-4-SY	Load cell	LC-BLK-4	20	21	-6.970087	kips/mV	0.09637	kips/mV
BLK-4-MX	Load cell	LC-BLK-4	21	22	-22.303535	kips/mV	9.467426	kips/mV
BLK-4-MY	Load cell	LC-BLK-4	22	23	20.223184	kips/mV	0.417213	kips/mV
YEL-11-N	Load cell	352-52-53	23	24	0.00333676	kips/mV	0.19454912	kips/mV
YEL-N-SX	Load cell	217-53-54	24	25	-0.0006186	kips/mV	0.01491197	kips/mV
YEL-N-SY	Load cell	31-54-55	25	26	-0.0006229	kips/mV	0.03227542	kips/mV
YEL-N-MX	Load cell	125-55-56	26	27	-0.0023896	kips/mV	0.60842732	kips/mV
YEL-N-MY	Load cell	350-56-57	27	28	0.00247788	kips/mV	-0.9402776	kips/mV
YEL-S-N	Load cell	155-57-58	107	108	0.00335217	kips/mV	0.13854618	kips/mV
YEL-S-SX	Load cell	33-58-59	100	101	-0.0006768	kips/mV	-0.047936	kips/mV
YEL-S-SY	Load cell	306-59-60	31	32	0.00063047	kips/mV	0.01468955	kips/mV
YEL-S-MX	Load cell	30-60-61	32	33	-0.0024643	kips/mV	-0.512575	kips/mV
YEL-S-MY	Load cell	307-62-63	33	34	0.00244702	kips/mV	1.14819219	kips/mV
Damp-LC-E	Load cell	715-79-81	112	113	0.00305022	kips/mV	0.12582933	kips/mV
Damp-LC-W	Load cell	715-79-80	113	114	-0.0028244	kips/mV	0.16177121	kips/mV

Table C.3. List of the string potentiometers and their properties

Sensor Label	Sensor Type	Serial Number	DA Channel Number	Channel Name	Calibration Constant		Zero Offset	
					Value	Units	Value	Units
SP-L1	Stringpot	38040	44	45	-0.0025582	in/mV	-0.0159885	in/mV
SP-L2	Stringpot	38007	45	46	-0.0026955	in/mV	0.00252702	in/mV
SP-L3	Stringpot	34799	46	47	0.00253697	in/mV	-0.0023784	in/mV
SP-L4	Stringpot	34790	47	48	-0.0025828	in/mV	0.00484282	in/mV
SP-L5	Stringpot	34785	48	49	0.00539078	in/mV	-0.0084231	in/mV
SP-L6	Stringpot	38046	49	50	-0.0026624	in/mV	-8.32E-04	in/mV
SP-L7	Stringpot	38036	52	53	-0.0028228	in/mV	0.00529269	in/mV
SP-L8	Stringpot	31765	53	54	0.00270013	in/mV	-0.0067503	in/mV
SP-L9	Stringpot	38023	54	55	-0.002338	in/mV	0.00511432	in/mV
SP-L10	Stringpot	31776	55	56	-0.0024952	in/mV	0.0054582	in/mV
SP-L11	Stringpot	38014	56	57	0.00252971	in/mV	-0.0047432	in/mV
SP-L12	Stringpot	38049	57	58	-0.0027428	in/mV	0.0051427	in/mV
SP-L13	Stringpot	38053	58	59	-0.0025768	in/mV	0.00322097	in/mV
SP-L14	Stringpot	38064	59	60	-0.0025907	in/mV	0.004048	in/mV
SP-L15	Stringpot	31781	60	61	0.00271449	in/mV	-0.0025448	in/mV
SP-L16	Stringpot	38013	62	63	0.00257747	in/mV	0	in/mV
SP-T1	Stringpot	37916	68	69	0.00233776	in/mV	-0.0029222	in/mV
SP-T2	Stringpot	34783	69	70	0.00260746	in/mV	-0.0024445	in/mV
SP-T3	Stringpot	38006	70	71	0.00256941	in/mV	-0.0032118	in/mV
SP-T4	Stringpot	38021	71	72	0.00255236	in/mV	-0.0063809	in/mV
SP-RN	Stringpot	9022981	72	73	0.00508767	in/mV	-0.0031798	in/mV
SP-RS	Stringpot	9099276	101	102	0.00539016	in/mV	-0.0067377	in/mV
SP-Table	Stringpot	38045	75	76	0.00275387	in/mV	0.00E+00	in/mV
SP-L-LC1	Stringpot	37994	76	77	-0.0026001	in/mV	0.00162508	in/mV
SP-L-LC2	Stringpot	31769	82	83	-0.0027778	in/mV	-0.0017361	in/mV
SP-L-LC3	Stringpot	38017	78	79	0.00269892	in/mV	-0.0042171	in/mV
SP-RE-DAMP	Stringpot	34786	115	116	0.00542058	in/mV	0	in/mV
SP-RW-DAMP	Stringpot	31782	116	117	0.00537617	in/mV	0.00E+00	in/mV

D.   Fabrication Drawings of the Bridge Model
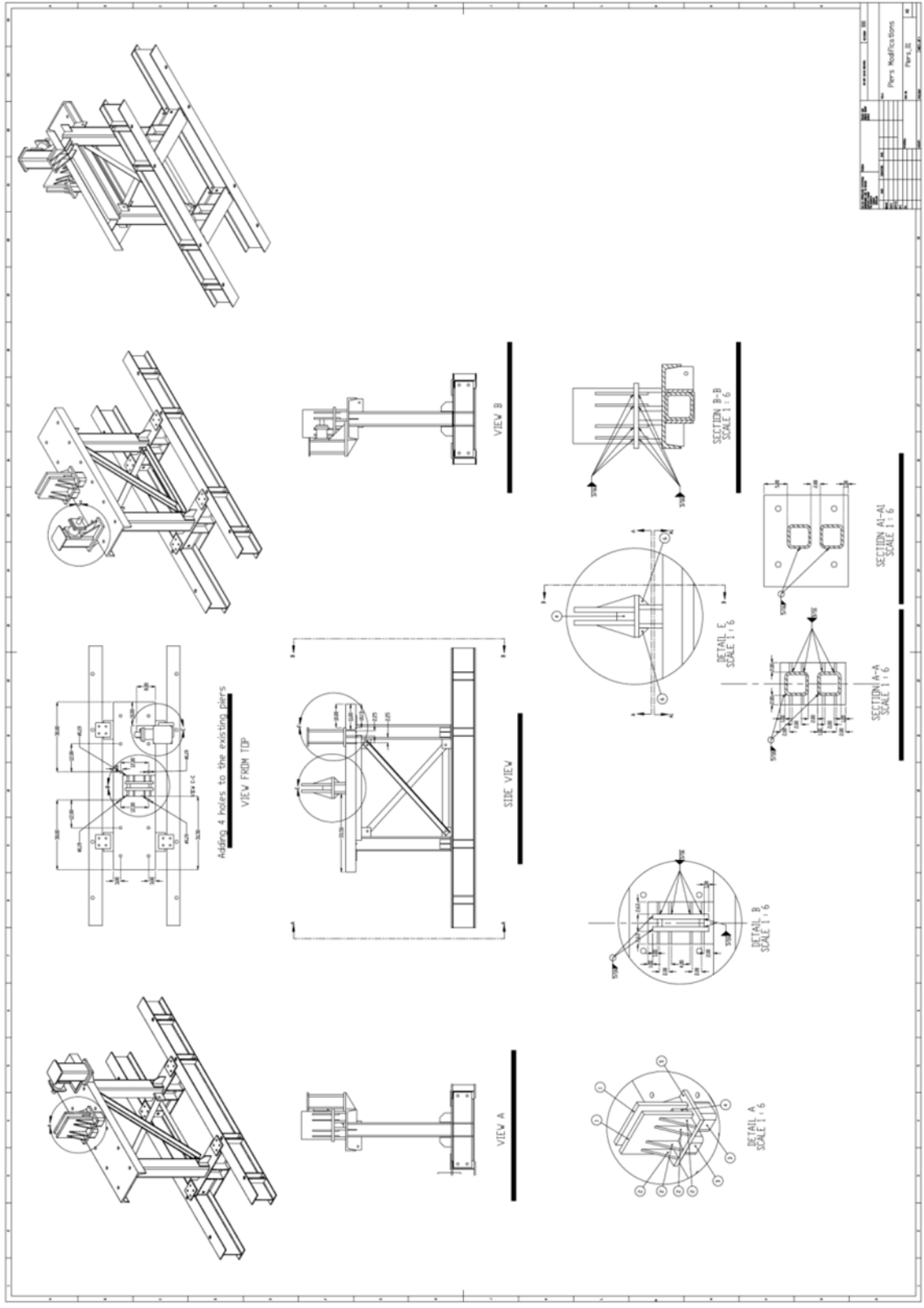
Figure D.1. Pier modification

188
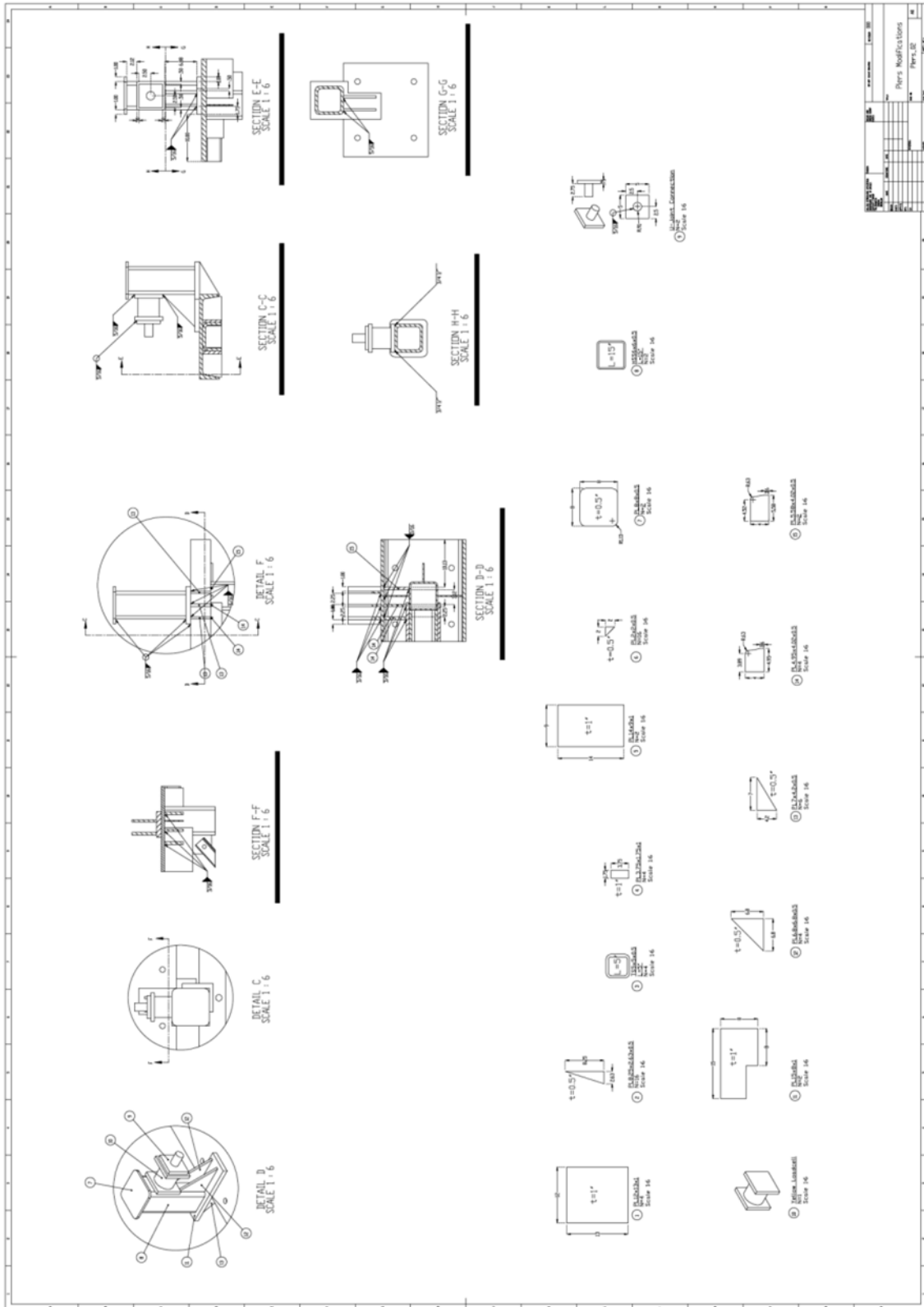
Figure D.2. Details of the pier modification
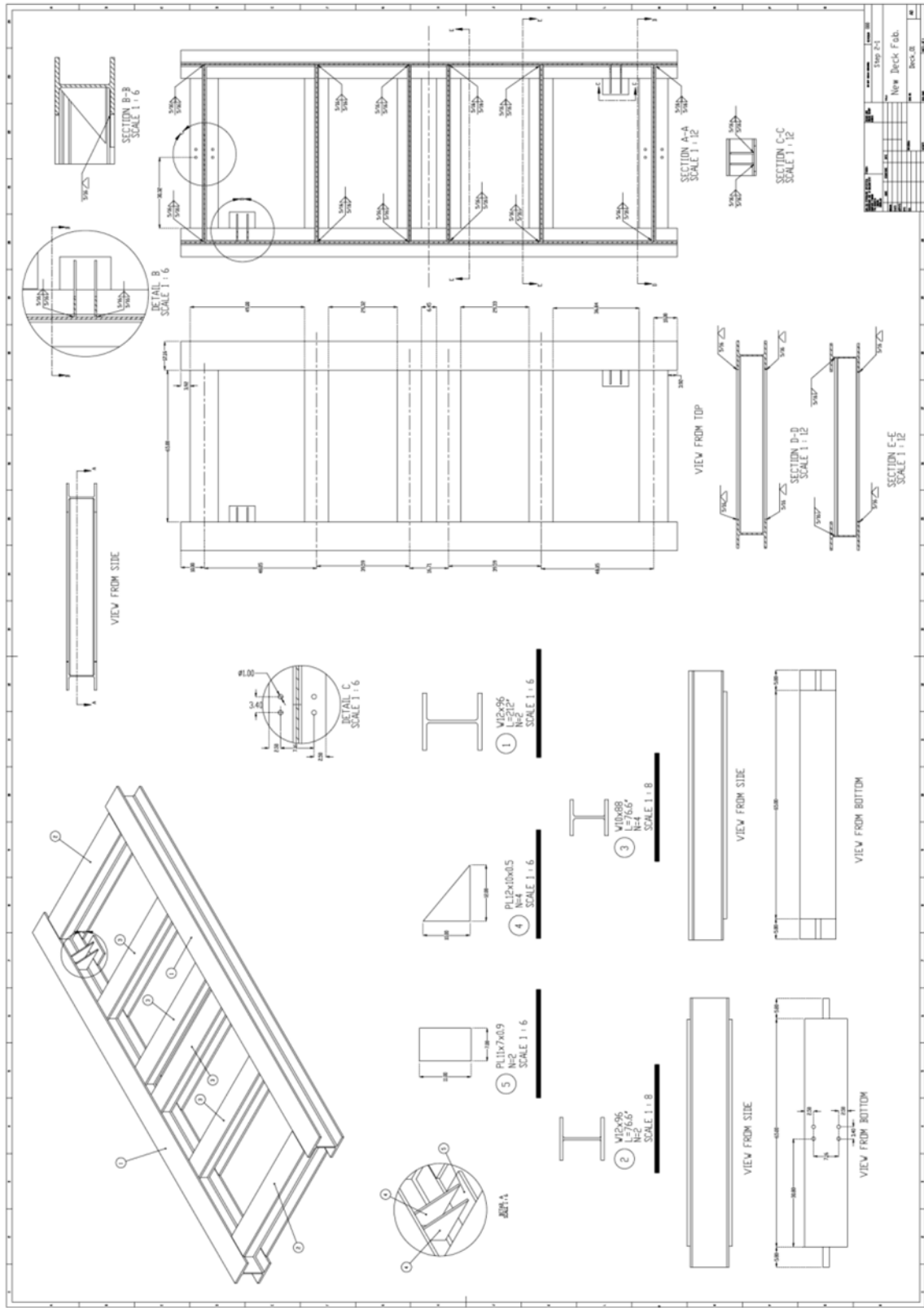
Figure D.3. Details of the bridge deck
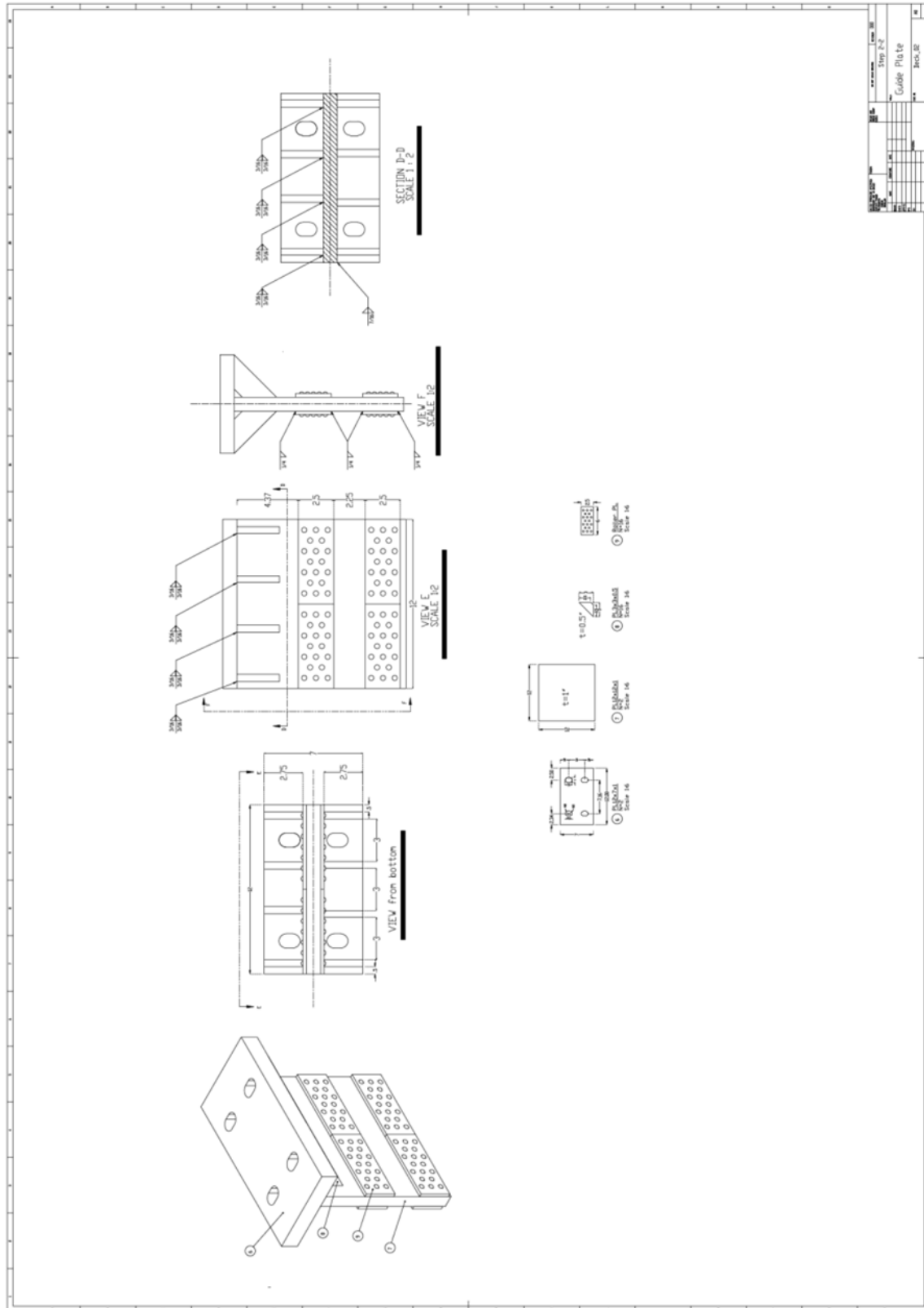
Figure D.4. Details of the torsional restraint guide
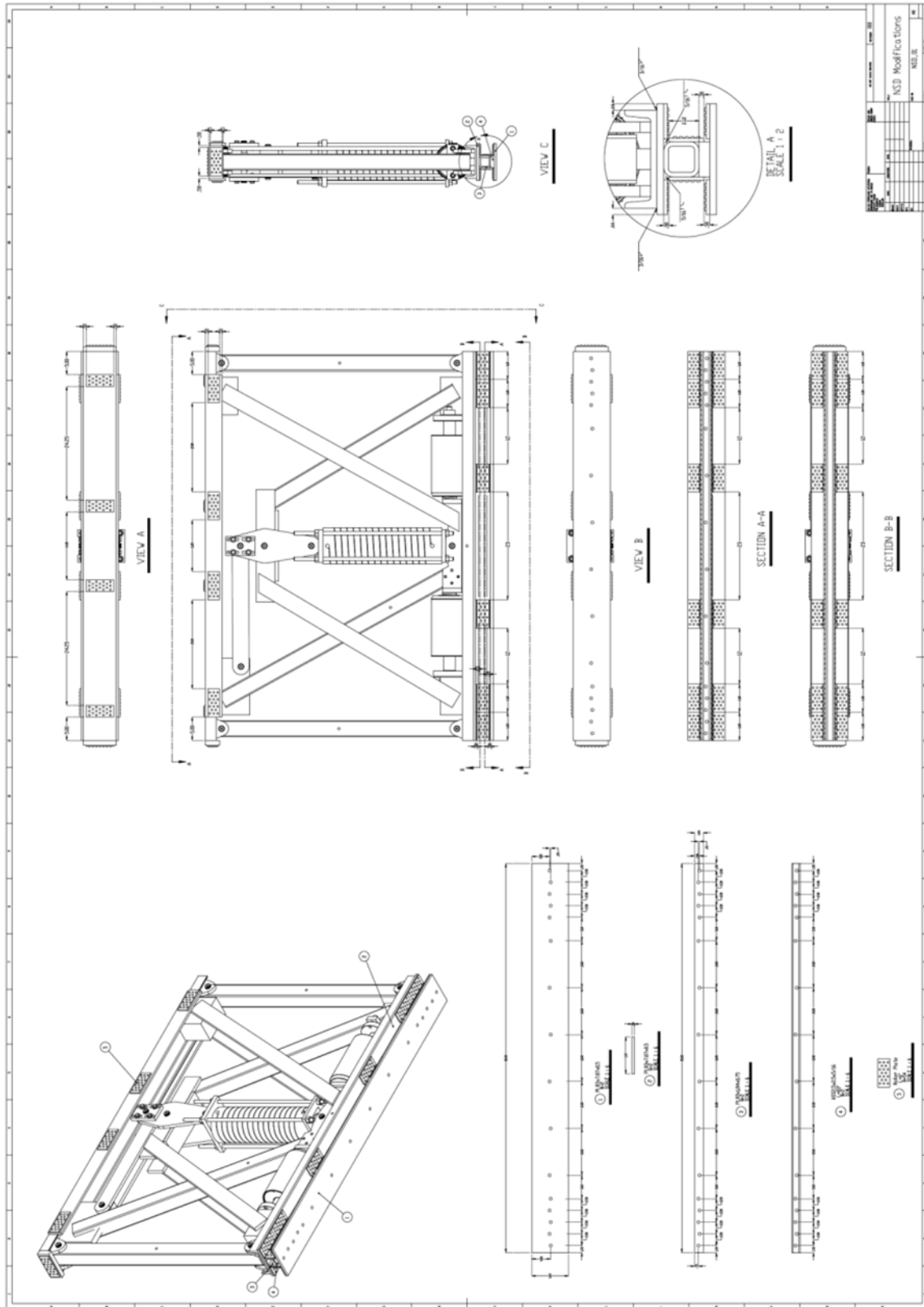
Figure D.5. NSD modifications

192
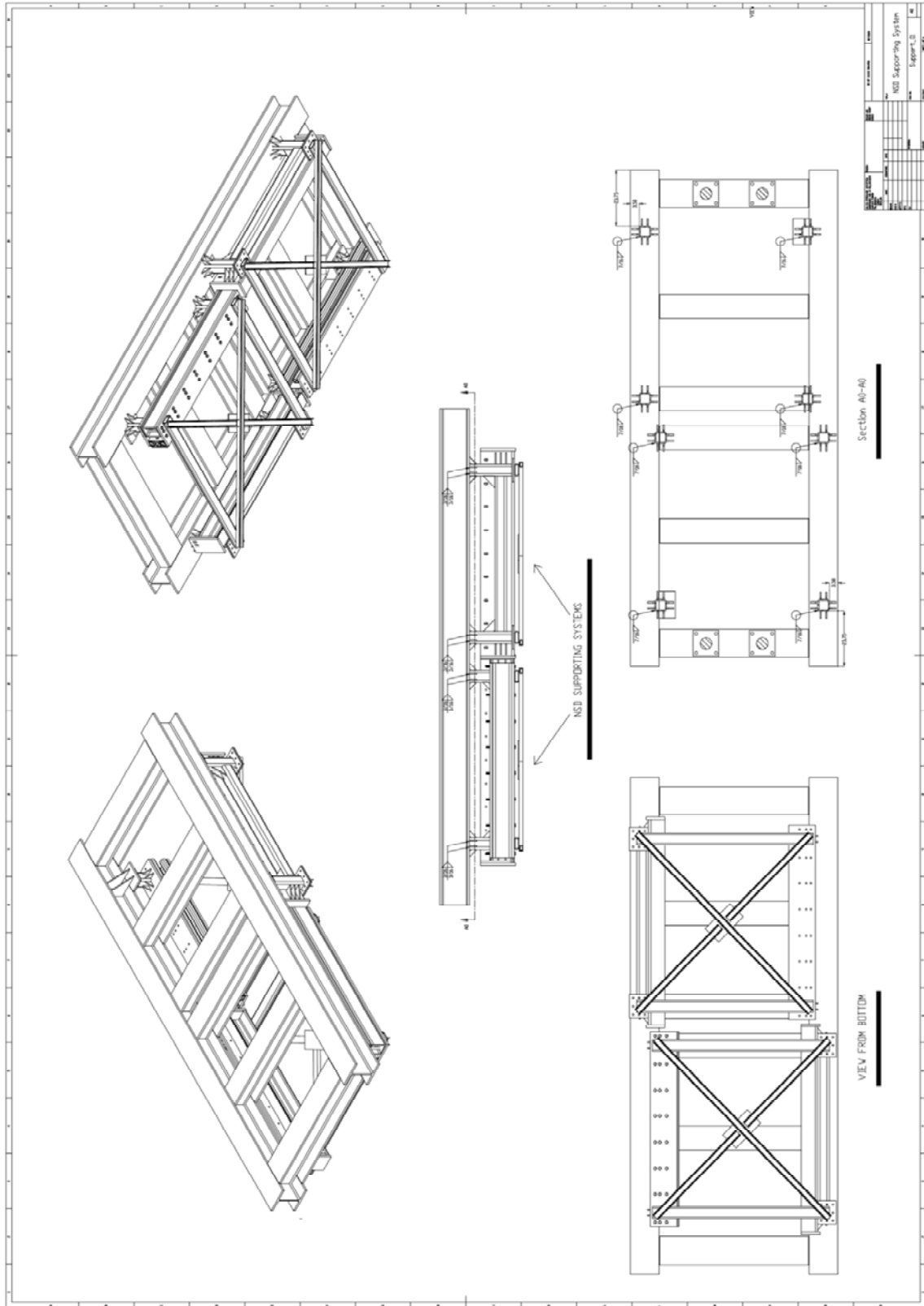
Figure D.6. The two NSD supporting systems under the deck
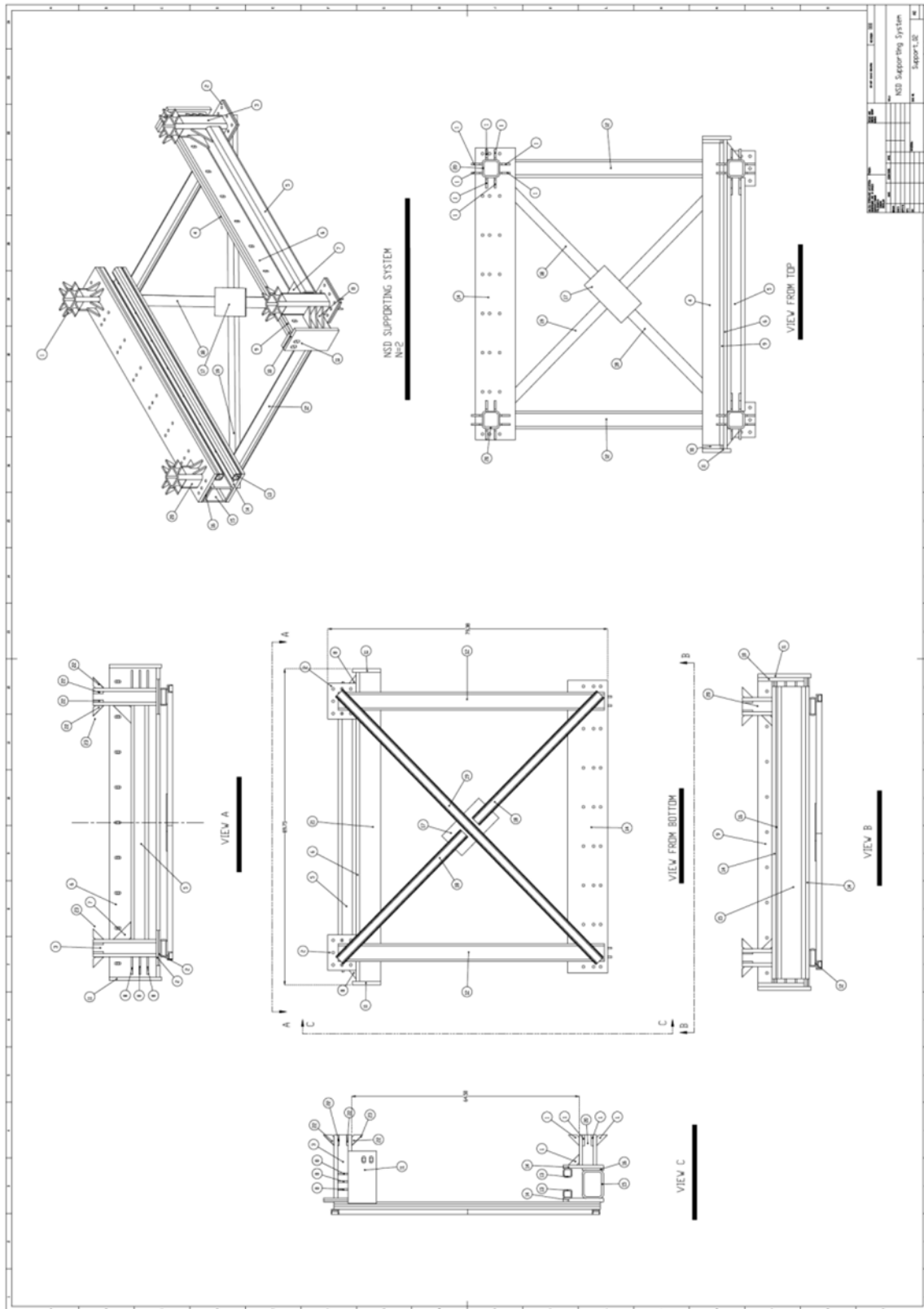
Figure D.7. Details (1) of the NSD supporting systems
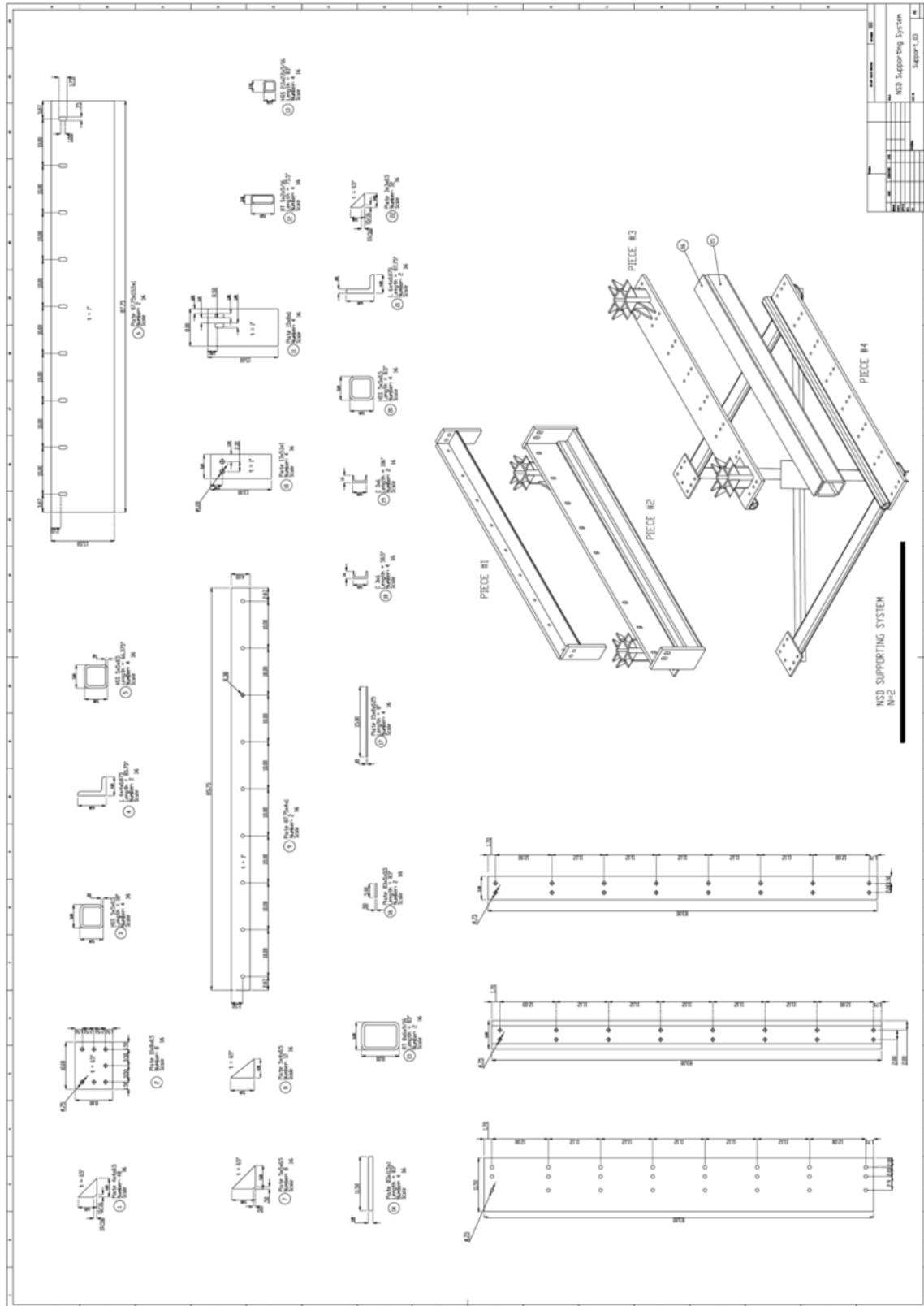
Figure D.8. Details (2) of the NSD supporting systems
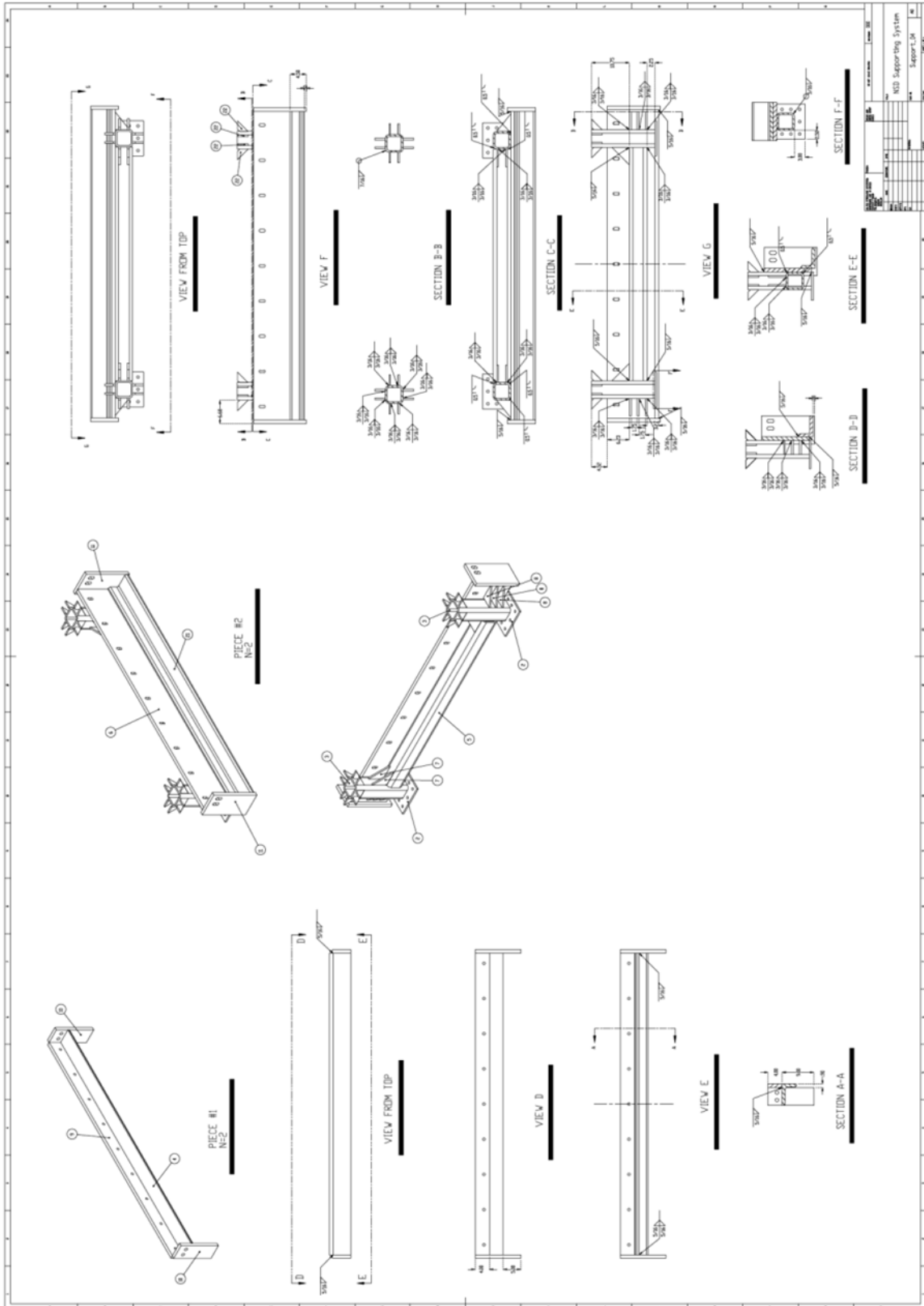
Figure D.9. Details (3) of the NSD supporting systems
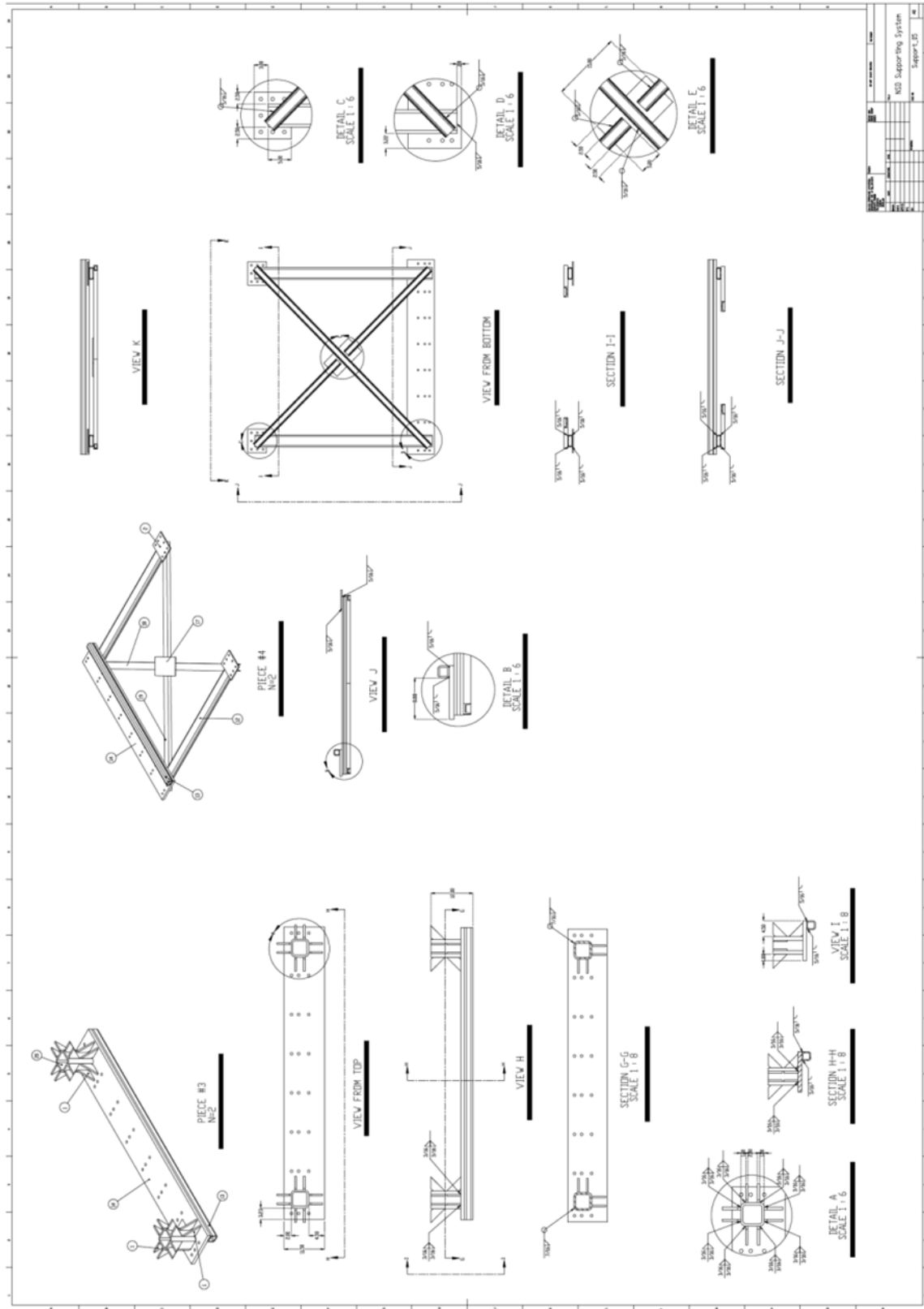
Figure D.10. Details (4) of the NSD supporting systems
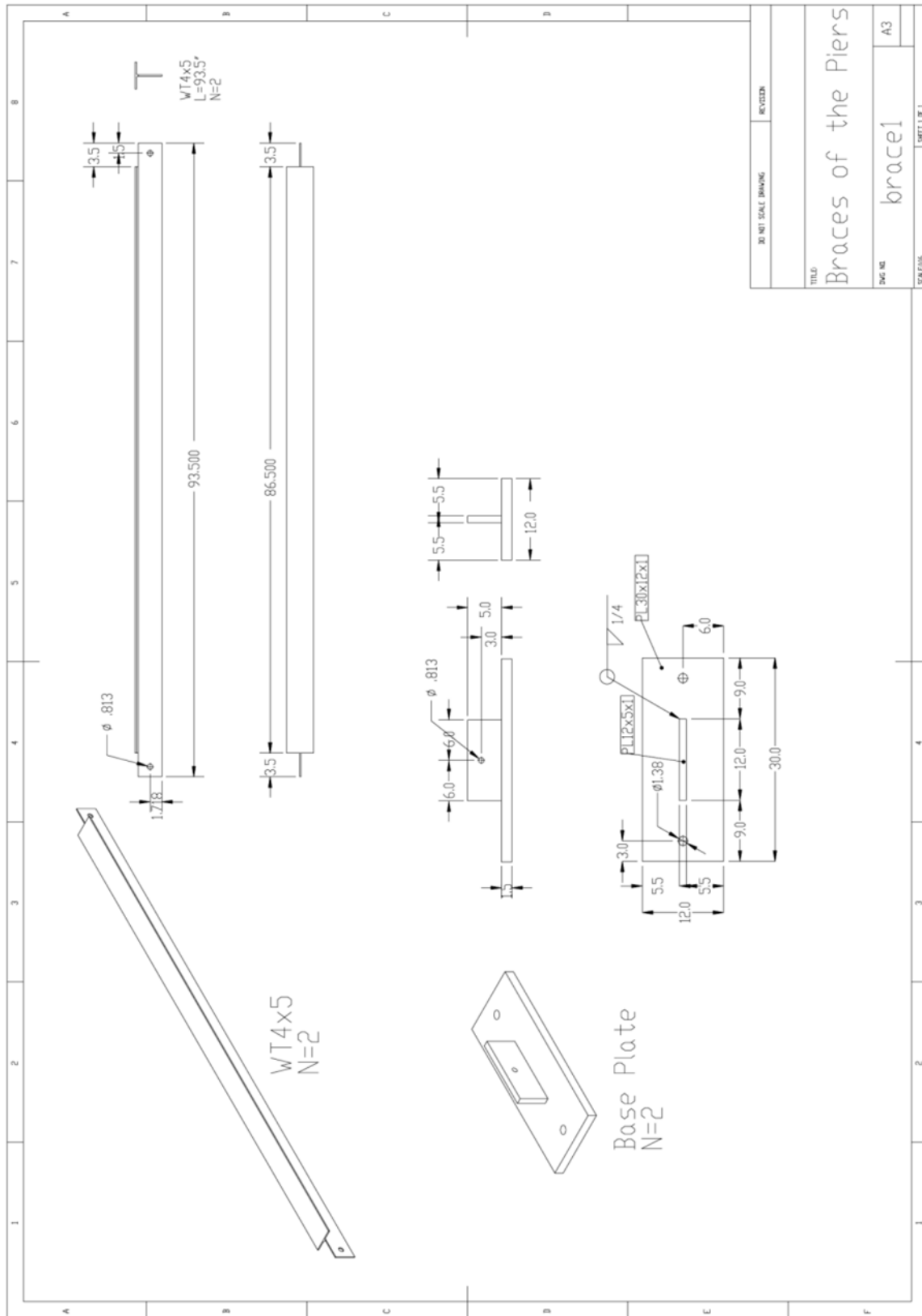
Figure D.11. Details of the pier braces

198
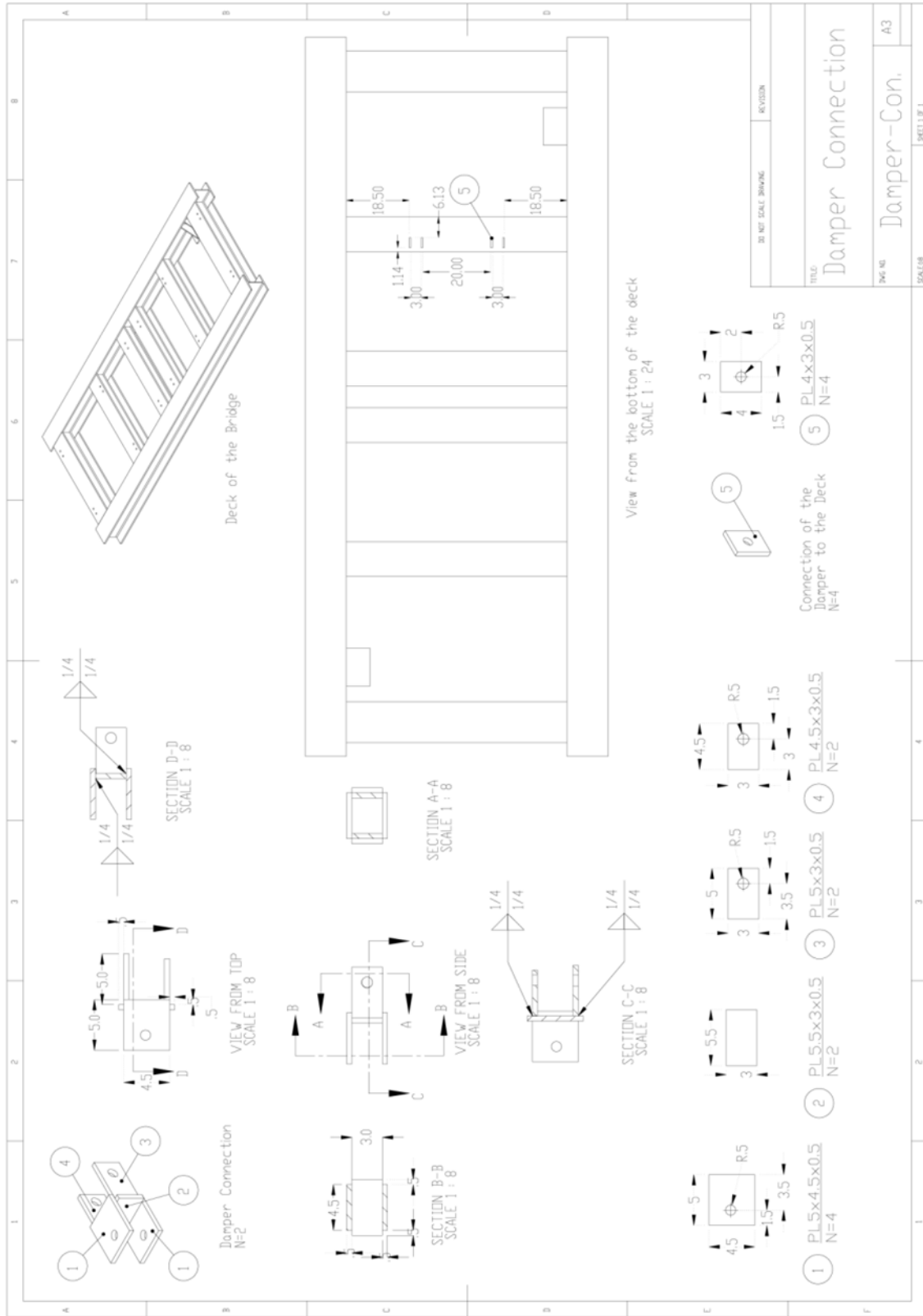
Figure D.12. Details of the damper connections

199

No.	Series	No. in Series	Type	N	L (in)	Shape	W (lb)
1	Pier	1	PL 12×13×1	4		□	177.2
2	Pier	2	PL 8.25×2.63×0.5	16		◁	49.3
3	Pier	3	TS 5×5×0.5	4	5	□	47.5
4	Pier	4	PL 3.75×1.75×1	4		□	7.5
5	Pier	5	PL 14×9×1	2		□	71.6
6	Pier	6	PL 2×2×0.5	16		▽	4.6
7	Pier	7	PL 8×8×0.5	2		□	18.2
8	Pier	8	HSS 6×6×0.5	2	15	□	88.6
9	Pier	9	U-Joint Con.	2		⊙	10.2
10	Pier	10	Yellow Loadcell	2			0
11	Pier	11	PL 15×8×1	2			68.2
12	Pier	12	PL 6.8×6.8×0.5	4		◁	13.15
13	Pier	13	PL 7×4.2×0.5	6		▷	12.5
14	Pier	14	PL 4.95×4.02×0.5	4		□	11.3
15	Pier	15	PL 5.58×4.02×0.5	2		□	6.4
16	Deck	1	W12×96	2	212	H	3396
17	Deck	2	W12×96	2	76.6	H	1227
18	Deck	3	W10×88	4	76.6	H	2254
19	Deck	4	PL 12×10×0.5	4			68.2
20	Deck	5	PL 11×7×0.9	2		□	39.4
21	Deck	6	PL 12×7×1	2			47.7
22	Deck	7	PL 12×12×1	2		□	81.8
23	Deck	8	PL 3×3×0.5	16		◁	10.2
24	Deck	9	McMaster-5764k31	16			0
25	NSD	1	PL 83×7.87×0.5	2			185.5
26	NSD	2	PL 83×7.87×0.5	2			185.5
27	NSD	3	PL 83×1.84×0.75	2			32.5
28	NSD	4	HSS2.5×2.5×5/16	2	83		146.6
29	NSD	5	McMaster-5764k31	54			0
30	Sup.	1	PL 4×4×0.5	48		△	54.6
31	Sup.	2	PL 10×8×0.5	8			90.9
32	Sup.	3	HSS 5×5×0.5	4	18	□	170.9
33	Sup.	4	L 6×4×7/8	2	85.75	L	397.7
34	Sup.	5	HSS 5×5×0.5	4	66.375	□	650.7
35	Sup.	6	PL 87.75×13.5×1	2			630.4
36	Sup.	7	PL 5×5×0.5	8		△	14.2
37	Sup.	8	PL 5×4×0.5	12		△	17.1
38	Sup.	9	PL 87.75×4×1	2			199.4
39	Sup.	10	PL 13×5.1×1	4			75.3
40	Sup.	11	PL 15×8×1	4			136.3
41	Sup.	12	RT 5×2×5/16	4	75.5	□	319.9
42	Sup.	13	HSS2.5×2.5×5/16	4	83	□	293.2
43	Sup.	14	PL 83×11.5×1	4			1084.3
44	Sup.	15	RT 8×6×9/16	2	83	□	645.9
45	Sup.	16	PL 83×5×0.5	2			117.9
46	Sup.	17	PL 15×8×0.25	4	8		34.1
47	Sup.	18	C 3×6	4	50.5	⊏	101
48	Sup.	19	C 3×6	2	106	⊏	106
49	Sup.	20	HSS 5×5×0.5	4	8.5	□	80.7
50	Sup.	21	PL 6×4×7/8	2	87.75	L	11.9
51	Sup.	22	PL 3×3×0.5	32		△	20.5
52	Bolt		McMaster-91257A868	48			
53	Bolt		McMaster-91257A880	32			
54	Bolt		McMaster-91257A961	8			
55	Bolt		McMaster-92620A877	18			
56	Bolt		McMaster-91257A847	28			
57	Bolt		McMaster-91257A803	32			
58	U-Joint		McMaster-8285k24	2			
			TOTAL				13513.6

Figure D.13. Summary of the sections that were used in the fabrication of the specimen

MCEER Technical Reports

MCEER publishes technical reports on a variety of subjects written by authors funded through MCEER. These reports are available from both MCEER Publications and the National Technical Information Service (NTIS). Requests for reports should be directed to MCEER Publications, MCEER, University at Buffalo, State University of New York, 133A Ketter Hall, Buffalo, New York 14260. Reports can also be requested through NTIS, P.O. Box 1425, Springfield, Virginia 22151. NTIS accession numbers are shown in parenthesis, if available.

NCEER-87-0001 "First-Year Program in Research, Education and Technology Transfer," 3/5/87, (PB88-134275, A04, MF-A01).

NCEER-87-0002 "Experimental Evaluation of Instantaneous Optimal Algorithms for Structural Control," by R.C. Lin, T.T. Soong and A.M. Reinhorn, 4/20/87, (PB88-134341, A04, MF-A01).

NCEER-87-0003 "Experimentation Using the Earthquake Simulation Facilities at University at Buffalo," by A.M. Reinhorn and R.L. Ketter, not available.

NCEER-87-0004 "The System Characteristics and Performance of a Shaking Table," by J.S. Hwang, K.C. Chang and G.C. Lee, 6/1/87, (PB88-134259, A03, MF-A01). This report is available only through NTIS (see address given above).

NCEER-87-0005 "A Finite Element Formulation for Nonlinear Viscoplastic Material Using a Q Model," by O. Gyebi and G. Dasgupta, 11/2/87, (PB88-213764, A08, MF-A01).

NCEER-87-0006 "Symbolic Manipulation Program (SMP) - Algebraic Codes for Two and Three Dimensional Finite Element Formulations," by X. Lee and G. Dasgupta, 11/9/87, (PB88-218522, A05, MF-A01).

NCEER-87-0007 "Instantaneous Optimal Control Laws for Tall Buildings Under Seismic Excitations," by J.N. Yang, A. Akbarpour and P. Ghaemmaghami, 6/10/87, (PB88-134333, A06, MF-A01). This report is only available through NTIS (see address given above).

NCEER-87-0008 "IDARC: Inelastic Damage Analysis of Reinforced Concrete Frame - Shear-Wall Structures," by Y.J. Park, A.M. Reinhorn and S.K. Kunnath, 7/20/87, (PB88-134325, A09, MF-A01). This report is only available through NTIS (see address given above).

NCEER-87-0009 "Liquefaction Potential for New York State: A Preliminary Report on Sites in Manhattan and Buffalo," by M. Budhu, V. Vijayakumar, R.F. Giese and L. Baumgras, 8/31/87, (PB88-163704, A03, MF-A01). This report is available only through NTIS (see address given above).

NCEER-87-0010 "Vertical and Torsional Vibration of Foundations in Inhomogeneous Media," by A.S. Veletsos and K.W. Dotson, 6/1/87, (PB88-134291, A03, MF-A01). This report is only available through NTIS (see address given above).

NCEER-87-0011 "Seismic Probabilistic Risk Assessment and Seismic Margins Studies for Nuclear Power Plants," by Howard H.M. Hwang, 6/15/87, (PB88-134267, A03, MF-A01). This report is only available through NTIS (see address given above).

NCEER-87-0012 "Parametric Studies of Frequency Response of Secondary Systems Under Ground-Acceleration Excitations," by Y. Yong and Y.K. Lin, 6/10/87, (PB88-134309, A03, MF-A01). This report is only available through NTIS (see address given above).

NCEER-87-0013 "Frequency Response of Secondary Systems Under Seismic Excitation," by J.A. HoLung, J. Cai and Y.K. Lin, 7/31/87, (PB88-134317, A05, MF-A01). This report is only available through NTIS (see address given above).

NCEER-87-0014 "Modelling Earthquake Ground Motions in Seismically Active Regions Using Parametric Time Series Methods," by G.W. Ellis and A.S. Cakmak, 8/25/87, (PB88-134283, A08, MF-A01). This report is only available through NTIS (see address given above).

NCEER-87-0015 "Detection and Assessment of Seismic Structural Damage," by E. DiPasquale and A.S. Cakmak, 8/25/87, (PB88-163712, A05, MF-A01). This report is only available through NTIS (see address given above).

NCEER-87-0016   "Pipeline Experiment at Parkfield, California," by J. Isenberg and E. Richardson, 9/15/87, (PB88-163720, A03, MF-A01). This report is available only through NTIS (see address given above).

NCEER-87-0017   "Digital Simulation of Seismic Ground Motion," by M. Shinozuka, G. Deodatis and T. Harada, 8/31/87, (PB88-155197, A04, MF-A01). This report is available only through NTIS (see address given above).

NCEER-87-0018   "Practical Considerations for Structural Control: System Uncertainty, System Time Delay and Truncation of Small Control Forces," J.N. Yang and A. Akbarpour, 8/10/87, (PB88-163738, A08, MF-A01). This report is only available through NTIS (see address given above).

NCEER-87-0019   "Modal Analysis of Nonclassically Damped Structural Systems Using Canonical Transformation," by J.N. Yang, S. Sarkani and F.X. Long, 9/27/87, (PB88-187851, A04, MF-A01).

NCEER-87-0020   "A Nonstationary Solution in Random Vibration Theory," by J.R. Red-Horse and P.D. Spanos, 11/3/87, (PB88-163746, A03, MF-A01).

NCEER-87-0021   "Horizontal Impedances for Radially Inhomogeneous Viscoelastic Soil Layers," by A.S. Veletsos and K.W. Dotson, 10/15/87, (PB88-150859, A04, MF-A01).

NCEER-87-0022   "Seismic Damage Assessment of Reinforced Concrete Members," by Y.S. Chung, C. Meyer and M. Shinozuka, 10/9/87, (PB88-150867, A05, MF-A01). This report is available only through NTIS (see address given above).

NCEER-87-0023   "Active Structural Control in Civil Engineering," by T.T. Soong, 11/11/87, (PB88-187778, A03, MF-A01).

NCEER-87-0024   "Vertical and Torsional Impedances for Radially Inhomogeneous Viscoelastic Soil Layers," by K.W. Dotson and A.S. Veletsos, 12/87, (PB88-187786, A03, MF-A01).

NCEER-87-0025   "Proceedings from the Symposium on Seismic Hazards, Ground Motions, Soil-Liquefaction and Engineering Practice in Eastern North America," October 20-22, 1987, edited by K.H. Jacob, 12/87, (PB88-188115, A23, MF-A01). This report is available only through NTIS (see address given above).

NCEER-87-0026   "Report on the Whittier-Narrows, California, Earthquake of October 1, 1987," by J. Pantelic and A. Reinhorn, 11/87, (PB88-187752, A03, MF-A01). This report is available only through NTIS (see address given above).

NCEER-87-0027   "Design of a Modular Program for Transient Nonlinear Analysis of Large 3-D Building Structures," by S. Srivastav and J.F. Abel, 12/30/87, (PB88-187950, A05, MF-A01). This report is only available through NTIS (see address given above).

NCEER-87-0028   "Second-Year Program in Research, Education and Technology Transfer," 3/8/88, (PB88-219480, A04, MF-A01).

NCEER-88-0001   "Workshop on Seismic Computer Analysis and Design of Buildings With Interactive Graphics," by W. McGuire, J.F. Abel and C.H. Conley, 1/18/88, (PB88-187760, A03, MF-A01). This report is only available through NTIS (see address given above).

NCEER-88-0002   "Optimal Control of Nonlinear Flexible Structures," by J.N. Yang, F.X. Long and D. Wong, 1/22/88, (PB88-213772, A06, MF-A01).

NCEER-88-0003   "Substructuring Techniques in the Time Domain for Primary-Secondary Structural Systems," by G.D. Manolis and G. Juhn, 2/10/88, (PB88-213780, A04, MF-A01).

NCEER-88-0004   "Iterative Seismic Analysis of Primary-Secondary Systems," by A. Singhal, L.D. Lutes and P.D. Spanos, 2/23/88, (PB88-213798, A04, MF-A01).

NCEER-88-0005   "Stochastic Finite Element Expansion for Random Media," by P.D. Spanos and R. Ghanem, 3/14/88, (PB88-213806, A03, MF-A01).

NCEER-88-0006   "Combining Structural Optimization and Structural Control," by F.Y. Cheng and C.P. Pantelides, 1/10/88, (PB88-213814, A05, MF-A01).

NCEER-88-0007   "Seismic Performance Assessment of Code-Designed Structures," by H.H-M. Hwang, J-W. Jaw and H-J. Shau, 3/20/88, (PB88-219423, A04, MF-A01). This report is only available through NTIS (see address given above).

NCEER-88-0008   "Reliability Analysis of Code-Designed Structures Under Natural Hazards," by H.H-M. Hwang, H. Ushiba and M. Shinozuka, 2/29/88, (PB88-229471, A07, MF-A01). This report is only available through NTIS (see address given above).

NCEER-88-0009   "Seismic Fragility Analysis of Shear Wall Structures," by J-W Jaw and H.H-M. Hwang, 4/30/88, (PB89-102867, A04, MF-A01).

NCEER-88-0010   "Base Isolation of a Multi-Story Building Under a Harmonic Ground Motion - A Comparison of Performances of Various Systems," by F-G Fan, G. Ahmadi and I.G. Tadjbakhsh, 5/18/88, (PB89-122238, A06, MF-A01). This report is only available through NTIS (see address given above).

NCEER-88-0011   "Seismic Floor Response Spectra for a Combined System by Green's Functions," by F.M. Lavelle, L.A. Bergman and P.D. Spanos, 5/1/88, (PB89-102875, A03, MF-A01).

NCEER-88-0012   "A New Solution Technique for Randomly Excited Hysteretic Structures," by G.Q. Cai and Y.K. Lin, 5/16/88, (PB89-102883, A03, MF-A01).

NCEER-88-0013   "A Study of Radiation Damping and Soil-Structure Interaction Effects in the Centrifuge," by K. Weissman, supervised by J.H. Prevost, 5/24/88, (PB89-144703, A06, MF-A01).

NCEER-88-0014   "Parameter Identification and Implementation of a Kinematic Plasticity Model for Frictional Soils," by J.H. Prevost and D.V. Griffiths, not available.

NCEER-88-0015   "Two- and Three- Dimensional Dynamic Finite Element Analyses of the Long Valley Dam," by D.V. Griffiths and J.H. Prevost, 6/17/88, (PB89-144711, A04, MF-A01).

NCEER-88-0016   "Damage Assessment of Reinforced Concrete Structures in Eastern United States," by A.M. Reinhorn, M.J. Seidel, S.K. Kunnath and Y.J. Park, 6/15/88, (PB89-122220, A04, MF-A01). This report is only available through NTIS (see address given above).

NCEER-88-0017   "Dynamic Compliance of Vertically Loaded Strip Foundations in Multilayered Viscoelastic Soils," by S. Ahmad and A.S.M. Israil, 6/17/88, (PB89-102891, A04, MF-A01).

NCEER-88-0018   "An Experimental Study of Seismic Structural Response With Added Viscoelastic Dampers," by R.C. Lin, Z. Liang, T.T. Soong and R.H. Zhang, 6/30/88, (PB89-122212, A05, MF-A01). This report is available only through NTIS (see address given above).

NCEER-88-0019   "Experimental Investigation of Primary - Secondary System Interaction," by G.D. Manolis, G. Juhn and A.M. Reinhorn, 5/27/88, (PB89-122204, A04, MF-A01).

NCEER-88-0020   "A Response Spectrum Approach For Analysis of Nonclassically Damped Structures," by J.N. Yang, S. Sarkani and F.X. Long, 4/22/88, (PB89-102909, A04, MF-A01).

NCEER-88-0021   "Seismic Interaction of Structures and Soils: Stochastic Approach," by A.S. Veletsos and A.M. Prasad, 7/21/88, (PB89-122196, A04, MF-A01). This report is only available through NTIS (see address given above).

NCEER-88-0022   "Identification of the Serviceability Limit State and Detection of Seismic Structural Damage," by E. DiPasquale and A.S. Cakmak, 6/15/88, (PB89-122188, A05, MF-A01). This report is available only through NTIS (see address given above).

NCEER-88-0023   "Multi-Hazard Risk Analysis: Case of a Simple Offshore Structure," by B.K. Bhartia and E.H. Vanmarcke, 7/21/88, (PB89-145213, A05, MF-A01).

NCEER-88-0024   "Automated Seismic Design of Reinforced Concrete Buildings," by Y.S. Chung, C. Meyer and M. Shinozuka, 7/5/88, (PB89-122170, A06, MF-A01). This report is available only through NTIS (see address given above).

NCEER-88-0025   "Experimental Study of Active Control of MDOF Structures Under Seismic Excitations," by L.L. Chung, R.C. Lin, T.T. Soong and A.M. Reinhorn, 7/10/88, (PB89-122600, A04, MF-A01).

NCEER-88-0026   "Earthquake Simulation Tests of a Low-Rise Metal Structure," by J.S. Hwang, K.C. Chang, G.C. Lee and R.L. Ketter, 8/1/88, (PB89-102917, A04, MF-A01).

NCEER-88-0027   "Systems Study of Urban Response and Reconstruction Due to Catastrophic Earthquakes," by F. Kozin and H.K. Zhou, 9/22/88, (PB90-162348, A04, MF-A01).

NCEER-88-0028   "Seismic Fragility Analysis of Plane Frame Structures," by H.H-M. Hwang and Y.K. Low, 7/31/88, (PB89-131445, A06, MF-A01).

NCEER-88-0029   "Response Analysis of Stochastic Structures," by A. Kardara, C. Bucher and M. Shinozuka, 9/22/88, (PB89-174429, A04, MF-A01).

NCEER-88-0030   "Nonnormal Accelerations Due to Yielding in a Primary Structure," by D.C.K. Chen and L.D. Lutes, 9/19/88, (PB89-131437, A04, MF-A01).

NCEER-88-0031   "Design Approaches for Soil-Structure Interaction," by A.S. Veletsos, A.M. Prasad and Y. Tang, 12/30/88, (PB89-174437, A03, MF-A01). This report is available only through NTIS (see address given above).

NCEER-88-0032   "A Re-evaluation of Design Spectra for Seismic Damage Control," by C.J. Turkstra and A.G. Tallin, 11/7/88, (PB89-145221, A05, MF-A01).

NCEER-88-0033   "The Behavior and Design of Noncontact Lap Splices Subjected to Repeated Inelastic Tensile Loading," by V.E. Sagan, P. Gergely and R.N. White, 12/8/88, (PB89-163737, A08, MF-A01).

NCEER-88-0034   "Seismic Response of Pile Foundations," by S.M. Mamoon, P.K. Banerjee and S. Ahmad, 11/1/88, (PB89-145239, A04, MF-A01).

NCEER-88-0035   "Modeling of R/C Building Structures With Flexible Floor Diaphragms (IDARC2)," by A.M. Reinhorn, S.K. Kunnath and N. Panahshahi, 9/7/88, (PB89-207153, A07, MF-A01).

NCEER-88-0036   "Solution of the Dam-Reservoir Interaction Problem Using a Combination of FEM, BEM with Particular Integrals, Modal Analysis, and Substructuring," by C-S. Tsai, G.C. Lee and R.L. Ketter, 12/31/88, (PB89-207146, A04, MF-A01).

NCEER-88-0037   "Optimal Placement of Actuators for Structural Control," by F.Y. Cheng and C.P. Pantelides, 8/15/88, (PB89-162846, A05, MF-A01).

NCEER-88-0038   "Teflon Bearings in Aseismic Base Isolation: Experimental Studies and Mathematical Modeling," by A. Mokha, M.C. Constantinou and A.M. Reinhorn, 12/5/88, (PB89-218457, A10, MF-A01). This report is available only through NTIS (see address given above).

NCEER-88-0039   "Seismic Behavior of Flat Slab High-Rise Buildings in the New York City Area," by P. Weidlinger and M. Ettouney, 10/15/88, (PB90-145681, A04, MF-A01).

NCEER-88-0040   "Evaluation of the Earthquake Resistance of Existing Buildings in New York City," by P. Weidlinger and M. Ettouney, 10/15/88, not available.

NCEER-88-0041   "Small-Scale Modeling Techniques for Reinforced Concrete Structures Subjected to Seismic Loads," by W. Kim, A. El-Attar and R.N. White, 11/22/88, (PB89-189625, A05, MF-A01).

NCEER-88-0042   "Modeling Strong Ground Motion from Multiple Event Earthquakes," by G.W. Ellis and A.S. Cakmak, 10/15/88, (PB89-174445, A03, MF-A01).

NCEER-88-0043   "Nonstationary Models of Seismic Ground Acceleration," by M. Grigoriu, S.E. Ruiz and E. Rosenblueth, 7/15/88, (PB89-189617, A04, MF-A01).

NCEER-88-0044   "SARCF User's Guide: Seismic Analysis of Reinforced Concrete Frames," by Y.S. Chung, C. Meyer and M. Shinozuka, 11/9/88, (PB89-174452, A08, MF-A01).

NCEER-88-0045   "First Expert Panel Meeting on Disaster Research and Planning," edited by J. Pantelic and J. Stoyle, 9/15/88, (PB89-174460, A05, MF-A01).

NCEER-88-0046   "Preliminary Studies of the Effect of Degrading Infill Walls on the Nonlinear Seismic Response of Steel Frames," by C.Z. Chrysostomou, P. Gergely and J.F. Abel, 12/19/88, (PB89-208383, A05, MF-A01).

NCEER-88-0047   "Reinforced Concrete Frame Component Testing Facility - Design, Construction, Instrumentation and Operation," by S.P. Pessiki, C. Conley, T. Bond, P. Gergely and R.N. White, 12/16/88, (PB89-174478, A04, MF-A01).

NCEER-89-0001   "Effects of Protective Cushion and Soil Compliancy on the Response of Equipment Within a Seismically Excited Building," by J.A. HoLung, 2/16/89, (PB89-207179, A04, MF-A01).

NCEER-89-0002   "Statistical Evaluation of Response Modification Factors for Reinforced Concrete Structures," by H.H-M. Hwang and J-W. Jaw, 2/17/89, (PB89-207187, A05, MF-A01).

NCEER-89-0003   "Hysteretic Columns Under Random Excitation," by G-Q. Cai and Y.K. Lin, 1/9/89, (PB89-196513, A03, MF-A01).

NCEER-89-0004   "Experimental Study of `Elephant Foot Bulge' Instability of Thin-Walled Metal Tanks," by Z-H. Jia and R.L. Ketter, 2/22/89, (PB89-207195, A03, MF-A01).

NCEER-89-0005   "Experiment on Performance of Buried Pipelines Across San Andreas Fault," by J. Isenberg, E. Richardson and T.D. O'Rourke, 3/10/89, (PB89-218440, A04, MF-A01). This report is available only through NTIS (see address given above).

NCEER-89-0006   "A Knowledge-Based Approach to Structural Design of Earthquake-Resistant Buildings," by M. Subramani, P. Gergely, C.H. Conley, J.F. Abel and A.H. Zaghw, 1/15/89, (PB89-218465, A06, MF-A01).

NCEER-89-0007   "Liquefaction Hazards and Their Effects on Buried Pipelines," by T.D. O'Rourke and P.A. Lane, 2/1/89, (PB89-218481, A09, MF-A01).

NCEER-89-0008   "Fundamentals of System Identification in Structural Dynamics," by H. Imai, C-B. Yun, O. Maruyama and M. Shinozuka, 1/26/89, (PB89-207211, A04, MF-A01).

NCEER-89-0009   "Effects of the 1985 Michoacan Earthquake on Water Systems and Other Buried Lifelines in Mexico," by A.G. Ayala and M.J. O'Rourke, 3/8/89, (PB89-207229, A06, MF-A01).

NCEER-89-R010   "NCEER Bibliography of Earthquake Education Materials," by K.E.K. Ross, Second Revision, 9/1/89, (PB90-125352, A05, MF-A01). This report is replaced by NCEER-92-0018.

NCEER-89-0011   "Inelastic Three-Dimensional Response Analysis of Reinforced Concrete Building Structures (IDARC-3D), Part I - Modeling," by S.K. Kunnath and A.M. Reinhorn, 4/17/89, (PB90-114612, A07, MF-A01). This report is available only through NTIS (see address given above).

NCEER-89-0012   "Recommended Modifications to ATC-14," by C.D. Poland and J.O. Malley, 4/12/89, (PB90-108648, A15, MF-A01).

NCEER-89-0013   "Repair and Strengthening of Beam-to-Column Connections Subjected to Earthquake Loading," by M. Corazao and A.J. Durrani, 2/28/89, (PB90-109885, A06, MF-A01).

NCEER-89-0014   "Program EXKAL2 for Identification of Structural Dynamic Systems," by O. Maruyama, C-B. Yun, M. Hoshiya and M. Shinozuka, 5/19/89, (PB90-109877, A09, MF-A01).

NCEER-89-0015   "Response of Frames With Bolted Semi-Rigid Connections, Part I - Experimental Study and Analytical Predictions," by P.J. DiCorso, A.M. Reinhorn, J.R. Dickerson, J.B. Radziminski and W.L. Harper, 6/1/89, not available.

NCEER-89-0016   "ARMA Monte Carlo Simulation in Probabilistic Structural Analysis," by P.D. Spanos and M.P. Mignolet, 7/10/89, (PB90-109893, A03, MF-A01).

NCEER-89-P017   "Preliminary Proceedings from the Conference on Disaster Preparedness - The Place of Earthquake Education in Our Schools," Edited by K.E.K. Ross, 6/23/89, (PB90-108606, A03, MF-A01).

NCEER-89-0017   "Proceedings from the Conference on Disaster Preparedness - The Place of Earthquake Education in Our Schools," Edited by K.E.K. Ross, 12/31/89, (PB90-207895, A012, MF-A02). This report is available only through NTIS (see address given above).

NCEER-89-0018   "Multidimensional Models of Hysteretic Material Behavior for Vibration Analysis of Shape Memory Energy Absorbing Devices, by E.J. Graesser and F.A. Cozzarelli, 6/7/89, (PB90-164146, A04, MF-A01).

NCEER-89-0019   "Nonlinear Dynamic Analysis of Three-Dimensional Base Isolated Structures (3D-BASIS)," by S. Nagarajaiah, A.M. Reinhorn and M.C. Constantinou, 8/3/89, (PB90-161936, A06, MF-A01). This report has been replaced by NCEER-93-0011.

NCEER-89-0020   "Structural Control Considering Time-Rate of Control Forces and Control Rate Constraints," by F.Y. Cheng and C.P. Pantelides, 8/3/89, (PB90-120445, A04, MF-A01).

NCEER-89-0021   "Subsurface Conditions of Memphis and Shelby County," by K.W. Ng, T-S. Chang and H-H.M. Hwang, 7/26/89, (PB90-120437, A03, MF-A01).

NCEER-89-0022   "Seismic Wave Propagation Effects on Straight Jointed Buried Pipelines," by K. Elhmadi and M.J. O'Rourke, 8/24/89, (PB90-162322, A10, MF-A02).

NCEER-89-0023   "Workshop on Serviceability Analysis of Water Delivery Systems," edited by M. Grigoriu, 3/6/89, (PB90-127424, A03, MF-A01).

NCEER-89-0024   "Shaking Table Study of a 1/5 Scale Steel Frame Composed of Tapered Members," by K.C. Chang, J.S. Hwang and G.C. Lee, 9/18/89, (PB90-160169, A04, MF-A01).

NCEER-89-0025   "DYNA1D: A Computer Program for Nonlinear Seismic Site Response Analysis - Technical Documentation," by Jean H. Prevost, 9/14/89, (PB90-161944, A07, MF-A01). This report is available only through NTIS (see address given above).

NCEER-89-0026   "1:4 Scale Model Studies of Active Tendon Systems and Active Mass Dampers for Aseismic Protection," by A.M. Reinhorn, T.T. Soong, R.C. Lin, Y.P. Yang, Y. Fukao, H. Abe and M. Nakai, 9/15/89, (PB90-173246, A10, MF-A02). This report is available only through NTIS (see address given above).

NCEER-89-0027   "Scattering of Waves by Inclusions in a Nonhomogeneous Elastic Half Space Solved by Boundary Element Methods," by P.K. Hadley, A. Askar and A.S. Cakmak, 6/15/89, (PB90-145699, A07, MF-A01).

NCEER-89-0028   "Statistical Evaluation of Deflection Amplification Factors for Reinforced Concrete Structures," by H.H.M. Hwang, J-W. Jaw and A.L. Ch'ng, 8/31/89, (PB90-164633, A05, MF-A01).

NCEER-89-0029   "Bedrock Accelerations in Memphis Area Due to Large New Madrid Earthquakes," by H.H.M. Hwang, C.H.S. Chen and G. Yu, 11/7/89, (PB90-162330, A04, MF-A01).

NCEER-89-0030   "Seismic Behavior and Response Sensitivity of Secondary Structural Systems," by Y.Q. Chen and T.T. Soong, 10/23/89, (PB90-164658, A08, MF-A01).

NCEER-89-0031   "Random Vibration and Reliability Analysis of Primary-Secondary Structural Systems," by Y. Ibrahim, M. Grigoriu and T.T. Soong, 11/10/89, (PB90-161951, A04, MF-A01).

NCEER-89-0032   "Proceedings from the Second U.S. - Japan Workshop on Liquefaction, Large Ground Deformation and Their Effects on Lifelines, September 26-29, 1989," Edited by T.D. O'Rourke and M. Hamada, 12/1/89, (PB90-209388, A22, MF-A03).

NCEER-89-0033   "Deterministic Model for Seismic Damage Evaluation of Reinforced Concrete Structures," by J.M. Bracci, A.M. Reinhorn, J.B. Mander and S.K. Kunnath, 9/27/89, (PB91-108803, A06, MF-A01).

NCEER-89-0034   "On the Relation Between Local and Global Damage Indices," by E. DiPasquale and A.S. Cakmak, 8/15/89, (PB90-173865, A05, MF-A01).

NCEER-89-0035   "Cyclic Undrained Behavior of Nonplastic and Low Plasticity Silts," by A.J. Walker and H.E. Stewart, 7/26/89, (PB90-183518, A10, MF-A01).

NCEER-89-0036   "Liquefaction Potential of Surficial Deposits in the City of Buffalo, New York," by M. Budhu, R. Giese and L. Baumgrass, 1/17/89, (PB90-208455, A04, MF-A01).

NCEER-89-0037   "A Deterministic Assessment of Effects of Ground Motion Incoherence," by A.S. Veletsos and Y. Tang, 7/15/89, (PB90-164294, A03, MF-A01).

NCEER-89-0038   "Workshop on Ground Motion Parameters for Seismic Hazard Mapping," July 17-18, 1989, edited by R.V. Whitman, 12/1/89, (PB90-173923, A04, MF-A01).

NCEER-89-0039   "Seismic Effects on Elevated Transit Lines of the New York City Transit Authority," by C.J. Costantino, C.A. Miller and E. Heymsfield, 12/26/89, (PB90-207887, A06, MF-A01).

NCEER-89-0040   "Centrifugal Modeling of Dynamic Soil-Structure Interaction," by K. Weissman, Supervised by J.H. Prevost, 5/10/89, (PB90-207879, A07, MF-A01).

NCEER-89-0041   "Linearized Identification of Buildings With Cores for Seismic Vulnerability Assessment," by I-K. Ho and A.E. Aktan, 11/1/89, (PB90-251943, A07, MF-A01).

NCEER-90-0001   "Geotechnical and Lifeline Aspects of the October 17, 1989 Loma Prieta Earthquake in San Francisco," by T.D. O'Rourke, H.E. Stewart, F.T. Blackburn and T.S. Dickerman, 1/90, (PB90-208596, A05, MF-A01).

NCEER-90-0002   "Nonnormal Secondary Response Due to Yielding in a Primary Structure," by D.C.K. Chen and L.D. Lutes, 2/28/90, (PB90-251976, A07, MF-A01).

NCEER-90-0003   "Earthquake Education Materials for Grades K-12," by K.E.K. Ross, 4/16/90, (PB91-251984, A05, MF-A05). This report has been replaced by NCEER-92-0018.

NCEER-90-0004   "Catalog of Strong Motion Stations in Eastern North America," by R.W. Busby, 4/3/90, (PB90-251984, A05, MF-A01).

NCEER-90-0005   "NCEER Strong-Motion Data Base: A User Manual for the GeoBase Release (Version 1.0 for the Sun3)," by P. Friberg and K. Jacob, 3/31/90 (PB90-258062, A04, MF-A01).

NCEER-90-0006   "Seismic Hazard Along a Crude Oil Pipeline in the Event of an 1811-1812 Type New Madrid Earthquake," by H.H.M. Hwang and C-H.S. Chen, 4/16/90, (PB90-258054, A04, MF-A01).

NCEER-90-0007   "Site-Specific Response Spectra for Memphis Sheahan Pumping Station," by H.H.M. Hwang and C.S. Lee, 5/15/90, (PB91-108811, A05, MF-A01).

NCEER-90-0008   "Pilot Study on Seismic Vulnerability of Crude Oil Transmission Systems," by T. Ariman, R. Dobry, M. Grigoriu, F. Kozin, M. O'Rourke, T. O'Rourke and M. Shinozuka, 5/25/90, (PB91-108837, A06, MF-A01).

NCEER-90-0009   "A Program to Generate Site Dependent Time Histories: EQGEN," by G.W. Ellis, M. Srinivasan and A.S. Cakmak, 1/30/90, (PB91-108829, A04, MF-A01).

NCEER-90-0010   "Active Isolation for Seismic Protection of Operating Rooms," by M.E. Talbott, Supervised by M. Shinozuka, 6/8/9, (PB91-110205, A05, MF-A01).

NCEER-90-0011   "Program LINEARID for Identification of Linear Structural Dynamic Systems," by C-B. Yun and M. Shinozuka, 6/25/90, (PB91-110312, A08, MF-A01).

NCEER-90-0012   "Two-Dimensional Two-Phase Elasto-Plastic Seismic Response of Earth Dams," by A.N. Yiagos, Supervised by J.H. Prevost, 6/20/90, (PB91-110197, A13, MF-A02).

NCEER-90-0013   "Secondary Systems in Base-Isolated Structures: Experimental Investigation, Stochastic Response and Stochastic Sensitivity," by G.D. Manolis, G. Juhn, M.C. Constantinou and A.M. Reinhorn, 7/1/90, (PB91-110320, A08, MF-A01).

NCEER-90-0014   "Seismic Behavior of Lightly-Reinforced Concrete Column and Beam-Column Joint Details," by S.P. Pessiki, C.H. Conley, P. Gergely and R.N. White, 8/22/90, (PB91-108795, A11, MF-A02).

NCEER-90-0015   "Two Hybrid Control Systems for Building Structures Under Strong Earthquakes," by J.N. Yang and A. Danielians, 6/29/90, (PB91-125393, A04, MF-A01).

NCEER-90-0016   "Instantaneous Optimal Control with Acceleration and Velocity Feedback," by J.N. Yang and Z. Li, 6/29/90, (PB91-125401, A03, MF-A01).

NCEER-90-0017   "Reconnaissance Report on the Northern Iran Earthquake of June 21, 1990," by M. Mehrain, 10/4/90, (PB91-125377, A03, MF-A01).

NCEER-90-0018   "Evaluation of Liquefaction Potential in Memphis and Shelby County," by T.S. Chang, P.S. Tang, C.S. Lee and H. Hwang, 8/10/90, (PB91-125427, A09, MF-A01).

NCEER-90-0019   "Experimental and Analytical Study of a Combined Sliding Disc Bearing and Helical Steel Spring Isolation System," by M.C. Constantinou, A.S. Mokha and A.M. Reinhorn, 10/4/90, (PB91-125385, A06, MF-A01). This report is available only through NTIS (see address given above).

NCEER-90-0020   "Experimental Study and Analytical Prediction of Earthquake Response of a Sliding Isolation System with a Spherical Surface," by A.S. Mokha, M.C. Constantinou and A.M. Reinhorn, 10/11/90, (PB91-125419, A05, MF-A01).

NCEER-90-0021   "Dynamic Interaction Factors for Floating Pile Groups," by G. Gazetas, K. Fan, A. Kaynia and E. Kausel, 9/10/90, (PB91-170381, A05, MF-A01).

NCEER-90-0022   "Evaluation of Seismic Damage Indices for Reinforced Concrete Structures," by S. Rodriguez-Gomez and A.S. Cakmak, 9/30/90, PB91-171322, A06, MF-A01).

NCEER-90-0023   "Study of Site Response at a Selected Memphis Site," by H. Desai, S. Ahmad, E.S. Gazetas and M.R. Oh, 10/11/90, (PB91-196857, A03, MF-A01).

NCEER-90-0024   "A User's Guide to Strongmo: Version 1.0 of NCEER's Strong-Motion Data Access Tool for PCs and Terminals," by P.A. Friberg and C.A.T. Susch, 11/15/90, (PB91-171272, A03, MF-A01).

NCEER-90-0025   "A Three-Dimensional Analytical Study of Spatial Variability of Seismic Ground Motions," by L-L. Hong and A.H.-S. Ang, 10/30/90, (PB91-170399, A09, MF-A01).

NCEER-90-0026   "MUMOID User's Guide - A Program for the Identification of Modal Parameters," by S. Rodriguez-Gomez and E. DiPasquale, 9/30/90, (PB91-171298, A04, MF-A01).

NCEER-90-0027   "SARCF-II User's Guide - Seismic Analysis of Reinforced Concrete Frames," by S. Rodriguez-Gomez, Y.S. Chung and C. Meyer, 9/30/90, (PB91-171280, A05, MF-A01).

NCEER-90-0028   "Viscous Dampers: Testing, Modeling and Application in Vibration and Seismic Isolation," by N. Makris and M.C. Constantinou, 12/20/90 (PB91-190561, A06, MF-A01).

NCEER-90-0029   "Soil Effects on Earthquake Ground Motions in the Memphis Area," by H. Hwang, C.S. Lee, K.W. Ng and T.S. Chang, 8/2/90, (PB91-190751, A05, MF-A01).

NCEER-91-0001   "Proceedings from the Third Japan-U.S. Workshop on Earthquake Resistant Design of Lifeline Facilities and Countermeasures for Soil Liquefaction, December 17-19, 1990," edited by T.D. O'Rourke and M. Hamada, 2/1/91, (PB91-179259, A99, MF-A04).

NCEER-91-0002   "Physical Space Solutions of Non-Proportionally Damped Systems," by M. Tong, Z. Liang and G.C. Lee, 1/15/91, (PB91-179242, A04, MF-A01).

NCEER-91-0003   "Seismic Response of Single Piles and Pile Groups," by K. Fan and G. Gazetas, 1/10/91, (PB92-174994, A04, MF-A01).

NCEER-91-0004   "Damping of Structures: Part 1 - Theory of Complex Damping," by Z. Liang and G. Lee, 10/10/91, (PB92-197235, A12, MF-A03).

NCEER-91-0005   "3D-BASIS - Nonlinear Dynamic Analysis of Three Dimensional Base Isolated Structures: Part II," by S. Nagarajaiah, A.M. Reinhorn and M.C. Constantinou, 2/28/91, (PB91-190553, A07, MF-A01). This report has been replaced by NCEER-93-0011.

NCEER-91-0006   "A Multidimensional Hysteretic Model for Plasticity Deforming Metals in Energy Absorbing Devices," by E.J. Graesser and F.A. Cozzarelli, 4/9/91, (PB92-108364, A04, MF-A01).

NCEER-91-0007   "A Framework for Customizable Knowledge-Based Expert Systems with an Application to a KBES for Evaluating the Seismic Resistance of Existing Buildings," by E.G. Ibarra-Anaya and S.J. Fenves, 4/9/91, (PB91-210930, A08, MF-A01).

NCEER-91-0008   "Nonlinear Analysis of Steel Frames with Semi-Rigid Connections Using the Capacity Spectrum Method," by G.G. Deierlein, S-H. Hsieh, Y-J. Shen and J.F. Abel, 7/2/91, (PB92-113828, A05, MF-A01).

NCEER-91-0009   "Earthquake Education Materials for Grades K-12," by K.E.K. Ross, 4/30/91, (PB91-212142, A06, MF-A01). This report has been replaced by NCEER-92-0018.

NCEER-91-0010   "Phase Wave Velocities and Displacement Phase Differences in a Harmonically Oscillating Pile," by N. Makris and G. Gazetas, 7/8/91, (PB92-108356, A04, MF-A01).

NCEER-91-0011   "Dynamic Characteristics of a Full-Size Five-Story Steel Structure and a 2/5 Scale Model," by K.C. Chang, G.C. Yao, G.C. Lee, D.S. Hao and Y.C. Yeh," 7/2/91, (PB93-116648, A06, MF-A02).

NCEER-91-0012   "Seismic Response of a 2/5 Scale Steel Structure with Added Viscoelastic Dampers," by K.C. Chang, T.T. Soong, S-T. Oh and M.L. Lai, 5/17/91, (PB92-110816, A05, MF-A01).

NCEER-91-0013   "Earthquake Response of Retaining Walls; Full-Scale Testing and Computational Modeling," by S. Alampalli and A-W.M. Elgamal, 6/20/91, not available.

NCEER-91-0014   "3D-BASIS-M: Nonlinear Dynamic Analysis of Multiple Building Base Isolated Structures," by P.C. Tsopelas, S. Nagarajaiah, M.C. Constantinou and A.M. Reinhorn, 5/28/91, (PB92-113885, A09, MF-A02).

NCEER-91-0015   "Evaluation of SEAOC Design Requirements for Sliding Isolated Structures," by D. Theodossiou and M.C. Constantinou, 6/10/91, (PB92-114602, A11, MF-A03).

NCEER-91-0016   "Closed-Loop Modal Testing of a 27-Story Reinforced Concrete Flat Plate-Core Building," by H.R. Somaprasad, T. Toksoy, H. Yoshiyuki and A.E. Aktan, 7/15/91, (PB92-129980, A07, MF-A02).

NCEER-91-0017   "Shake Table Test of a 1/6 Scale Two-Story Lightly Reinforced Concrete Building," by A.G. El-Attar, R.N. White and P. Gergely, 2/28/91, (PB92-222447, A06, MF-A02).

NCEER-91-0018   "Shake Table Test of a 1/8 Scale Three-Story Lightly Reinforced Concrete Building," by A.G. El-Attar, R.N. White and P. Gergely, 2/28/91, (PB93-116630, A08, MF-A02).

NCEER-91-0019   "Transfer Functions for Rigid Rectangular Foundations," by A.S. Veletsos, A.M. Prasad and W.H. Wu, 7/31/91, not available.

NCEER-91-0020 "Hybrid Control of Seismic-Excited Nonlinear and Inelastic Structural Systems," by J.N. Yang, Z. Li and A. Danielians, 8/1/91, (PB92-143171, A06, MF-A02).

NCEER-91-0021 "The NCEER-91 Earthquake Catalog: Improved Intensity-Based Magnitudes and Recurrence Relations for U.S. Earthquakes East of New Madrid," by L. Seeber and J.G. Armbruster, 8/28/91, (PB92-176742, A06, MF-A02).

NCEER-91-0022 "Proceedings from the Implementation of Earthquake Planning and Education in Schools: The Need for Change - The Roles of the Changemakers," by K.E.K. Ross and F. Winslow, 7/23/91, (PB92-129998, A12, MF-A03).

NCEER-91-0023 "A Study of Reliability-Based Criteria for Seismic Design of Reinforced Concrete Frame Buildings," by H.H.M. Hwang and H-M. Hsu, 8/10/91, (PB92-140235, A09, MF-A02).

NCEER-91-0024 "Experimental Verification of a Number of Structural System Identification Algorithms," by R.G. Ghanem, H. Gavin and M. Shinozuka, 9/18/91, (PB92-176577, A18, MF-A04).

NCEER-91-0025 "Probabilistic Evaluation of Liquefaction Potential," by H.H.M. Hwang and C.S. Lee," 11/25/91, (PB92-143429, A05, MF-A01).

NCEER-91-0026 "Instantaneous Optimal Control for Linear, Nonlinear and Hysteretic Structures - Stable Controllers," by J.N. Yang and Z. Li, 11/15/91, (PB92-163807, A04, MF-A01).

NCEER-91-0027 "Experimental and Theoretical Study of a Sliding Isolation System for Bridges," by M.C. Constantinou, A. Kartoum, A.M. Reinhorn and P. Bradford, 11/15/91, (PB92-176973, A10, MF-A03).

NCEER-92-0001 "Case Studies of Liquefaction and Lifeline Performance During Past Earthquakes, Volume 1: Japanese Case Studies," Edited by M. Hamada and T. O'Rourke, 2/17/92, (PB92-197243, A18, MF-A04).

NCEER-92-0002 "Case Studies of Liquefaction and Lifeline Performance During Past Earthquakes, Volume 2: United States Case Studies," Edited by T. O'Rourke and M. Hamada, 2/17/92, (PB92-197250, A20, MF-A04).

NCEER-92-0003 "Issues in Earthquake Education," Edited by K. Ross, 2/3/92, (PB92-222389, A07, MF-A02).

NCEER-92-0004 "Proceedings from the First U.S. - Japan Workshop on Earthquake Protective Systems for Bridges," Edited by I.G. Buckle, 2/4/92, (PB94-142239, A99, MF-A06).

NCEER-92-0005 "Seismic Ground Motion from a Haskell-Type Source in a Multiple-Layered Half-Space," A.P. Theoharis, G. Deodatis and M. Shinozuka, 1/2/92, not available.

NCEER-92-0006 "Proceedings from the Site Effects Workshop," Edited by R. Whitman, 2/29/92, (PB92-197201, A04, MF-A01).

NCEER-92-0007 "Engineering Evaluation of Permanent Ground Deformations Due to Seismically-Induced Liquefaction," by M.H. Baziar, R. Dobry and A-W.M. Elgamal, 3/24/92, (PB92-222421, A13, MF-A03).

NCEER-92-0008 "A Procedure for the Seismic Evaluation of Buildings in the Central and Eastern United States," by C.D. Poland and J.O. Malley, 4/2/92, (PB92-222439, A20, MF-A04).

NCEER-92-0009 "Experimental and Analytical Study of a Hybrid Isolation System Using Friction Controllable Sliding Bearings," by M.Q. Feng, S. Fujii and M. Shinozuka, 5/15/92, (PB93-150282, A06, MF-A02).

NCEER-92-0010 "Seismic Resistance of Slab-Column Connections in Existing Non-Ductile Flat-Plate Buildings," by A.J. Durrani and Y. Du, 5/18/92, (PB93-116812, A06, MF-A02).

NCEER-92-0011 "The Hysteretic and Dynamic Behavior of Brick Masonry Walls Upgraded by Ferrocement Coatings Under Cyclic Loading and Strong Simulated Ground Motion," by H. Lee and S.P. Prawel, 5/11/92, not available.

NCEER-92-0012 "Study of Wire Rope Systems for Seismic Protection of Equipment in Buildings," by G.F. Demetriades, M.C. Constantinou and A.M. Reinhorn, 5/20/92, (PB93-116655, A08, MF-A02).

NCEER-92-0013   "Shape Memory Structural Dampers: Material Properties, Design and Seismic Testing," by P.R. Witting and F.A. Cozzarelli, 5/26/92, (PB93-116663, A05, MF-A01).

NCEER-92-0014   "Longitudinal Permanent Ground Deformation Effects on Buried Continuous Pipelines," by M.J. O'Rourke, and C. Nordberg, 6/15/92, (PB93-116671, A08, MF-A02).

NCEER-92-0015   "A Simulation Method for Stationary Gaussian Random Functions Based on the Sampling Theorem," by M. Grigoriu and S. Balopoulou, 6/11/92, (PB93-127496, A05, MF-A01).

NCEER-92-0016   "Gravity-Load-Designed Reinforced Concrete Buildings: Seismic Evaluation of Existing Construction and Detailing Strategies for Improved Seismic Resistance," by G.W. Hoffmann, S.K. Kunnath, A.M. Reinhorn and J.B. Mander, 7/15/92, (PB94-142007, A08, MF-A02).

NCEER-92-0017   "Observations on Water System and Pipeline Performance in the Limón Area of Costa Rica Due to the April 22, 1991 Earthquake," by M. O'Rourke and D. Ballantyne, 6/30/92, (PB93-126811, A06, MF-A02).

NCEER-92-0018   "Fourth Edition of Earthquake Education Materials for Grades K-12," Edited by K.E.K. Ross, 8/10/92, (PB93-114023, A07, MF-A02).

NCEER-92-0019   "Proceedings from the Fourth Japan-U.S. Workshop on Earthquake Resistant Design of Lifeline Facilities and Countermeasures for Soil Liquefaction," Edited by M. Hamada and T.D. O'Rourke, 8/12/92, (PB93-163939, A99, MF-E11).

NCEER-92-0020   "Active Bracing System: A Full Scale Implementation of Active Control," by A.M. Reinhorn, T.T. Soong, R.C. Lin, M.A. Riley, Y.P. Wang, S. Aizawa and M. Higashino, 8/14/92, (PB93-127512, A06, MF-A02).

NCEER-92-0021   "Empirical Analysis of Horizontal Ground Displacement Generated by Liquefaction-Induced Lateral Spreads," by S.F. Bartlett and T.L. Youd, 8/17/92, (PB93-188241, A06, MF-A02).

NCEER-92-0022   "IDARC Version 3.0: Inelastic Damage Analysis of Reinforced Concrete Structures," by S.K. Kunnath, A.M. Reinhorn and R.F. Lobo, 8/31/92, (PB93-227502, A07, MF-A02).

NCEER-92-0023   "A Semi-Empirical Analysis of Strong-Motion Peaks in Terms of Seismic Source, Propagation Path and Local Site Conditions, by M. Kamiyama, M.J. O'Rourke and R. Flores-Berrones, 9/9/92, (PB93-150266, A08, MF-A02).

NCEER-92-0024   "Seismic Behavior of Reinforced Concrete Frame Structures with Nonductile Details, Part I: Summary of Experimental Findings of Full Scale Beam-Column Joint Tests," by A. Beres, R.N. White and P. Gergely, 9/30/92, (PB93-227783, A05, MF-A01).

NCEER-92-0025   "Experimental Results of Repaired and Retrofitted Beam-Column Joint Tests in Lightly Reinforced Concrete Frame Buildings," by A. Beres, S. El-Borgi, R.N. White and P. Gergely, 10/29/92, (PB93-227791, A05, MF-A01).

NCEER-92-0026   "A Generalization of Optimal Control Theory: Linear and Nonlinear Structures," by J.N. Yang, Z. Li and S. Vongchavalitkul, 11/2/92, (PB93-188621, A05, MF-A01).

NCEER-92-0027   "Seismic Resistance of Reinforced Concrete Frame Structures Designed Only for Gravity Loads: Part I - Design and Properties of a One-Third Scale Model Structure," by J.M. Bracci, A.M. Reinhorn and J.B. Mander, 12/1/92, (PB94-104502, A08, MF-A02).

NCEER-92-0028   "Seismic Resistance of Reinforced Concrete Frame Structures Designed Only for Gravity Loads: Part II - Experimental Performance of Subassemblages," by L.E. Aycardi, J.B. Mander and A.M. Reinhorn, 12/1/92, (PB94-104510, A08, MF-A02).

NCEER-92-0029   "Seismic Resistance of Reinforced Concrete Frame Structures Designed Only for Gravity Loads: Part III - Experimental Performance and Analytical Study of a Structural Model," by J.M. Bracci, A.M. Reinhorn and J.B. Mander, 12/1/92, (PB93-227528, A09, MF-A01).

NCEER-92-0030   "Evaluation of Seismic Retrofit of Reinforced Concrete Frame Structures: Part I - Experimental Performance of Retrofitted Subassemblages," by D. Choudhuri, J.B. Mander and A.M. Reinhorn, 12/8/92, (PB93-198307, A07, MF-A02).

NCEER-92-0031   "Evaluation of Seismic Retrofit of Reinforced Concrete Frame Structures: Part II - Experimental Performance and Analytical Study of a Retrofitted Structural Model," by J.M. Bracci, A.M. Reinhorn and J.B. Mander, 12/8/92, (PB93-198315, A09, MF-A03).

NCEER-92-0032   "Experimental and Analytical Investigation of Seismic Response of Structures with Supplemental Fluid Viscous Dampers," by M.C. Constantinou and M.D. Symans, 12/21/92, (PB93-191435, A10, MF-A03). This report is available only through NTIS (see address given above).

NCEER-92-0033   "Reconnaissance Report on the Cairo, Egypt Earthquake of October 12, 1992," by M. Khater, 12/23/92, (PB93-188621, A03, MF-A01).

NCEER-92-0034   "Low-Level Dynamic Characteristics of Four Tall Flat-Plate Buildings in New York City," by H. Gavin, S. Yuan, J. Grossman, E. Pekelis and K. Jacob, 12/28/92, (PB93-188217, A07, MF-A02).

NCEER-93-0001   "An Experimental Study on the Seismic Performance of Brick-Infilled Steel Frames With and Without Retrofit," by J.B. Mander, B. Nair, K. Wojtkowski and J. Ma, 1/29/93, (PB93-227510, A07, MF-A02).

NCEER-93-0002   "Social Accounting for Disaster Preparedness and Recovery Planning," by S. Cole, E. Pantoja and V. Razak, 2/22/93, (PB94-142114, A12, MF-A03).

NCEER-93-0003   "Assessment of 1991 NEHRP Provisions for Nonstructural Components and Recommended Revisions," by T.T. Soong, G. Chen, Z. Wu, R-H. Zhang and M. Grigoriu, 3/1/93, (PB93-188639, A06, MF-A02).

NCEER-93-0004   "Evaluation of Static and Response Spectrum Analysis Procedures of SEAOC/UBC for Seismic Isolated Structures," by C.W. Winters and M.C. Constantinou, 3/23/93, (PB93-198299, A10, MF-A03).

NCEER-93-0005   "Earthquakes in the Northeast - Are We Ignoring the Hazard? A Workshop on Earthquake Science and Safety for Educators," edited by K.E.K. Ross, 4/2/93, (PB94-103066, A09, MF-A02).

NCEER-93-0006   "Inelastic Response of Reinforced Concrete Structures with Viscoelastic Braces," by R.F. Lobo, J.M. Bracci, K.L. Shen, A.M. Reinhorn and T.T. Soong, 4/5/93, (PB93-227486, A05, MF-A02).

NCEER-93-0007   "Seismic Testing of Installation Methods for Computers and Data Processing Equipment," by K. Kosar, T.T. Soong, K.L. Shen, J.A. HoLung and Y.K. Lin, 4/12/93, (PB93-198299, A07, MF-A02).

NCEER-93-0008   "Retrofit of Reinforced Concrete Frames Using Added Dampers," by A. Reinhorn, M. Constantinou and C. Li, not available.

NCEER-93-0009   "Seismic Behavior and Design Guidelines for Steel Frame Structures with Added Viscoelastic Dampers," by K.C. Chang, M.L. Lai, T.T. Soong, D.S. Hao and Y.C. Yeh, 5/1/93, (PB94-141959, A07, MF-A02).

NCEER-93-0010   "Seismic Performance of Shear-Critical Reinforced Concrete Bridge Piers," by J.B. Mander, S.M. Waheed, M.T.A. Chaudhary and S.S. Chen, 5/12/93, (PB93-227494, A08, MF-A02).

NCEER-93-0011   "3D-BASIS-TABS: Computer Program for Nonlinear Dynamic Analysis of Three Dimensional Base Isolated Structures," by S. Nagarajaiah, C. Li, A.M. Reinhorn and M.C. Constantinou, 8/2/93, (PB94-141819, A09, MF-A02).

NCEER-93-0012   "Effects of Hydrocarbon Spills from an Oil Pipeline Break on Ground Water," by O.J. Helweg and H.H.M. Hwang, 8/3/93, (PB94-141942, A06, MF-A02).

NCEER-93-0013   "Simplified Procedures for Seismic Design of Nonstructural Components and Assessment of Current Code Provisions," by M.P. Singh, L.E. Suarez, E.E. Matheu and G.O. Maldonado, 8/4/93, (PB94-141827, A09, MF-A02).

NCEER-93-0014   "An Energy Approach to Seismic Analysis and Design of Secondary Systems," by G. Chen and T.T. Soong, 8/6/93, (PB94-142767, A11, MF-A03).

NCEER-93-0015   "Proceedings from School Sites: Becoming Prepared for Earthquakes - Commemorating the Third Anniversary of the Loma Prieta Earthquake," Edited by F.E. Winslow and K.E.K. Ross, 8/16/93, (PB94-154275, A16, MF-A02).

NCEER-93-0016   "Reconnaissance Report of Damage to Historic Monuments in Cairo, Egypt Following the October 12, 1992 Dahshur Earthquake," by D. Sykora, D. Look, G. Croci, E. Karaesmen and E. Karaesmen, 8/19/93, (PB94-142221, A08, MF-A02).

NCEER-93-0017   "The Island of Guam Earthquake of August 8, 1993," by S.W. Swan and S.K. Harris, 9/30/93, (PB94-141843, A04, MF-A01).

NCEER-93-0018   "Engineering Aspects of the October 12, 1992 Egyptian Earthquake," by A.W. Elgamal, M. Amer, K. Adalier and A. Abul-Fadl, 10/7/93, (PB94-141983, A05, MF-A01).

NCEER-93-0019   "Development of an Earthquake Motion Simulator and its Application in Dynamic Centrifuge Testing," by I. Krstelj, Supervised by J.H. Prevost, 10/23/93, (PB94-181773, A-10, MF-A03).

NCEER-93-0020   "NCEER-Taisei Corporation Research Program on Sliding Seismic Isolation Systems for Bridges: Experimental and Analytical Study of a Friction Pendulum System (FPS)," by M.C. Constantinou, P. Tsopelas, Y-S. Kim and S. Okamoto, 11/1/93, (PB94-142775, A08, MF-A02).

NCEER-93-0021   "Finite Element Modeling of Elastomeric Seismic Isolation Bearings," by L.J. Billings, Supervised by R. Shepherd, 11/8/93, not available.

NCEER-93-0022   "Seismic Vulnerability of Equipment in Critical Facilities: Life-Safety and Operational Consequences," by K. Porter, G.S. Johnson, M.M. Zadeh, C. Scawthorn and S. Eder, 11/24/93, (PB94-181765, A16, MF-A03).

NCEER-93-0023   "Hokkaido Nansei-oki, Japan Earthquake of July 12, 1993, by P.I. Yanev and C.R. Scawthorn, 12/23/93, (PB94-181500, A07, MF-A01).

NCEER-94-0001   "An Evaluation of Seismic Serviceability of Water Supply Networks with Application to the San Francisco Auxiliary Water Supply System," by I. Markov, Supervised by M. Grigoriu and T. O'Rourke, 1/21/94, (PB94-204013, A07, MF-A02).

NCEER-94-0002   "NCEER-Taisei Corporation Research Program on Sliding Seismic Isolation Systems for Bridges: Experimental and Analytical Study of Systems Consisting of Sliding Bearings, Rubber Restoring Force Devices and Fluid Dampers," Volumes I and II, by P. Tsopelas, S. Okamoto, M.C. Constantinou, D. Ozaki and S. Fujii, 2/4/94, (PB94-181740, A09, MF-A02 and PB94-181757, A12, MF-A03).

NCEER-94-0003   "A Markov Model for Local and Global Damage Indices in Seismic Analysis," by S. Rahman and M. Grigoriu, 2/18/94, (PB94-206000, A12, MF-A03).

NCEER-94-0004   "Proceedings from the NCEER Workshop on Seismic Response of Masonry Infills," edited by D.P. Abrams, 3/1/94, (PB94-180783, A07, MF-A02).

NCEER-94-0005   "The Northridge, California Earthquake of January 17, 1994: General Reconnaissance Report," edited by J.D. Goltz, 3/11/94, (PB94-193943, A10, MF-A03).

NCEER-94-0006   "Seismic Energy Based Fatigue Damage Analysis of Bridge Columns: Part I - Evaluation of Seismic Capacity," by G.A. Chang and J.B. Mander, 3/14/94, (PB94-219185, A11, MF-A03).

NCEER-94-0007   "Seismic Isolation of Multi-Story Frame Structures Using Spherical Sliding Isolation Systems," by T.M. Al-Hussaini, V.A. Zayas and M.C. Constantinou, 3/17/94, (PB94-193745, A09, MF-A02).

NCEER-94-0008   "The Northridge, California Earthquake of January 17, 1994: Performance of Highway Bridges," edited by I.G. Buckle, 3/24/94, (PB94-193851, A06, MF-A02).

NCEER-94-0009   "Proceedings of the Third U.S.-Japan Workshop on Earthquake Protective Systems for Bridges," edited by I.G. Buckle and I. Friedland, 3/31/94, (PB94-195815, A99, MF-A06).

NCEER-94-0010   "3D-BASIS-ME: Computer Program for Nonlinear Dynamic Analysis of Seismically Isolated Single and Multiple Structures and Liquid Storage Tanks," by P.C. Tsopelas, M.C. Constantinou and A.M. Reinhorn, 4/12/94, (PB94-204922, A09, MF-A02).

NCEER-94-0011   "The Northridge, California Earthquake of January 17, 1994: Performance of Gas Transmission Pipelines," by T.D. O'Rourke and M.C. Palmer, 5/16/94, (PB94-204989, A05, MF-A01).

NCEER-94-0012   "Feasibility Study of Replacement Procedures and Earthquake Performance Related to Gas Transmission Pipelines," by T.D. O'Rourke and M.C. Palmer, 5/25/94, (PB94-206638, A09, MF-A02).

NCEER-94-0013   "Seismic Energy Based Fatigue Damage Analysis of Bridge Columns: Part II - Evaluation of Seismic Demand," by G.A. Chang and J.B. Mander, 6/1/94, (PB95-18106, A08, MF-A02).

NCEER-94-0014   "NCEER-Taisei Corporation Research Program on Sliding Seismic Isolation Systems for Bridges: Experimental and Analytical Study of a System Consisting of Sliding Bearings and Fluid Restoring Force/Damping Devices," by P. Tsopelas and M.C. Constantinou, 6/13/94, (PB94-219144, A10, MF-A03).

NCEER-94-0015   "Generation of Hazard-Consistent Fragility Curves for Seismic Loss Estimation Studies," by H. Hwang and J-R. Huo, 6/14/94, (PB95-181996, A09, MF-A02).

NCEER-94-0016   "Seismic Study of Building Frames with Added Energy-Absorbing Devices," by W.S. Pong, C.S. Tsai and G.C. Lee, 6/20/94, (PB94-219136, A10, A03).

NCEER-94-0017   "Sliding Mode Control for Seismic-Excited Linear and Nonlinear Civil Engineering Structures," by J. Yang, J. Wu, A. Agrawal and Z. Li, 6/21/94, (PB95-138483, A06, MF-A02).

NCEER-94-0018   "3D-BASIS-TABS Version 2.0: Computer Program for Nonlinear Dynamic Analysis of Three Dimensional Base Isolated Structures," by A.M. Reinhorn, S. Nagarajaiah, M.C. Constantinou, P. Tsopelas and R. Li, 6/22/94, (PB95-182176, A08, MF-A02).

NCEER-94-0019   "Proceedings of the International Workshop on Civil Infrastructure Systems: Application of Intelligent Systems and Advanced Materials on Bridge Systems," Edited by G.C. Lee and K.C. Chang, 7/18/94, (PB95-252474, A20, MF-A04).

NCEER-94-0020   "Study of Seismic Isolation Systems for Computer Floors," by V. Lambrou and M.C. Constantinou, 7/19/94, (PB95-138533, A10, MF-A03).

NCEER-94-0021   "Proceedings of the U.S.-Italian Workshop on Guidelines for Seismic Evaluation and Rehabilitation of Unreinforced Masonry Buildings," Edited by D.P. Abrams and G.M. Calvi, 7/20/94, (PB95-138749, A13, MF-A03).

NCEER-94-0022   "NCEER-Taisei Corporation Research Program on Sliding Seismic Isolation Systems for Bridges: Experimental and Analytical Study of a System Consisting of Lubricated PTFE Sliding Bearings and Mild Steel Dampers," by P. Tsopelas and M.C. Constantinou, 7/22/94, (PB95-182184, A08, MF-A02).

NCEER-94-0023   "Development of Reliability-Based Design Criteria for Buildings Under Seismic Load," by Y.K. Wen, H. Hwang and M. Shinozuka, 8/1/94, (PB95-211934, A08, MF-A02).

NCEER-94-0024   "Experimental Verification of Acceleration Feedback Control Strategies for an Active Tendon System," by S.J. Dyke, B.F. Spencer, Jr., P. Quast, M.K. Sain, D.C. Kaspari, Jr. and T.T. Soong, 8/29/94, (PB95-212320, A05, MF-A01).

NCEER-94-0025   "Seismic Retrofitting Manual for Highway Bridges," Edited by I.G. Buckle and I.F. Friedland, published by the Federal Highway Administration (PB95-212676, A15, MF-A03).

NCEER-94-0026   "Proceedings from the Fifth U.S.-Japan Workshop on Earthquake Resistant Design of Lifeline Facilities and Countermeasures Against Soil Liquefaction," Edited by T.D. O'Rourke and M. Hamada, 11/7/94, (PB95-220802, A99, MF-E08).

NCEER-95-0001 "Experimental and Analytical Investigation of Seismic Retrofit of Structures with Supplemental Damping: Part 1 - Fluid Viscous Damping Devices," by A.M. Reinhorn, C. Li and M.C. Constantinou, 1/3/95, (PB95-266599, A09, MF-A02).

NCEER-95-0002 "Experimental and Analytical Study of Low-Cycle Fatigue Behavior of Semi-Rigid Top-And-Seat Angle Connections," by G. Pekcan, J.B. Mander and S.S. Chen, 1/5/95, (PB95-220042, A07, MF-A02).

NCEER-95-0003 "NCEER-ATC Joint Study on Fragility of Buildings," by T. Anagnos, C. Rojahn and A.S. Kiremidjian, 1/20/95, (PB95-220026, A06, MF-A02).

NCEER-95-0004 "Nonlinear Control Algorithms for Peak Response Reduction," by Z. Wu, T.T. Soong, V. Gattulli and R.C. Lin, 2/16/95, (PB95-220349, A05, MF-A01).

NCEER-95-0005 "Pipeline Replacement Feasibility Study: A Methodology for Minimizing Seismic and Corrosion Risks to Underground Natural Gas Pipelines," by R.T. Eguchi, H.A. Seligson and D.G. Honegger, 3/2/95, (PB95-252326, A06, MF-A02).

NCEER-95-0006 "Evaluation of Seismic Performance of an 11-Story Frame Building During the 1994 Northridge Earthquake," by F. Naeim, R. DiSulio, K. Benuska, A. Reinhorn and C. Li, not available.

NCEER-95-0007 "Prioritization of Bridges for Seismic Retrofitting," by N. Basöz and A.S. Kiremidjian, 4/24/95, (PB95-252300, A08, MF-A02).

NCEER-95-0008 "Method for Developing Motion Damage Relationships for Reinforced Concrete Frames," by A. Singhal and A.S. Kiremidjian, 5/11/95, (PB95-266607, A06, MF-A02).

NCEER-95-0009 "Experimental and Analytical Investigation of Seismic Retrofit of Structures with Supplemental Damping: Part II - Friction Devices," by C. Li and A.M. Reinhorn, 7/6/95, (PB96-128087, A11, MF-A03).

NCEER-95-0010 "Experimental Performance and Analytical Study of a Non-Ductile Reinforced Concrete Frame Structure Retrofitted with Elastomeric Spring Dampers," by G. Pekcan, J.B. Mander and S.S. Chen, 7/14/95, (PB96-137161, A08, MF-A02).

NCEER-95-0011 "Development and Experimental Study of Semi-Active Fluid Damping Devices for Seismic Protection of Structures," by M.D. Symans and M.C. Constantinou, 8/3/95, (PB96-136940, A23, MF-A04).

NCEER-95-0012 "Real-Time Structural Parameter Modification (RSPM): Development of Innervated Structures," by Z. Liang, M. Tong and G.C. Lee, 4/11/95, (PB96-137153, A06, MF-A01).

NCEER-95-0013 "Experimental and Analytical Investigation of Seismic Retrofit of Structures with Supplemental Damping: Part III - Viscous Damping Walls," by A.M. Reinhorn and C. Li, 10/1/95, (PB96-176409, A11, MF-A03).

NCEER-95-0014 "Seismic Fragility Analysis of Equipment and Structures in a Memphis Electric Substation," by J-R. Huo and H.H.M. Hwang, 8/10/95, (PB96-128087, A09, MF-A02).

NCEER-95-0015 "The Hanshin-Awaji Earthquake of January 17, 1995: Performance of Lifelines," Edited by M. Shinozuka, 11/3/95, (PB96-176383, A15, MF-A03).

NCEER-95-0016 "Highway Culvert Performance During Earthquakes," by T.L. Youd and C.J. Beckman, available as NCEER-96-0015.

NCEER-95-0017 "The Hanshin-Awaji Earthquake of January 17, 1995: Performance of Highway Bridges," Edited by I.G. Buckle, 12/1/95, not available.

NCEER-95-0018 "Modeling of Masonry Infill Panels for Structural Analysis," by A.M. Reinhorn, A. Madan, R.E. Valles, Y. Reichmann and J.B. Mander, 12/8/95, (PB97-110886, MF-A01, A06).

NCEER-95-0019 "Optimal Polynomial Control for Linear and Nonlinear Structures," by A.K. Agrawal and J.N. Yang, 12/11/95, (PB96-168737, A07, MF-A02).

NCEER-95-0020   "Retrofit of Non-Ductile Reinforced Concrete Frames Using Friction Dampers," by R.S. Rao, P. Gergely and R.N. White, 12/22/95, (PB97-133508, A10, MF-A02).

NCEER-95-0021   "Parametric Results for Seismic Response of Pile-Supported Bridge Bents," by G. Mylonakis, A. Nikolaou and G. Gazetas, 12/22/95, (PB97-100242, A12, MF-A03).

NCEER-95-0022   "Kinematic Bending Moments in Seismically Stressed Piles," by A. Nikolaou, G. Mylonakis and G. Gazetas, 12/23/95, (PB97-113914, MF-A03, A13).

NCEER-96-0001   "Dynamic Response of Unreinforced Masonry Buildings with Flexible Diaphragms," by A.C. Costley and D.P. Abrams," 10/10/96, (PB97-133573, MF-A03, A15).

NCEER-96-0002   "State of the Art Review: Foundations and Retaining Structures," by I. Po Lam, not available.

NCEER-96-0003   "Ductility of Rectangular Reinforced Concrete Bridge Columns with Moderate Confinement," by N. Wehbe, M. Saiidi, D. Sanders and B. Douglas, 11/7/96, (PB97-133557, A06, MF-A02).

NCEER-96-0004   "Proceedings of the Long-Span Bridge Seismic Research Workshop," edited by I.G. Buckle and I.M. Friedland, not available.

NCEER-96-0005   "Establish Representative Pier Types for Comprehensive Study: Eastern United States," by J. Kulicki and Z. Prucz, 5/28/96, (PB98-119217, A07, MF-A02).

NCEER-96-0006   "Establish Representative Pier Types for Comprehensive Study: Western United States," by R. Imbsen, R.A. Schamber and T.A. Osterkamp, 5/28/96, (PB98-118607, A07, MF-A02).

NCEER-96-0007   "Nonlinear Control Techniques for Dynamical Systems with Uncertain Parameters," by R.G. Ghanem and M.I. Bujakov, 5/27/96, (PB97-100259, A17, MF-A03).

NCEER-96-0008   "Seismic Evaluation of a 30-Year Old Non-Ductile Highway Bridge Pier and Its Retrofit," by J.B. Mander, B. Mahmoodzadegan, S. Bhadra and S.S. Chen, 5/31/96, (PB97-110902, MF-A03, A10).

NCEER-96-0009   "Seismic Performance of a Model Reinforced Concrete Bridge Pier Before and After Retrofit," by J.B. Mander, J.H. Kim and C.A. Ligozio, 5/31/96, (PB97-110910, MF-A02, A10).

NCEER-96-0010   "IDARC2D Version 4.0: A Computer Program for the Inelastic Damage Analysis of Buildings," by R.E. Valles, A.M. Reinhorn, S.K. Kunnath, C. Li and A. Madan, 6/3/96, (PB97-100234, A17, MF-A03).

NCEER-96-0011   "Estimation of the Economic Impact of Multiple Lifeline Disruption: Memphis Light, Gas and Water Division Case Study," by S.E. Chang, H.A. Seligson and R.T. Eguchi, 8/16/96, (PB97-133490, A11, MF-A03).

NCEER-96-0012   "Proceedings from the Sixth Japan-U.S. Workshop on Earthquake Resistant Design of Lifeline Facilities and Countermeasures Against Soil Liquefaction, Edited by M. Hamada and T. O'Rourke, 9/11/96, (PB97-133581, A99, MF-A06).

NCEER-96-0013   "Chemical Hazards, Mitigation and Preparedness in Areas of High Seismic Risk: A Methodology for Estimating the Risk of Post-Earthquake Hazardous Materials Release," by H.A. Seligson, R.T. Eguchi, K.J. Tierney and K. Richmond, 11/7/96, (PB97-133565, MF-A02, A08).

NCEER-96-0014   "Response of Steel Bridge Bearings to Reversed Cyclic Loading," by J.B. Mander, D-K. Kim, S.S. Chen and G.J. Premus, 11/13/96, (PB97-140735, A12, MF-A03).

NCEER-96-0015   "Highway Culvert Performance During Past Earthquakes," by T.L. Youd and C.J. Beckman, 11/25/96, (PB97-133532, A06, MF-A01).

NCEER-97-0001   "Evaluation, Prevention and Mitigation of Pounding Effects in Building Structures," by R.E. Valles and A.M. Reinhorn, 2/20/97, (PB97-159552, A14, MF-A03).

NCEER-97-0002   "Seismic Design Criteria for Bridges and Other Highway Structures," by C. Rojahn, R. Mayes, D.G. Anderson, J. Clark, J.H. Hom, R.V. Nutt and M.J. O'Rourke, 4/30/97, (PB97-194658, A06, MF-A03).

NCEER-97-0003 "Proceedings of the U.S.-Italian Workshop on Seismic Evaluation and Retrofit," Edited by D.P. Abrams and G.M. Calvi, 3/19/97, (PB97-194666, A13, MF-A03).

NCEER-97-0004 "Investigation of Seismic Response of Buildings with Linear and Nonlinear Fluid Viscous Dampers," by A.A. Seleemah and M.C. Constantinou, 5/21/97, (PB98-109002, A15, MF-A03).

NCEER-97-0005 "Proceedings of the Workshop on Earthquake Engineering Frontiers in Transportation Facilities," edited by G.C. Lee and I.M. Friedland, 8/29/97, (PB98-128911, A25, MR-A04).

NCEER-97-0006 "Cumulative Seismic Damage of Reinforced Concrete Bridge Piers," by S.K. Kunnath, A. El-Bahy, A. Taylor and W. Stone, 9/2/97, (PB98-108814, A11, MF-A03).

NCEER-97-0007 "Structural Details to Accommodate Seismic Movements of Highway Bridges and Retaining Walls," by R.A. Imbsen, R.A. Schamber, E. Thorkildsen, A. Kartoum, B.T. Martin, T.N. Rosser and J.M. Kulicki, 9/3/97, (PB98-108996, A09, MF-A02).

NCEER-97-0008 "A Method for Earthquake Motion-Damage Relationships with Application to Reinforced Concrete Frames," by A. Singhal and A.S. Kiremidjian, 9/10/97, (PB98-108988, A13, MF-A03).

NCEER-97-0009 "Seismic Analysis and Design of Bridge Abutments Considering Sliding and Rotation," by K. Fishman and R. Richards, Jr., 9/15/97, (PB98-108897, A06, MF-A02).

NCEER-97-0010 "Proceedings of the FHWA/NCEER Workshop on the National Representation of Seismic Ground Motion for New and Existing Highway Facilities," edited by I.M. Friedland, M.S. Power and R.L. Mayes, 9/22/97, (PB98-128903, A21, MF-A04).

NCEER-97-0011 "Seismic Analysis for Design or Retrofit of Gravity Bridge Abutments," by K.L. Fishman, R. Richards, Jr. and R.C. Divito, 10/2/97, (PB98-128937, A08, MF-A02).

NCEER-97-0012 "Evaluation of Simplified Methods of Analysis for Yielding Structures," by P. Tsopelas, M.C. Constantinou, C.A. Kircher and A.S. Whittaker, 10/31/97, (PB98-128929, A10, MF-A03).

NCEER-97-0013 "Seismic Design of Bridge Columns Based on Control and Repairability of Damage," by C-T. Cheng and J.B. Mander, 12/8/97, (PB98-144249, A11, MF-A03).

NCEER-97-0014 "Seismic Resistance of Bridge Piers Based on Damage Avoidance Design," by J.B. Mander and C-T. Cheng, 12/10/97, (PB98-144223, A09, MF-A02).

NCEER-97-0015 "Seismic Response of Nominally Symmetric Systems with Strength Uncertainty," by S. Balopoulou and M. Grigoriu, 12/23/97, (PB98-153422, A11, MF-A03).

NCEER-97-0016 "Evaluation of Seismic Retrofit Methods for Reinforced Concrete Bridge Columns," by T.J. Wipf, F.W. Klaiber and F.M. Russo, 12/28/97, (PB98-144215, A12, MF-A03).

NCEER-97-0017 "Seismic Fragility of Existing Conventional Reinforced Concrete Highway Bridges," by C.L. Mullen and A.S. Cakmak, 12/30/97, (PB98-153406, A08, MF-A02).

NCEER-97-0018 "Loss Asssessment of Memphis Buildings," edited by D.P. Abrams and M. Shinozuka, 12/31/97, (PB98-144231, A13, MF-A03).

NCEER-97-0019 "Seismic Evaluation of Frames with Infill Walls Using Quasi-static Experiments," by K.M. Mosalam, R.N. White and P. Gergely, 12/31/97, (PB98-153455, A07, MF-A02).

NCEER-97-0020 "Seismic Evaluation of Frames with Infill Walls Using Pseudo-dynamic Experiments," by K.M. Mosalam, R.N. White and P. Gergely, 12/31/97, (PB98-153430, A07, MF-A02).

NCEER-97-0021 "Computational Strategies for Frames with Infill Walls: Discrete and Smeared Crack Analyses and Seismic Fragility," by K.M. Mosalam, R.N. White and P. Gergely, 12/31/97, (PB98-153414, A10, MF-A02).

NCEER-97-0022 "Proceedings of the NCEER Workshop on Evaluation of Liquefaction Resistance of Soils," edited by T.L. Youd and I.M. Idriss, 12/31/97, (PB98-155617, A15, MF-A03).

MCEER-98-0001 "Extraction of Nonlinear Hysteretic Properties of Seismically Isolated Bridges from Quick-Release Field Tests," by Q. Chen, B.M. Douglas, E.M. Maragakis and I.G. Buckle, 5/26/98, (PB99-118838, A06, MF-A01).

MCEER-98-0002 "Methodologies for Evaluating the Importance of Highway Bridges," by A. Thomas, S. Eshenaur and J. Kulicki, 5/29/98, (PB99-118846, A10, MF-A02).

MCEER-98-0003 "Capacity Design of Bridge Piers and the Analysis of Overstrength," by J.B. Mander, A. Dutta and P. Goel, 6/1/98, (PB99-118853, A09, MF-A02).

MCEER-98-0004 "Evaluation of Bridge Damage Data from the Loma Prieta and Northridge, California Earthquakes," by N. Basoz and A. Kiremidjian, 6/2/98, (PB99-118861, A15, MF-A03).

MCEER-98-0005 "Screening Guide for Rapid Assessment of Liquefaction Hazard at Highway Bridge Sites," by T. L. Youd, 6/16/98, (PB99-118879, A06, not available on microfiche).

MCEER-98-0006 "Structural Steel and Steel/Concrete Interface Details for Bridges," by P. Ritchie, N. Kauhl and J. Kulicki, 7/13/98, (PB99-118945, A06, MF-A01).

MCEER-98-0007 "Capacity Design and Fatigue Analysis of Confined Concrete Columns," by A. Dutta and J.B. Mander, 7/14/98, (PB99-118960, A14, MF-A03).

MCEER-98-0008 "Proceedings of the Workshop on Performance Criteria for Telecommunication Services Under Earthquake Conditions," edited by A.J. Schiff, 7/15/98, (PB99-118952, A08, MF-A02).

MCEER-98-0009 "Fatigue Analysis of Unconfined Concrete Columns," by J.B. Mander, A. Dutta and J.H. Kim, 9/12/98, (PB99-123655, A10, MF-A02).

MCEER-98-0010 "Centrifuge Modeling of Cyclic Lateral Response of Pile-Cap Systems and Seat-Type Abutments in Dry Sands," by A.D. Gadre and R. Dobry, 10/2/98, (PB99-123606, A13, MF-A03).

MCEER-98-0011 "IDARC-BRIDGE: A Computational Platform for Seismic Damage Assessment of Bridge Structures," by A.M. Reinhorn, V. Simeonov, G. Mylonakis and Y. Reichman, 10/2/98, (PB99-162919, A15, MF-A03).

MCEER-98-0012 "Experimental Investigation of the Dynamic Response of Two Bridges Before and After Retrofitting with Elastomeric Bearings," by D.A. Wendichansky, S.S. Chen and J.B. Mander, 10/2/98, (PB99-162927, A15, MF-A03).

MCEER-98-0013 "Design Procedures for Hinge Restrainers and Hinge Sear Width for Multiple-Frame Bridges," by R. Des Roches and G.L. Fenves, 11/3/98, (PB99-140477, A13, MF-A03).

MCEER-98-0014 "Response Modification Factors for Seismically Isolated Bridges," by M.C. Constantinou and J.K. Quarshie, 11/3/98, (PB99-140485, A14, MF-A03).

MCEER-98-0015 "Proceedings of the U.S.-Italy Workshop on Seismic Protective Systems for Bridges," edited by I.M. Friedland and M.C. Constantinou, 11/3/98, (PB2000-101711, A22, MF-A04).

MCEER-98-0016 "Appropriate Seismic Reliability for Critical Equipment Systems: Recommendations Based on Regional Analysis of Financial and Life Loss," by K. Porter, C. Scawthorn, C. Taylor and N. Blais, 11/10/98, (PB99-157265, A08, MF-A02).

MCEER-98-0017 "Proceedings of the U.S. Japan Joint Seminar on Civil Infrastructure Systems Research," edited by M. Shinozuka and A. Rose, 11/12/98, (PB99-156713, A16, MF-A03).

MCEER-98-0018 "Modeling of Pile Footings and Drilled Shafts for Seismic Design," by I. PoLam, M. Kapuskar and D. Chaudhuri, 12/21/98, (PB99-157257, A09, MF-A02).

MCEER-99-0001 "Seismic Evaluation of a Masonry Infilled Reinforced Concrete Frame by Pseudodynamic Testing," by S.G. Buonopane and R.N. White, 2/16/99, (PB99-162851, A09, MF-A02).

MCEER-99-0002 "Response History Analysis of Structures with Seismic Isolation and Energy Dissipation Systems: Verification Examples for Program SAP2000," by J. Scheller and M.C. Constantinou, 2/22/99, (PB99-162869, A08, MF-A02).

MCEER-99-0003 "Experimental Study on the Seismic Design and Retrofit of Bridge Columns Including Axial Load Effects," by A. Dutta, T. Kokorina and J.B. Mander, 2/22/99, (PB99-162877, A09, MF-A02).

MCEER-99-0004 "Experimental Study of Bridge Elastomeric and Other Isolation and Energy Dissipation Systems with Emphasis on Uplift Prevention and High Velocity Near-source Seismic Excitation," by A. Kasalanati and M. C. Constantinou, 2/26/99, (PB99-162885, A12, MF-A03).

MCEER-99-0005 "Truss Modeling of Reinforced Concrete Shear-flexure Behavior," by J.H. Kim and J.B. Mander, 3/8/99, (PB99-163693, A12, MF-A03).

MCEER-99-0006 "Experimental Investigation and Computational Modeling of Seismic Response of a 1:4 Scale Model Steel Structure with a Load Balancing Supplemental Damping System," by G. Pekcan, J.B. Mander and S.S. Chen, 4/2/99, (PB99-162893, A11, MF-A03).

MCEER-99-0007 "Effect of Vertical Ground Motions on the Structural Response of Highway Bridges," by M.R. Button, C.J. Cronin and R.L. Mayes, 4/10/99, (PB2000-101411, A10, MF-A03).

MCEER-99-0008 "Seismic Reliability Assessment of Critical Facilities: A Handbook, Supporting Documentation, and Model Code Provisions," by G.S. Johnson, R.E. Sheppard, M.D. Quilici, S.J. Eder and C.R. Scawthorn, 4/12/99, (PB2000-101701, A18, MF-A04).

MCEER-99-0009 "Impact Assessment of Selected MCEER Highway Project Research on the Seismic Design of Highway Structures," by C. Rojahn, R. Mayes, D.G. Anderson, J.H. Clark, D'Appolonia Engineering, S. Gloyd and R.V. Nutt, 4/14/99, (PB99-162901, A10, MF-A02).

MCEER-99-0010 "Site Factors and Site Categories in Seismic Codes," by R. Dobry, R. Ramos and M.S. Power, 7/19/99, (PB2000-101705, A08, MF-A02).

MCEER-99-0011 "Restrainer Design Procedures for Multi-Span Simply-Supported Bridges," by M.J. Randall, M. Saiidi, E. Maragakis and T. Isakovic, 7/20/99, (PB2000-101702, A10, MF-A02).

MCEER-99-0012 "Property Modification Factors for Seismic Isolation Bearings," by M.C. Constantinou, P. Tsopelas, A. Kasalanati and E. Wolff, 7/20/99, (PB2000-103387, A11, MF-A03).

MCEER-99-0013 "Critical Seismic Issues for Existing Steel Bridges," by P. Ritchie, N. Kauhl and J. Kulicki, 7/20/99, (PB2000-101697, A09, MF-A02).

MCEER-99-0014 "Nonstructural Damage Database," by A. Kao, T.T. Soong and A. Vender, 7/24/99, (PB2000-101407, A06, MF-A01).

MCEER-99-0015 "Guide to Remedial Measures for Liquefaction Mitigation at Existing Highway Bridge Sites," by H.G. Cooke and J. K. Mitchell, 7/26/99, (PB2000-101703, A11, MF-A03).

MCEER-99-0016 "Proceedings of the MCEER Workshop on Ground Motion Methodologies for the Eastern United States," edited by N. Abrahamson and A. Becker, 8/11/99, (PB2000-103385, A07, MF-A02).

MCEER-99-0017 "Quindío, Colombia Earthquake of January 25, 1999: Reconnaissance Report," by A.P. Asfura and P.J. Flores, 10/4/99, (PB2000-106893, A06, MF-A01).

MCEER-99-0018 "Hysteretic Models for Cyclic Behavior of Deteriorating Inelastic Structures," by M.V. Sivaselvan and A.M. Reinhorn, 11/5/99, (PB2000-103386, A08, MF-A02).

MCEER-99-0019   "Proceedings of the 7th U.S.- Japan Workshop on Earthquake Resistant Design of Lifeline Facilities and Countermeasures Against Soil Liquefaction," edited by T.D. O'Rourke, J.P. Bardet and M. Hamada, 11/19/99, (PB2000-103354, A99, MF-A06).

MCEER-99-0020   "Development of Measurement Capability for Micro-Vibration Evaluations with Application to Chip Fabrication Facilities," by G.C. Lee, Z. Liang, J.W. Song, J.D. Shen and W.C. Liu, 12/1/99, (PB2000-105993, A08, MF-A02).

MCEER-99-0021   "Design and Retrofit Methodology for Building Structures with Supplemental Energy Dissipating Systems," by G. Pekcan, J.B. Mander and S.S. Chen, 12/31/99, (PB2000-105994, A11, MF-A03).

MCEER-00-0001   "The Marmara, Turkey Earthquake of August 17, 1999: Reconnaissance Report," edited by C. Scawthorn; with major contributions by M. Bruneau, R. Eguchi, T. Holzer, G. Johnson, J. Mander, J. Mitchell, W. Mitchell, A. Papageorgiou, C. Scaethorn, and G. Webb, 3/23/00, (PB2000-106200, A11, MF-A03).

MCEER-00-0002   "Proceedings of the MCEER Workshop for Seismic Hazard Mitigation of Health Care Facilities," edited by G.C. Lee, M. Ettouney, M. Grigoriu, J. Hauer and J. Nigg, 3/29/00, (PB2000-106892, A08, MF-A02).

MCEER-00-0003   "The Chi-Chi, Taiwan Earthquake of September 21, 1999: Reconnaissance Report," edited by G.C. Lee and C.H. Loh, with major contributions by G.C. Lee, M. Bruneau, I.G. Buckle, S.E. Chang, P.J. Flores, T.D. O'Rourke, M. Shinozuka, T.T. Soong, C-H. Loh, K-C. Chang, Z-J. Chen, J-S. Hwang, M-L. Lin, G-Y. Liu, K-C. Tsai, G.C. Yao and C-L. Yen, 4/30/00, (PB2001-100980, A10, MF-A02).

MCEER-00-0004   "Seismic Retrofit of End-Sway Frames of Steel Deck-Truss Bridges with a Supplemental Tendon System: Experimental and Analytical Investigation," by G. Pekcan, J.B. Mander and S.S. Chen, 7/1/00, (PB2001-100982, A10, MF-A02).

MCEER-00-0005   "Sliding Fragility of Unrestrained Equipment in Critical Facilities," by W.H. Chong and T.T. Soong, 7/5/00, (PB2001-100983, A08, MF-A02).

MCEER-00-0006   "Seismic Response of Reinforced Concrete Bridge Pier Walls in the Weak Direction," by N. Abo-Shadi, M. Saiidi and D. Sanders, 7/17/00, (PB2001-100981, A17, MF-A03).

MCEER-00-0007   "Low-Cycle Fatigue Behavior of Longitudinal Reinforcement in Reinforced Concrete Bridge Columns," by J. Brown and S.K. Kunnath, 7/23/00, (PB2001-104392, A08, MF-A02).

MCEER-00-0008   "Soil Structure Interaction of Bridges for Seismic Analysis," I. PoLam and H. Law, 9/25/00, (PB2001-105397, A08, MF-A02).

MCEER-00-0009   "Proceedings of the First MCEER Workshop on Mitigation of Earthquake Disaster by Advanced Technologies (MEDAT-1), edited by M. Shinozuka, D.J. Inman and T.D. O'Rourke, 11/10/00, (PB2001-105399, A14, MF-A03).

MCEER-00-0010   "Development and Evaluation of Simplified Procedures for Analysis and Design of Buildings with Passive Energy Dissipation Systems, Revision 01," by O.M. Ramirez, M.C. Constantinou, C.A. Kircher, A.S. Whittaker, M.W. Johnson, J.D. Gomez and C. Chrysostomou, 11/16/01, (PB2001-105523, A23, MF-A04).

MCEER-00-0011   "Dynamic Soil-Foundation-Structure Interaction Analyses of Large Caissons," by C-Y. Chang, C-M. Mok, Z-L. Wang, R. Settgast, F. Waggoner, M.A. Ketchum, H.M. Gonnermann and C-C. Chin, 12/30/00, (PB2001-104373, A07, MF-A02).

MCEER-00-0012   "Experimental Evaluation of Seismic Performance of Bridge Restrainers," by A.G. Vlassis, E.M. Maragakis and M. Saiid Saiidi, 12/30/00, (PB2001-104354, A09, MF-A02).

MCEER-00-0013   "Effect of Spatial Variation of Ground Motion on Highway Structures," by M. Shinozuka, V. Saxena and G. Deodatis, 12/31/00, (PB2001-108755, A13, MF-A03).

MCEER-00-0014   "A Risk-Based Methodology for Assessing the Seismic Performance of Highway Systems," by S.D. Werner, C.E. Taylor, J.E. Moore, II, J.S. Walton and S. Cho, 12/31/00, (PB2001-108756, A14, MF-A03).

MCEER-01-0001   "Experimental Investigation of P-Delta Effects to Collapse During Earthquakes," by D. Vian and M. Bruneau, 6/25/01, (PB2002-100534, A17, MF-A03).

MCEER-01-0002   "Proceedings of the Second MCEER Workshop on Mitigation of Earthquake Disaster by Advanced Technologies (MEDAT-2)," edited by M. Bruneau and D.J. Inman, 7/23/01, (PB2002-100434, A16, MF-A03).

MCEER-01-0003   "Sensitivity Analysis of Dynamic Systems Subjected to Seismic Loads," by C. Roth and M. Grigoriu, 9/18/01, (PB2003-100884, A12, MF-A03).

MCEER-01-0004   "Overcoming Obstacles to Implementing Earthquake Hazard Mitigation Policies: Stage 1 Report," by D.J. Alesch and W.J. Petak, 12/17/01, (PB2002-107949, A07, MF-A02).

MCEER-01-0005   "Updating Real-Time Earthquake Loss Estimates: Methods, Problems and Insights," by C.E. Taylor, S.E. Chang and R.T. Eguchi, 12/17/01, (PB2002-107948, A05, MF-A01).

MCEER-01-0006   "Experimental Investigation and Retrofit of Steel Pile Foundations and Pile Bents Under Cyclic Lateral Loadings," by A. Shama, J. Mander, B. Blabac and S. Chen, 12/31/01, (PB2002-107950, A13, MF-A03).

MCEER-02-0001   "Assessment of Performance of Bolu Viaduct in the 1999 Duzce Earthquake in Turkey" by P.C. Roussis, M.C. Constantinou, M. Erdik, E. Durukal and M. Dicleli, 5/8/02, (PB2003-100883, A08, MF-A02).

MCEER-02-0002   "Seismic Behavior of Rail Counterweight Systems of Elevators in Buildings," by M.P. Singh, Rildova and L.E. Suarez, 5/27/02. (PB2003-100882, A11, MF-A03).

MCEER-02-0003   "Development of Analysis and Design Procedures for Spread Footings," by G. Mylonakis, G. Gazetas, S. Nikolaou and A. Chauncey, 10/02/02, (PB2004-101636, A13, MF-A03, CD-A13).

MCEER-02-0004   "Bare-Earth Algorithms for Use with SAR and LIDAR Digital Elevation Models," by C.K. Huyck, R.T. Eguchi and B. Houshmand, 10/16/02, (PB2004-101637, A07, CD-A07).

MCEER-02-0005   "Review of Energy Dissipation of Compression Members in Concentrically Braced Frames," by K.Lee and M. Bruneau, 10/18/02, (PB2004-101638, A10, CD-A10).

MCEER-03-0001   "Experimental Investigation of Light-Gauge Steel Plate Shear Walls for the Seismic Retrofit of Buildings" by J. Berman and M. Bruneau, 5/2/03, (PB2004-101622, A10, MF-A03, CD-A10).

MCEER-03-0002   "Statistical Analysis of Fragility Curves," by M. Shinozuka, M.Q. Feng, H. Kim, T. Uzawa and T. Ueda, 6/16/03, (PB2004-101849, A09, CD-A09).

MCEER-03-0003   "Proceedings of the Eighth U.S.-Japan Workshop on Earthquake Resistant Design f Lifeline Facilities and Countermeasures Against Liquefaction," edited by M. Hamada, J.P. Bardet and T.D. O'Rourke, 6/30/03, (PB2004-104386, A99, CD-A99).

MCEER-03-0004   "Proceedings of the PRC-US Workshop on Seismic Analysis and Design of Special Bridges," edited by L.C. Fan and G.C. Lee, 7/15/03, (PB2004-104387, A14, CD-A14).

MCEER-03-0005   "Urban Disaster Recovery: A Framework and Simulation Model," by S.B. Miles and S.E. Chang, 7/25/03, (PB2004-104388, A07, CD-A07).

MCEER-03-0006   "Behavior of Underground Piping Joints Due to Static and Dynamic Loading," by R.D. Meis, M. Maragakis and R. Siddharthan, 11/17/03, (PB2005-102194, A13, MF-A03, CD-A00).

MCEER-04-0001   "Experimental Study of Seismic Isolation Systems with Emphasis on Secondary System Response and Verification of Accuracy of Dynamic Response History Analysis Methods," by E. Wolff and M. Constantinou, 1/16/04 (PB2005-102195, A99, MF-E08, CD-A00).

MCEER-04-0002   "Tension, Compression and Cyclic Testing of Engineered Cementitious Composite Materials," by K. Kesner and S.L. Billington, 3/1/04, (PB2005-102196, A08, CD-A08).

MCEER-04-0003 "Cyclic Testing of Braces Laterally Restrained by Steel Studs to Enhance Performance During Earthquakes," by O.C. Celik, J.W. Berman and M. Bruneau, 3/16/04, (PB2005-102197, A13, MF-A03, CD-A00).

MCEER-04-0004 "Methodologies for Post Earthquake Building Damage Detection Using SAR and Optical Remote Sensing: Application to the August 17, 1999 Marmara, Turkey Earthquake," by C.K. Huyck, B.J. Adams, S. Cho, R.T. Eguchi, B. Mansouri and B. Houshmand, 6/15/04, (PB2005-104888, A10, CD-A00).

MCEER-04-0005 "Nonlinear Structural Analysis Towards Collapse Simulation: A Dynamical Systems Approach," by M.V. Sivaselvan and A.M. Reinhorn, 6/16/04, (PB2005-104889, A11, MF-A03, CD-A00).

MCEER-04-0006 "Proceedings of the Second PRC-US Workshop on Seismic Analysis and Design of Special Bridges," edited by G.C. Lee and L.C. Fan, 6/25/04, (PB2005-104890, A16, CD-A00).

MCEER-04-0007 "Seismic Vulnerability Evaluation of Axially Loaded Steel Built-up Laced Members," by K. Lee and M. Bruneau, 6/30/04, (PB2005-104891, A16, CD-A00).

MCEER-04-0008 "Evaluation of Accuracy of Simplified Methods of Analysis and Design of Buildings with Damping Systems for Near-Fault and for Soft-Soil Seismic Motions," by E.A. Pavlou and M.C. Constantinou, 8/16/04, (PB2005-104892, A08, MF-A02, CD-A00).

MCEER-04-0009 "Assessment of Geotechnical Issues in Acute Care Facilities in California," by M. Lew, T.D. O'Rourke, R. Dobry and M. Koch, 9/15/04, (PB2005-104893, A08, CD-A00).

MCEER-04-0010 "Scissor-Jack-Damper Energy Dissipation System," by A.N. Sigaher-Boyle and M.C. Constantinou, 12/1/04 (PB2005-108221).

MCEER-04-0011 "Seismic Retrofit of Bridge Steel Truss Piers Using a Controlled Rocking Approach," by M. Pollino and M. Bruneau, 12/20/04 (PB2006-105795).

MCEER-05-0001 "Experimental and Analytical Studies of Structures Seismically Isolated with an Uplift-Restraint Isolation System," by P.C. Roussis and M.C. Constantinou, 1/10/05 (PB2005-108222).

MCEER-05-0002 "A Versatile Experimentation Model for Study of Structures Near Collapse Applied to Seismic Evaluation of Irregular Structures," by D. Kusumastuti, A.M. Reinhorn and A. Rutenberg, 3/31/05 (PB2006-101523).

MCEER-05-0003 "Proceedings of the Third PRC-US Workshop on Seismic Analysis and Design of Special Bridges," edited by L.C. Fan and G.C. Lee, 4/20/05, (PB2006-105796).

MCEER-05-0004 "Approaches for the Seismic Retrofit of Braced Steel Bridge Piers and Proof-of-Concept Testing of an Eccentrically Braced Frame with Tubular Link," by J.W. Berman and M. Bruneau, 4/21/05 (PB2006-101524).

MCEER-05-0005 "Simulation of Strong Ground Motions for Seismic Fragility Evaluation of Nonstructural Components in Hospitals," by A. Wanitkorkul and A. Filiatrault, 5/26/05 (PB2006-500027).

MCEER-05-0006 "Seismic Safety in California Hospitals: Assessing an Attempt to Accelerate the Replacement or Seismic Retrofit of Older Hospital Facilities," by D.J. Alesch, L.A. Arendt and W.J. Petak, 6/6/05 (PB2006-105794).

MCEER-05-0007 "Development of Seismic Strengthening and Retrofit Strategies for Critical Facilities Using Engineered Cementitious Composite Materials," by K. Kesner and S.L. Billington, 8/29/05 (PB2006-111701).

MCEER-05-0008 "Experimental and Analytical Studies of Base Isolation Systems for Seismic Protection of Power Transformers," by N. Murota, M.Q. Feng and G-Y. Liu, 9/30/05 (PB2006-111702).

MCEER-05-0009 "3D-BASIS-ME-MB: Computer Program for Nonlinear Dynamic Analysis of Seismically Isolated Structures," by P.C. Tsopelas, P.C. Roussis, M.C. Constantinou, R. Buchanan and A.M. Reinhorn, 10/3/05 (PB2006-111703).

MCEER-05-0010 "Steel Plate Shear Walls for Seismic Design and Retrofit of Building Structures," by D. Vian and M. Bruneau, 12/15/05 (PB2006-111704).

MCEER-05-0011   "The Performance-Based Design Paradigm," by M.J. Astrella and A. Whittaker, 12/15/05 (PB2006-111705).

MCEER-06-0001   "Seismic Fragility of Suspended Ceiling Systems," H. Badillo-Almaraz, A.S. Whittaker, A.M. Reinhorn and G.P. Cimellaro, 2/4/06 (PB2006-111706).

MCEER-06-0002   "Multi-Dimensional Fragility of Structures," by G.P. Cimellaro, A.M. Reinhorn and M. Bruneau, 3/1/06 (PB2007-106974, A09, MF-A02, CD A00).

MCEER-06-0003   "Built-Up Shear Links as Energy Dissipators for Seismic Protection of Bridges," by P. Dusicka, A.M. Itani and I.G. Buckle, 3/15/06 (PB2006-111708).

MCEER-06-0004   "Analytical Investigation of the Structural Fuse Concept," by R.E. Vargas and M. Bruneau, 3/16/06 (PB2006-111709).

MCEER-06-0005   "Experimental Investigation of the Structural Fuse Concept," by R.E. Vargas and M. Bruneau, 3/17/06 (PB2006-111710).

MCEER-06-0006   "Further Development of Tubular Eccentrically Braced Frame Links for the Seismic Retrofit of Braced Steel Truss Bridge Piers," by J.W. Berman and M. Bruneau, 3/27/06 (PB2007-105147).

MCEER-06-0007   "REDARS Validation Report," by S. Cho, C.K. Huyck, S. Ghosh and R.T. Eguchi, 8/8/06 (PB2007-106983).

MCEER-06-0008   "Review of Current NDE Technologies for Post-Earthquake Assessment of Retrofitted Bridge Columns," by J.W. Song, Z. Liang and G.C. Lee, 8/21/06 (PB2007-106984).

MCEER-06-0009   "Liquefaction Remediation in Silty Soils Using Dynamic Compaction and Stone Columns," by S. Thevanayagam, G.R. Martin, R. Nashed, T. Shenthan, T. Kanagalingam and N. Ecemis, 8/28/06 (PB2007-106985).

MCEER-06-0010   "Conceptual Design and Experimental Investigation of Polymer Matrix Composite Infill Panels for Seismic Retrofitting," by W. Jung, M. Chiewanichakorn and A.J. Aref, 9/21/06 (PB2007-106986).

MCEER-06-0011   "A Study of the Coupled Horizontal-Vertical Behavior of Elastomeric and Lead-Rubber Seismic Isolation Bearings," by G.P. Warn and A.S. Whittaker, 9/22/06 (PB2007-108679).

MCEER-06-0012   "Proceedings of the Fourth PRC-US Workshop on Seismic Analysis and Design of Special Bridges: Advancing Bridge Technologies in Research, Design, Construction and Preservation," Edited by L.C. Fan, G.C. Lee and L. Ziang, 10/12/06 (PB2007-109042).

MCEER-06-0013   "Cyclic Response and Low Cycle Fatigue Characteristics of Plate Steels," by P. Dusicka, A.M. Itani and I.G. Buckle, 11/1/06 06 (PB2007-106987).

MCEER-06-0014   "Proceedings of the Second US-Taiwan Bridge Engineering Workshop," edited by W.P. Yen, J. Shen, J-Y. Chen and M. Wang, 11/15/06 (PB2008-500041).

MCEER-06-0015   "User Manual and Technical Documentation for the REDARS^{TM} Import Wizard," by S. Cho, S. Ghosh, C.K. Huyck and S.D. Werner, 11/30/06 (PB2007-114766).

MCEER-06-0016   "Hazard Mitigation Strategy and Monitoring Technologies for Urban and Infrastructure Public Buildings: Proceedings of the China-US Workshops," edited by X.Y. Zhou, A.L. Zhang, G.C. Lee and M. Tong, 12/12/06 (PB2008-500018).

MCEER-07-0001   "Static and Kinetic Coefficients of Friction for Rigid Blocks," by C. Kafali, S. Fathali, M. Grigoriu and A.S. Whittaker, 3/20/07 (PB2007-114767).

MCEER-07-0002   "Hazard Mitigation Investment Decision Making: Organizational Response to Legislative Mandate," by L.A. Arendt, D.J. Alesch and W.J. Petak, 4/9/07 (PB2007-114768).

MCEER-07-0003   "Seismic Behavior of Bidirectional-Resistant Ductile End Diaphragms with Unbonded Braces in Straight or Skewed Steel Bridges," by O. Celik and M. Bruneau, 4/11/07 (PB2008-105141).

MCEER-07-0004   "Modeling Pile Behavior in Large Pile Groups Under Lateral Loading," by A.M. Dodds and G.R. Martin, 4/16/07(PB2008-105142).

MCEER-07-0005   "Experimental Investigation of Blast Performance of Seismically Resistant Concrete-Filled Steel Tube Bridge Piers," by S. Fujikura, M. Bruneau and D. Lopez-Garcia, 4/20/07 (PB2008-105143).

MCEER-07-0006   "Seismic Analysis of Conventional and Isolated Liquefied Natural Gas Tanks Using Mechanical Analogs," by I.P. Christovasilis and A.S. Whittaker, 5/1/07, not available.

MCEER-07-0007   "Experimental Seismic Performance Evaluation of Isolation/Restraint Systems for Mechanical Equipment – Part 1: Heavy Equipment Study," by S. Fathali and A. Filiatrault, 6/6/07 (PB2008-105144).

MCEER-07-0008   "Seismic Vulnerability of Timber Bridges and Timber Substructures," by A.A. Sharma, J.B. Mander, I.M. Friedland and D.R. Allicock, 6/7/07 (PB2008-105145).

MCEER-07-0009   "Experimental and Analytical Study of the XY-Friction Pendulum (XY-FP) Bearing for Bridge Applications," by C.C. Marin-Artieda, A.S. Whittaker and M.C. Constantinou, 6/7/07 (PB2008-105191).

MCEER-07-0010   "Proceedings of the PRC-US Earthquake Engineering Forum for Young Researchers," Edited by G.C. Lee and X.Z. Qi, 6/8/07 (PB2008-500058).

MCEER-07-0011   "Design Recommendations for Perforated Steel Plate Shear Walls," by R. Purba and M. Bruneau, 6/18/07, (PB2008-105192).

MCEER-07-0012   "Performance of Seismic Isolation Hardware Under Service and Seismic Loading," by M.C. Constantinou, A.S. Whittaker, Y. Kalpakidis, D.M. Fenz and G.P. Warn, 8/27/07, (PB2008-105193).

MCEER-07-0013   "Experimental Evaluation of the Seismic Performance of Hospital Piping Subassemblies," by E.R. Goodwin, E. Maragakis and A.M. Itani, 9/4/07, (PB2008-105194).

MCEER-07-0014   "A Simulation Model of Urban Disaster Recovery and Resilience: Implementation for the 1994 Northridge Earthquake," by S. Miles and S.E. Chang, 9/7/07, (PB2008-106426).

MCEER-07-0015   "Statistical and Mechanistic Fragility Analysis of Concrete Bridges," by M. Shinozuka, S. Banerjee and S-H. Kim, 9/10/07, (PB2008-106427).

MCEER-07-0016   "Three-Dimensional Modeling of Inelastic Buckling in Frame Structures," by M. Schachter and AM. Reinhorn, 9/13/07, (PB2008-108125).

MCEER-07-0017   "Modeling of Seismic Wave Scattering on Pile Groups and Caissons," by I. Po Lam, H. Law and C.T. Yang, 9/17/07 (PB2008-108150).

MCEER-07-0018   "Bridge Foundations: Modeling Large Pile Groups and Caissons for Seismic Design," by I. Po Lam, H. Law and G.R. Martin (Coordinating Author), 12/1/07 (PB2008-111190).

MCEER-07-0019   "Principles and Performance of Roller Seismic Isolation Bearings for Highway Bridges," by G.C. Lee, Y.C. Ou, Z. Liang, T.C. Niu and J. Song, 12/10/07 (PB2009-110466).

MCEER-07-0020   "Centrifuge Modeling of Permeability and Pinning Reinforcement Effects on Pile Response to Lateral Spreading," by L.L Gonzalez-Lagos, T. Abdoun and R. Dobry, 12/10/07 (PB2008-111191).

MCEER-07-0021   "Damage to the Highway System from the Pisco, Perú Earthquake of August 15, 2007," by J.S. O'Connor, L. Mesa and M. Nykamp, 12/10/07, (PB2008-108126).

MCEER-07-0022   "Experimental Seismic Performance Evaluation of Isolation/Restraint Systems for Mechanical Equipment – Part 2: Light Equipment Study," by S. Fathali and A. Filiatrault, 12/13/07 (PB2008-111192).

MCEER-07-0023   "Fragility Considerations in Highway Bridge Design," by M. Shinozuka, S. Banerjee and S.H. Kim, 12/14/07 (PB2008-111193).

MCEER-07-0024   "Performance Estimates for Seismically Isolated Bridges," by G.P. Warn and A.S. Whittaker, 12/30/07 (PB2008-112230).

MCEER-08-0001   "Seismic Performance of Steel Girder Bridge Superstructures with Conventional Cross Frames," by L.P. Carden, A.M. Itani and I.G. Buckle, 1/7/08, (PB2008-112231).

MCEER-08-0002   "Seismic Performance of Steel Girder Bridge Superstructures with Ductile End Cross Frames with Seismic Isolators," by L.P. Carden, A.M. Itani and I.G. Buckle, 1/7/08 (PB2008-112232).

MCEER-08-0003   "Analytical and Experimental Investigation of a Controlled Rocking Approach for Seismic Protection of Bridge Steel Truss Piers," by M. Pollino and M. Bruneau, 1/21/08 (PB2008-112233).

MCEER-08-0004   "Linking Lifeline Infrastructure Performance and Community Disaster Resilience: Models and Multi-Stakeholder Processes," by S.E. Chang, C. Pasion, K. Tatebe and R. Ahmad, 3/3/08 (PB2008-112234).

MCEER-08-0005   "Modal Analysis of Generally Damped Linear Structures Subjected to Seismic Excitations," by J. Song, Y-L. Chu, Z. Liang and G.C. Lee, 3/4/08 (PB2009-102311).

MCEER-08-0006   "System Performance Under Multi-Hazard Environments," by C. Kafali and M. Grigoriu, 3/4/08 (PB2008-112235).

MCEER-08-0007   "Mechanical Behavior of Multi-Spherical Sliding Bearings," by D.M. Fenz and M.C. Constantinou, 3/6/08 (PB2008-112236).

MCEER-08-0008   "Post-Earthquake Restoration of the Los Angeles Water Supply System," by T.H.P. Tabucchi and R.A. Davidson, 3/7/08 (PB2008-112237).

MCEER-08-0009   "Fragility Analysis of Water Supply Systems," by A. Jacobson and M. Grigoriu, 3/10/08 (PB2009-105545).

MCEER-08-0010   "Experimental Investigation of Full-Scale Two-Story Steel Plate Shear Walls with Reduced Beam Section Connections," by B. Qu, M. Bruneau, C-H. Lin and K-C. Tsai, 3/17/08 (PB2009-106368).

MCEER-08-0011   "Seismic Evaluation and Rehabilitation of Critical Components of Electrical Power Systems," S. Ersoy, B. Feizi, A. Ashrafi and M. Ala Saadeghvaziri, 3/17/08 (PB2009-105546).

MCEER-08-0012   "Seismic Behavior and Design of Boundary Frame Members of Steel Plate Shear Walls," by B. Qu and M. Bruneau, 4/26/08 . (PB2009-106744).

MCEER-08-0013   "Development and Appraisal of a Numerical Cyclic Loading Protocol for Quantifying Building System Performance," by A. Filiatrault, A. Wanitkorkul and M. Constantinou, 4/27/08 (PB2009-107906).

MCEER-08-0014   "Structural and Nonstructural Earthquake Design: The Challenge of Integrating Specialty Areas in Designing Complex, Critical Facilities," by W.J. Petak and D.J. Alesch, 4/30/08 (PB2009-107907).

MCEER-08-0015   "Seismic Performance Evaluation of Water Systems," by Y. Wang and T.D. O'Rourke, 5/5/08 (PB2009-107908).

MCEER-08-0016   "Seismic Response Modeling of Water Supply Systems," by P. Shi and T.D. O'Rourke, 5/5/08 (PB2009-107910).

MCEER-08-0017   "Numerical and Experimental Studies of Self-Centering Post-Tensioned Steel Frames," by D. Wang and A. Filiatrault, 5/12/08 (PB2009-110479).

MCEER-08-0018   "Development, Implementation and Verification of Dynamic Analysis Models for Multi-Spherical Sliding Bearings," by D.M. Fenz and M.C. Constantinou, 8/15/08 (PB2009-107911).

MCEER-08-0019   "Performance Assessment of Conventional and Base Isolated Nuclear Power Plants for Earthquake Blast Loadings," by Y.N. Huang, A.S. Whittaker and N. Luco, 10/28/08 (PB2009-107912).

MCEER-08-0020	"Remote Sensing for Resilient Multi-Hazard Disaster Response – Volume I: Introduction to Damage Assessment Methodologies," by B.J. Adams and R.T. Eguchi, 11/17/08 (PB2010-102695).

MCEER-08-0021	"Remote Sensing for Resilient Multi-Hazard Disaster Response – Volume II: Counting the Number of Collapsed Buildings Using an Object-Oriented Analysis: Case Study of the 2003 Bam Earthquake," by L. Gusella, C.K. Huyck and B.J. Adams, 11/17/08 (PB2010-100925).

MCEER-08-0022	"Remote Sensing for Resilient Multi-Hazard Disaster Response – Volume III: Multi-Sensor Image Fusion Techniques for Robust Neighborhood-Scale Urban Damage Assessment," by B.J. Adams and A. McMillan, 11/17/08 (PB2010-100926).

MCEER-08-0023	"Remote Sensing for Resilient Multi-Hazard Disaster Response – Volume IV: A Study of Multi-Temporal and Multi-Resolution SAR Imagery for Post-Katrina Flood Monitoring in New Orleans," by A. McMillan, J.G. Morley, B.J. Adams and S. Chesworth, 11/17/08 (PB2010-100927).

MCEER-08-0024	"Remote Sensing for Resilient Multi-Hazard Disaster Response – Volume V: Integration of Remote Sensing Imagery and VIEWS^{TM} Field Data for Post-Hurricane Charley Building Damage Assessment," by J.A. Womble, K. Mehta and B.J. Adams, 11/17/08 (PB2009-115532).

MCEER-08-0025	"Building Inventory Compilation for Disaster Management: Application of Remote Sensing and Statistical Modeling," by P. Sarabandi, A.S. Kiremidjian, R.T. Eguchi and B. J. Adams, 11/20/08 (PB2009-110484).

MCEER-08-0026	"New Experimental Capabilities and Loading Protocols for Seismic Qualification and Fragility Assessment of Nonstructural Systems," by R. Retamales, G. Mosqueda, A. Filiatrault and A. Reinhorn, 11/24/08 (PB2009-110485).

MCEER-08-0027	"Effects of Heating and Load History on the Behavior of Lead-Rubber Bearings," by I.V. Kalpakidis and M.C. Constantinou, 12/1/08 (PB2009-115533).

MCEER-08-0028	"Experimental and Analytical Investigation of Blast Performance of Seismically Resistant Bridge Piers," by S.Fujikura and M. Bruneau, 12/8/08 (PB2009-115534).

MCEER-08-0029	"Evolutionary Methodology for Aseismic Decision Support," by Y. Hu and G. Dargush, 12/15/08.

MCEER-08-0030	"Development of a Steel Plate Shear Wall Bridge Pier System Conceived from a Multi-Hazard Perspective," by D. Keller and M. Bruneau, 12/19/08 (PB2010-102696).

MCEER-09-0001	"Modal Analysis of Arbitrarily Damped Three-Dimensional Linear Structures Subjected to Seismic Excitations," by Y.L. Chu, J. Song and G.C. Lee, 1/31/09 (PB2010-100922).

MCEER-09-0002	"Air-Blast Effects on Structural Shapes," by G. Ballantyne, A.S. Whittaker, A.J. Aref and G.F. Dargush, 2/2/09 (PB2010-102697).

MCEER-09-0003	"Water Supply Performance During Earthquakes and Extreme Events," by A.L. Bonneau and T.D. O'Rourke, 2/16/09 (PB2010-100923).

MCEER-09-0004	"Generalized Linear (Mixed) Models of Post-Earthquake Ignitions," by R.A. Davidson, 7/20/09 (PB2010-102698).

MCEER-09-0005	"Seismic Testing of a Full-Scale Two-Story Light-Frame Wood Building: NEESWood Benchmark Test," by I.P. Christovasilis, A. Filiatrault and A. Wanitkorkul, 7/22/09 (PB2012-102401).

MCEER-09-0006	"IDARC2D Version 7.0: A Program for the Inelastic Damage Analysis of Structures," by A.M. Reinhorn, H. Roh, M. Sivaselvan, S.K. Kunnath, R.E. Valles, A. Madan, C. Li, R. Lobo and Y.J. Park, 7/28/09 (PB2010-103199).

MCEER-09-0007	"Enhancements to Hospital Resiliency: Improving Emergency Planning for and Response to Hurricanes," by D.B. Hess and L.A. Arendt, 7/30/09 (PB2010-100924).

MCEER-09-0008   "Assessment of Base-Isolated Nuclear Structures for Design and Beyond-Design Basis Earthquake Shaking," by Y.N. Huang, A.S. Whittaker, R.P. Kennedy and R.L. Mayes, 8/20/09 (PB2010-102699).

MCEER-09-0009   "Quantification of Disaster Resilience of Health Care Facilities," by G.P. Cimellaro, C. Fumo, A.M Reinhorn and M. Bruneau, 9/14/09 (PB2010-105384).

MCEER-09-0010   "Performance-Based Assessment and Design of Squat Reinforced Concrete Shear Walls," by C.K. Gulec and A.S. Whittaker, 9/15/09 (PB2010-102700).

MCEER-09-0011   "Proceedings of the Fourth US-Taiwan Bridge Engineering Workshop," edited by W.P. Yen, J.J. Shen, T.M. Lee and R.B. Zheng, 10/27/09 (PB2010-500009).

MCEER-09-0012   "Proceedings of the Special International Workshop on Seismic Connection Details for Segmental Bridge Construction," edited by W. Phillip Yen and George C. Lee, 12/21/09 (PB2012-102402).

MCEER-10-0001   "Direct Displacement Procedure for Performance-Based Seismic Design of Multistory Woodframe Structures," by W. Pang and D. Rosowsky, 4/26/10 (PB2012-102403).

MCEER-10-0002   "Simplified Direct Displacement Design of Six-Story NEESWood Capstone Building and Pre-Test Seismic Performance Assessment," by W. Pang, D. Rosowsky, J. van de Lindt and S. Pei, 5/28/10 (PB2012-102404).

MCEER-10-0003   "Integration of Seismic Protection Systems in Performance-Based Seismic Design of Woodframed Structures," by J.K. Shinde and M.D. Symans, 6/18/10 (PB2012-102405).

MCEER-10-0004   "Modeling and Seismic Evaluation of Nonstructural Components: Testing Frame for Experimental Evaluation of Suspended Ceiling Systems," by A.M. Reinhorn, K.P. Ryu and G. Maddaloni, 6/30/10 (PB2012-102406).

MCEER-10-0005   "Analytical Development and Experimental Validation of a Structural-Fuse Bridge Pier Concept," by S. El-Bahey and M. Bruneau, 10/1/10 (PB2012-102407).

MCEER-10-0006   "A Framework for Defining and Measuring Resilience at the Community Scale: The PEOPLES Resilience Framework," by C.S. Renschler, A.E. Frazier, L.A. Arendt, G.P. Cimellaro, A.M. Reinhorn and M. Bruneau, 10/8/10 (PB2012-102408).

MCEER-10-0007   "Impact of Horizontal Boundary Elements Design on Seismic Behavior of Steel Plate Shear Walls," by R. Purba and M. Bruneau, 11/14/10 (PB2012-102409).

MCEER-10-0008   "Seismic Testing of a Full-Scale Mid-Rise Building: The NEESWood Capstone Test," by S. Pei, J.W. van de Lindt, S.E. Pryor, H. Shimizu, H. Isoda and D.R. Rammer, 12/1/10 (PB2012-102410).

MCEER-10-0009   "Modeling the Effects of Detonations of High Explosives to Inform Blast-Resistant Design," by P. Sherkar, A.S. Whittaker and A.J. Aref, 12/1/10 (PB2012-102411).

MCEER-10-0010   "L'Aquila Earthquake of April 6, 2009 in Italy: Rebuilding a Resilient City to Withstand Multiple Hazards," by G.P. Cimellaro, I.P. Christovasilis, A.M. Reinhorn, A. De Stefano and T. Kirova, 12/29/10.

MCEER-11-0001   "Numerical and Experimental Investigation of the Seismic Response of Light-Frame Wood Structures," by I.P. Christovasilis and A. Filiatrault, 8/8/11 (PB2012-102412).

MCEER-11-0002   "Seismic Design and Analysis of a Precast Segmental Concrete Bridge Model," by M. Anagnostopoulou, A. Filiatrault and A. Aref, 9/15/11.

MCEER-11-0003   'Proceedings of the Workshop on Improving Earthquake Response of Substation Equipment," Edited by A.M. Reinhorn, 9/19/11 (PB2012-102413).

MCEER-11-0004   "LRFD-Based Analysis and Design Procedures for Bridge Bearings and Seismic Isolators," by M.C. Constantinou, I. Kalpakidis, A. Filiatrault and R.A. Ecker Lay, 9/26/11.

MCEER-11-0005   "Experimental Seismic Evaluation, Model Parameterization, and Effects of Cold-Formed Steel-Framed Gypsum Partition Walls on the Seismic Performance of an Essential Facility," by R. Davies, R. Retamales, G. Mosqueda and A. Filiatrault, 10/12/11.

MCEER-11-0006   "Modeling and Seismic Performance Evaluation of High Voltage Transformers and Bushings," by A.M. Reinhorn, K. Oikonomou, H. Roh, A. Schiff and L. Kempner, Jr., 10/3/11.

MCEER-11-0007   "Extreme Load Combinations: A Survey of State Bridge Engineers," by G.C. Lee, Z. Liang, J.J. Shen and J.S. O'Connor, 10/14/11.

MCEER-12-0001   "Simplified Analysis Procedures in Support of Performance Based Seismic Design," by Y.N. Huang and A.S. Whittaker.

MCEER-12-0002   "Seismic Protection of Electrical Transformer Bushing Systems by Stiffening Techniques," by M. Koliou, A. Filiatrault, A.M. Reinhorn and N. Oliveto, 6/1/12.

MCEER-12-0003   "Post-Earthquake Bridge Inspection Guidelines," by J.S. O'Connor and S. Alampalli, 6/8/12.

MCEER-12-0004   "Integrated Design Methodology for Isolated Floor Systems in Single-Degree-of-Freedom Structural Fuse Systems," by S. Cui, M. Bruneau and M.C. Constantinou, 6/13/12.

MCEER-12-0005   "Characterizing the Rotational Components of Earthquake Ground Motion," by D. Basu, A.S. Whittaker and M.C. Constantinou, 6/15/12.

MCEER-12-0006   "Bayesian Fragility for Nonstructural Systems," by C.H. Lee and M.D. Grigoriu, 9/12/12.

MCEER-12-0007   "A Numerical Model for Capturing the In-Plane Seismic Response of Interior Metal Stud Partition Walls," by R.L. Wood and T.C. Hutchinson, 9/12/12.

MCEER-12-0008   "Assessment of Floor Accelerations in Yielding Buildings," by J.D. Wieser, G. Pekcan, A.E. Zaghi, A.M. Itani and E. Maragakis, 10/5/12.

MCEER-13-0001   "Experimental Seismic Study of Pressurized Fire Sprinkler Piping Systems," by Y. Tian, A. Filiatrault and G. Mosqueda, 4/8/13.

MCEER-13-0002   "Enhancing Resource Coordination for Multi-Modal Evacuation Planning," by D.B. Hess, B.W. Conley and C.M. Farrell, 2/8/13.

MCEER-13-0003   "Seismic Response of Base Isolated Buildings Considering Pounding to Moat Walls," by A. Masroor and G. Mosqueda, 2/26/13.

MCEER-13-0004   "Seismic Response Control of Structures Using a Novel Adaptive Passive Negative Stiffness Device," by D.T.R. Pasala, A.A. Sarlis, S. Nagarajaiah, A.M. Reinhorn, M.C. Constantinou and D.P. Taylor, 6/10/13.

MCEER-13-0005   "Negative Stiffness Device for Seismic Protection of Structures," by A.A. Sarlis, D.T.R. Pasala, M.C. Constantinou, A.M. Reinhorn, S. Nagarajaiah and D.P. Taylor, 6/12/13.

MCEER-13-0006   "Emilia Earthquake of May 20, 2012 in Northern Italy: Rebuilding a Resilient Community to Withstand Multiple Hazards," by G.P. Cimellaro, M. Chiriatti, A.M. Reinhorn and L. Tirca, June 30, 2013.

MCEER-13-0007   "Precast Concrete Segmental Components and Systems for Accelerated Bridge Construction in Seismic Regions," by A.J. Aref, G.C. Lee, Y.C. Ou and P. Sideris, with contributions from K.C. Chang, S. Chen, A. Filiatrault and Y. Zhou, June 13, 2013.

MCEER-13-0008   "A Study of U.S. Bridge Failures (1980-2012)," by G.C. Lee, S.B. Mohan, C. Huang and B.N. Fard, June 15, 2013.

MCEER-13-0009   "Development of a Database Framework for Modeling Damaged Bridges," by G.C. Lee, J.C. Qi and C. Huang, June 16, 2013.

MCEER-13-0010 "Model of Triple Friction Pendulum Bearing for General Geometric and Frictional Parameters and for Uplift Conditions," by A.A. Sarlis and M.C. Constantinou, July 1, 2013.

MCEER-13-0011 "Shake Table Testing of Triple Friction Pendulum Isolators under Extreme Conditions," by A.A. Sarlis, M.C. Constantinou and A.M. Reinhorn, July 2, 2013.

MCEER-13-0012 "Theoretical Framework for the Development of MH-LRFD," by G.C. Lee (coordinating author), H.A Capers, Jr., C. Huang, J.M. Kulicki, Z. Liang, T. Murphy, J.J.D. Shen, M. Shinozuka and P.W.H. Yen, July 31, 2013.

MCEER-13-0013 "Seismic Protection of Highway Bridges with Negative Stiffness Devices," by N.K.A. Attary, M.D. Symans, S. Nagarajaiah, A.M. Reinhorn, M.C. Constantinou, A.A. Sarlis, D.T.R. Pasala, and D.P. Taylor, September 3, 2014.